$$\hat{D} = \alpha_{ij} + \alpha\, b_i^M * H_j^M \qquad (3)$$

where $\vec{H}/H$ is the unit crystal lattice translation $[0\bar{1}1]_M$ in the slip direction, $\vec{H}_M$ is the reciprocal vector corresponding to the $(011)_M$ martensitic plane, α is the value of the relative distortion which is a slip $\sqrt{b_M^2 + c_M^2}$ to the distance $\frac{mc_M}{\sqrt{1+(b_M/c_M)^2}}$ between the nearest slip planes, i.e.,

$$\alpha = \frac{1}{m}\left[1 + (b_M/c_M)^2\right] \qquad (4)$$

where m is the number of interplanar distances between the nearest slip planes (see Fig. 1). Since both the matrix $\hat{D}$ and the matrix $\hat{B}$ should be represented in the same coordinate system related to the austenite axes it is convenient to express the vectors $\vec{b}_M$ and $\vec{H}_M$ by means of the following equations:

$$\vec{b}_M = \hat{B}\,\vec{b}_A\,, \quad \vec{H}_M = \vec{H}_A\,\hat{B}^{-1} \qquad (5)$$

where $\vec{b}_A = \frac{1}{6}\left(a_A,\ a_A,\ -2a_A\right)$ and $\vec{H}_A = \frac{1}{\sqrt{3}}\left(\frac{1}{a_A}\,,\ \frac{1}{a_A}\,,\ \frac{1}{a_A}\right)$

are the reference vector $[11\bar{2}]_A$ and $(111)_A$ reciprocal vectors of the austenite lattice which according to Eq. (5) are transformed into $\vec{b}_M = [0\bar{1}1]_M$ reference vector and $(011)_M$ reciprocal vector of martensite.

There is another way to interpret the matrix $\hat{D}$ as well. The matrix $\hat{D}$ can be treated as the matrix describing the macroscopic change of the shape of the martensitic crystal produced by the glide of the perfect dislocations $[0\bar{1}1](011)_M$ through the martensitic crystal in each $m^{\underline{th}}$ $(011)_M$ plane (compare with Oshima-Wayman mechanism [6]). This dislocations form steps on the $\gamma \rightarrow \alpha$ interphase but leave the perfect martensite lattice behind (Fig. 1).

To find the number m of interplanar distances between the nearest slip planes and the habit plane we shall proceed from the invariant plane conception. According to [12,13] the invariant plane strain transformation produces the minimum elastic strain energy if the habit plane of a new phase coherent inclusion coincides with invariant plane since the main elastic energy term--the bulk elastic energy vanishes.

The requirement that the macroscopic strain is an invariant plane strain is reduced to the equation

$$\hat{\bar{A}} = \hat{R}\hat{A}(m) = \hat{1} + \varepsilon_o\,\vec{d} * \vec{1} \qquad (6)$$

where $\vec{1}$ is the unit vector being normal to the invariant plane, $\vec{d}$ is the unit vector in the direction of the macroscopic shear, ε_o is the

strain, $\hat{R}$ is a rigid body rotation which eliminates the crystal lattice discontinuity on the interphase (invariant) plane caused by the crystal lattice rearrangement $\hat{A}$, $\vec{d}*\vec{1}$ is a tensor product of the vectors $\vec{d}$ and $\vec{1}$. The subsequence of Eq. (6) is

$$\left(\hat{R}\hat{A}(m)\right)^{+}\left(\hat{R}\hat{A}(m)\right) = \hat{A}^{+}(m)\hat{R}^{+}\hat{R}\hat{A}(m) = \hat{A}^{+}(m)\hat{A}(m) = \hat{1} + \varepsilon_{o}\left[\left(\vec{d} + \frac{\varepsilon_{o}}{2}\vec{1}\right) * \vec{\ell} + \vec{1} * \left(\vec{d} + \frac{\varepsilon_{o}}{2}\vec{1}\right)\right] \tag{7}$$

Since $\hat{R}$ is a unitary matrix we have $\hat{R}^{+} = \hat{R}^{-1}$ where $\hat{R}^{-1}$ is an inverse matrix, $\hat{R}^{+}$ is the transposed matrix. Matrix $\hat{A}^{+}(m)\hat{A}(m)$ as any Hermitian matrix can be represented as the sum of three tensor products of its orthonormal eigenvectors:

$$\hat{A}^{+}(m)\hat{A}(m) = \lambda_1^2(M)\vec{e}_1 * \vec{e}_1 + \lambda_2^2(M)\vec{e}_2 * \vec{e}_2 + \lambda_3(m)\vec{e}_3 * \vec{e}_3 \tag{8a}$$

or

$$\hat{A}^{+}(m)\hat{A}(m)-1 = \left(\lambda_1^2(m)-1\right)\vec{e}_1 * \vec{e}_1 + \left(\lambda_2^2(m)-1\right)\vec{e}_2 * \vec{e}_2 + \left(\lambda_3^2(m)-1\right)\vec{e}_3 * \vec{e}_3 \tag{8b}$$

where $\lambda_1^2(m)$, $\lambda_2^2(m)$, $\lambda_3^2(m)$ and $\vec{e}_1$, $\vec{e}_2$, $\vec{e}_3$ are eigenvalues and corresponding eigenvectors of $\hat{A}^{+}\hat{A}$ respectively. Matrix (8b) can be represented in the form (7) if one of the eigenvalues is equal to unity (for instance $\lambda_2(m) = 1$), the second more than unity (for instance $\lambda_1^2 > 1$) and the third one less than unity ($\lambda_3^2 < 1$). Then the simple but tedious calculations show that

$$\vec{\ell} = \sqrt{\frac{\lambda_1^2 - 1}{\lambda_1^2 - \lambda_3^2}}\,\vec{e}_1 + \sqrt{\frac{1 - \lambda_3^2}{\lambda_1^2 - \lambda_3^2}}\,\vec{e}_3 \tag{9a}$$

$$\varepsilon_o^2 = \left(\lambda_1 - \lambda_3\right)^2 \tag{9b}$$

Equation (9a) determines the normal vector $\vec{\ell}$ for the invariant plane. Therefore it determines the habit through the eigenvalues and eigenvectors of the known matrix $\hat{A}^{+}(m)\hat{A}(m)$ calculated for the quantity $m = m_o$ providing the equality $\lambda_2^2(m) = 1$

The easiest way to find $m = m_o$ is to solve equation

$$\det\left|\hat{A}^{+}(m)\hat{A}(m)-1\right| = \left(\lambda_3^2(m)-1\right)\left(\lambda_2^2(m)-1\right)\left(\lambda_3^2(m)-1\right) = 0 \tag{10}$$

where symbol det means the determinant.

Therefore the procedure of finding the invariant plane strain is reduced to the following operations:

(i) the calculation of the matrix $\hat{A}$ employing Eqs. (1) to (3) at the arbitrary value of m. The result of calculations is presented in Appendix 1. (Eq. AI-3).

(ii) the solution of Eq. (10) with respect to m.

(iii) finding of matrix $\hat{A}^{+}\hat{A}$ and its eigenvectors and eigenvectors.

(iv) finding the habit and macroscopic shear from Eq. (9a) and (9b) respectively.

The orientational relationships are determined by equations:

$$\vec{r}_M = \hat{A}\vec{r}_A = (\hat{1} + \varepsilon_o \vec{d} * \vec{\ell})\vec{r}_A = \vec{r}_A + \varepsilon_o \vec{d}(\vec{\ell}\vec{r}_A) \tag{11}$$

$$\vec{H}_M = \vec{H}_A \hat{A}^{-1} = \vec{H}_A \left(\hat{1} - \frac{\varepsilon_o \vec{d} * \vec{\ell}}{1 + \varepsilon_o (\vec{d}\vec{\ell})} \right) = \vec{H}_A - \frac{\varepsilon_o \vec{\ell}(\vec{d}\vec{H}_A)}{1 + \varepsilon_o (\vec{d}\vec{\ell})}$$

where $\vec{r}_A$ and $\vec{H}_A$ are any reference vectors of real and reciprocal lattice of austenite which transforms into $\vec{r}_M$ and $\vec{H}_M$ and reciprocal lattice vectors of martensite respectively after $\gamma \to \alpha$ rearrangement.

3. The habit plane and orientational relationship for freshly formed martensite of Fe-6%Mn-1%C steel

Below we shall consider the case of Fe-6%Mn-1%C martensite. This case has been chosen since it has been studied by the most detail way. According to [14] the crystal lattice parameters of κ'-martensite (freshly formed orthorhombic martensite) in this alloy calculated at the temperature ($M_s = -100°C$) are $a = 2{,}861031$ Å $c = 2{,}9498583$ Å (12) (the temperature expansion coefficient is 23.10^{-6} 1/grad. The crystal lattice parameter of austenite has been found from [15].

$$a_\gamma = \left(3{,}578 + 0.0005\ X_{Mn} + 0.03\ X_C\right)\left(1 + 23.10^{-6}\Delta T\right) \cdot \text{Å} \tag{13}$$

where X_{Mn} and X_C are the weight percents of Mn and C in the alloy. Employing Eqs. (12), (13) and (2) we have the values:

$$a_\gamma = 3{,}601133, \quad \eta_1 = 1{,}1235579;\ \eta_2 = 1{,}1298305,\ \eta_3 = 0{,}8131472 \tag{14}$$

The substitution of (14) into Eq. (A1-4) gives two solutions

$$\begin{aligned} m_1 &= 5{,}5210642 \\ m_2 &= 7{,}7662248 \end{aligned} \tag{15}$$

Both solutions provide the macroscopically invariant plane strain with the same amount of shear $\vec{\xi}_o d$. However, it is useful to remember that the calculated habit plane is an invariant plane within the macroscopic scale only. Locally this habit plane is not invariant plane at all and, therefore the connection of austenite and martensite at this plane produces the stress field which is concentrated near the habit plane within the layer whose thickness if of the order of the typical heterogeneity thickness $md_{(011)}$ (the distance between the nearest slip planes). Therefore, the less value m, the less elastic energy associated with the local elastic strain [12].* Thus it is just the reason why one should choose the solution $m_o = 5,521$ rather than $m_o = 7,766$. The value $m_o = 5,521$ is in excellent agreement with the electron microscopic observation [17] where for the Fe-6%-Mn-1%C κ'-martensite the value m_o within the range 5,5 to 6 was reported.

However, one should bear in mind that the value m_o (being the number of the interplanar distance between the nearest slip planes) cannot be equal to a fractional number 5,521. Therefore, we should choose one of the nearest integer number: either 5 or 6. As a result of that, the macroscopic strain will not be already the invariant plane strain. However, the invariant plane strain can be restored by means of the usual addition of $(112)_M$ transformation twins. The later procedure may be carried out if we substitute m=5 or m=6 into Eq. (A1-3) for the macroscopic distortion with the Bain axis $[001]_A$ and into (I) for the distortion $\hat{A}_1$ with the Bain axis $[100]_A$ (both of them, of course, will not be invariant plane at $\gamma \rightarrow \alpha$ rearrangement).

Making use of the new macroscopic distortion

$$\hat{\bar{A}}_{13} = (1 - x)\hat{A}_3 + x\hat{R}_1\hat{A}_1 \qquad (16)$$

where x is the volume fraction of austenite transformed into martensite by means of the distortion $\hat{A}_1$, $\hat{R}_1$ is the rigid body rotation restoring the continuity of the martensitic lattice along $(112)_M$ plane - the boundary between the martensitic domains arises by means of the distortion $\hat{A}_3$ and $\hat{A}_2$ respectively. The volume fraction x is chosen so that the macroscopic distortion $\hat{\bar{A}}_{13}$ would be the invariant plane strain again.

For the case $m_o = 6$ the numerical calculation gives the habit plane orientation

$$\vec{\ell} = (0,2889621,\ 0,3395651,\ 0,8950958) \qquad (17)$$

---

*According to [12] the elastic energy caused by the heterogeneity of the habit plane is of the order of $E \sim \lambda\varepsilon_o^2 Sh$, where λ are the typical elastic modulus, ε_o is transformation strain, S is the area of the habit plane, h is the heterogeneity length.

which is close to $(225)_A$ plane, (see Fig. 2) and the macroscopic shear

$$\varepsilon_o \vec{d} = (0{,}0098823,\ 0{,}1792044,\ -0{,}045091) \tag{18}$$

for the magnitude

$$\varepsilon_o = 0{,}1850542$$

The calculated value of x is very small and equal to 0,0684219.

The measurement by D. P. Dunne and J. S. Bowles [11] for the Fe-6.14%Mn-0,95%C alloy gives $(225)_A$ habit. It is in good agreement with the calculated habit plane orientation (17). The measured complimentary shear being in the range 0.16 to 0.19 is in good agreement with the value $\frac{1}{m_o} = \frac{1}{6} = 0.166$.

The calculation of orientational relationship based on Eq. (11) gives

$$\begin{aligned} &(1\bar{1}\bar{1})_A \parallel (10\bar{1})_M \quad \text{(deviation is } 0{,}6710496^o\text{)} \\ &[01\bar{1}]_A \parallel [\bar{1}1\bar{1}]_M \quad \text{(deviation is } 0{,}1766081^o\text{)} \end{aligned} \tag{20}$$

The relationships (20) are Kurdjumov-Sacks orientational relationships with very good accuracy, i.e., are in the agreement with x-ray measurement [11].

The case m = 5 does not give any solution and, therefore, cannot take place.

4. The relationship between crystal lattice parameters of freshly formed κ'-martensite and room temperature α-martensite

The above-considered theory results in the conclusion that the $(112)_M$ twinned martensite crystal consists of the 6 plane packs slipped with respect to each other for the same elementary reference vector $[0\bar{1}1](011)_M$. This structure can be also interpreted as the periodical alternation of one-layer $[0\bar{1}1](011)_M$ twins.

According to [4] within such a twin, C-atoms pass from 0_z octahedral positions to 0_y positions. Let introduce the values n_1, n_2, n_3 which are the fractions of interstitial atoms occupying 0_x, 0_y, 0_z interstices respectively. Then according to [4], if the occupation probability to C-atom in each of three octahedral interstices 0_x, 0_y, 0_z is different, the crystal lattice parameters can be calculated from Eqs. [4]

$$\begin{aligned} a_M &= a_o\left[1 + U_{11}(n_2 + n_3) + U_{33}\, n_1\right] \\ b_M &= a_o\left[1 + U_{11}(n_1 + n_3) + U_{33}\, n_2\right] \\ c_M &= a_o\left[1 + U_{11}(n_1 + n_2) + U_{33}\, n_3\right] \end{aligned} \tag{21}$$

where a_o is the crystal lattice parameter of pure αFe; U_{11} and U_{33} one the concent-rational coefficient of the crystal lattice expansion of martensite if C-atoms occupy 0_z octahedral sites only.

In the frame of present approach when we accept 0_y site occupation within one-layer $(011)_M$ twins and 0_2 site occupation within the rest of the crystal we have

$$n_1 = 0, \quad n_2 = \frac{1}{m}\bar{c}, \quad n_3 = \left(1 - \frac{1}{m}\right)\bar{c} \tag{22}$$

The crystal lattice paramters of room temperature martensite (all C-atoms occupy 0_z interstices only) can be obtained from (21) if one puts $n_1 = n_2 = 0$ $n_3 = \bar{c}$:

$$a_M^\alpha = b_M^\alpha = a_o\left(1 + U_{11}\bar{c}\right) \quad c_M^\alpha = a_o\left(1 + U_{33}\bar{c}\right) \tag{23}$$

The substitution of Eq. (22) into (21), taking into account Eq. (23) and the condition

$$\frac{c_M^\alpha}{a_M^\alpha} - 1 \simeq \left(U_{33} - U_{11}\right)\bar{c}$$

which is valid at small values $U_{33}\bar{c}$ and $U_{11}\bar{c}$ results in the final relationships

$$a_M = a_M^\alpha, \quad b_M = a_M^\alpha + \left(\frac{c_M^\alpha}{a_M^\alpha} - 1\right)\frac{a_o}{m}, \quad c_M = c_M^\alpha - \left(\frac{c_M^\alpha}{a_M^\alpha} - 1\right)\frac{a_o}{m} \tag{24}$$

between crystal lattice parameters of κ' and α martensite.

It follows from (24) that

$$b_M + c_M = c_M^\alpha + a_M^\alpha \tag{25}$$

Equation (25) can be checked. According to [14] for Fe-6%Mn-1%C we have

$$c_M = 2{,}955 \text{ Å}, \quad b_M = 2{,}882 \text{ Å} \quad \text{and} \quad c_M + b_M = 5{,}837 \text{ Å}$$

$$c_M^\alpha = 2{,}975 \text{ Å}, \quad b_M^\alpha = 2{,}864 \text{ Å} \quad \text{and} \quad c_M^\alpha + b_M = 5{,}839 \text{ Å}$$

i.e., Eq. (25) hold with accuracy of experimental measurement.

Since we know the crystal lattice paramters of α martensite of Fe-6%Mn-1%C alloy from [14] and the number m (m=6 according to the previous habit plane calculation and positions of extra spots on the electron diffraction pattern [6,7]) we can calculate the crystal lattice

parameters of κ'-martensite employing Eq. (24) and compare them with X-ray data. The results of the calculation and comparison are displayed in the Table 1.

Table 1

Experimental data [14] in Å		Data according to Eq. (24) in Å
$a_M^{\alpha} = 2{,}864$	$a_M = 2{,}866$	$a_M = 2{,}864$
$a_M^{\alpha} = 2{,}864$	$b_M = 2{,}882$	$b_M = 2{,}884$
$c_M^{\alpha} = 2{,}975$	$c_M = 2{,}955$	$c_M = 2{,}955$

5. Discussion

The combination of the $\langle 0\bar{1}1\rangle > (011)_M$ slip and of the $(112)_M$ twinning mechanisms of relaxation of internal stresses at $\gamma \rightarrow \alpha$ rearrangement enables to explain the group of the different phenomena observed in the freshly formed martensite, (κ'-martensite), of manganese steel. We mean the crystal lattice abnormalities [1,2,3,14], extra spots on the selected area diffraction patterns [6], the $(225)_A$ habit [11] and the orientational relationship [11]. The elementary slip along the $(011)_M$ plane may be considered as the formulation of the one layer $(011)_M$ twin. Therefore the $(011)_M$ twinning model [4], the proposed slip model and the dislocation model [6] as a matter of fact, are very close to each other.

The requirement that the shape strain is to be an invariant plane strain enables to get the value $m = 6$, which determines the separation between the extra spots and the nearest fundamental reflections as well as the magnitude of the crystal lattice paramters of orthorhombic κ'-martensite. All of the values calculated and measured are in good agreement with each other.

As known, $(225)_A$ habit could not be satisfactorily obtained in the frame of the conventional scheme of $\gamma \rightarrow \alpha$ rearrangement. However, the proposed mechanism of $\gamma \rightarrow \alpha$ rearrangement enables to obtain the habit being close to the $(hhl)_A$ line on the stereographic projection (Fig. 2).

Since the $(011)_M$ slip in martensite corresponds to the $(111)_A$ shear in austenite one may conclude that the proposed slip mechanism seems to be especially significant for alloys with low stacking fault energy. The observation of f.c.c. $\rightleftharpoons$ h.c.p. transformation in the Fe-Mn-C equilibrium diagram (this transformation is associated with regular formation of the stacking faults) just means that Fe-6%Mn-1%C alloy is an alloy with the low stacking fault energy and, therefore, the alloy, where all above mentioned phenomena take place. The same

might be expected for any iron-based alloy whose equilibrium diagram contains the h.c.p. field.

As for the effect of C-atoms on the mechanism of $\gamma \to \alpha$ rearrangement we can assume that C-atoms are the obstacles for the dislocation glide along $(011)_M$ plane, and therefore, should depress the proposed slip mechanism of the formation of the invariant plane. It means that the increase of the carbon content seems to be able to change the habit plane orientation from $(225)_A$ kind to $(259)_A$ kind.

APPENDIX

We shall determine matrix $\hat{A}$ using the values η_1, η_2, η_3. From (5) we can get

$$\vec{b}_M = \left(\frac{\eta_1}{\sqrt{\eta_1^2 + \eta_2^2 + 4\eta_3^2}} ; \quad \frac{\eta_2}{\sqrt{\eta_1^2 + \eta_2^2 + 4\eta_3^2}} ; \quad \frac{\eta_2}{\sqrt{\eta_1^2 + \eta_2^2 + 4\eta_3^2}} \right) \tag{A-1}$$

$$\vec{H}_M = \left(\frac{\eta_1\eta_2}{\sqrt{\eta_1^2\eta_2^2 + \eta_1^2\eta_3^3 + \eta_2^2\eta_3^2}} ; \quad \frac{\eta_1\eta_3}{\sqrt{\eta_1^2\eta_2^2 + \eta_1^2\eta_2^2 + \eta_2^2\eta_3^2}} ; \quad \frac{\eta_2\eta_2}{\sqrt{\eta_1^2\eta_2^2 + \eta_1^2\eta_3^2 + \eta_2^2\eta_3^2}} \right) \tag{A-2}$$

and from Eqs. (1), (2) and (3)

$$\hat{A} = \begin{pmatrix} \eta_1(1+\gamma) & \gamma\eta_1 & \gamma\eta_1 \\ \gamma\eta_2 & \eta_2(1+\gamma) & \gamma\eta_2 \\ -2\gamma\eta_3 & -2\gamma\eta_3 & \eta_3(1-2\gamma) \end{pmatrix} \tag{A-3}$$

where

$$\gamma = \frac{\alpha\eta_1\eta_2\eta_3}{\sqrt{(\eta_1^2 + \eta_2^2 + 4\eta_2^2)(\eta_1^2\eta_2^2 + \eta_1^2\eta_3^2 + \eta_2^2\eta_2^2)}} \tag{A-4}$$

Now the Eq. (14) we can write as

$$\det|\hat{A}^+\hat{A}-1| = 0 = \begin{vmatrix} \xi\gamma^2 + 2\eta_1^2\gamma + \eta_1^2 - 1 & \xi\gamma^2 + \gamma(\eta_1^2 + \eta_2^2) & \xi\gamma^2 + \gamma(\eta_1^2 - 2\eta_3^2) \\ \xi\gamma^2 + \gamma(\eta_1^2 + \eta_2^2) & \xi\gamma^2 + 2\eta_2^2\gamma + \eta_2^2 - 1 & \xi\gamma^2 + \gamma(\eta_2^2 - 2\eta_3^2) \\ \xi\gamma^2 + \gamma(\eta_1^2 - 2\eta_3^2) & \xi\gamma^2 + \gamma(\eta_2^2\ 2\eta_3^2) & \xi\gamma^2 - 4\gamma\eta_3^2 + \eta_3^2 - 1 \end{vmatrix}$$

where $\xi = \eta_1^2 + \eta_2^2 + 4\eta_3^2$ (A-5)

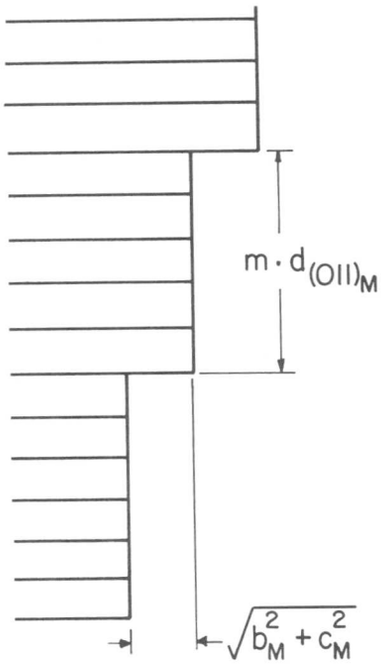

Fig. 1 $[0\bar{1}1]$ $(011)_M$

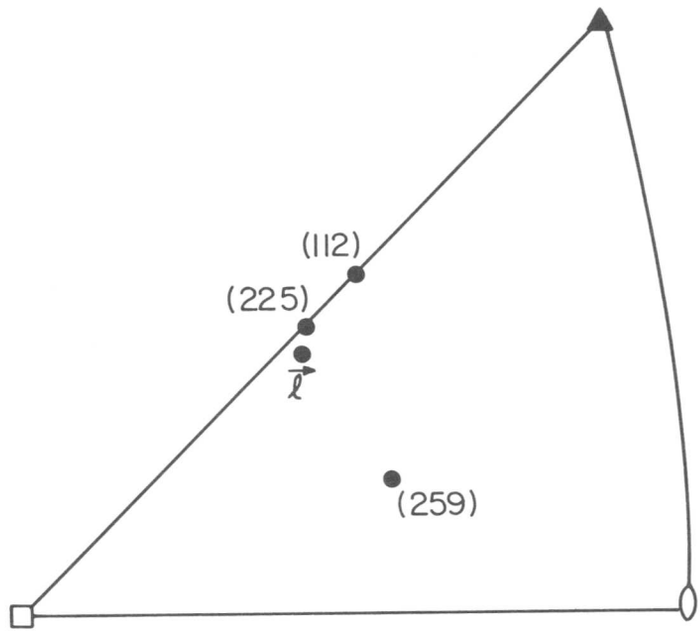

Fig. 2 Stereographic projection

REFERENCES

1. L. I. Lyssak, Ja. N. Vovk, Fiz. Metal. Metalloved 20, (1965), 540. L. I. Lyssak, V. E. Danilchenko, ibid. 32, (1971), 639.
2. Ju. Alshevsky, G. Kurdjumov, Fiz. Metal. Metallov. 25, (1968) 172.
3. L. I. Lyssak, Ja. N. Vovk, A. P. Drachinskaya, Ju. M. Polishtchuk Fiz. Met. Metalloved. 24, (1967), 299.
4. G. V. Kurdjumov, A. G. Khachaturyan, Acta Met. 23, (1975), 1077.
5. I. Entin, V. Somenkov, S. Shilshtein, Dokl. Acad. Nauk SSSR 195, (1970), 595.
6. R. Oshima, C. M. Wayman, Scripta Met. 8, (1974), 223.
7. R. Oshima, H. Azuma, F. E. Fujita, "New Aspects of Martensitic Transformation," Proceedings of the International Symposium, Kobe, Japan, (1976).
8. M. S. Wechsler, D. S. Lieberman, T. A. Read, Trans. AIME 197, (1953) 1503.
9. J. S. Bowles, J. K. Mackenzie Acta Met. 2, (1954), pp. 123, 138, 324.
10. C. M. Wayman, "Introduction to the Crystallography of Martensitic Transformation," MacMillan Co., New York, (1964).
11. D. P. Dunne, J. S. Bowles, Acta Met. 17, (1969), 201.
12. A. G. Khachaturyan, G. A. Shatalov, Sov. Phys. JETP 29, (1969), 557.
13. A. G. Khachaturyan, A. Rymynina, Phys. Stat. Sol. (a) 45, (1978), 393.
14. L. I. Lyssak, S. P. Kondratjev, Ju. M. Polishtchuk, Fiz. Metal. Metalloved. 36, (1973), 546.
15. C. S. Roberts, Trans. AIME 197, (1953), 203.

A General Method of Determining Habit Planes and Orientation Relationships in Bainitic Steels

S. Hoekstra and C.A. Verbraak

A new and accurate method is given for the experimental determination of habit planes and orientation relationships in specimens of a commercial 35NiCr18 steel, to check the invariant plane strain (I.P.S.) theory. This new method is based on the orientation determination of the austenite prior to the bainite transformation using non-parallel {111} twin intersections. A comparison between the new method of habit plane determination based on a single surface analysis and the old method based on a two surface analysis, shows that the new method is an in situ determination, because of the early stage of transformation at which the habit planes are determined. This means that two important conditions can be fulfilled for an accurate determination of the habit plane, which are missing in the case of a two surface analysis. The orientation relationship is rather accurate as well, because of the correlation with the new method of habit plane determination.

I. Introduction

The I.P.S. theory of martensitic transformations, developed by Wechsler et al. [1] and Bowles and MacKenzie [2,3] have been succesful in accounting for the crystallographic characteristics of these and many other transformations. However, the full crystallography of some transformations can not be explained by this theory because of the large dilatation of the order of 2% which must be invoked to be able to account for the observed habit planes [4]. One such anamolous case is the bainitic transformation in steel, as has been pointed out by Bowles and Kennon [5]. These workers demonstrated the failure of the theory to account for the observed habit planes and emphasized the need for experimental determination of bainite habit planes and orientation relationships. Therefore, it is the purpose of the present paper to present a new and accurate method of determining habit planes and orientation relationships in bainitic steels without the aid of the I.P.S. theory. This method depends on the orientation determination of the austenite using non-parallel {111} twin intersections.

II. Experimental Procedure

The experiments were carried out with the commercial steel 35NiCr18 with the following composition: 0.34 wt.% C, 0.25 wt.% Si, 0.60 wt.% Mn, 0.03 wt.% P, 0.06 wt.% S, 4.50 wt.% Ni and 1.30 wt.% Cr. From this steel a number of rectangular-shaped specimens were cut out mechanically to the dimensions 5 × 8 × 0.2 mm, and were abraded on 220-600 grade SiC-paper followed by an electrolytical polishing for 20 s. The heat treatment of the specimens (in a Leitz hot stage microscope and at a pressure

---

Department of Mechanical Engineering, Section Materials Science (WB/MK) Technical University Twente, P.O. Box 217, Enschede, The Netherlands.

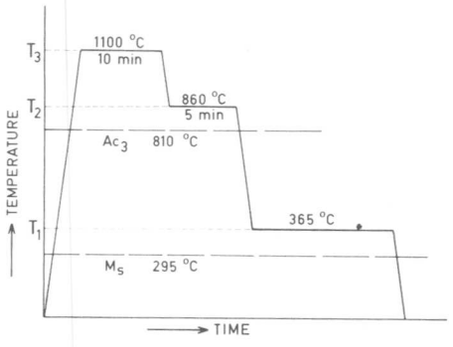

Fig. 1. Schematic representation of the heat treatment.

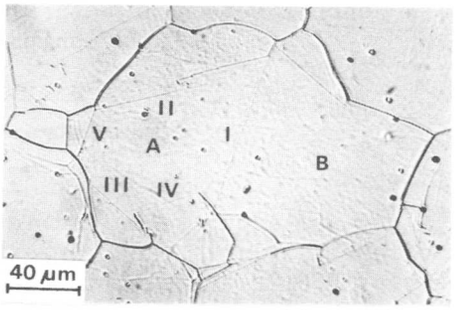

N = -0.5292 -0.1066 0.8418 } B
D = 0.5514 -0.7972 0.2458

Fig. 2. Optical micrograph of an austenitic grain taken at 365°C.

of 10^{-6} Torr) is shown schematically in Fig. 1 and is based on earlier investigations of Beyer [6]. During the austenitizing process at the temperature T_3, thermal etching occurs and annealing twins will arise from which the orientation of the austenitic grain can be determined. After an austenitic grain is found at the temperature T_2 containing four non-parallel {111} twin intersections, the isothermal transformation from metastable austenite to bainite takes place at the temperature T_1. This temperature will be lowered to room temperature as soon as the bainite plates start to influence each other in their growth. This means that the remaining part of the matrix will transform into martensite. During the transformation from austenite to bainite many optical micrographs are taken in order to record the history of the bainite plates. Foils for transmission electron microscopy on a Philips EM 300, are then prepared by mechanical thinning and ionic etching of the fully transformed specimens, to determine the orientation of the same bainite plates as observed in the hot stage microscope.

III. Orientation Determination of the Austenite

Fig. 2 represents an optical micrograph of an austenitic grain containing two parts A and B in twin relationship to each other. Part A contains the {111} twin intersections I, II, III, IV and V, of which I and V are parallel. With the aid of the mutual angles between the twin intersections I, II, III and IV the orientation of part A can be calculated with an accuracy better than 0.1°. This calculation method is described in detail by Hoekstra et al. [7] and in view of the need for brevity we will not go further into this matter. The orientation of part B can now be calculated by mathematical twinning of the orientation of part A. The indicated direction D in Fig. 2 is the direction of the common twin intersection I which is perpendicular to the calculated plane normal N of part B.

IV. Habit Plane Determination of the Bainite

The optical micrographs of Fig. 3 show three successive stages during the isothermal transformation from metastable austenite to bainite (compare also Fig. 2). The indicated three non-parallel trace directions of bainite intersections 1, 2 and 3 in part B are selected to

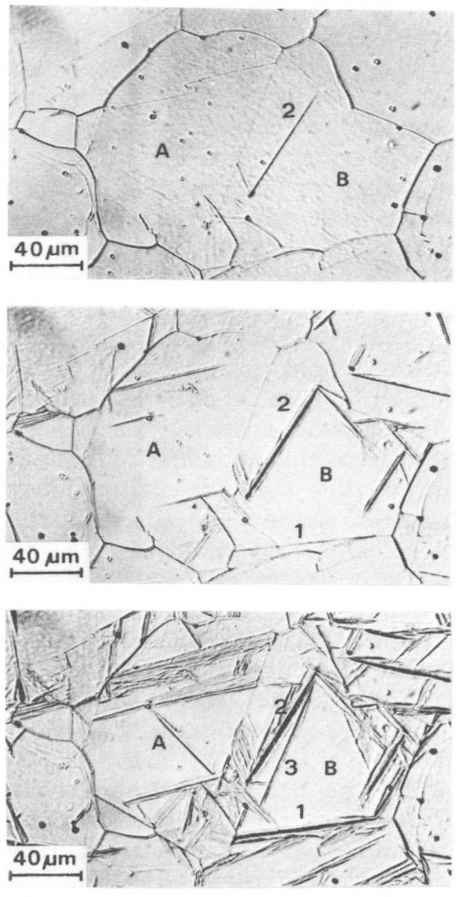

Fig. 3. Optical micrographs of the same grain in Fig. 2.

determine the habit plane, because the midribs of these intersections are straight lines and well defined. We assume that inside of one grain the pole of the habit plane is the same for all bainite plates apart from mutations. This pole is lying on a line which is perpendicular to the midrib of each bainite intersection. The lines in question, 1', 2' and 3', are indicated in the stereographic projection plot of Fig. 4 with the calculated plane normal of part B in the centre of the plot and the calculated direction along the axis AB. The {hkl} poles of the habit planes belonging to the bainite intersections 1, 2 and 3 are lying somewhere on the lines 1', 2' and 3' respectively. The positions of these poles are defined by the fact that they all should be a mutation of one and the same {hkl} pole because of the assumption mentioned above. These positions can be found by permuting all four lines in Fig. 4 in only one and the same unit triangle as indicated in Fig. 5. If our assumption is correct, then all four lines must intersect each other at one point. As can be seen from Fig. 5, such a point can be found and is indicated by X_1, which is the pole of the bainite habit plane. With the aid of the irrational indices of the X_1 pole, it is possible to plot in Fig. 4 the exact podition of X_1 with regard to each individual line, i.e. P, Q and R. For a more detailed description of this new method of habit

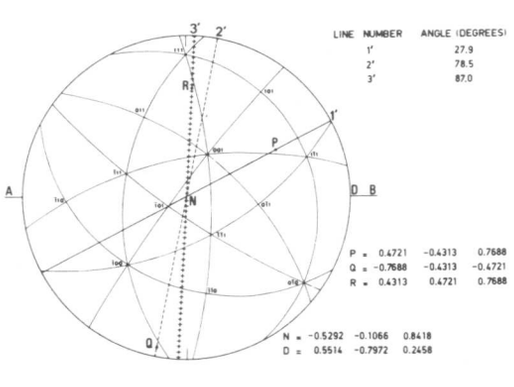

Fig. 4. Stereogr. proj. of the orientation of part B in Fig. 2.

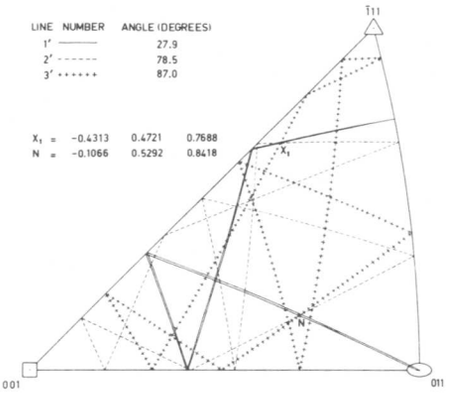

Fig. 5. Representation of the lines 1', 2' and 3' in one unit triangle.

plane determination, the reader is referred to Hoekstra et al. [8].

V. Determination of the Orientation Relationship

The grain in Fig. 2 is shown again in Fig. 6a after the isothermal transformation temperature from metastable austenite to bainite was lowered to room temperature. At that moment (8 min. after the isothermal transformation temperature was reached) about 30% of the parent phase was transformed into bainite. This means that the remaining part has been transformed into martensite on cooling to room temperature. After mechanical thinning and ionic etching of the fully transformed specimens it is possible to determine the orientation of the same bainite plates 1, 2 and 3 in Fig. 3 by means of electron diffraction, as shown in Fig. 6b and Fig. 7a (bainite plate 1), Fig. 6c and Fig. 7b (bainite plate 2), and Fig. 6d and Fig. 7c (bainite plate 3). With the aid of bright field images the direction of each bainite intersection can be determined for a correct transfer of the stereographic projection plots of the diffraction patterns to the plot of Fig. 4, defining the orientation relationship, as indicated in Fig. 7. As can be seen, the orientation relationship for each bainite plate with the austenitic matrix is approximately of the type Kurdjumov-Sachs. Now two conditions must be satisfied at the same time. In the first place the poles of the bainite habit planes must also be mutations of each other relative to the bcc structure, and in the second place the orientation relationship of each bainite plate with the austenitic matrix in which it originated must be the same. These two conditions can be satisfied at the same time by rotating the calculated orientation of the austenitic grain into an exact Kurdjumov-Sachs orientation relationship with the orientations of the bainite plates 1, 2 and 3 (Fig. 7), because it appears that as a result of this rotation the new positions of P, Q and R, i.e. P', Q' and R', are mutations of each other relative to the bcc structure within an accuracy of 1^{o}. In our case P', Q' and R' are exact mutations of each other. This means that the orientation relationship for each bainite plate is a Kurdjumov-Sachs orientation relationship within 1^{o}. The necessary rotations are justified because they are in the order of magnitude of the inaccuracy of the electron diffraction patterns [9].

VI. Results and Discussion

The new method of habit plane determination has been employed to a number of specimens of which the results are shown in the upper half of Fig. 8. As can be seen, the mean habit plane pole relative to the fcc structure ($MHPP_{\gamma}$) is irrational but close to $(569)_{\gamma}$. The accuracy of the habit plane determination is estimated to be better than $\pm 0.5^{o}$. Apart from this accuracy, the new method is more reliable than a two-surface analysis, because of the stage at which the habit planes are determined. This stage is the very beginning of the transformation process, resulting in an unambiguous indication of the midrib for the bainite plates corresponding to the true habit plane. Besides the bainite plates will not be influenced by internal stresses. These two important conditions for the determination of a correct habit plane are missing in the case of a two-surface analysis because this method can only be used after the transformation is complete with regard to the steel used in this investigation [10]. From nine specimens of which the habit plane

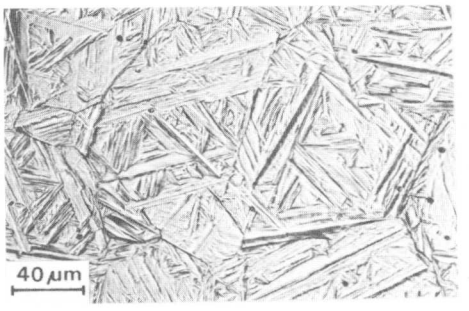

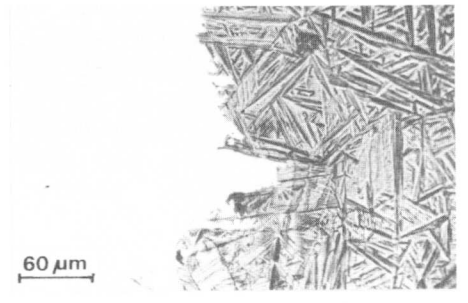

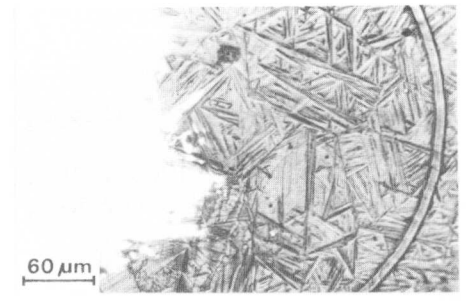

Fig. 6. Optical micrographs of different ionic etching stages of the specimen containing the transformed grain indicated in Fig. 2 and Fig. 3.

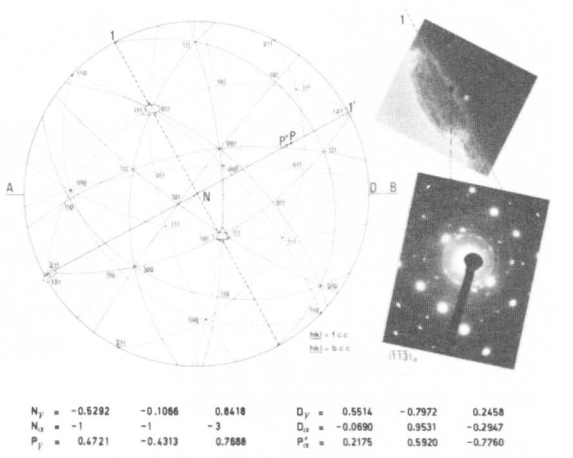

(a)

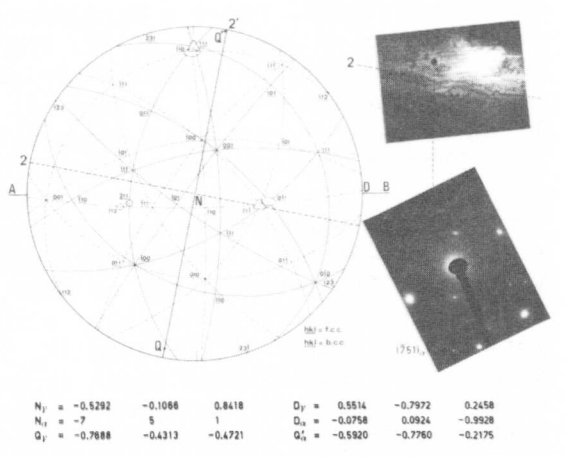

(b)

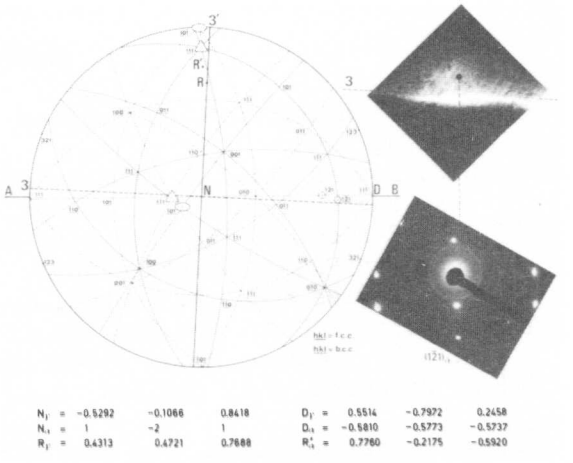

(c) 2.0 μm

Fig. 7. Orientation relationships of the bainite plates 1, 2 and 3.

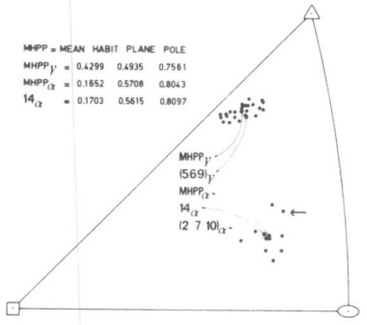

Fig. 8. Results of habit plane pole measurements.

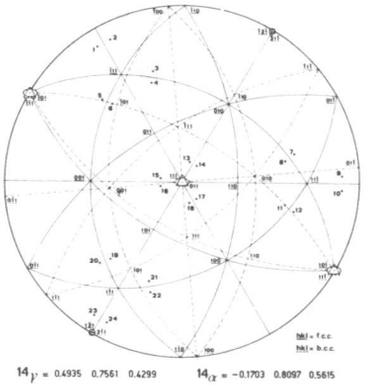

Fig. 9. Stereogr. proj. plot of an exact Kurdjumov-Sachs orientation relationship in which all 24 permutations of MHPP$_\gamma$ are plotted.

poles are shown in the upper half of Fig. 8, the orientation relationship was determined of each bainite plate in a way as described in Section V. In all cases a Kurdjumov-Sachs orientation relationship was found within an accuracy of 1°. The habit plane poles belonging to the observed orientation relationship relative to the bcc structure are shown in the lower half of Fig. 8. For example the black dot indicated by an arrow represents the three mutations P', Q' and R' in Fig. 7. The mean habit plane pole relative to the bcc structure (MHPP$_\alpha$) is irrational but close to (2 7 10)$_\alpha$. Now, an ultimate check can be made concerning the question whether the correlation between MHPP$_\gamma$ and MHPP$_\alpha$ results in a Kurdjumov-Sachs orientation relationship. As can be seen from Fig. 9, where all 24 permutations of MHPP$_\gamma$ are plotted in an exact Kurdjumov-Sachs orientation relationship, such a correlation is only given by permutation number 14, because 14$_\alpha$ is very close to MHPP$_\alpha$ and (2 7 10)$_\alpha$, as shown in Fig. 8. From these experiments it can be concluded that the observed orientation relationship is stable within an accuracy of 1°, in contradistinction to the total spread in all measured habit plane poles which is much more than the accuracy of measurement of 0.5°, and this means a discrepancy between the experiments and the I.P.S. theory.

References

[1] M.S. Wechsler, D.S. Liebermann and T.A. Read, Trans. A.I.M.E. 197 (1953), 1503.
[2] J.S. Bowles and J.K. MacKenzie, Acta Metall. 2 (1954), 129.
[3] J.K. MacKenzie and J.S. Bowles, Acta Metall. 2 (1954), 138.
[4] J.W. Christian, The Theory of Transformations in Metals and Alloys, Pergamon Press, Oxford (1965).
[5] J.S. Bowles and N.F. Kennon, J. Aust. Inst. Metals, 5 (1960), 106.
[6] J. Beyer, Proc. 2nd Int. Conf. Mechanical Behaviour of Materials, p. 1687, Boston, Mass. (16-20 August, 1976).
[7] S. Hoekstra, R.K. Ohm and C.A. Verbraak, Acta Metall. 26 (1978), 1505.
[8] S. Hoekstra, H.M.M. van der Lelie and C.A. Verbraak, Acta Metall. 26 (1978), 1517.
[9] S. Hoekstra, J.W.H.G. Slakhorst and J. Huber, Acta Metall. 25 (1977), 395.
[10] F.J. Schoen, J.L. Nilles and W.S. Owen, Metall. Trans. 2 (1971), 2489.

On Minimization of Elastic Energy and Crystallography of Martensite Transformations

A.L. Roitburd

The major results of thermodynamic analysis of martensite structures are compared with some of the conclusions of recent works based on the minimization of elastic energy of an ellipsoidal inclusion.

1. Introduction

A great deal of literature has appeared in recent years [1-5] concerning the morphological and structural characteristics of martenistic transformation as determined through the minimization of the elastic energy of internal stresses arising during the transformation. These studies are based on the solution the elastic energy problem for an ellipsoidal inclusions, achieved by Eshelby [6], and on its generalization to the elastic anisotropic medium [7]. The problem of martensitic structure as described in these references lies in finding such orientations for an ellipsoidal inclusion at a given axial ratio so as to obtain a minimum elastic energy, secondary deformations in the martensitic phase also being varied and found. In a more general case the contribution of the secondary deformation to the elastic energy is taken account in [4], where the arbitrary periodic distribution of the secondary deformation in the martensite is considered. It follows from [4, 5] that the variable secondary deformation inside the inclusion brings about a substantial increase of its volume elastic energy, which comprises $\approx 10^5$ cal/mol for Fe - 31% Ni alloys (per unit volume of martensite phase). This estimate however leaves some doubt. In order to clarify its sense as well as to discuss some other conclusions of the above-mentioned theoretical works [1-5] it seems more reasonable to compare them with the conclusions made on the thermodynamic theory of heterophase structures in which the equilibrium structure - the size of the phase components, their shape, orientation, mutual arrangement and structure were found as a result of minimization of free energy [8-14].

2. Plane-Parallel Plates - the Equilibrium Form of Structure Components in Martensitic Transformation

The variational problems of equilibrium form, orientation and secondary deformation of a martensite crystal formulated in [8]. It was assumed that the shape of a crys-

Central Scientific Research Institute of Ferrous Metallurgy, Moscow

tal in matrix was an elliptic cylinder. The free energy made up of the interphase surface energy and the elastic energy depending on the secondary deformation, has been minimized. It was shown that the equilibrium structural characteristics of martensite crystal depend on its sizes. At large sizes the equilibrium shape crystal is plate parallel to a definite crystallographic plane. In the case when the combination of the lattice and secondary deformations allows achieving an invariant plane (IP) macrodeformation, the plate is oriented along this plane, the macrostresses therein being absent and the elastic energy being equal to zero. Thus the conclusion was made about the identity of the principle of minimum elastic energy with the fundamental statement of the phenomenological theory of the crystallography of martensitic transformations (IP - theory). At the same time it was shown that the plate-like shape of the inclusion is responsible for the minimum energy, even if the intrinsic deformation differs from IP-deformation.

The shortcoming of analysis in [8] as well as in the investigations postulating the ellipsoidal form of inclusions [1-5] is that the martensite crystal "is referred to as" a definite kind of form. A more strict approach should be tried to find an equilibrium form by minimizing the energy of a crystal of an arbitrary form in the course of its arbitrary variation. The elastic energy minimum corresponds to zero of the local configuration force on each interphase boundary element [11-16]:

$$f = \Delta\mu - \sigma_{ik}\,\Delta\,\varepsilon^{\circ}_{ik} \qquad (1)$$

where $\Delta\mu$ and $\Delta\,\varepsilon^{\circ}_{ik}$ are the differences of free energies and intrinsic deformations across a boundary at site under consideration, σ_{ik} is the stress acting upon the site minus the field of the boundary element itself and equal to the half-sum of the stresses across the boundary.

Since σ_{ik} is created by all the interphase boundaries being the sources of the internal stresses, it depends on the boundaries configuration. Therefore (1) is an equation determining the boundary configuration. The analysis of this equation supports the conclusion that with a fine degree of approximation one can consider that the equilibrium inclusion form is a special oriented plane-parallel plate. The hierarchy of the plate-like formations makes up the typical equilibrium heterophase structures [14]. This essentially simplifies the mathematical aspect of the problem since for the plate-like structures the elastic field and energy can be found from the solving one-dimensional problems [12]. For the metastable and stable structures together with the equality of the configuration force (1), it is necessary to fulfil zero-equality of its moment.

This gives in addition to (1) the following equation:

$$\partial e(\vec{n})/\partial n_i = 0 \qquad e(\vec{n}) = \frac{1}{2}\Delta\varepsilon^{o}_{ij} G^{*}_{ijk\ell}(\vec{n})\Delta\varepsilon^{o}_{k\ell} \tag{2}$$

where $e(\vec{n})$ is the elastic energy of stress field of boundary itself, $G^{*}_{ijk\ell}(\vec{n})$ is the effective elastic module depending on orientation [12-14]. The set of equations (1) and (2) determines the interphase boundary orientations and the relative volume of the phase components responding to the the elastic energy minimum. Taking into account the surface energy of the interphase boundaries it is possible to determine the size of different structure elements.

3. Plate Substructure: Secondary Deformation as a Result of Elastic Domains Formation

Since the time Greninger and Troiano [17] stated the fundamental fact that martensite plate macrodeformation does not coincide with the deformation of the lattice but distinguishes from it by some secondary shear, studying the secondary deformation is the major directions of investigation of the martensite substructure. It is often interpreted as some plastic deformation whose combination with lattice deformation leads to an IP-deformation. Yet the physical sense of the secondary deformation remains obscure, and it is assumed that it may be any kind of invariant lattice deformation. Nevertheless, the presentation of a more justified treatment of the problem from the physical point of view is the one referring to the first work of Read et al [18-19] where the macrodeformation is regarded as the result of combining different lattice deformations in alternating martensite phase regions. Further development of this approach leads to viewing the martensite plate as a polydomain aggregate constituting of elastic domains. As in the case of magnetic domains the breaking-down into domains is a result of the tendency toward decreasing the long-range fields [9]. In case one phase only arises during transformation, the intrinsic deformations in the neighbouring domains related by twin or translation operations differ by an IP-deformation, and no stresses arise at interdomain boundaries. If the domains combination leads to an average over plate IP-macrodeformation, the macrostress and elastic energy is absent, provided the habitus plate face coincides with the invariant plane. It is this case, that the IP - theory considers.

The additional energy involving the formation of domains is made up of energy of microdistortion on the interphase surface of the polydomain plates and energy of the interdomain boundaries. In per unit volume of martensite it is equal to an order of magnitude

$$\Delta E/V \approx \gamma\varepsilon_{o}/b + \Gamma_{d}/H \tag{3}$$

in case when the stacking faults are the domains boundaries. Here, γ is the stacking fault energy, b - the interatomic distance, H - the plate thickness, ε_o - the intrinsic lattice deformation, $\Gamma_d \approx G\varepsilon_o b$ - the microdistortion energy due to the partial dislocations on the plate surface. In the case of twin domains we have

$$\Delta E/V \approx J/H^{1/2}, \quad J=(\gamma_{tw} e_r)^{1/2} \tag{4}$$

where $e_r \approx G\varepsilon_o^2$, γ_{tw} is the coherent twin boundary energy. The estimation for fcc → bcc transformations in Fe alloys shows that even for $H \approx 10^4 b$ responsible for the midrib thickness, $\Delta E/V$ is much less than 10^5 kal/mol given in [4, 5]. Most likely the periodic secondary deformation considered in [4, 5] is less advantageous from the energy viewpoint than breaking-down into domains and must not be realized.

If the elastic domain conception solves the problem regarding the thermodynamic causes of the secondary deformation, the problem concerning its mechanism and feasible modes still remains obscure. At any rate it may be stated that only special kinds of invariant lattice deformation can serve as a secondary deformation and that the development of a secondary deformation need not necessarily involve the overcoming of the barrier typical peculiar to plastic deformation to secure the generation and movement of dislocations. Attention should be focussed on another important aspect of secondary deformations: the polydomain region can be macroscopically regarded as a homogeneous phase with an additional internal parameter - domain composition [20]. The existence of several secondary deformation modes results in different martensitic phases distinguishing themselves by the number and type of interdomain boundaries and correspondingly by their properties. The number of "phases" increases still more in the external field [20-21]. In this case the equilibrium domain composition is determined by the stress value and the orientation of the interfaces relative to the external fields. Therefore the plates representing the equivalent orientational variant in the absence of the field require different substructures and assume physically different features. The comparison of energies of different substructures allows designing the equilibrium diagram of structure states [22], whereby the external parameters determining the substructure are the sizes of the martensite plates as well as temperature and stresses.

The synthesis of the IP-theory and thermodynamic analysis appears to be very perspective in making a quantitative description of the morphology and substructure of the plates. In the framework of the thermodynamic theory the characteristics corresponding to a small deviation from the unstres-

sed state can be determined with a precision of no less than that of an experimental determination. The choice from the point of reference of deformations of such a state with the interfaces lying along the invariant planes [23] instead of the unstrain original phase allows one to substantially lessen the inaccuracy of the calculations carried out with the linear elasticity theory. Thus it is possible for instance to calculate rather precisely the changes in the structure and the internal stresses arising in the course of the martensitic transformation under external stress. The calculation results for the Fe - 30% Ni alloy [24] are in good agreement with the data of the electron microscopic study of the influence of the uniaxial load on the habitus orientation of the martensite plates [25].

Everything referring to the substructure of the martensitic phases as well as to the polydomain formations can also be related to product of other phase transformations in solids, vis. ordering, decomposition of solid solutions, formation of antiferromagnetic and antiferroelectric. This allows one to regard the martensitic transformation as a typical solid-state transformation [26].

References

1. M. Shibata, K. Ono, Acta Met., 23 (1975) 587, 25 (1977), 35.
2. D.R. Clarke, Met. Trans., 7A (1976), 723.
3. K.E. Easterling, R. Tholen, Acta Met. 24 (1976), 333.
4. T. Mura, I. Mori, M. Kato, J. Mech. Phys. Sol., 24 (1976), 305.
5. M. Kato, T. Miyazaki, V. Sunago, Scr. Met., 11 (1977), 915.
6. J.D. Eshelby, Progress in Sol. Mech., V. 2, p. 116, Nort-Hol (1961).
7. N. Kinoshita, T. Mura, Phys. Stat. Sol., a5 (1971), 759.
8. A.L. Roitburd, VIII Int. Crystallogr. Congr. Thesis, p. 231, ANSSSR, Moscow 1966, Krystallografy, 12 (1967), 567 (Sov. Phys. - Crystall., 12 (1967), 499).
9. A.L. Roitburd, Fiz. Tverd. Tela, 10 (1968), 3619 (Sov. Phys. - Solid State, 10 (1969), 2870).
10. A.L. Roitburd, Fiz. Tverd. Tela, 11 (1969), 1465 (Sov. Phys/ - Solid State, 11 (1969), 1191).
11. A.L. Roitburd, Dokladi ANSSSR, 197 (1971), 1051 (Sov. Phys. - Doklady, 16 (1971), 305).
12. A.L. Roitburd, Phys. Stat. Sol., a16 (1973), 329.
13. A.L. Roitburd, in "Nesoversh. Kristal. Stroen. i Mart. Prevrashch." ("Crystal Imperfection and Martensitic Transformations"), p. 7, Nauka, Moscow, 1972.
14. A.L. Roitburd, Usp. Fiz. Nauk, 113 (1974), 69 (Sov. Phys. - Uspehi, 17 (1974), 326).
15. J.J. Gitomirskiy, P.P. Nechiporenko, Fiz. Tverd. Tela, 19 (1977), 859.
16. S.D. Gavazza, Scr. Met., 11 (1977), 979.
17. A.B. Greninger, A.R. Troiano, Trans. AIME, 185 (1949), 590.

18. M.V. Burkart, T.A. Read, Trans. AIME, 197 (1953), 1516.
19. M.S. Wechsler, D.S. Lieberman, T.A. Read, Trans. AIME, 197 (1953), 1503.
20. A.L. Roitburd, Fiz. Tverd. Tela, 19 (1977), 2879.
21. N.S. Kosenko, A.L. Roitburd, L.G. Khandros, Fiz. Metallov i Metalloved, 44 (1977), 956.
22. A.L. Roitburd, Phys. Stat. Sol., a40 (1977), 333.
23. A.L. Roitburd, N.S. Kosenko, Ser. Met., 11 (1977), 1039.
24. N.S. Kosenko, A.L. Roitburd, Ukr. Fiz. J., 23 (1978), 490.
25. M.N. Pankova, L.M. Utevskiy, Dokladi ANSSSR, 236 (1977), 1353; G.V. Kurdjumov, L.M. Utevskiy, R.I. Entin, "Prevrashch. v stali geleze ("Transformations in ferrum and steel"), Nauka, Moscow, 1977.
26. A.L. Roitburd, Solid State Physics, 33 (1978), 317.

Computer Simulation of the Martensite Transformation In a Model Two-Dimensional Body

by

Sheree Chen,* A. G. Khachaturyan,** and J. W. Morris, Jr.*

Abstract

An analytical model of a martensitic transformation in an idealized body is constructed and used to carry out a computer simulation of the transformation in a pseudo-two-dimensional crystal. The reaction is assumed to proceed through the sequential transformation of elementary volumes (elementary martensitic particles, EMP) via the Bain strain. The elastic interaction between these volumes is computed and the transformation path chosen so as to minimize the total free energy. The model transformation shows interesting qualitative correspondencies with the known features of martensitic transformations in typical solids.

I. Introduction

It is widely recognized that many of the most interesting and least understood features of martensitic transformations reflect the need to accommodate the substantial internal elastic strains which develop as the transformation proceeds. Theoretical studies of the heterogeneous nucleation of martensite[1,2] have focused on the identification of crystal defects or distributions of defects whose strain fields may serve to relieve the large strain energy associated with a single-variant martensite nucleus. The more successful theories of the internal structure, shape, and habit of fresh martensite are crystallographic models[3,4] which are predicated on the assumption that the preferred martensite substructure, shape, and habit is that combination which most nearly insures a net invariant plane strain, the internal strain state which minimizes the elastic energy.[5] Elastic effects are also believed to participate in the continuation of the transformation through the autocatalytic nucleation of sequential martensite plates, to influence the thermal characteristics of the transformation, and to affect the retention of high-temperature phase in "fully-transformed" product.

Given the prominence of elastic effects in the nucleation, growth, and morphology of martensite, tractable analytic models of the transformation which include elastic interactions should prove particularly fruitful in new theoretical insight. One such model has been under development by the authors for some time, and has recently been used to carry out computer simulation studies of martensitic transformations in simple sys-

*Department of Materials, Science and Mineral Engineering, and Materials and Molecular Research Division, Lawrence Berkeley Laboratory, University of California, Berkeley

**On leave from the Institute of Crystallography, Academy of Sciences of the USSR, Moscow 11733

stems.[6] This model is briefly described and an example of its initial results presented in the following.

II. Model of the Martensite Transformation

The linear theory of elastic inclusions in anisotropic media, as developed by Khachaturyan[7], permits the straightforward computation of the elastic energy associated with an arbitrary distribution of inclusions under the assumption that the elastic constants are uniform. The relevant equations can be written so that the elastic energy is the sum of the self-energies of the inclusions plus a simple sum of binary interactions between them. The real-space form of the elastic potential which determines the binary interactions can be easily calculated. Moreover, the formulation insures a simple kinematics for a process involving the appearance of elastic inclusions since in a linear model a macroscopic inclusion may be regarded as the direct sum of elementary inclusions which make it up.

To construct a model of the martensite transformation based on the theory of elastic inclusions we refer the crystal to a superlattice whose Wigner-Seitz cells define elementary volumes which transform. Following the FCC→BCC transformation the parent lattice is assumed cubic and the Bain strain is taken to be tetragonal. In dyadic form

$$\underset{\sim}{\varepsilon}^{\circ}=\varepsilon^{\circ}_{11}(\underset{\sim}{e}_1\underset{\sim}{e}_1+\underset{\sim}{e}_2\underset{\sim}{e}_2)+\varepsilon^{\circ}_{33}\,\underset{\sim}{e}_3\underset{\sim}{e}_3 \tag{1}$$

where the $\underset{\sim}{e}_i$ are unit victors along the cubic axes. A given tetragonal strain, specified by the values of ε_{11} and ε_{33}, yields three distinct variants of the elementary martensite particle which differ only in the selection of the tetragonal axis, $\underset{\sim}{e}_3$, from among the three cubic axes.

The distribution of EMP over the superlattice is described by the distribution functions $\zeta_p(\underset{\sim}{R})$ (p=1,2,3), which take the value one if there is an EMP of type p at $\underset{\sim}{R}$ and are zero otherwise. A configuration (α) of the body is defined by making a particular choice of the three $\zeta_p(\underset{\sim}{R})$. A configuration, α, may evolve to the immediately succeeding configuration, α+1, by adding an EMP of type p at any site $\underset{\sim}{R}$ which is unoccupied, or by deleting an EMP from any occupied site. The free energy change on either modification is (neglecting a chemical contribution to the surface energy) governed by the thermoelastic potential:

$$\phi^{\alpha}_p(\underset{\sim}{R})=N_o\Delta\mu+\Delta\phi^{\alpha}_p(\underset{\sim}{R}) \tag{2}$$

where $\Delta\mu$ is the chemical free energy change per atom, N_o is the number of atoms in an EMP, and $\Delta\phi^{\alpha}_p(\underset{\sim}{R})$ is the change in elastic energy

$$\Delta\phi^{\alpha}_p(\underset{\sim}{R})=\phi^{o}_p+\sum_q\sum_{\underset{\sim}{R}'}\omega_{pq}(\underset{\sim}{R}-\underset{\sim}{R}')\,\zeta_q(\underset{\sim}{R}') \tag{3}$$

The evaluation of the elastic self-energy ϕ^{o}_p and the binary potential $\omega_{pq}(\underset{\sim}{R})$ in terms of fundamental quantities is straightforward and is given in reference (6). If an EMP of type p at $\underset{\sim}{R}$ is eliminated the associated free energy change is $-\phi^{\alpha}_p(\underset{\sim}{R})$.

Given a configuration, α, the values of the thermoelastic potentials for the possible elementary changes in α, and the value of any inherent activation barrier, the mean and variance of the time required for the evolution of α through a thermally-activated process may be computed, and the particular elementary event causing the evolution of α may be chosen statistically. By iterating this procedure the kinetics and the "path" of the model transformation (i.e., the sequence of successive configurations) may be found. It is, in fact, only necessary to use computer simulation to determine the transformation path; the kinetics of transformation may be computed exactly once the path is known.[6]

If the martensite transformation is thermally activated the transformation will follow a path determined by a biased random walk over the space of possible configurations. Particularly if there are metastable intermediate configurations the transformation path will be complex and very difficult to analyze. A relatively simple and useful representative path may be defined by requiring that each net forward step be chosen so as to minimize the free energy. Choosing this "minimum energy" transformation path, neglecting any inherent activation barrier to the appearance of an EMP, and making a first-order-correction for the "correlation effect" due to the reversibility of the transformation we obtain the equation

$$<t_\alpha> \simeq (\frac{1}{\nu})[1+\exp(\beta\phi_\alpha)][1+\exp(\beta(\phi_\alpha+\phi_{\alpha+1}))] \qquad (4)$$

for the time required to accomplish the $\alpha^{\underline{th}}$ transformation step, where ν is a frequency of the order of the Debye frequency, $\beta=(kT)^{-1}$, and ϕ_α is the least of the thermoelastic potentials $\phi_p^\alpha(\underset{\sim}{R})$ for the addition of EMP to the $\alpha^{\underline{th}}$ configuration. If ϕ_α remains positive, $<t_\alpha>$ increases without bound as T approaches zero and the transformation eventually becomes athermal.

The quantitative plausibility of equation (4) was checked by comparing its predictions for the nucleation of martensite to the experimental results of Pati and Cohen[8], who studied thermally-activated nucleation of martensite in Fe-Ni-Mn alloys and found an effective activation energy

$$\Delta G^* = 72.8\Delta\mu + 2.95\times10^{-12} \text{ ergs/event} \qquad (5)$$

where $\Delta\mu$ has units ergs/atom. Assuming an EMP with $\sim$24 atoms, using the elastic constants and transformation strain for the similar case of Fe-31 Ni as reported by Wayman[9], and assuming a heterogeneous nucleation site having the effective strain field of an elementary martensite particle, equation (4) predicts that the formation of the first EMP (the nucleation step), will be governed by an Arrhenius equation with an effective activation energy

$$\Delta G^* = 72\Delta\mu + 2.74\times10^{-12} \text{ ergs/event} \qquad (6)$$

in reasonable quantitative argument with the Pati-Cohen result.

III. Example of a Transformation in Two Dimensions

To define a simple transformation case for computer simulation let the solid be a psuedo-two-dimensional body (in the sense that its elementary particles are infinite rods perpendicular to the representation

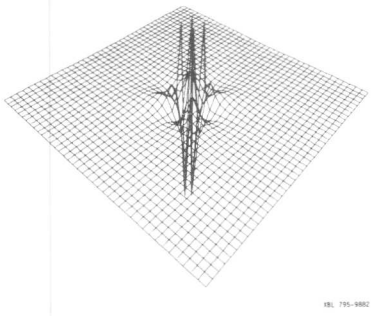

Fig. 1

plane), let the solid have isotropic elastic constants, and let the Bain strain be a simple shear involving an expansion along one of the axes of the two-dimensional grid and a compensating contracting along the other. In this case there are two variants of the elementary martensite particle which differ in orientation of the expansion axis. The elastic potential ($\omega_{pp}(\underset{\sim}{R})$) for the interaction of like particles is shown in Figure 1. By symmetry the interaction potential ($\omega_{pq}(\underset{\sim}{R})$) for unlike particles is the negative of the potential shown. The chemical driving force ($\Delta\mu$) is assumed to be a linear function of the undercooling (ΔT).

Since the martensite transformation is known to be heterogeneously nucleated we simulate the transformation of a defective lattice. For simplicity the pre-existing defects are taken to be a random distribution of elementary martensite particles. In the particular case illustrated here ten such particles are randomly distributed over a 40x40 grid. We further assume that the transformation follows the "minimum energy path", and that the transformation can proceed only if the associated free energy change is negative, as follows naturally if the elementary martensite particle is very large or if the temperature at which the transformation occurs is very low.

Under the assumptions listed the martensitic transformation is athermal, and occurs progressively on continuous cooling. The variation of the fraction of martensite with undercooling, measured in energy units, is illustrated in Figure 2. The transformation is seen to initiate at an undercooling of approximately 0.09, and to reach completion at an undercooling of approximately 0.6. For comparison, the undercooling required to homogeneously nucleate the martensite phase in this case is 0.6447.

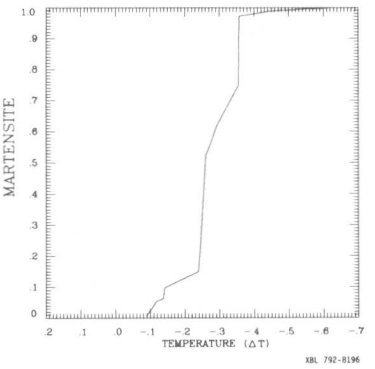

Fig. 2

The nucleation of the martensite transformation is illustrated in Figure 3. The transformation nucleates as a two layer twinned plate, and grows along the (11) habit plane until it nearly closes on itself, as shown in Figure 4. However, before closing on itself the growing plate encounters the strain fields of other pre-existing defects, which causes the transformation to stop, to be resumed after further undercooling. This phenomenon illustrates the dual role of pre-existing defects. The strain fields of these defects promote the nucleation of martensite but interfere with its growth.

Microstructures: (□)=Austenite, (-)= X-Martensite, (ˈ)=y-Martensite

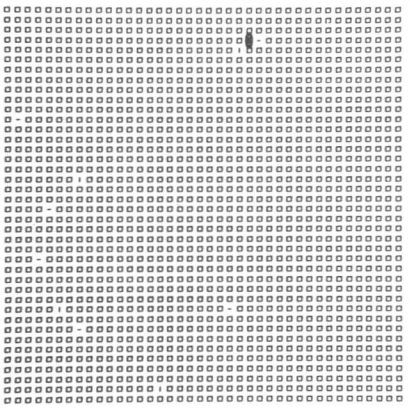

Fig. 3

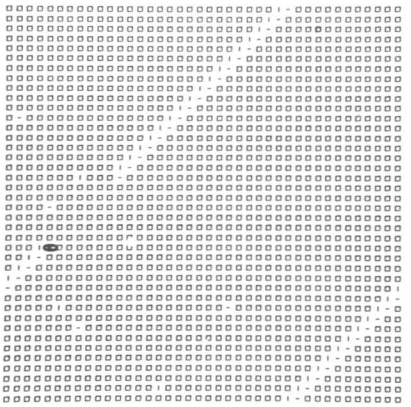

Fig. 4

The transformation develops further on decreasing temperature. Additional plates nucleate and grow, and may be oriented either parallel to or perpendicular to the original martensite plate. These autocatalytically nucleated plates sometimes initiate from pre-existing defects, and are sometimes homogeneously nucleated in defect-free regions of the lattice. Interestingly, the parallel martensite plates often form in an aggregate twin orientation to one another with a layer of retained austenite in the intervening space. An intermediate stage in the transformation illustrating some of these features is shown in Figure 5. As the transformation nears completion, only a small residue of isolated austenite particles is retained. This residue of austenite is extremely stable, and a large undercooling is required to eliminate it and bring the transformation to completion.

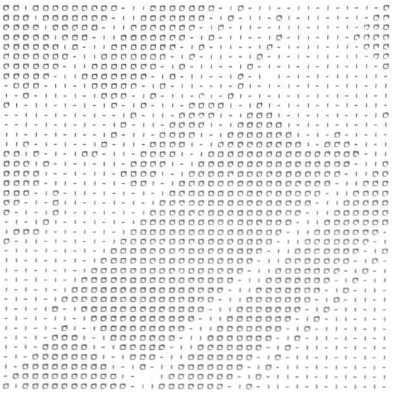

Fig. 5

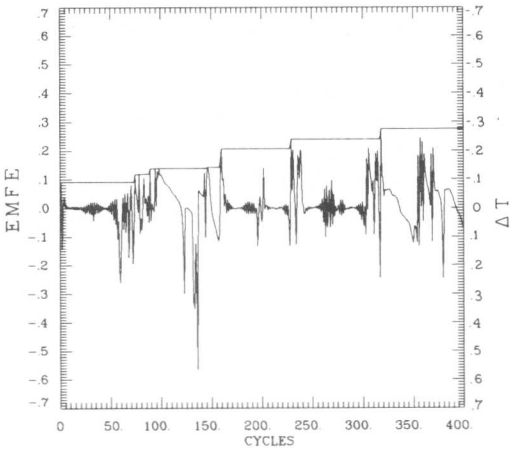

Fig. 6

The energetics of the transformation are illustrated in Figure 6, which shows the magnitude of the chemical driving force as a horizontal line, and the magnitude of the elastic energy per step as an oscillating function for the first 400 transformation steps. The elastic energy is a noisy function which oscillates about the value zero. The transformation is stopped by occasional, large excursions from the value zero which exceed the chemical driving force. These excursions identify the nucleation steps along the transformation path. They are responsible for the progression of the martensite transformation through a sequence of transformation bursts as the temperature is lowered, and

the chemical driving force raised.

V. Conclusion

A model of the martensitic transformation in a simple system has been developed which allows the transformation to occur through the sequential appearance of elementary volumes of martensite in the parent matrix and accounts for the energetic contribution of the elastic interaction between these elementary volumes. The model has been used for the computer simulation of a martensitic transformation in two dimensions. Despite the simplicity of the model the features observed in the simulated transformation are encouragingly real. The initial martensite phase is heterogeneously nucleated and grows as a twinned plate along a definite habit plane. The overall transformation occurs through a series of bursts which are sequentially triggered as the temperature is lowered. These bursts involve the autocatalytic nucleation and growth of martensite plates which may parallel or branch with respect to the original plate. Bands of retained austenite are occasionally observed between parallel plates which are in an aggregate twin-orientation to one another. Residual austenite is retained to a very late stage in the transformation, and is elastically stabilized to the extent that very large undercoolings are required to eliminate it.

Acknowledgment

This work was supported by the Division of Materials Sciences, Office of Basic Energy Sciences, U. S. Department of Energy under Contract No. W-7405-Eng-48.

References

[1] K. E. Easterling and A. R. Thölén: Acta Met. 24, 333 (1976).
[2] G. B. Olson and M. Cohen: Met. Trans. A, 17A, 1897 (1976).
[3] J. S. Bowles and J. K. Mackenzie: Acta Met., 2, 129 (1954); 2, 138 (1954); 2, 224 (1954); 5, 137 (1957) 10, 625 (1962).
[4] D. S. Lieberman, M. S. Wechsler and T. A. Read: J. Apply. Phys., 26, 473 (1955).
[5] A. G. Khachaturyan and G. A. Shatalov: Sov. Phys- JETP, 29, 557 (1969).
[6] Sheree Chen: PhD. Thesis, U. C. Berkeley (1979).
[7] A. G. Khachaturyan: Soviet Phys.-Solid State, 4, 2081 (1963); 7, 2040 (1968); 9, 2249 (1968); 13, 2024 (1972).
[8] S. R. Pati, and M. Cohen, Acta Met. 17, 189 (1966).
[9] J. E. Breedis, and C. M. Wayman: Trans. AIME 224, 1128 (1962).

Theory of Martensitic Transformations

S. Mendelson

This paper reports on a crystallographic theory for martensite formation by multiple lattice-variant shears. The transformations are accomplished by (i) a primary shear which transforms the Bravis lattice, (ii) a habit plane shear which accomodates the volume change, and (iii) one or more secondary shears in the intermediate martensite. The transformations are represented by vector and matrix algebra in terms of lattice parameters, orientation relationships, shear strains and shear planes. The theory is applied to the $(3,\bar{1}\bar{5},10)_f$ habit plane in the fcc→bcc (bct) transformation in ferrous alloys where (i) and (ii) are sufficient to complete the transformation. The primary shear has degenerate stress-sense and periodically alternates its direction to satisfy the "minimum long range stress field criterion", with the result that the product is twinned on the $(112)_b$ plane. The orientation relationship corresponds to that of Greninger and Troiano and the habit plane is 1.5° from $(3,\bar{1}\bar{5},10)_f$ for Fe-C alloys and 1° from $(1\bar{4}3)_f$ for the Fe-29.5%Ni alloy.

I. Introduction

The martensitic transformation is a coordinated response of an unstable lattice under conditions which deny it the option of transforming by uncoordinated atomic diffusion. Since lattice parameters are changed and a new structure created a successful theory must include mechanisms to accomplish this. Early geometric models [1-6] attempted to do this by low index lattice-variant shears; in each case the shears occur with one of the three principle strains being zero, one positive, and one negative, satisfying the condition for an invariant plane strain. Although the models had some success this approach was abandoned when it failed to predict the more prominent habit planes in various alloys.

The Bain distortion represents the most obvious lattice correspondence between the two phases and the phenomenological theories [7-10] were designed to accomplish it, but since all three of its principle strains are non zero, it cannot be accomplished with an invariant plane strain by a simple deformation. The theory overcomes this difficulty to satisfy the invariant plane strain condition over macroscopic (but not microscopic) dimensions in the interface by combining the Bain strain with a lattice-invariant strain (slip or twinning). Since this gives the correct shape deformation, habit plane , and orientation relationship for certain data the theories have had wide support. Because the theories are phenomenological the manner in which the Bain distortion is accomplished is not addressed; it is assumed to occur instantaneously in the interface as the lattice-invariant strain extends into the austenite. A consequence of this is a large activated volume for the Bain strain and no insights into the problem of nucleation. The theory does not include habit planes in the regions of $\{225\}_f$ and $\{111\}_f$, and the wide scatter around $\{3,\bar{1}\bar{5},10\}_f$ requires the inclusion of an adjustable dilatation parameter.

The City University of New York, New York, New York 10001, USA.

In the present theory the transformations are accomplished by two or more lattice-variant shears which transform the structure and lattice parameters. Each shear is an invariant plane strain with one positive, one negative, and one zero principle strain. The lattice-variant shears include (i) a primary shear which has degenerate stress-sense and transforms the Bravis lattice, (ii) a habit plane shear which accomodates the volume change, and (iii) one or more smaller secondary shears may occur on twin systems in the intermediate martensite product. Both the primary and secondary shears periodically alternate their direction to satisfy the "minimum long range stress field criterion", with the result that the product is twinned, faulted, or has a long period stacking order structure.

II. Mathematical Representations

The transformation shear is accomplished by transformation dislocations on the κ_1 shear plane in the $\vec{\eta}_1$ shear direction. The atomic displacements are represented by the Burgers vector $\vec{b}_s$ along $\vec{\eta}_1$ (shear strain $S_s=b_s/nd$), and the volume change displacement vector $\vec{b}_n$ along $\vec{\kappa}_1$ ($\vec{\kappa}_1$ strain $S_n=b_n/nd$); These are defined by the components of low index lattice translations, $\vec{t}$ vectors, which lie in the S_m plane of shear. $\vec{b}_s$ is the component of $\vec{t}_f-\vec{t}_b$ resolved parallel to $\vec{\eta}_1$, and $\vec{b}_n$ the component resolved parallel to $\vec{\kappa}_1$; these are given by:

$$\vec{b}_s = [(\vec{t}_f\cdot\vec{\eta}_{1f})/\eta_{1f}^2]\vec{\eta}_{1f} - [(\vec{t}_b\cdot\vec{\eta}_{1b})/\eta_{1b}^2]\vec{\eta}_{1b} \qquad (1)$$

$$\vec{b}_n = [(\vec{t}_b\cdot\vec{\kappa}_{1b})/\kappa_{1b}^2]\vec{\kappa}_{1b} - [(\vec{t}_f\cdot\vec{\kappa}_{1f})/\kappa_{1f}^2]\vec{\kappa}_{1f} \qquad (2)$$

where the subscripts f and b refer to fcc and bcc respectively, but could represent any two strucutres. The transformation equations in martx form are given by

$$(hkl)_f=({}_fA_b)(hkl)_b, \quad [uvw]_f=[{}_fS_b][uvw]_b, \quad [{}_fS_b]=({}_fA_b^{-1})^t \qquad (3)$$

The A matrices are for planes and the S matrices for directions. The matrices are evaluated by the simultaneous solution of three non-coplanar vector equations, represented by

$$\vec{\eta}_{1b}=\vec{\eta}_{1f}, \quad \vec{S}_{mb}=\vec{S}_{mf}, \quad \vec{t}_b=\vec{t}_f-\vec{b}_s+\vec{b}_n \qquad (4)$$

The matrices for multiple shear transformations are represented by

$$({}_fA_b) = ({}_fA_{bn})({}_{bn}A_{bn-1})({}_{bn-1}A_{bn-2}) \text{ --- } ({}_{b1}A_b) \qquad (5)$$

III. Transformation Theory For A Double Shear Transformation

The double shear transformation applies to $\{3,\bar{1}\bar{5},10\}_f$ habit planes in ferrous alloys and is accomplished by a primary shear which transforms the Bravis lattice, and a habit plane shear which accomodates the volume change to complete the transformation.

A. The Primary Shear

The primary shear has the following characteristics: (i) it has degenerate stress-sense, (ii) it results in a cell in which one cell edge,

$\vec{u}_3'=\vec{u}_3$, is completely transformed to its final dimension, (iii) $\vec{u}_3$ is orthogonal to $\vec{u}_1$ and $\vec{u}_2$ in both the intermediate and final martensite products. (iv) it periodically alternates its direction to satisfy the "minimum long range stress-field criterion" with the result that (v) the product is twinned, faulted, or has a long period stacking order structure on the primary shear system.

B. The habit plane Shear

The habit plane shear has the following characteristics: (i) it occurs with $\vec{S}_{m2}||\vec{u}_3$, (ii) it occurs along a direction represented by $\vec{\eta}_1=\rho\vec{u}_1+\sigma\vec{u}_2$, where ρ and σ are integers, (iii) it accomodates the volume change for the transformation by a small relaxation strain $S_n=b_n/nd$, normal to the κ_1 shear plane, and (iv) it transforms $\vec{u}_1$ and $\vec{u}_2$ to their final dimensions and angular relations to complete the transformation.

IV. The FCC→BCC(BCT) Transformation

A. Primary Shear

The primary shear for fcc→bcc(bct) occurs on the $(101)[10\bar{1}]_f$ system and is represented by:

$$\vec{\eta}_1=[10\bar{1}]_f=[11\bar{1}]_b,\quad \vec{S}_m=[010]_f=[\bar{1}10]_b,\text{ and }\quad [001]_f=[001]_b\pm C[\bar{1}\bar{1}1]_b \tag{6}$$

and

$$({}_fA_{b_1})=\begin{pmatrix}1\mp C & 1\mp C & \pm C\\ -1 & 1 & 0\\ \mp C & \mp C & 1\pm C\end{pmatrix},\quad ({}_{b_1}A_f)=\tfrac{1}{2}\begin{pmatrix}1\pm C & -1 & \mp C\\ 1\pm C & 1 & \mp C\\ \pm 2C & 0 & 2\mp 2C\end{pmatrix} \tag{7}$$

where $$C=b_s/\sqrt{2}a_f \tag{8}$$

The $\pm$ sign represents the degenerate stress-sese of the primary shear. The value of C depends on the lattice parameters and is determined by conditions (ii) and (iii) for the primary shear. With $\vec{u}_3=[u0w]_f$ it is satisfied when the following two equations are solved simultaneously.

$$\frac{u}{w}=\frac{[-2(1-2C)+(1+2C)(c_b/a_b)^2]}{2[2(C-C^2)-(C+C^2)(c_b/a_b)^2]} \pm \frac{\{[2(1-2C)-(1+2C)(c_b/a_b)^2]^2+4[2(C-C^2)-(C+C^2)(c_b/a_b)^2]\}^{1/2}}{2[2(C-C^2)-(C+C^2)(c_b/a_b)^2]} \tag{9}$$

$$C=\frac{[2u-w(c_b/a_b)^2]}{(u+w)[2+(c_b/a_b)^2]} \pm \frac{\{[w(c_b/a_b)^2-2u]^2-[2+(c_b/a_b)^2][2u^2+w^2(c_b/a_b)^2-(a_f/a_b)^2(u^2+w^2)]\}^{1/2}}{(u+w)[2+(c_b/a_b)^2]} \tag{10}$$

For the alloy Fe-0.908%C, $a_b/a_f=0.7945$, and $c_b/a_b=1.041$; this leads to $u/w=-59/20$, and $C=7/58$, and the transformation matrices for the primary shear are:

$$({}_fA_{b1})=\tfrac{1}{58}\begin{pmatrix} 51 & 51 & 7 \\ -58 & 58 & 0 \\ -7 & -7 & 65 \end{pmatrix}, \quad ({}_{b1}A_f)=\tfrac{1}{116}\begin{pmatrix} 65 & -58 & -7 \\ 65 & 58 & -7 \\ 14 & 0 & 102 \end{pmatrix} \tag{11}$$

This primary shear transformed the Bain cell to an intermediate product which is a distortion of the tetragonal martensite. The transformation is completed by the habit plane shear.

B. Habit Plane Shear

The three orthogonal cell dimensions for the habit plane shear, represented in the fcc basis, are $\vec{u}_1=[010]_f$, $\vec{S}_m=[u0w]_f$, and $\vec{u}_2=\vec{u}_1 x \vec{S}_m$. Taking $\vec{\eta}_1=\rho\vec{u}_1+\sigma\vec{u}_2$ we obtain

$$\vec{\eta}_1 = 2[580,1303\ 1711]_f=[\bar{1}\bar{9}\bar{9}\bar{9},3213,3975]_b \tag{12}$$

$$\kappa_1 = (2606,\bar{1}\bar{1}2549,76877)_f||(7683603,\bar{5}372081,8206294)_b \tag{13}$$

The shear strain is $S_s=b_s/nd=0.189$ along $\vec{\eta}_1$ and the volume change strain is $S_n=b_n/nd=0.0441$ along $\vec{\kappa}_1$. The three non-coplanar vector equations which represent the habit plane shear are:

$$\vec{\eta}_1 = [\bar{1}\bar{9}\bar{9}\bar{9},3213,3975]_b=2[580,1303,1711]_f \tag{14}$$

$$\vec{S}_m = [3149,3149,\bar{8}\bar{8}\bar{7}]_b=58[59,0,\bar{2}\bar{0}]_f \tag{15}$$

$$\vec{\kappa}_1 = [143\ \bar{1}\bar{0}\bar{0},141]_b=C[26060,\bar{1}\bar{1}2549,76877] \tag{16}$$

where $$C=(a_b/a_f)\{[30449+19881(c_b/a_b)^2]/19256474130\}^{1/2}=0.0013055 \tag{17}$$

and the final matrix is

$$({}_bA_f) = \tfrac{1}{6}\begin{pmatrix} 3.245035 & -3.412981 & -0.709089 \\ 3.44389 & 3.203515 & -0.119456 \\ 0.599143 & -0.448368 & 4.905235 \end{pmatrix} \tag{18}$$

This corresponds to:

$$\begin{aligned} \theta &= [11\bar{1}]_b \measuredangle [10\bar{1}]_f=2.8°, & \alpha_1 &= [010]_b \measuredangle [110]_f=1.9° \\ \phi &= (101) \measuredangle (1\bar{1}1)_f=0.21°, & \alpha_2 &= [10\bar{1}]_b \measuredangle [\bar{1}\bar{1}2]_f=1.9° \end{aligned} \tag{19}$$

This is between the K-S [1] and N [3] orientation relationships and is close to the Greninger-Troiano (G-T) [11] orientation relationship.

The habit planes for this and other ferrous alloys, Fe-1.765%C ($a_b/a_f=0.78319$, $c_b/a_b=1.080$) and Fe-29.5%Ni ($a_b/a_f=0.800$) are summarized in Table I.

TABLE I. Habit Planes For Ferrous Alloys

Alloy	η_1	κ_1	DEVIATION OF κ_1
Fe-0.908%C	$[1,2.25,2.95]_f$	$(3.39,\bar{1}\bar{4}.\bar{6}\bar{4},10)_f$	1.52° from $(3,\bar{1}\bar{5},10)_f$
Fe-1.765%C	$[1,2.67,3.51]_f$	$(2.85,\bar{1}\bar{4}.\bar{1}\bar{6},10)_f$	1.47° from $(3,\bar{1}\bar{5},10)_f$
Fe-29.5%Ni	$[1,2.75,3.28]_f$	$(1,\bar{4}.\bar{2}\bar{7},3.29)_f$	1.05° from $(1\bar{4}3)_f$

V. Discussion

The $(101)[10\bar{1}]_f$ primary shear system transforms to $(112)[11\bar{1}]_b$ and, since $(101)[10\bar{1}]_f$ has degenerate stress-sense, the product is twinned on $(112)_b$ when the primary shear periodically alternates its direction to satisfy the "minimum long range stress field criterion". Habit planes in the region of $\{225\}_f$ are accomplished by other multiple shears. In transformations of β alloys (bcc→orthorhombic) a three shear mechanism (primary shear, habit plane shear, and secondary shear) is found to apply. The primary shear system $(110)[\bar{1}10]_b$ has degenerate stress-sense, leading to the various reported long period stacking order structures when it periodically alternates its direction. The habit plane shear in AuCd results in the $\kappa_1 \simeq (13\bar{3})_b$ habit plane with the $\vec{\eta}_1 \simeq [133]_b$ shear direction. The secondary shear system $(02\bar{1})[0\bar{1}2]_o$ which completes the transformation is equivalent to $\{\bar{1}011\}\langle\bar{1}01\bar{2}\rangle_h$ in hcp, the reported twin system in β alloys.

The thickness of the twins and the period of the stacking order structures can be related to the short range stress field, as represented by the microscopic shear strain. This is consistent with the twin thickness and periods of stacking order structures in various alloys. The primary shear in ferrous and β alloys is large, leading to fine twins in ferrous alloys and a comparable period in β alloys, whereas the secondary shear in β alloys occurs on a twin system with a much smaller microscopic shear strain, and consequently relatively thick twins. Depending on how the primary shear periodically alternates its direction in β alloys the product can have any of the reported long period stacking order structures. The $(110)[\bar{1}10]_b$ system in bcc→fcc' (or hcp' or orthorhombic') is known to be soft [4], and since $(101)[10\bar{1}]_f$ in fcc→bct' has the same degenerate stress-sense and symmetry characteristics this primary shear is probably also soft, at least in a relative if not absolute sense.

Since the shears in the present theory are lattice-variant, and those in the phenomenological theories, lattice-invariant, the two theories cannot be compared directly. Nevertheless the fact that both theories account for similar data suggest that there are some features of the theories worthy of comparison. (i) Both theories transform the Bain cell; by lattice-variant shears in the present theory, and assumed to occur spontaneously in the phenomenological theory when the lattice-invariant shear extends the interface into the austenite. (ii) In both theories the $[001]_b$ tetragonal axis is derived from $[001]_f$ and (iii) the ordering of the carbon atoms along the c-axis predicted. (iv) The phenomenological theories include a lattice-invariant shear on $(112)[11\bar{1}]_b$, whereas the present theory requires a lattice-variant shear on the same

system. (v) Both theories result in a twinned product on the above system; by a lattice-invariant twinning shear in the phenomenological theories, and by a lattice-variant primary shear which periodically alternates its direction in the present theory. (vi) In each theory the two twinned regions have equivalent orientation relationships with the austensite lattice, although it is not clear how this is accomplished by the phenomenological theories, since the manner in which the Bain distortion is accomplished is not addressed, (vii) The microscopic shear strain for the twins in the phenomenological theory is that for deformation twinning, whereas in the present theory it is half this. (viii) The macroscopic shear strain for these twins is close to zero in the present theory, whereas it is a principal part of the total shape strain in the phenomenological theories. (ix) The total shape strain in the phenomenological theory is factorized into the Bain strain and the lattice-invariant strain, whereas in the present theory it is equal to that for the habit plane shear. (x) The activated volume for the Bain strain in the phenomenological theories is related to the region in the interface between slipped or twinned regions, whereas in the present theory it is the small region between K_1 shear planes. (xi) The phenomenological theories give no insights into the nucleation event, whereas the present theory does, and allows for the inclusion of soft modes, charge density waves, lattice instabilities and embryo formation by transformation dislocations.

Evaluations show that the low strain energy which leads to pseudoelasticity and SIM can be rationalized if the domains and their stress fields fluctuate, with a zero macroscopic strain, on different variants of the primary system at temperatures above M_s but below T_c; there is some evidence for this view. If each souce can fluctuate on more than one domain variant of the primary shear system a small strain energy will be effective when it changes the entropy of the fluctuating domains so that more than the mean distribution of them fluctuate on those variants with large Schmid factors. The net result is a non-zero macroscopic strain and consequently pseudoelasticity or SIM with a relative small strain energy.

In summary the present theory shows that lattice-variant shears account for the shape strains, magnitude and direction, the habit planes, the orientation relationships, and the internal structure without the need for lattice-invariant shears or phenomenological representations.

References

[1] G. Kurdjumow and G. Sachs, Z. Phys. 64, 325 (1930).
[2] W. G. Burgers, Physica 1, 561 (1934).
[3] Z. Nishyama, Sci Rep. Res. Inst. Tohoko Univ. 23, 537 (1934).
[4] C. Zener, Elasticity and Anelasticity of Metals, The University of Chicago Press, Chicago 1948).
[5] A. J. Bogers and W. G. Burgers, Acta Met. 12, 255 (1964).
[6] S. Mendelson, Scripta Met. 11, 375 (1977).
[7] M. S. Weschsler, D. S. Lieberman and T. A. Read, Trans. AIME 197, 1503 (1953); J. Appl. Phys. 26, 473 (1955).
[8] J. S. Bowles and J. K. Makenzie, Acta Met. 2, 129, 137 (1954)
[9] B. A. Bilby and J. W. Christian, The Mechanisms of Phase Transformations in Metals, Inst. Met. Monographs 18, 121 (1956).
[10] R Bullough and B. A. Bilby, Proc. Phys Soc. B69, 1276 (1956).
[11] A. B. Greninger and A. R. Troiano, Trans. AIME 185, 590 (1949).

Comparison of FCC-BCC and BCC-HCP-FCC Lattice Deformations

Francisco Eiichi Fujita

According to the generally accepted concept that the shear movement along $[11\bar{2}]_f/(111)_f$ of fcc lattice plays the main role in the lattice deformation in the martensite transformation of steels, cobalt and its alloys and, similarly, the $[10\bar{1}]_b/(101)_b$ shear movement of bcc lattice does so in the lattice transformation of zirconium, titanium and many other non-ferrous bcc alloys, a generalized picture of martensite transformation paths of metals and alloys is composed by connecting the concerned crystal structures with the units of shear movement well defined and with certain limited number. A simple mathematical treatment for various shear movements, which was proposed by the author in a previous paper, is extended to describe the lattice deformations in the generalized picture. Unified view points on the shear modes, intermediate structures, and pre-martensitic phenomena are given accordingly through ferrous and non-ferrous martensite transformations.

I. Introduction

Since Kurdjumov and Sachs'[1] and Nishiyama's[2] first models of lattice deformation in the martensite transformation of steel, it has been accepted that the shear movement along $[11\bar{2}]_f$ direction and $(111)_f$ plane of the fcc austenite lattice plays the main role in the lattice transformation. This main shear mode was enough convincing since it is along the closest packing direction and plane and can account for the lattice relations found by the above and other investigators [1,2,3] if accompanied by other additional shears and axial contractions and dilatations.

The role of the $[11\bar{2}]_f/(111)_f$ shear movement was not always confined within the problem of lattice transformation of steel. For instance, in the cases of martensite transformation of some Fe-Ni and stainless steels and cobalt and cobalt alloys in which fcc lattice transforms to hcp lattice, the same sort of shear movement was employed by Christian [4], in the form of motion of half dislocation on every second $(111)_f$ plane, to explain the lattice deformation mechanism. It was further utilized by Venables [5] and others [6,7,8] in the proposal that the fcc austenite lattice of steel would first transform to the hcp lattice by Christian's mechanism and then to the ultimate bcc martensite lattice by the alternate shears along $[11\bar{2}]_f/(111)_f$ or $[1\bar{1}00]_h/(0001)_h$, that is the shuffling, where subscripts, f and h, mean the fcc and hcp lattice respectively. It is also possible to reach from fcc to bcc even if the order of the above two processes is reversed. This idea was actually employed by the author [9] to interpret the appearance of the intermediate six layer structure of Fe-Mn-C steel martensite, which was found by Oshima and Wayman [10] by using electron diffraction and microscopy,

Department of Material Physics, Faculty of Engineering Science, Osaka University, Toyonaka, Osaka 560 Japan.

and to interpret the 1 : 1 occupancy of octahedral and tetrahedral interstices by carbon in steel martensite at low temperature, which was investigated by the author and others by Mössbauer spectroscopy[11 15] and neutron diffraction[16].

According to the above studies, the fcc-bcc martensite transformationlinks can be completed, as are shown in Fig. 1. All the concerned structures are linked by transformation paths consisting of various $[11\bar{2}]_f/(111)_f$ shear modes; for instance, the direct uniform shear of the fcc austenite lattice along $[11\bar{2}]_f/(111)_f$ by 19°28' together with some other deformations to reach the bcc (bct) martensite lattice, which was proposed by Kurdjumov and Sachs and Nishiyama as before mentioned, is expressed by $a/12\cdot[11\bar{2}]_f/(111)_f$, two step transformation mechanism from fcc to bcc through hcp by Venables and others is described by $a/6\cdot[11\bar{2}]_f/(111)_f$ half dislocation motion on every second plane and $a/12\cdot[11\bar{2}]_f/(111)_f$ shuffling (or $a''/6\cdot[1\bar{1}00]_h/(0001)_h$ in hexagonal notations), and the author's proposal of transformation through the intermediate six layer structure is by the $a/12\cdot[11\bar{2}]_f/(111)_f$ shuffling followed by the $a'/3\cdot[10\bar{1}]_b/(101)_b$ half dislocation motion on every second plane which are quite the same as Venables' two steps but in the reversed order. In these expressions, a, a', and a'' are lattice parameter of fcc, bcc, and hcp ;attice respectively and subscript b means the bcc lattice. It should be noted that the six layer structure experimentally determined is regarded as a stacking modification of the ultimate bcc lattice[17], and, therefrore, the half dislocation shear mode has to be figured out according to the bcc notations, a' and subscript b. By using Nishiyama's lattice relation, $(111)_f // (101)_b$, $[11\bar{2}]_f // [10\bar{1}]_b$, it is readily seen that the above two modes of half dislocation type shears are topologically correspondent with each other.

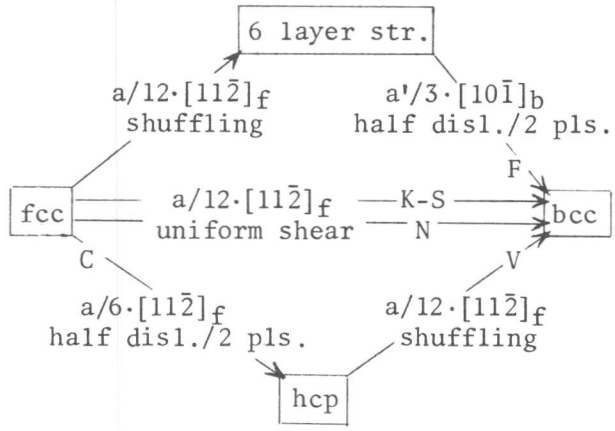

Fig. 1 fcc-bcc martensite transformation links

Further applications of the transformation links of Fig. 1 to martensite transformations other than that of steels seem to be possible. Many bcc metals and alloys, such as titanium, zirconium, Au-Cd, Cu-Al-Ni, and Cu-Zn-Al, are known to transform martensitically to the hcp or its modification structures of further to the fcc structure. Their transformations are mainly by the shear motion of $(101)_b$ palnes along the $[10\bar{1}]_b$ direction, which is again topologically equivalent to $[11\bar{2}]_f/(111)_f$ shear in fcc lattice.

In this paper, it is attempted bo complete a generalized picture of martensite transformation paths of various metals, including steels and non-ferrous alloys, by connecting the concerned crystal structures and their observed modifications with links of mathematically and crystallographically defined shear modes. The purpose of the composition of the transformation links is to obtain the unified view point on the lattice deformation mechanisms and associated phenomena covering ferrous and

non-ferrous martensite transformations.

2. Mathematical Expressions for Shear Modes and Structures

As was introduced in the previous paper[9], first consider the Nishiyama's relation, $(111)_f // (101)_b$ and $[11\bar{2}]_f // [10\bar{1}]_b$, and denote the stacking configurations of atomic planes by A, a, B, b, C, and c, common to $(111)_f$ and $(101)_b$, as in Fig. 2. a, b, and c do not appear in the fcc lattice since its stacking sequence is ABCABC..., and only two configurations appear in the bcc structure, i. e., AbAbAb... The three fcc configurations can be converted into each other by the lateral displacement vector, $a/6\cdot[11\bar{2}]_f$, which corresponds to the Burgers vector of half dislocation in this structure, or its multiples, while the displacements in bcc structure are in the units of $a'/2\cdot[10\bar{1}]_b$. For the transition between the two structures, the difference of the above two displacement vectors in the topological sense, $\overline{Ab} - \overline{AB}$, that is $a/12\cdot[11\bar{2}]_f$ or $a'/6[10\bar{1}]_b$, must appear in the translational operations in the lattice deformation. Accordingly we employ it as the unitoperator in the transformation processes denoting it by [**1**]. Then, the direct uniform shear along $[11\bar{2}]_f/(111)_f$ in the Kurdjumov and Sachs' and Nishiyama's mechanism is simply represented by [**1**], and the half dislocation on every two planes mechnism by Christian to transform fcc to hcp is denoted as [**20**] where **0** means no operation on the second plane of every two planes. Shuffling is represented by [$\mathbf{1}^{\pm}$]. As mentioned before, some additional deformations are required for fcc-bcc marrensite transformation, and they are summarized in the notation [**D**]. When [**D**] is not operated, the lattice belongs to fcc or hcp system including their stacking modifications in which closest packing of atoms is maintained. When the starting structure is bcc, [$\bar{\mathbf{D}}$]should be operated for the transformation to the closest packing system.

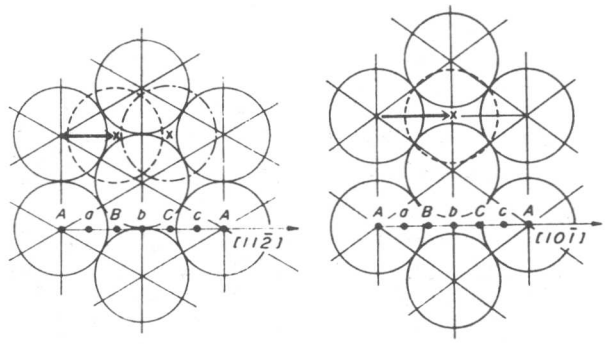

$(111)_f$ $(101)_b$

Fig. 2 Nishiyama's lattice relation and stacking sequence correspondence between the fcc and bcc structure.

Essentially the same cipherization is used to express the concerned crystal structures. For instance, the normal fcc structure is written as [2], since its ABCABC... stacking is regarded as the sequence of displacements each in two units. Similarly, hcp is represented by $[2\bar{2}]$, and bcc is [3]. More precise description of the above notations and rules between them have been given in the previous papers[9]. According to the above expressions, Kurdjumov and Sachs' and Nishiyama's mechanism is simplywritten as $[2]_f[\mathbf{1}][\mathbb{D}] \doteq [3]_b$, which simply means $2 + 1 = 3$, and Christian's mechanism is $[2]_f[\mathbf{20}] = [42]_f = [\bar{2}2]_h$ where 4 is equivalent to $\bar{2}$ since one cycle of the displacements is in six units. Shuffling

of hcp to produce bcc is $[\bar{2}2]_h[1^{\mp}][\mathbb{D}] = [3]_b$, and likewise shuffling of fcc is $[2]_f[1^{\pm}][\mathbb{D}] = [31]_b$ which is the six layer structure with the sequence of AbCaBc... mentioned before. With these notations, the fcc-bcc transformation links in Fig. 1 can be redrawn as in Fig. 3. Many other ways of lattice deformation by various shear modes as described in the previous reports are mathematically possible, but only four comparatively simple paths exist in the fcc-bcc martensite transformation and, therefore, no other ways are shown in the figure.

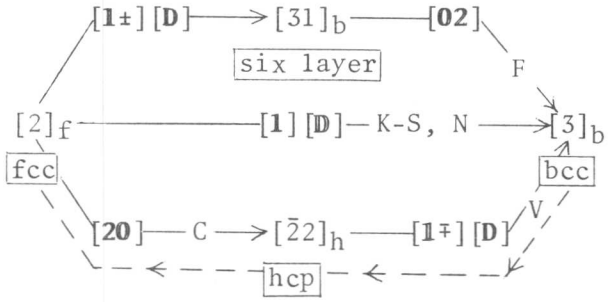

Fig. 3 fcc-bcc lattice transformation links redrawn with the new cipherization.

3. Extension of the Mathematical Expressions to Non-ferrous Alloys' Cases

Recent developments in the study of martensie transformation are remarkable in the cases of non-ferrous alloys, since new topics, such as of the shape memory effect, super-elesticity, lattice softening phenomena, and appearance of various modification structures, have risen from them[18]. Many alloys with these peculiar characteristics show transformations starting from the bcc structure. For instance, similar to the first order transformation by cooling of titanium, zirconium, and hafnium from bcc to hcp with the lattice relation equivalent to that in Fig. 2, the Cu-Al-Ni thermo-elastic or super-elastic alloy martensitically transforms from bcc (β_1) to 2H (γ_1') by cooling[19,20]. This correspond to the V path in the reversed direction from bcc to hcp shown in Fig. 1 and Fig. 3. Further, by applying stress and/or temperature change, the alloy exhibits rhombohedral modifications, β_1' ($18R_1$) and β_1'' ($18R_2$), and with the highest stress application it turns to the α_1' phase (6R) which is equivqlent to the fcc structure except the atomic ordering. Au-47.5 Cd β_1 alloy also transforms to the hexagonal γ_2' (M2H) phase or an intermediate structure, β_2' (9R). Cu-29Zn-5.5 Al alloy also transforms from β to β_1' and α_1' phase[21]. Other modification structures of martensite from normal or ordered β phases are, for instance, fct of Ni-Al alloy[22], β_2' (N9R) and β_2'' (M9R) of β Cu-Zn[23,24], and α_2' fct and its 2H and 9R modifications of β_2 Ni-Zn-Cu alloy[25].

Generally speaking, many β phase alloys martensitically transform from the bcc type structure, either normal or ordered, to the fcc (fct) or hcp type structures or their closest packing modifications, such as 2H, 6R, 9R, and 18R. Therefore, it looks quite reasonable to put this group of martensite transformation of non-ferrous alloys into the lower part of the before mentioned fcc-bcc transformation links for steel provided that the direction of transformation is from the righthand side to the left, as shown by the broken line in Fig. 3. This means that the first deformation process will most likely be by shuffling, which is actually widely accepted concept and useful to interpret the experimental facts in conjunction with the lattice softening phenomena.

In order to unify the non-ferrous martensite transformation cases from the above view point and analyze the modes of shear in lattice deformations, we first apply the new notations to the structures mentioned in the above and, then, figure out the deformation processes especially of shuffling. Correspondences between the former and new notations for the non-ferrous concerned structures are as follows.

Notations	phases								
Metallurgical	β,β_1,β_2 (bcc,CsCl, etc.)	α (fct)	α'_1,α'_2 (fct)	γ'_1 (hcp)	γ'_2 (mod. hcp)	β'_2 (mod.)	β''_2 (mod.)	β'_1 (mod.)	β''_2 (mod.)
Ramsdell	-	3R	6R	2H	M2H	N9R	M9R	$18R_1$	$18R_2$
Zhdanov	-	Z(1)	$Z(1)_6$	$Z(1\bar{1})$	$Z(1\bar{1})$	$Z(2\bar{1})$	$Z(2\bar{1})$	$Z(2\bar{1})_6$	$Z(1\bar{1}3\bar{1})_3$
Fujita	$[3]_b$	$[2]_f$	$[2]_f$	$[2\bar{2}]_h$	$[''\pm\delta]$	$[22\bar{2}]_f$	$[''\pm\delta]$	$[22\bar{2}]_f$	$[2\bar{2}222\bar{2}]_f$

Only the notations by the present author enable the cipherization of deformation processes between the cited structures and, thereby, the classification of the main shear modes discussed in the preceding sections. For instance, transformations from β, β_1 and β_2 to γ'_1 (hcp) is simply described as $[3]_b[\mathbf{1}^{\mp}][\bar{\mathbf{D}}] = [2\bar{2}]_h$, which showsthat the shuffling plays the main role in the lattice deformation. From the β to the α group is $[3]_b[\bar{\mathbf{1}}][\bar{\mathbf{D}}] = [2]_f$. However, this doesn't always imply that the deformation is by the large uniform shear along $[10\bar{1}]_b/(101)_b$ corresponding to the reversed K-S or N path but probably means that a compound shearprocess starting from shuffling takes place still following the broken line in Fig. 3. Other important transformations are from β to 9R or $18R_1$ and from β to $18R_2$. The former is expressed as $[3]_b[\bar{\mathbf{1}}\bar{\mathbf{1}}\mathbf{1}][\bar{\mathbf{D}}] = [22\bar{2}]_f$, and the latter is as $[3]_b[\bar{\mathbf{1}}\mathbf{1}\bar{\mathbf{1}}\bar{\mathbf{1}}\mathbf{1}\bar{\mathbf{1}}][\bar{\mathbf{D}}] = [2\bar{2}222\bar{2}]_f$. In both cases, the deformation operators in the equations have asymmetrical forms, which might suggest that the soft phonon mode with an asymmetrical wave form is induced and ultimately give rise to the shuffling with the inherited asymmetry. Another possible explanation is that, even if the initial mode was symmetrical, the ordered lattice structure would have an intrinsic asymmetrical constraints and accordingly deform the vibrational mode, leading to the asymmetrical shear transformation. It could also be considered that the shuffling is essentially combined with another deformation mode, such as half dislocation like displacements with certain regular intervals, and produce various modification structures. In either case, the deformation operator should be further decomposed into the deformation elements to find the unit processes and their nature. For example, the operator for β to $18R_2$ transformation can be decomposed as $[\bar{\mathbf{1}}\mathbf{1}\bar{\mathbf{1}}\bar{\mathbf{1}}\mathbf{1}\bar{\mathbf{1}}] = [\bar{\mathbf{1}}\mathbf{1}\bar{\mathbf{1}}\mathbf{1}\bar{\mathbf{1}}] + [\mathbf{000200}]$. This is no other than the combination of the symmetrical normal shuffling $[\mathbf{1}^{\mp}]$ and half dislocation like displacement on the fourth plane of every six layers. Nevertheless, a straightforward explanation of the large interval layer sliding is not given and a reasonable way of decomposition is not always possible. Therefore, to solve this problem, closer investigation taking account of precise crystal structure is required.

It is worthy of note that sometimes the martensite structure is a

distorted one with monoclinic or other low symmetry. The distortion often comes from the oblique shear along the main shear plane which can not be expressed by the integral numbers as used in this paper. A rather simple example is M9R (β'_2) phase of Cu-39Zn alloy in which c axis is inclined against the main shear plane by the orderof 1 degree. This is most likely due to the atomic size effect in the ordered structure, and taking it into consideration the structure is cipherized as $[2+\delta\ 2+\delta\ \bar{2}-\delta]_f$ where δ measures the deviation from the unit shear displacement between two successive layers. Similar expression has been employed in the analysis of the six layer structure of Fe-Mn-C martensite[17].

More improvements of the present notations and calculations are required, including more precise treatment of [D] in which other shear plane and direction as large and important as $[10\bar{1}]_b/(101)_b$ as in the case of Au-50Cd and Au-Cu-Zn alloy.

The generalized fcc-hcp-bcc lattice deformation links seems to suggest that the martensitic transformation of steels is induced by the lattice softening along the main shear mode as well as the cases of β phase non-ferrous alloys. However, experimental evidences are not always clear and enough,so that this problem still remains unsolved.

References

(1) G.Kurdjumov and G.Sachs: Z.Phys., **64**(1930)325.
(2) Z.Nishiyama: Sci.Rep.Tohoku Univ., **23**(1934)637; **25**(1936)79.
(3) A.B.Greninger and A.R.Troiano: Trans.AIMME, **185**(1949)590.
(4) J.W.Christian: Proc.Roy.Soc.London, **A206**(1951)51.
(5) A.Venables: Phil.Mag. **7**(1962)35.
(6) B.Cina: Acta Met., **6**(1958)748.
(7) H.Otte: Acta Met., **5**(1957)614.
(8) S.Dash and N.Brown: Acta Met., **14**(1966)595.
(9) F.E.Fujita: Bull.Japan Inst.Metals **13**, No.10(1974)713; Proc.Met. Trans.A, **8A**, Nov.(1977)1727.
(10) R.Oshima and C.M.Wayman: Script.Met., **8**(1974)223.
(11) T.Moriya, H.Ino, F.E.Fujita and Y.Maeda: J.Phys.Soc.Japan, **24**(1968)60.
(12) F.E.Fujita, T.Moriya and H.Ino: Proc.ICSTIS,Suppl.Trans.ISIJ, **11** (1971)1273.
(13) F.E.Fujita, C.Shiga, T.Moriya and H.Ino: J.Japan Inst.Met., **38**(1974) 1030.
(14) C.Shiga, F.E.Fujita and M.Kimura: J.Japan Inst.Met., **39**(1975)1205.
(15) F.E.Fujita and C.Shiga: Proc.1st Int.Sym.Mart.Trans.,Suppl.Trans. JIM, **17**(1976)287.
(16) R.Oshima,A.Kajikawa and F.E.Fujita: in this issue.
(17) R.Oshima, H.Azuma and F.E.Fujita: Proc.1st Int.Sym.Mart.Trans., suppl.Trans.JIM, **17**(1976)293.
(18) Z.Nishiyama: "Martensite Transformation" (Maruzen,1971)
(19) G.U.Kurdjumov and L.G.Khandros: Dokl.Akad.Nauk.SSSR, **66**(1949)211.
(20) K.Otsuka, M.Tokonami, K.Shimizu, Y.Iwata and I.Shibuya: Acta Met., **27**(1979)
(21) K.Takezawa and S.Sato: Proc.1st Int.Sym.Mart.Trans.,suppl.Trans.JIM, **17**(1976)233.
(22) S.Chakravorty and C.M.Wayman:Metal.Trans., **7A**(1976)569.
(23) I.Cornelis and C.M.Wayman: Acta Met., **22**(1974)291.
(24) T.Tadaki: Doctor's Thesis, Osaka Univ. (1978).
(25) Y.Murakami and S.Kachi: Trans. JIM, **18**(1977)423.

The Mössbauer Effect Study of an Intermediate Phase in Martensite Transformation of Fe-Mn-C Steel

Ryuichiro Oshima, Akira Kajikawa and Francisco E. Fujita

The Mössbauer spectroscopy of Fe-Mn-C steel was carried out to examine the intermediate six layer structure which was previously found in the process of martensite transformation. 50 μm thick specimen of Fe-5.5wt%Mn-1wt%C steel were first quenched from 1200°C into water and then cooled down below Ms temperature. The Mössbauer effect was measured between room temperature and -196°C. In the paramagnetic retained austenite spectrum, a new component with larger quadrupole splitting appeared when the martensite transformation started, and it disappeared irreversibly as the specimen was warmed to room temperature. This characteristic spectral component was identified to be of the intermediate phase with low crystal symmetry. No remarkable change of the recoil-free fraction of iron atoms was observed near the Ms temperature, suggesting that the lattice softening did not occur in the martensite transformation.

The neutron diffraction experiment was also done to examine the carbon positions in martensite structure, and it was concluded that carbon atoms sit at the octahedral and tetrahedral interstitial sites with equal probabilities in freshly formed martensite at low temperature.

I. Introduction

The martensite transformation in steels has long been treated by the direct shear mechanisms proposed by Kurdjumov and Sachs [1] and Nishiyama [2]. Occupancy of octahedral interstitial sites by carbon atoms in the martensite phase was suggested by the lattice parameter measurements at room temperature and well interpreted by the above mechanisms. However, recent Mössbauer studies [3,4] have indicated that carbon atoms in freshly formed martensite at low temperatures occupy both tetrahedral and octahedral interstitial sites. Since the tetrahedral interstitial carbon atoms can not be introduced by the above direct shear mechanisms, Fujita [5] proposed another transformation process in which the austenite lattice transforms first by shuffling of fcc lattice on (111) along $[11\bar{2}]$ and then by half dislocation type shearing along the same plane and direction to reach the bct martensite lattice. By this transformation process, formation of an intermediate phase with a six layer structure was predicted. While, Oshima et al.[6,7] investigated freshly formed martensite of Fe-Mn-C steel at low temperature by electron diffraction and electron microscopy, and found an intermediate phase with a monoclinic six layer structure with a = b = 2.476A, c = 12.13A and γ = 70°32', which corresponded to the bove structure expected from Fujita's model.

With respect to the carbon positions in martensite, Entin et al.[8] concluded from their neutron diffraction study on Fe-8at%Ni-6.7at%C steel that about 80% of carbon atoms occupy one of the three octahedral interstitial sublattices and less than 20% of carbon sit on the other

Department of Material Physics, Faculty of Engineering Science, Osaka University, Toyonaka, Osaka, Japan 560.

two sublattices in as formed martensite at 80K. However, recalculation showed that the O and T sites half and half configuration is also possible to interpret their observation of diffraction intensities [9]. Since manganese has a negative atomic scattering amplitude and carbon has a relatively large amplitude for neutrons, the Fe-Mn-C alloy is suitable for the neutron diffraction study too.

In the present study, the electronic and magnetic structure of the six layer are examined by the Mössbauer effect, the carbon positions in the martensite by neutron diffraction, and they are compared with former results.

II. Experimental

Plates of Fe-5.5wt%Mn-1wt%C with the sizes of 10x20x0.1 mm were sealed in evacuated quratz capsules, austenitized at 1200°C for 3.6 ks and quenched into iced water. The specimens were chemically and electrolytically thinned to 50 μm thick. The Mössbauer spectroscopy was carried out between room temperature and -196°C using a 30 mCi ^{57}Co source diffused in copper. For the neutron spectroscopy, tips of about 100g in weight was put in a cylindrical aluminum specimen holder. The diffraction patterns were first obtained at room temperature, at -193°C by cooling the specimen, and their at -80°C, -50°C, -25°C, 0°C and 40°C by warming up successively.

III. Experimental Results

(I) Mössbuer effect

Fig.1 shows a Mössbauer spectrum obtained from austenite of Fe-5.5wt%Mn-1wt%C steel at room temperature. The spectrum consists of a central main peak and split sub-peaks, as was already reported for the retained austenite of various steels [3,4,10]. The main peak arises from the iron atoms unaffected by solute carbon atoms, and the sub-peaks with the quadrupole splitting from those with first neighboring interstitial carbon atoms. The isomer shift of the main peak is -0.26 mm/s and that of the sub-peaks -0.24 mm/s, and the latter's quadrupole splitting is -0.71 mm/s. When cooling the specimen to a temperature a few degrees higher than the Ms, the spectrum shifted due to the second doppler effect but the profile did not change. The area of resonant absorption, which corresponds to the recoil-free fraction, increased monotonically by lowering the temperature across the Ms temperature. This means that lattice softening did not occur appreciably around the martensite transformation temperature. On the other hand, the spectrum of the paramagnetic component

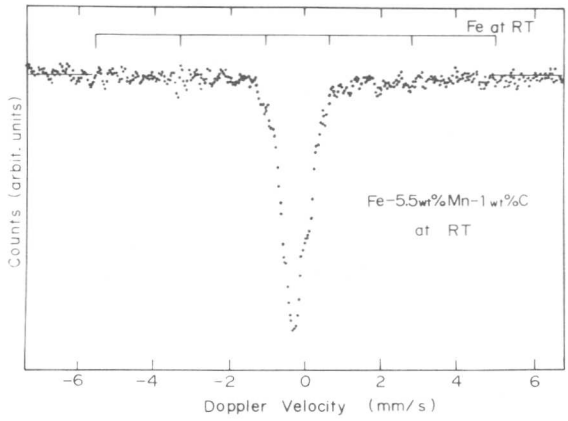

Fig.1 Mössbauer spectrum of Fe-5.5 wt%Mn-1wt%C Austenite at room temperature.

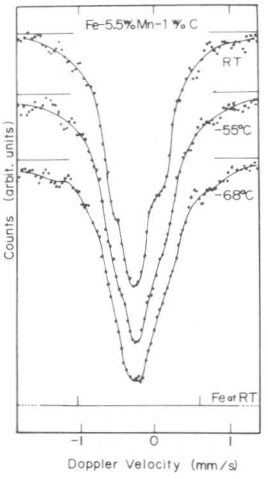

Fig.2 Change in Mössbauer spectrum of paramagnetic component of Fe-5.5wt%Mn-1wt%C.

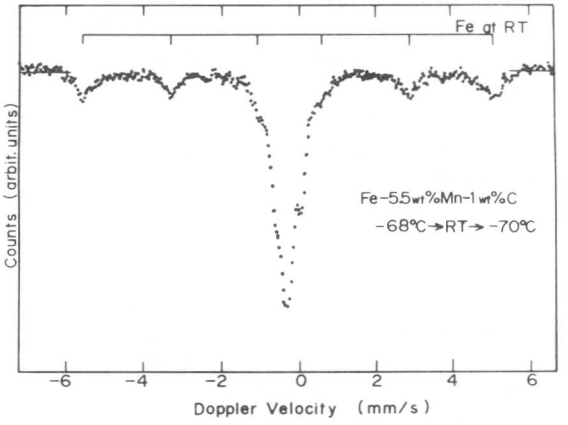

Fig.3 Mössbauer spectrum obtained from Fe-5.5wt%Mn-1wt%C at -70°C after transformed at -68°C, and annealed at room temperature.

became wider when the martensite transformation started. As shown in Fig.2, which was obtained from a specimen with Ms = -50°C, the main peak is wider than before the transformation and the sub-peak shoulders are hidden in the main peak. After measured at -68°C, the specimen was warmed up to room temperature and measured again. The ferromagnetic component of the martensite remained as it was, but the paramagnetic component turned back to the same profile as before the transformation. When it was again cooled to -70°C, no more remarkable change in the paramagnetic component took place, as shown in Fig.3. The above result strongly suggests that a structure change took place in the paramagnetic phase during the process of martensite formation at low temperature and it irreversibly disappeared by warming up to room temperature.

(II) Neutron diffraction

In the neutron diffraction study, {112} martensite reflection was carefully examined because the information in the carbon position was readily obtained from it. Actually, when the temperature was raised from -196°C after the martensite transformation, the profile change was already observed at -80°C especially in {112} reflection. Fig.4 shows diffraction patterns of {220} austenite and {112} martensite reflections taken at -196°C and 0°C after the transformation. When warmed to 0°C, broadening of peak width, change in line profile and peak shift to the higher angle side were found in the martensite reflection, while the austenite reflec-

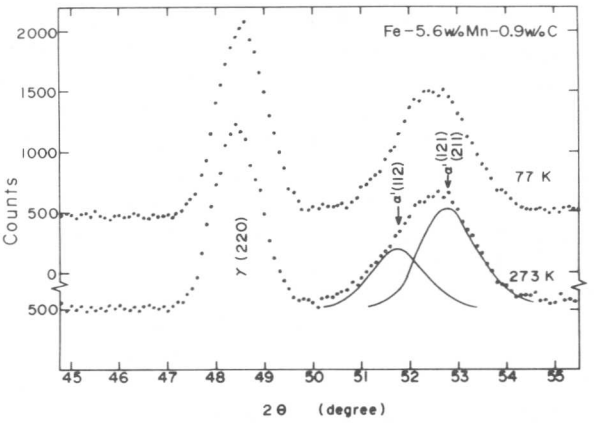

Fig.4 Neutron diffraction patterns of {220} austenite and {112} martensite reflections.

tion only moved to the lower angle side due to the thermal expansion. They suggest that the martensite structure at low temperature has a small tetragonality, different structure factor, and larger unit cell volume than at room temperature and these anomalies irreversibly disappear when warmed up. In the neutron powder patterns any satellite reflections corresponding to the intermediate six layer structure were not observed.

III. Discussion

In order to interpret the change of the profile of the paramagnetic spectrum at low temperature, three possibilities were taken into consideration. They were (1) the difference of the second doppler shift of the main peak and sub-peaks, (2) superposition of the paramagnetic peak and the ferromagnetic peaks, and (3) appearance of a new phase associated with the martensite transformation.

(1) Second doppler shift is proportional to the mean square velocity of atoms, $\langle v^2 \rangle$. Iron atoms with and without carbon neighbors could have different values and temperature dependences of $\langle v^2 \rangle$, and thereby produce the profile change. Accordingly, a specimen with Ms lower than -140°C was investigated between room temperature and the Ms temperature. The mean second doppler shift was only 3.8×10^{-4} mm/s, and the profile of the paramagnetic spectrum did not change.

(2) When the martensite transformation takes place, six line ferromagnetic peaks appear in the spectrum. Since the inner most two peaks more or less overlap the paramagnetic peak, the peak shape might be changed. However, the quantitative analysis showed that the ferromagnetic peaks did not affect the central part of the paramagnetic peak. In addition, as before mentioned, once the specimen was warmed to room temperature, appreciable change of the profile of the paramagnetic peak no longer took place. This can be accounted for by neither the second doppler shift difference nor the effect of the martensite peaks. Therefore, the appearance of a new paramagnetic phase was most likely considered.

Fig.5 shows the result of decomposition of the low temperature spectrum into most probable three components including the innermost two lines of ferromagnetic part. As compared with the spectrum at room temperature, the quadrupole splitting is slightly larger and the half value width of the central component is by 20% larger. Since the line broadening of the central peak most likely comes from the increase of the quadrupole effect, or of the electric field gradient on the iron atoms as well as in the sub-peaks, the crystal symmetry of the paramagnetic phase in problem must have become lower as a whole or at least partly. Taking into consideration of our previous results of the electron microscopy and diffraction experiment, it is concluded that a new paramagnetic phase with low crystal symmetry, which most probably corresponds to the intermediate six layer structure,

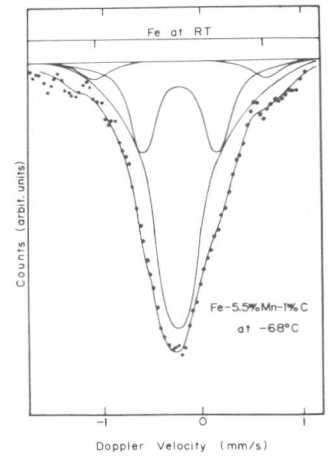

Fig.5 Decomposition of low temperature spectrum into most probable three components.

appears and coexists with martensite and retained austenite at low temperature. It may be worthy of note that the intermediate six layer structure is not ferromagnetic but paramagnetic although it was considered as a stacking modification of bcc martensite structure.

In the following, the result of the neutron diffraction study will be discussed with respect of the carbon positions in martensite. Possible carbon positions in martensite are shown in Fig.6. The crystal structure factor of this unit cell can be written as

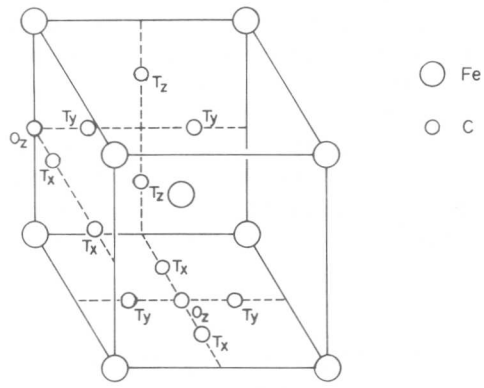

Fig.6 O and T sites of interstitial carbon positions.

$$F = \frac{1}{2}(1-c)b_i\{1+\exp\pi i(h+k+1)\} + \frac{1}{2}(1-\alpha-\beta-\gamma)c\,b_c\{\exp\pi il+\exp\pi i(h+k)\}$$
$$+ \frac{\alpha}{4}c\,b_c\{\exp\pi i(\frac{h}{2}+k) + \exp\pi i(\frac{3}{2}h+k) + \exp\pi i(\frac{h}{2}+1) + \exp\pi i(\frac{3}{2}h+1)\}$$
$$+ \frac{\beta}{4}c\,b_c\{\exp\pi i(h+\frac{k}{2}) + \exp\pi i(h+\frac{3}{2}k) + \exp\pi i(\frac{k}{2}+1) + \exp\pi i(\frac{3}{2}k+1)\}$$
$$+ \frac{\gamma}{4}c\,b_c\{\exp\pi i(h+\frac{1}{2}) + \exp\pi i(h+\frac{3}{2}1) + \exp\pi i(k+\frac{1}{2}) + \exp\pi i(k+\frac{3}{2}1)\},$$

where c is the carbon concentration, b_i the mean scattering amplitude of the substitutional Fe-Mn alloy, b_c the scattering amplitude of carbon atoms, and α, β and γ are the parameters to describe the carbon distribution in interstitial sub-lattices. Four cases are conceivable for carbon distribution, that is,

1) $\alpha = \beta = \gamma = 0$; 100% O_z configuration,
2) $\alpha = 1/2$, $\beta = \gamma = 0$; 50%O_z-50%T_x configuration,
3) $\alpha = \beta = 1/4$, $\gamma = 0$; 50%O_z-50%$T_{x,y}$ configuration, and
4) $\alpha = \beta = \gamma = 1/6$; 50%O_z-50%$T_{x,y,z}$ configuration.

In table 1 are shown the calculated intensities for various carbon configurations and the ratio of $(|F(211)|^2 + |F(121)|^2) / |F(112)|^2$. The ratio is 1.77 for O_z only configuration, and 1.88 and 1.91 for O_z-T con-

Table 1 Calculated Intensities for Various Carbon Configurations

Carbon Position	$\|F(211)\|^2$	$\|F(121)\|^2$	$\|F(112)\|^2$	$\frac{\|F(211)\|^2+\|F(121)\|^2}{\|F(112)\|^2}$
O_z	0.8207	0.8207	0.8749	1.76
1/2 O_z - 1/2 T_x	0.8478	0.8342	0.8613	1.91
1/2 O_z - 1/2 $T_{x,y}$	0.8410	0.8410	0.8613	1.91
1/2 O_z - 1/2 $T_{x,y,z}$	0.8387	0.8387	0.8658	1.88

figurations. The observed {112} diffraction line was decomposed into two components by using the tetragonal lattice parameters determined by the X-ray measurement. Assuming that the two components have the same profile and same half value width, the ratio was experimentally determined to be 1.90 at -196°C and 1.71 at 0°C. These values well agree with those calculated for the O_z-T and O_z configuration respectively. It is, therefore, concluded that the carbon atoms occupy both octahedral and tetrahedral interstitial sites with equal populations in freshly formed martensite, as the previous theory and experiments suggested.

IV. Conclusion

The Mössbauer spectroscopy of Fe-Mn-C steel between room temperature and -196°C showed that a new paramagnetic component with large quadrupole splitting appeared in austenite when martensite transformation just started. It is concluded that this component corresponds to the intermediate six layer structure previously reported. No evidence of lattice softening was obtained just above the Ms temperature. The neutron diffraction experiment showed that carbon atoms in freshly formed martensite occupy the octahedral and tetrahedral site with equal populations.

Acknowledgment

The authors wish to express their sincere thanks to Prof. M. Hirabayashi and Dr. H. Asano of Tohoku University for their cooperation in the neutron diffraction experiment at the Japan Atomic Research Institute, and also for helpful discussions.

References

[1] G. V. Kurdjumov and G. Sachs: Z. Phys., **64**(1930), 325.

[2] Z. Nishiyama: Sci. Rep. Tohoku Univ., **23**(1934), 637.

[3] H. Ino, T. Moriya, F. E. Fujita and Y. Maeda: J. Phys. Soc. Japan, **22**(1967), 346.

[4] C. Shiga, F. E. Fujita and M. Kimura: J. Japan Inst. Metals, **39** (1975), 1205.

[5] F. E. Fujita: J. Japan Inst. Metals, **39**(1975), 1082.

[6] R. Oshima and C. M. Wayman: Scripta Met., **8**(1974), 223.

[7] R. Oshima, H. Azuma and F. E. Fujita: Scripta Met., **10**(1976), 1011.

[8] I. R. Entin, V. A. Somenkov and S. Sh. Shil'shtein: Doklady Akad. Nauk S. S. S. R., **206**(1972), 1096.

[9] F. E. Fujita: Met. Trans., **8A**(1977), 1729.

[10] N. DeCristfaro and R. Kaplow: Met. Trans., **8A**(1977), 35.

The Inheritance of Lattice Defects during $\gamma \rightleftarrows \alpha$ Transformation and the Martensite Structure in Thermomechanically Treated Steel

M.L.Bernshtein[+], L.M.Kaputkina[+] and S.D.Prokoshkin[+]

The martensite crystals of any structural-morphological type formed by cooling or deformation inherit the hot-deformed austenite substructure during martensitic transformation. The exception is in the case of formation of perfect polygonized austenite substructure, when the subboundaries can serve as impenetrable barriers for martensite crystals propagation causing the most significant their refinement. The combination of the substructures formed due to transformation-induced hardening and of hot-deformed austenite substructure changes the martensite diffraction image obtained by X-ray topography in so manner that it become possible to distinguish between the martensite topograms in thermomechanically strengthened condition and that of the martensite formed from undeformed or recrystallized austenite. In the case of preliminary hot-deformed austenite the primary plate martensite crystals are of preferred orientation relatively to the rolling direction unlike their random orientation in control quenching. If the hot-deformed austenite substructure is sufficiently stable to prevent recrystallization in austenite and ferrite states in repeated austenitization, it remains in the course of martensitic transformation and austenite formation during repeated heating due to shear mechanism of metal atoms lattice reconstruction.

I. Introduction.

The formation of well-developed austenite substructure during hot deformation in a cycle of high-temperature thermomechanical treatment (HTMT) of steel leads to improvement in mechanical properties of the martensite [1,2]. In this connection the following problems are considered in present communication: a) determination of the conditions for the retention of hot-deformed austenite substructure and hence of thermomechanical strengthening during subsequent phase transformations including repeated heat treatment; b) obtaining of data concerning the influence of the austenite substructure upon martensite structure with the aim to control the latter and consequently the final properties of steel. The austenite structures formed in steels examined during hot deformation by rolling, post-deformation holdings, repeated heating and

---

[+]The Laboratory of Thermomechanical Treatment, Moscow Steel and Alloys Institute, Moscow II7936, USSR.

conventional (control) heat treatment were fixed by water cooling. In steels with M_s lower than room temperature the austenite structure was examined at room temperature, the martensite was obtained during cooling in liquid nitrogen.

II. Results and Discussion.

According to Bernshtein and Shtremel [3] the retention of dislocation substructure during phase transformation, i.e. the "inheritance" of primary phase substructure by the secondary one, is possible in the case of shear mechanism of martensitic transformation. In this case the atoms displace relatively to one another at the distances shorter than interatomic, the nearest neighbourhood does not disturb and therefore the dislocations of primary austenite must transfer into martensite. The inheritance of substructure is to be expected as a result of transformation during heating if the formation of austenite realizes by shear.

There are various types of substructure formed during hot deformation or post-deformation holding, fixed by rapid cooling: "hot-worked" substructure, to which the uniform distribution of dislocations and dislocated cellular structure belong, and polygonized substructure - elongated or equiaxed subgrains bordered by sharp dislocation subboundaries [4]. The realization of one or another substructure type depends on the austenite hot deformation regimen and the steel composition. High temperatures and degrees of deformation and post-deformation holdings promote the formation of polygonized substructure. The recrystallization exterminates the well-developed substructure of the austenite. There are known two main types of martensite morphology: lath(packet) dislocated and plate twinned martensite [5].

As it is seen from fig.I,a,b the crystals of plate martensite and of the lath one inherit the dislocation substrucre of any type. At the back-cloth of martensite crystals individual dislocations and various their configurations including polygonal subboundaries continuing from the retained austenite into martensite crystals, are seen. The austenite substructure is inherited not only by martensite formed during cooling, but also by the strain-induced martensite (fig.I,c). The differences in substructure and morphology of martensite formed during cooling and strain-induced martensite and in primary austenite substructure do not affect the degree of ordering of carbon atoms in martensite lattice [6].

It is important that the retention of austenite defects during martensitic transformation in combination with defects forming as a result of transformation and relaxation deformations introduces such differences in martensite during HTMT in comparison with conventional quenching, which can be fixed not only by electron microscopy, but also by such an integral method of structure unvestigation as X-ray topography. The

point is that at the present time no effective method is available for direct integral control of the structure state after HTMT in real industrial steels having completely martensitic structure.The results of X-ray diffractometry (especially for carbon steels) and light microscopy do not often enable one to provide unequivocal explanation,and the electron micriscopy method is rather consuming and local,the more so the high density of imperfections inherent to martensite itself veils the inherited substructure of austenite. Therefore the problem related to the control of martensite structure after HTMT with the aim to reveal the existence of strengthened state is of interest.At a proper geometry of topography the topograms of martensite (mixed packet-plate,fig. 2,and completely packet,fig.3) formed from the austenites with and without well-developed substructure can be distinguished.In the absence of preliminary austenite deformation the intensity of martensite reflections is distributed discretely along the line - the well-defined concentrations are present, which correspond to reflections from martensite crystals equally orientated within initial austenite grains (fig.2,a).The austenite hot deformation in the absence of recrystallization results in uniform or smoothly changed owing to texture effect distribution of intensity along the line due to strong broadening and overlapping of individual martensite spots (figs. 2,b,3,b).The topograms of martensite (fig.2,c) similar to the ones obtained from undeformed specimen (fig.2,a),with typical concentrations of intensity on lines,correspond to complete recrystallization of austenite after deformation.Thus,it has been found that in principle the X-ray topography method can be applied for the control in completely martensitic state of presence of well-developed austenite substructure,or in other words,of the existence of thermomechanical strengthening in martensite after HTMT.

The presence of well-developed substructure in austenite due to HTMT affects the dimensions of individual plate martensite crystals and of packets of lath crystals,refining them without changes in form-factor [4,7].The most significant refinement of martensite crystals is observed when the martensite is formed from the austenite with perfect polygonized substructure obtained at sufficiently high deformation temperatures and degrees and rather slow deformation rates.Such substructure represents itself equiaxed subgrains with low-angle,but sufficiently high (up to 10^{0}) misorientation.In this case it was for the first time detected,that subboundaries are not always inherited,but can serve as impenetrable barriers for the propagation of the martensite crystals,which therefore become localized in the limits of subgrains (fig.4).

Another peculiarity of martensite structure after HTMT is preferred orientation of martensite crystals relatively to rolling direction.It may be the consequence of hot-deformed austenite lattice (and subboundaries) preferred orientation and of influence of the orientated stresses on the formation of martensite crystals.The analysis of histograms of distribu-

tion of angles between any martensite crystal and rolling direction (fig.5) in Fe-Ni-C steel shows the anisotropy of the structure of martensite formed from hot-deformed austenite and the preferred orientation of long axes of crystals sections.This orientation is closer to the direction across rolling one.After conventional quenching all the directions of martensite crystals are equiprobable.

The inheritance of the substructure during $\alpha \rightarrow \gamma$ transformation was revealed in the time of repeated quenching after HTMT of I5Cr-8Ni steel with packet martensite,formed in 30% volume during first (subzero) cooling before short-time repeated heating in a salt bath.After repeated heating at I000°C, 3 min only a small number of polygonized regions are observed. All the remaining volume is occupied by recrystallized grains. Only after repeated heating at 950°C,3 min and rapid cooling noticeable effect of substructure inheritance during $\alpha \rightarrow \gamma$ transformation is observed.In this case the volume fraction of the polygonized substructure in hot-deformed austenite is about 60%.At that time in some areas at the back-cloth of polygonized substructure of primary austenite the systems of subboundaries are observed,which correspond to the former packets of martensite lath crystals by their morphology and size,but contain more lesser dislocation density inside subgrains (fig. 6).This fact directly indicates the inheritance by the secondary austenite of the substructure of martensite,from which it is formed,including the substructure of hot-deformed austenite.The latter,in it's turn,was inherited by martensite during direct $\gamma \rightarrow \alpha$ transformation.If the volume fraction of martensite formed during first cooling is higher (60%),then the transformation-induced hardening is so high,that the austenite structure after repeated heating represents itself only the grains formed as a result of austenite recrystallization after $\alpha \rightarrow \gamma$ transformation.Thus,for the retention of HTMT effect after repeated quenching it is necessary to limit as much as possible temperature and duration of heating for the repeated quenching and to create the austenite substructure stable to recrystallization.

Acknowledgements

The authors acknowledge research workers of the Laboratory of Thermomechanical Treatment N.A.Nikishov,A.V.Lutsau and V.G.Prokoshkina for kindly given illustrative material, obtained in joint with them experimental works.

References

[I] M.L.Bernshtein: Termomekhanicheskaja obrabotka metallov i splavov,vols.I,II,M.,Metallurgija,I968.
[2] M.L.Bernshtein: Prochnost staly,M.,Metallurgija,I974.
[3] M.L.Bernshtein and M.A.Shtremel: Fiz.Met.Metalloved.,I5 (I963),82.
[4] M.L.Bernshtein,L.M.Kaputkina and S.D.Prokoshkin: Acta Met., 25(I977),I47I.

[5] A.R.Marder and G.Krauss: Trans.ASM,60(1967),651.
[6] M.L.Bernshtein,L.M.Kaputkina,S.D.Prokoshkin and A.M.Glushets: Martensitic transformations,tez.dokl.ICOMAT-77, Kiev,1977,27.
[7] M.L.Bernshtein,V.A.Zaimovsky,L.M.Kaputkina,D.V.Laptev, A.P.Matevosjan,L.A.Smoljakova,M.N.Spassky,M.A.Shtremel: Metallofizika,55(1974),49.

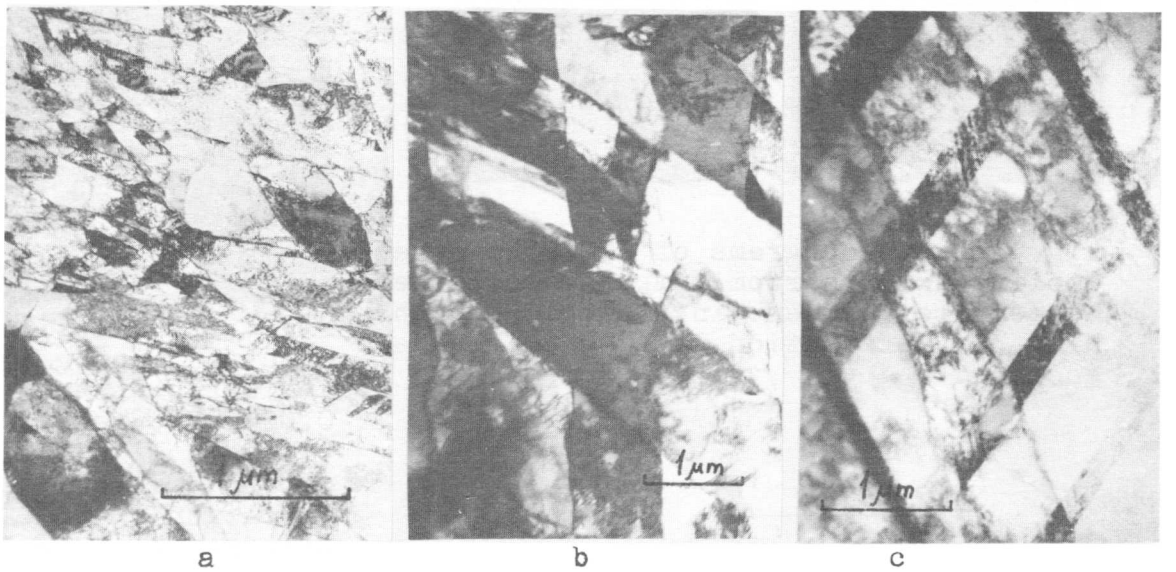

a b c

Fig.1.Transmission electron micrographs.The inheritance of substructure of hot-deformed austenite by martensite. a) 15Cr-8Ni steel,packet martensite, b)0.7C-5Cr-4Mn steel,plate martensite, c)0.7C-5Cr-4Mn steel,strain-induced martensite.

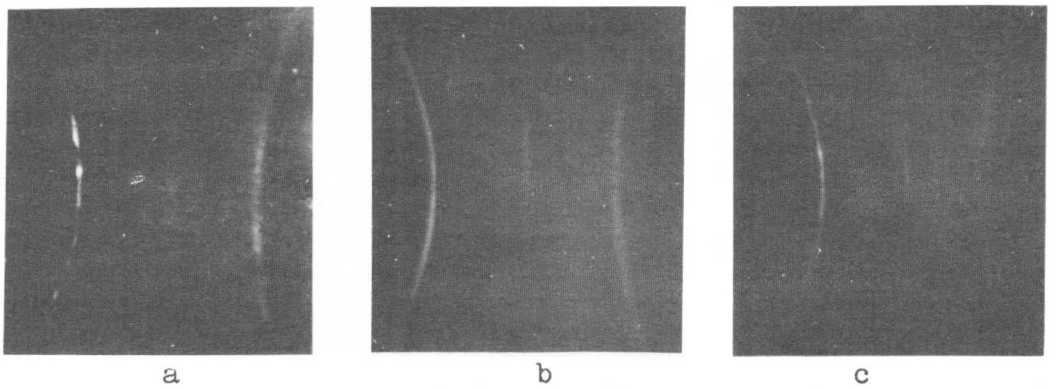

a b c

Fig.2.X-ray topograms of 0.8C-5Cr steel with mixed plate-packet martensite.Cooling in liquid nitrogen. a)quenching from 950°C, b)HTMT,30% deformation at 950°C,immediate cooling, c) HTMT,60% deformation at 950°C,cooling after 2-min holding at 950°C.

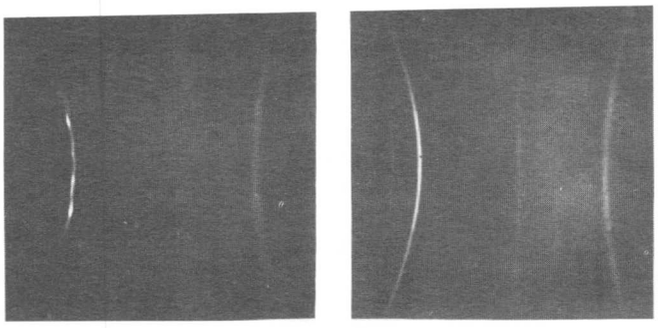

a b

Fig.3.X-ray topograms of I5Cr-5Ni steel. Cooling down to room temperature.Packet martensite. a)quenching from I050°C, b) HTMT,30% deformation at I050°C,immediate cooling.

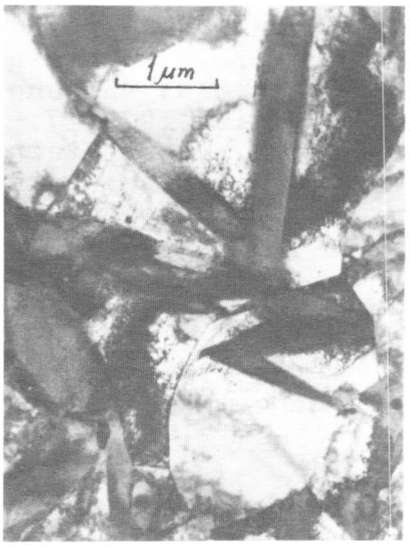

Fig.4.Transmission electron micrograph. The structure of 0.6C-20Ni steel.Cooling in liquid nitrogen.HTMT,60% deformation at I020°C, deformation rate 2 s^{-1}.

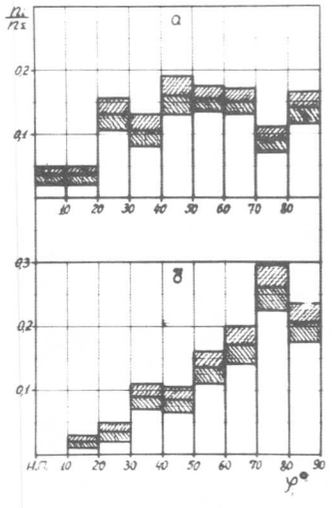

Fig.5.Histograms of distribution of angles between long axes of martensite crystals sections and rolling direction in 0.6C-20Ni steel.Cooling in liquid nitrogen. a)quenching from 950°C, b)HTMT,20% deformation at 950°C,deformation rate 20 s^{-1}.

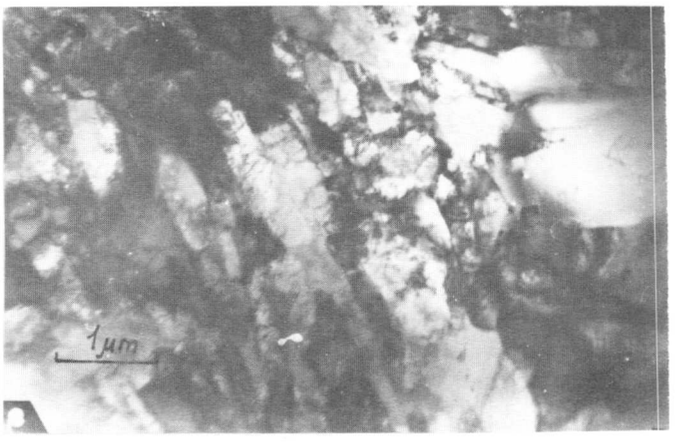

Fig.6.Transmission electron micrograph. The substructure of secondary austenite in I5Cr-8Ni steel. HTMT,30% deformation at I050°C,subzero cooling,repeated heating at 950°C,3 min, cooling down to room temperature.

Shear Transformations in the Laves Phase $TiCr_{\sim 2}$

C. W. Allen and K. C. Liao*

The nucleation and growth of thin lamellae during shear transformation are discussed in terms of glissile partial dislocation dipoles. Transformation of 2H to $6H_2$, 4H and $6H_1$, are considered, simple dislocation models for which are summarized. Estimates of activation energy and critical dipole pair separation for $TiCr_2$ are made for edge and screw dipoles. For 2H→4H, the specific model which is favored energetically is at variance with the limited conclusions deduced from TEM structure images.

I. Introduction

The Laves phases are topologically close packed structures of composition type AB_2 with a ratio of effective sizes of A and B equal 1.225. They may be cubic 3C (C15, $MgCu_2$ structure), hexagonal 2H (C14, $MgZn_2$ structure) or dihexagonal 4H (C36, $MgNi_2$ structure); in some cases, particularly in pseudobinary solutions, other structures also appear [1-4]. A number of Laves phases exhibit polymorphism with attendant polytypic transition structures. In $TiCr_2$, for example, which is 2H above about 1100°C and 3C at lower temperatures when equilibrated, 4, 6 and 12 layer variants have been observed by TEM structure imaging [5] in material in which the 2H→3C transformation is incomplete.

The purpose of this contribution is to examine a particular mechanism for the initiation and early growth period for such transformations, with particular emphasis on the 2H→4H and 2H→6H events observed in $TiCr_{\sim 2}$.

II. Structures and Shear Transformations

A convenient stacking sequence model for the Laves phase structures has been developed [5,6], the layer units being sandwiches each composed of two "slices" of A atoms (Ti) enclosing an almost close packed layer of B atoms (Cr); each layer sandwich is completed by a dispersion of B-atoms within one of the A-atom layers. These basic layer units are then stacked just as in other close-packed structures, as indicated in Fig. 1, in which the layer positions are labelled X, Y and Z. Thus the layer, of which the A-atoms shown in Fig. 1 are a part, has position X.

The stacking sequences of five possible structures thus realized are listed in Table 1 in order of decreasing hexagonal character of near neighbor layers. The characteristics of second and higher order relationships determine the relative internal energies of the various forms and thereby in part the driving force for interpolytypic shear transformations in these systems.

Department of Metallurgical Engineering and Materials Science, University of Notre Dame, Notre Dame, IN 46556. *Present address: National Steel Co., Weirton, W.VA 26062, U.S.A.

Table 1. Fractions of second and third neighbor layers in cubic (C) and hexagonal (H) relationship for several layer structures.

Structure	Stacking Sequence	Second		Third	
		C	H	C	H
2H	XY	0	1.00	0	1.00
$6H_2$	XYZYXY	0.33	0.67	0	1.00
4H	XYXZ	0.50	0.50	0	1.00
RANDOM STACKING SEQUENCE		0.50	0.50	0.50	0.50
$6H_1$	XYXZYZ	0.67	0.33	0.33	0.67
3C	XYZ	1.00	0	1.00	0

In Photo 1 a region of $TiCi_{\sim 2}$ is shown which has partially transformed from 2H to 4H. The transformation proceeds by the glide of arrays of Shockley type partial dislocations which are evidently highly mobile at practical transformation temperatures. In the case of the sample represented in Photo 1, a 15 g button of alloy from which the sample was prepared was cooled quickly on the water cooled hearth of a levitation crucible following an annealing treatment at about 1300°C. While the majority of lamellae of 4H in Photo 1 run completely across the thin observable area, the advancing 4H/2H interface at A has been quenched in. It is likely that such an interface separating a parent phase from a more stable growing product carries some record of birth of the new phase. Indeed detailed analysis of structure images around the steps of lamella A have led to the conclusion [7] that each step is a partial dislocation dipole such as B in Fig. 2a.

In the Laves phases, the most common transition structures seem to be 4H and $6H_1$ [5] and, to a lesser degree, $6H_2$[4], all of which may be formed from 2H by the passage of periodic partial dislocation dipoles, as illustrated in Figure 3. Such transformations thereby may be free of a net macroshear. On the other hand, no shear transformation involving the cubic phase (3C) can involve such dipoles. One expectation drawn from this simple geometrical fact is that transformations from 3C may be more sluggish than those from 2H.

III. Origin of Partial Dislocation Dipoles

The crucial problem, as in the case of more general martensite transformations, is what constitutes the nucleation event. The partial dislocation dipoles described above may arise in two ways depicted in Figure 2: (a) by nucleation from perfect crystal and (b) by dissociation of perfect dislocation dipoles as proposed by Cohen and Olson [8]. A third possibility is that they may be emitted by grain boundaries or similar interfaces, perhaps in a coordinated fashion, as represented in Figure 4.

The feasibility of nucleation of partial dislocation dipoles is most simply examined by considering straight dislocations (Figure 2a). The driving force for the nucleation event is the chemical energy change associated with the transformation, the internal energy (ΔE_{chem}) of which varies linearly with the separation (a) of the dipoles A and B shown in Figure 2a. Thus

$$\Delta E_{chem} = \alpha L a \, \Delta E_v'$$

where α is a geometrical factor which takes account of the fact that the thickness of the transformed lamella is not necessarily just the dipole spacking L, and $\Delta E_v'$ is the internal energy change per unit volume for the particular transformation. The chemical driving force is countered by the net elastic interaction of the four partial dislocations which make up the pair of dipoles. This is represented by the curve ΔE_{elas} in Figure 5. In the isotropic approximation, for edge dislocation dipoles,

$$\Delta E_{el}^{e} = \{Gb^2/[2\pi(1-\nu)]\}\{\ln[(a/a_o)^2[(a_o^2 + L^2)/(a^2 + L^2)]] + 2L^2(a^2 - a_o^2)/[(a_o^2 + L^2)(a^2 + L^2)]\}$$

and for screw dislocation dipoles

$$\Delta E_{el}^{s} = (Gb^2/2\pi)\ln\{(a/a_o)^2 \, [(a_o^2 + L^2)/(a^2 + L^2)]\}$$

in which a_o is the cut off parameter and G, ν and b have their usual meanings.

The net change in energy with dipole separation a is then just $\Delta E = \Delta E_{elas} + \Delta E_{chem}$, and the behavior is clearly characterized by an activation energy ΔE^* and critical separation a*, is shown schematically in Figure 5. For the models depicted in Figure 3, for the transformations of 2H to $6H_2$, 4H and $6H_1$, these critical values are summarized in Table 2. The value of $\Delta E_v(2H \rightarrow 3C)$ is assumed to be -100 cal/gmole (418J/gmole) for the calculation. In all cases the activation energies and critical sizes are much smaller for screw partials than for edge partials because of the differences in elastic energies involved. An activation energy ΔE^* of 0.3×10^{-9} J/m is comparable to approximately 0.3 eV per atom plane threaded by a pair of dipoles. The large difference in activation energy for edge and screw partials suggests that the advancing front of such a lamella would be substantially straight and the assumption of straight dislocations may not be so far fetched as it appears at first glance. On the other hand, a difference in dislocation mobilities may counteract this effect (in LiF, for instance, edge dislocation mobility is an order of magnitude larger than screw dislocation mobility for a wide range of glide forces [9]).

As for the relative values of activation energy for the various processes summarized in Table 2, the most likely processes are $2H \rightarrow 6H_2$ by mechanism (a) (Figure 3) and $2H \rightarrow 4H$ by mechanism (c). While 4H is certainly a common transition structure, there is good evidence [7] that in $TiCr_2$ it forms from 2H by the mechanism depicted in Figure 3(d) for which the activation energy by the dipole nucleation mechanism is three times that for the one of Figure 3(c). In addition it is felt that $6H_1$ appears more

Table 2. Nucleation of straight edge and screw partial dislocation dipoles, initiating several transformations.

				ΔE^* (J/m) x 10^9		a^* (nm)	
Transformation	Fig.3	α	L(nm)	Edge	Screw	Edge	Screw
$2H \rightarrow 6H_2$	(a)	6	0.4	1.24	0.32	3.8	2.3
	(b)	1.2	2.0	3.80	1.56	11.0	6.6
$2H \rightarrow 4H$	(c)	4	0.4	1.24	0.32	3.8	2.3
	(d)	1.33	1.2	3.02	1.10	7.9	4.7
$2H \rightarrow 6H_1$	(e)	2	1.2	2.93	1.05	6.2	3.7

$G = 4 \times 10^{10}$ N/m^2; $|b| = 0.285$ nm; $\Delta E_v(2H \rightarrow 3C) = -418$J/gmole; $\nu = 0.33$

frequently than does $6H_2$ and here too a similar problem exists with the activation energies. $6H_1$ has been observed to form from 4H [5] to limited extent, but this transformation requires the cooperation of groups of three dislocation dipoles if no net macroshear is to result [7]. This has not been examined at all, but does not seem as likely as the more simple direct $2H \rightarrow 6H_1$ transformation. It is clear that further investigation, especially involving good structure imaging techniques, is needed.

Finally, the resultant activation parameters are sensitive to the choice of chemical driving force, of course. For example, if $\Delta E_v(2H \rightarrow 3C)$ were assumed to be -1,000 cal/gmole rather than -100, $\Delta E^*(2H \rightarrow 4H)$ is reduced from 0.32×10^{-9} to 0.15×10^{-9} J/m, and a*, from 2.3 to 1.0 nm, for the screw dipole case, Figure 3(c).

This work was sponsored by the Metallurgy Section, Division of Materials Research, National Science Foundation, U.S.A.

References

[1] Y. Komura, M. Mitarai, I, Nakatani, H. Iba and T. Shimizu, Acta Cryst. B26 (1970) 666.
[2] Y. Komura, A. Nakaue and M. Mitarai, Acta Cryst, B28 (1972) 727.
[3] Y. Kitano, Y. Komura and H. Kajiwara, Trans. JIM, 18 (1977) 39.
[4] Y. Komura and Y. Kitano, Acta Cryst, B33 (1977) 2496.
[5] C. W. Allen, P. Delavignette and S. Amelinckx, Phys. Stat. Sol. (a) 9, (1972) 237.
[6] C. W. Allen, K. C. Liao and A. E. Miller, J. Less-Common Met, 52 (1977) 109.
[7] K. C. Liao and C. W. Allen, submitted to Phys. Stat. Sol. (1979).
[8] G. B. Olson and Morris Cohen, Met. Trans. 7A (1976) 1897.
[9] W. G. Johnson and J. J. Gilman, J. Appl. Phys. 30 (1959) 129.

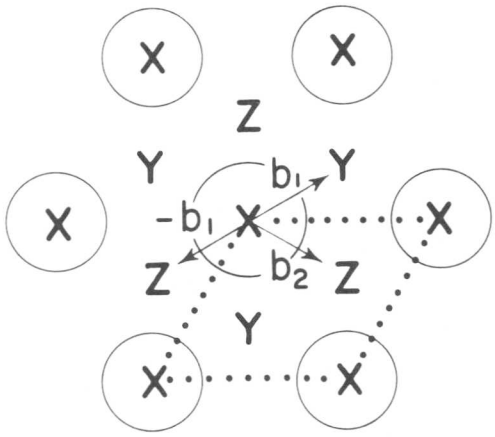

Figure 1. Key positions of A-atom layers in Laves phases AB_2. Burgers vectors of three Shockley partials.

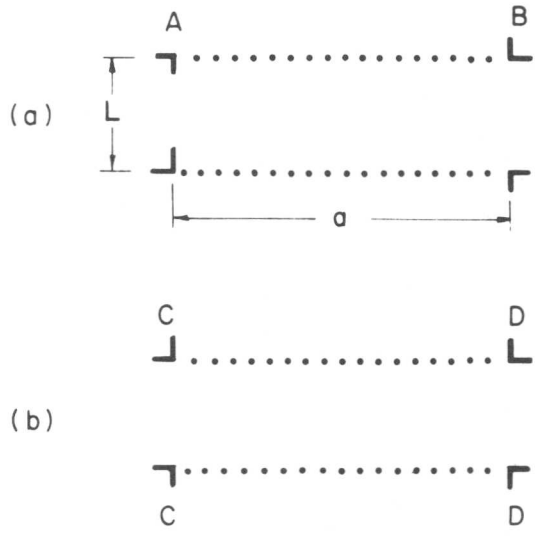

Figure 2. Partial dislocation dipole pairs formed (a) by nucleation and (b) by dissociation of perfect dipole.

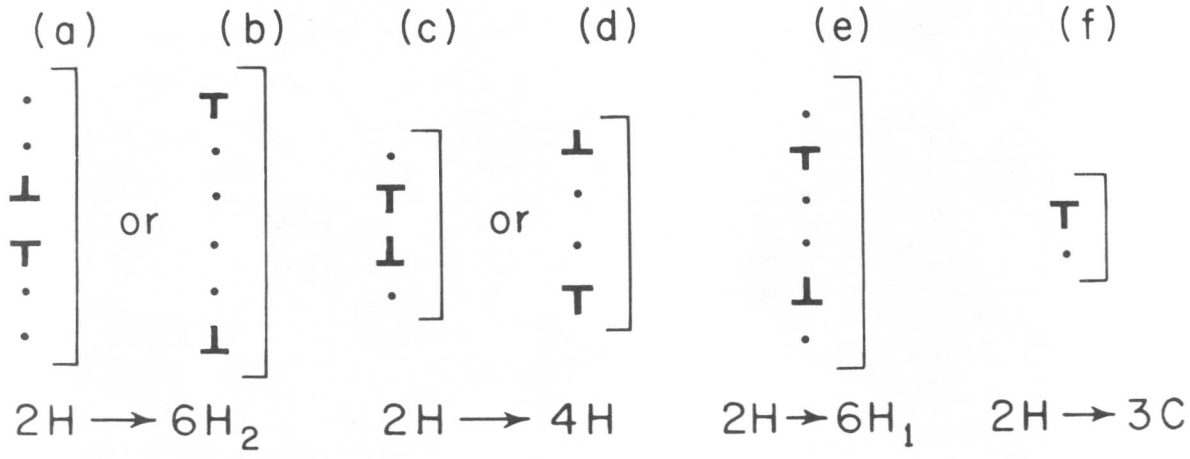

Figure 3. Perodic partial dislocation dipoles passing through 2H to produce 4H and 6H structures (a) - (e). Such a dipole mechanism is not possible for 2H→3C (f).

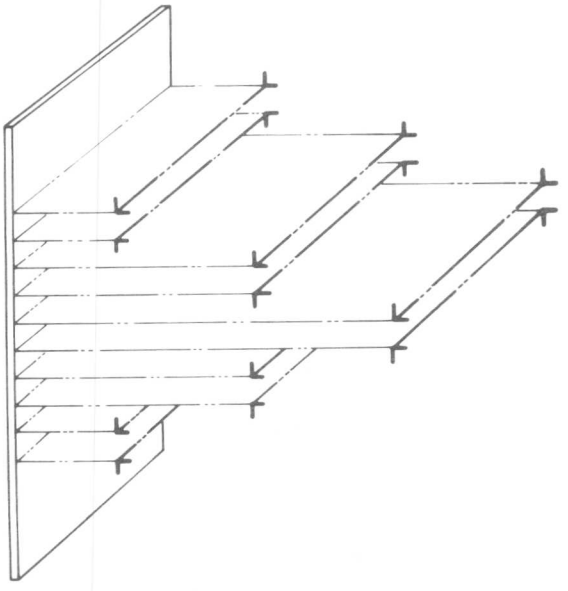

Figure 4. Coordinated emission of partial dislocation dipoles by a boundary.

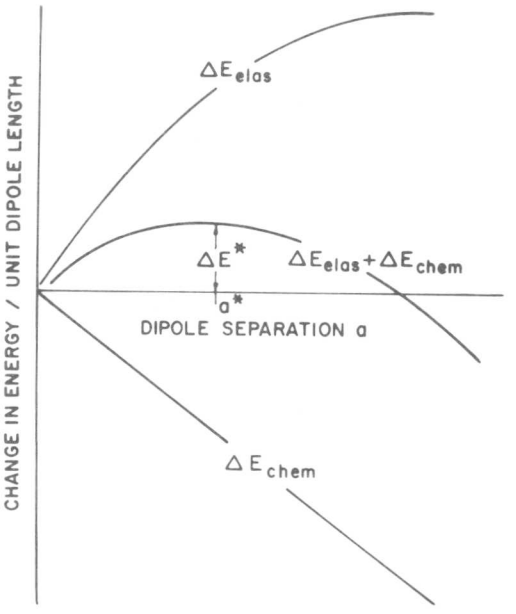

Figure 5. Nucleation of partial dislocation dipole pairs in a shear transformation.

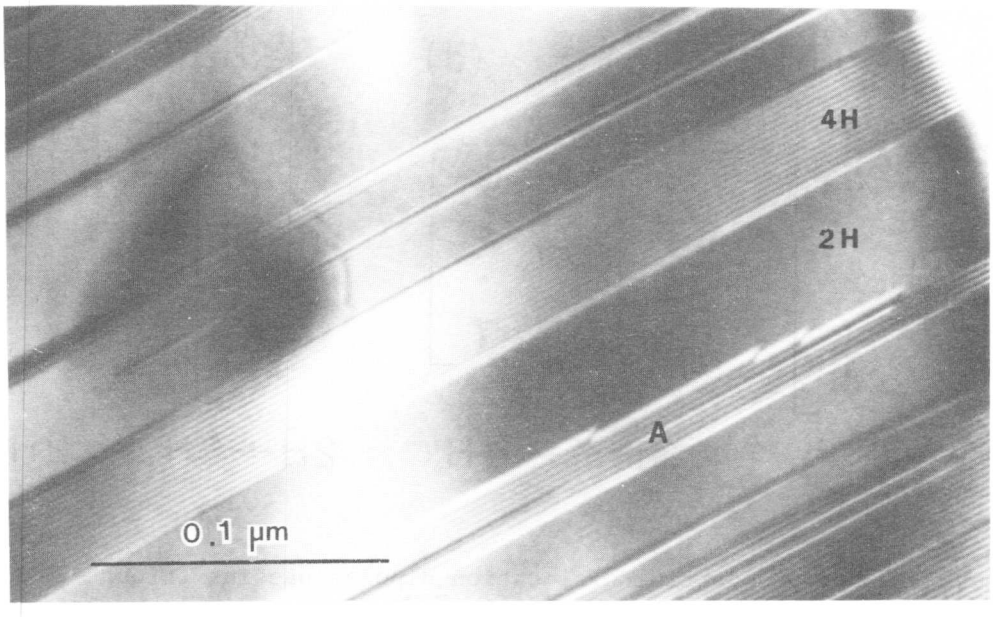

Photo 1. BF electron micrograph of mixed 2H + 4H in $TiCr_{\sim 2}$. Region I: 4H with fringe spacing 1.6 nm; Region II: 2H; Lamella A: 4H growing to the right into 2H. Each step corresponds to a partial dislocation dipole.

The Shape of the Parent-Product Interface for Twinned Martensite

K.M. Knowles and D.A. Smith

Faceted interfaces between parent and twinned martensite have been observed by previous workers in Ti-Mn and TaO_y. In the present work, it is shown that a possible reason why faceted interfaces may occur is that each twin-parent interface plane has the orientation with the minimum Burgers vector content in the zone of the invariant line. This approach is contrasted with previous theoretical work and is shown to give good agreement with available experimental results.

I. Introduction

It has been observed by Hammond and Kelly [1] that the interface between the parent and twinned martensite in titanium-5 wt.% manganese is faceted when the particular variant of the martensite corresponds to the Class A ($\alpha-,\omega+$) solution in the Bowles-MacKenzie theory of martensitic transformations [2]. Twinned martensite consistent with the Class A ($\alpha+,\omega+$) solution (Figure 6 of reference [1]) is also observed but without the interface faceting. Hammond and Kelly explain the faceting in the Class A ($\alpha-,\omega+$) solution on the basis of small scale dilatations which occur at each parent-twin interface to make the interface an invariant plane in an invariant plane strain. This explanation fails to account for the observed absence of faceting in the Class A ($\alpha+,\omega+$) solution; however, Hammond [3] has suggested that it may account for the faceting observed in the Ta(b.c.c.) $\rightarrow$ TaO_y(b.c.c.) transformation [4,5] which can be analysed in terms of martensitic crystallography. Furthermore, his approach suggests that since the macroscopic habit plane and the calculated interface facets do not all lie in the same zone, additional 'steps' or 'ledges' are required in the interfaces (Figure 15 of reference [1]).

A different analysis has been developed by Dunne [6], where he considers the $(3,15,10)_F$ martensites in steels and postulates that one of the facet plane normals may be unrotated, although it should be noted that distortions can occur for such facet planes.

II. The Surface Dislocation Approach

An alternative approach is based on the surface dislocation analysis of interfaces [7,8]. The Burgers vector content $\underline{B}'$ of a boundary can be defined through the formula

$$\underline{B}' = (\underline{\underline{S}}_+^{-1} - \underline{\underline{S}}_-^{-1})\ \underline{p} \qquad (1)$$

where $\underline{p}$ is a vector in the interface and $\underline{\underline{S}}_+$ and $\underline{\underline{S}}_-$ are the deformations carrying the reference lattice, in which $\underline{B}'$ and $\underline{p}$ are expressed, into the final orientations of the (+) and (-) lattices respectively. In applying

University of Oxford, Department of Metallurgy & Science of Materials, Parks Road, Oxford OX1 3PH, England.

this formula to martensitic transformations, we can choose the (+) lattice to be the reference lattice and $\underline{\underline{S}}$ to be an invariant line strain $\underline{\underline{L}}$, so that equation (1) becomes

$$\underline{B}' = (\underline{\underline{I}} - \underline{\underline{L}}^{-1})\ \underline{p} \tag{2}$$

If $\underline{p}$ is the invariant line $\underline{B}' = 0$, so that no dislocations are needed normal to $\underline{p}$, and thus, if an interface contains the invariant line, all dislocations in the interface can be parallel to the invariant line. Therefore, to define the Burgers vector content of such an interface, a vector $\underline{p}$ perpendicular to the invariant line and in the interface is chosen and put into equation (2). Consequently, if the reference lattice is the parent lattice, the Burgers vector content of the interface represented in Figure 1 by the line $\vec{AB}$ is:

$$\underline{B}_1' = (\underline{\underline{I}} - \underline{\underline{L}}_1^{-1})\ \vec{AB} \tag{3}$$

and a similar expression

$$\underline{B}_2' = (\underline{\underline{I}} - \underline{\underline{L}}_2^{-1})\ \vec{BC} \tag{4}$$

holds for the boundary represented by $\vec{BC}$. Since the macroscopic habit plane is assumed to be the invariant plane in an invariant plane strain, it follows that $\underline{B}_1'$ and $\underline{B}_2'$ are equal in magnitude and opposite in sign.

To assess the variation of $|\underline{B}_1'|$ and $|\underline{B}_2'|$ with facet orientation, it is convenient to define a new axis system designated by the subscript i, where a unit vector parallel to the invariant line $\underline{\ell}_{INV}$ is the z-axis, so that any unit vector normal to $\underline{\ell}_{INV}$ has the form $[\cos\theta, \sin\theta, 0]_i$. Thus, if the thickness of a pair of martensitic twins is 't', and the volume fraction of the larger twin is x, the Burgers vector content $\underline{B}_{2i}'$ of the interface represented by $\vec{BC}$ in the i-axis system satisfies the equation

$$\underline{B} = \frac{\underline{B}_{2i}'}{t} = \frac{x}{\sin(\theta-\theta_T)} \left(\underline{\underline{I}} - \underline{\underline{L}}_2^{-1}\right)_i \begin{bmatrix} \cos\theta \\ \sin\theta \\ 0 \end{bmatrix}_i \tag{5}$$

and again a similar expression holds for the Burgers vector content of the interface represented by $\vec{AB}$. The function $|\underline{B}|$ can then be plotted as a function of the angle θ for a given correspondence between the parent and the martensite twin; this determines $\underline{\underline{L}}_1$ in the reference (parent) lattice and hence by appropriate matrix transformation in the i-axis system. Figures 2-4 show $|\underline{B}|$ v θ plots for the Ti-Mn Class A ($\alpha-,\omega+$) solution, the TiMn Class A ($\alpha+,\omega+$) solution and the Ta → TaO_y case respectively. The lattice parameters of the parent and martensite phases for these systems are shown in Tables 1 and 2.

III. Results and Discussion

If we consider Figure 2 first, we notice that at the orientation corresponding to the macroscopic habit plane, denoted by θ_H, the magnitudes of the Burgers vector contents are both 0.064t; faceting can reduce the magnitudes to 0.420 of this value. The orientations of the

facets with minimum Burgers vector contents, denoted by θ_L and θ_S, correspond well to the experimentally observed facet orientations (Table 1).

The corresponding graph for the Ti-Mn Class A ($\alpha+,\omega+$) solution (Figure 3) shows that the magnitudes of the Burgers vector contents at the macroscopic habit plane are within 0.2% of their minimum values, and faceting is not expected and was not observed by Hammond and Kelly (Figure 6 of reference [1]). Figure 4, where the Ta $\rightarrow$ TaO_y transformation is studied, shows that the criterion of each twin-parent interface having the orientation with the minimum Burgers vector content again gives good agreement with experimental results [3,4,5].

Dunne's approach (Table 3 and reference [6]) when applied to Ti-Mn and the Ta $\rightarrow$ TaO_y transformation fails to predict the observed orientations of the facets, since none of the unrotated normals lies near the relevant experimentally determined orientations, and it seems doubtful that this approach has general applicability.

Hammond and Kelly's approach suggests that in general the facets will have 'steps' or 'ledges'; current experimental work on Ti-Mn and Ni-Ti in conjunction with the present theoretical work has not detected such ledges or steps and shows that the facets do indeed lie in the zone of the invariant line.

It is thus concluded that the surface dislocation approach gives the best agreement with the available experimental results although its physical basis is not yet worked out fully.

Acknowledgements

The authors would like to thank Professor Sir Peter Hirsch F.R.S. for the provision of laboratory facilities, Professor J.W. Christian F.R.S. for useful discussions, and one of us (KMK) would like to thank the Science Research Council for financial support.

REFERENCES

[1] C. Hammond and P.M. Kelly, 1969, Acta Met., 17, 869.
[2] J.K. MacKenzie and J.S. Bowles, 1957, Acta Met., 5, 137.
[3] C. Hammond, 1977, Scripta Met., 11, 857.
[4] J. Van Landuyt and C.M. Wayman, 1968, Acta Met., 16, 803.
[5] C.M. Wayman and J. Van Landuyt, 1968, Acta Met., 16, 815.
[6] D.P. Dunne, 1977, Scripta Met., 11, 1017.
[7] K.M. Knowles and D.A. Smith, 1979, Institution of Metallurgists Conference on Phase Transformations, York, U.K.
[8] R. Bullough and B.I. Bilby, 1956, Proc.Phys.Soc. B, 69, 1276.
[9] D.S. Lieberman, M.S. Wechsler and T.A. Read, 1955, J.Appl.Phys., 26, 473.

Table 1 - Comparison of Experimental and Theoretical Results for Ti-Mn

Input lattice parameters (1) Parent phase (b.c.c.) a_o = 3.259Å
(2) Martensite phase (h.c.p.) a = 2.950Å
c = 4.680Å

Class A ($\alpha-,\omega+$) solution with the dilatation parameter taken to be unity for the theoretical results from this paper. Hammond and Kelly's results [1] have been permuted to allow for a WLR formalism as used for the Au-Cd cubic to orthorhombic phase transformation [9]. The subscript c pertains to the b.c.c. phase of Ti-Mn.

	Experimental [1]	Theoretical (this paper)	Theoretical [1]
Fraction of larger twin, x	0.75 - 0.80	0.744	0.744
Twin plane, normal n'_T	-	$\begin{pmatrix} 0.029 \\ -0.710 \\ 0.704 \end{pmatrix}_c$	-
Invariant line, $\underline{\ell}_{INV}$	-	$\begin{bmatrix} 0.154 \\ 0.699 \\ 0.699 \end{bmatrix}_c$	-
Larger twin-parent facet, normal n'_L	$\begin{pmatrix} \frac{3}{4} \\ 3 \end{pmatrix}_c$	$\begin{pmatrix} 0.522 \\ -0.658 \\ 0.543 \end{pmatrix}_c$	$\begin{pmatrix} 0.489 \\ -0.722 \\ 0.489 \end{pmatrix}_c$
Smaller twin-parent facet, normal n'_S	$\begin{pmatrix} 3 \\ \frac{3}{4} \\ 4 \end{pmatrix}_c$	$\begin{pmatrix} 0.578 \\ 0.510 \\ -0.637 \end{pmatrix}_c$	$\begin{pmatrix} 0.489 \\ 0.489 \\ -0.722 \end{pmatrix}_c$
Angle between n'_L (EXP) and n'_L (THEOR)	-	2.3°	2.9°
Angle between n'_S (EXP) and n'_S (THEOR)	-	4.6°	2.9°

Table 2 - Comparison of Experimental and Theoretical Results for the $Ta \rightarrow TaO_y$ Transformation

Input lattice parameters (1) Parent phase (b.c.c.) $a_o = 3.322\text{Å}$
(2) Martensite phase (b.c.o.) $a = 3.271\text{Å}$
$b = 3.201\text{Å}$
$c = 3.610\text{Å}$

Class B solution with the dilatation parameter taken to be unity for the theoretical results from this paper. Van Languyt and Wayman's results [4,5] have been permuted to allow for a WLR formalism as used for the Au-Cd cubic to orthorhombic phase transformation [9]. The subscript c pertains to the b.c.c. phase.

	Experimental [4,5]	Theoretical (this paper)	Theoretical [3]
Fraction of larger twin, x	0.84 - 0.88	0.843	-
Twin plane, normal n'_T	derived from $(0\bar{1}1)_c$	$\begin{pmatrix} 0.033 \\ -0.682 \\ 0.731 \end{pmatrix}_c$	-
Invariant line ℓ_{INV}	-	$\begin{bmatrix} -0.716 \\ 0.494 \\ 0.494 \end{bmatrix}_c$	-
Larger twin-parent facet, normal n'_L	-	$\begin{pmatrix} 0.519 \\ 0.849 \\ -0.096 \end{pmatrix}_c$	$\begin{pmatrix} 0.403 \\ 0.915 \\ 0 \end{pmatrix}_c$
Smaller twin-parent facet, normal n'_S	-	$\begin{pmatrix} 0.656 \\ 0.234 \\ 0.717 \end{pmatrix}_c$	$\begin{pmatrix} 0.403 \\ 0 \\ 0.915 \end{pmatrix}_c$
Macroscopic habit plane normal n'_H	$\begin{pmatrix} 2 \\ 3 \\ 0 \end{pmatrix}_c$	$\begin{pmatrix} 0.575 \\ 0.818 \\ 0.016 \end{pmatrix}_c$	$\begin{pmatrix} 0.575 \\ 0.818 \\ 0.016 \end{pmatrix}_c$
Azimuthal angle between n'_H and n'_L in the zone $[\bar{1}11]_c$	6° - 7°	7.4°	7.6°
Azimuthal angle between n'_T and n'_L in the zone $[\bar{1}11]_c$	47.5° - 48.5°	50.3°	50.1°

Table 3 - Analysis of Dunne [6] applied to the Ti-Mn and the Ta→ TaO_y Transformations

System	Invariant line matrix	Eigenvalues	Unrotated planes
TiMn Class A ($\alpha-,\omega+$) solution	$\underline{\underline{L}}_1$	1.047	(0.988,-0.112,-0.106)$_c$
		1.000	(-0.657, 0.664,-0.356)$_c$
		0.974	(-0.382, 0.694,-0.610)$_c$
TiMn Class A ($\alpha+,\omega+$) solution	$\underline{\underline{L}}_2$	1.102	(0.544, 0.099, 0.833)$_c$
		1.000	(-0.657, 0.356, 0.663)$_c$
		0.926	(0.400, 0.893,-0.205)$_c$
Ta → TaO_y	$\underline{\underline{L}}_2$	1.052	(0.461, 0.865,-0.196)$_c$
		1.000	(0.664, 0.528,-0.528)$_c$
		0.980	(0.652, 0.221, 0.725)$_c$

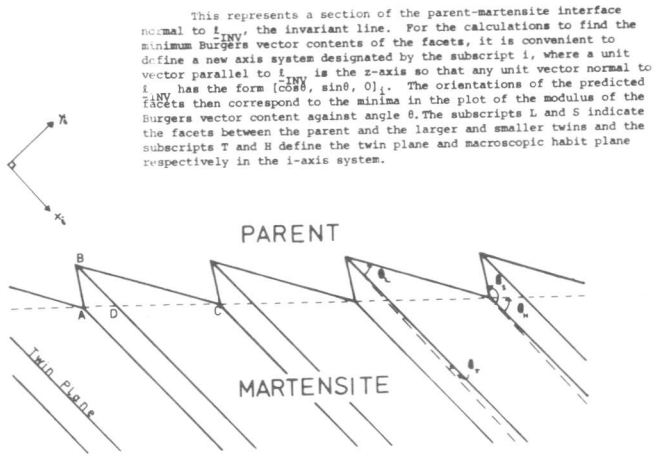

Figure 1

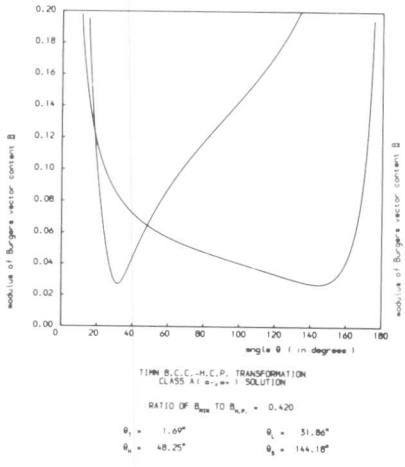

Figure 2

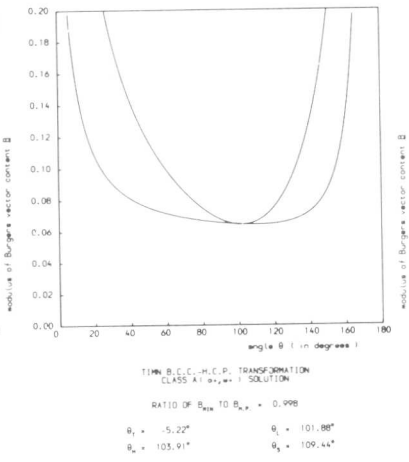

Figure 3

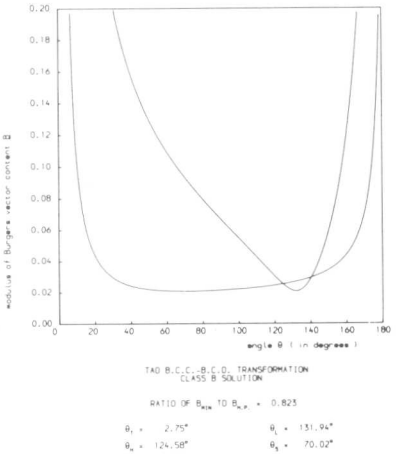

Figure 4

In Situ Observations of Diffusionless Transformations in NiTi

G.M. Michal* and R. Sinclair*

In situ heat treatments of NiTi were carried out in a Philips EM400 electron microscope. Because of the excellent vacuum, a single area of the specimen was able to be studied through several temperature cycles between austenite and martensite without noticable surface contamination. For the area of the foil observed, the M_s and M_f temperatures were found to be 55.5 and 38.5°C with A_s and A_f being 79 and 99°C. These temperatures were in close agreement with the bulk M_s temperature of 62°C and typical hysteresis behavior of bulk material. No premartensitic phase was observed. However diffraction effects possible due to large amplitde lattice vibrations in the austenite were clearly evident. Arguments are presented to support the contention that the transformations observed are characteristic of the bulk material.

I. Introduction

The alloy NiTi of nominal 50 at% composition has been the subject of numerous structural investigations since the discovery of its shape memory property. Both the following aspects of NiTi have given impetus to most of this research. Firstly of the dozen or so known alloys that exhibit the shape memory effect NiTi posesses the best combination of physical and mechanical properties. NiTi thus warrants investigation of its structure as a starting point for characterization and an understanding of its macroscopic memory properties. Secondly NiTi displays several solid state phase transformations that have been the subject of considerable controversy and interest as examples of the path of collapse of a β phase alloy into a closer packed structure. Almost every aspect of the transformation behavior of NiTi from eutectoid decomposition, the premartensitic lattice instability to the structure(s) of the low temperature martensite phase is under debate in the literature. The present research aims to clarify some of these conflicting ideas.

Most of the fundamental questions about the structures and mechanisms involved with the system remain ambiguous due to different observations and interpretations by various investigators [1]. The premise for the present investigation is with the advent of the present generation of high resolution electron microscopes it is possible to observe the system in ways more amenable to the determination of many of these fundamental questions. The specific object is to gain information concerning the mechanism of the memory effect by applying lattice imaging [2], 2½ D microscopy [3], and in situ heating and cooling experiments in conjunction with high resolution imaging. Specifically this paper is presented to show initial work on an in situ study of the transformation behavior of NiTi, as a basis for further more detailed experiments.

*Department of Materials Science and Engineering, Stanford University, Stanford, California 94305.

II. Experimental Procedure

The alloy used in this investigation was 50.0±0.1 at% Ni, balance Ti. As a check of the composition after heat treatment the bulk M_s temperature was determined to be 62°C. The hot rolled strip was annealed at 900°C for 5 minutes under a vacuum of 10^{-7} torr then water quenched by allowing water to enter the furnace tube. The alloy was saturated with oxygen at room temperature as evidenced by the presence of small amounts of Ti_4Ni_2O precipitates observed in the TEM. Specimens were spark-cut and jet-electropolished in a 3:1 by volume methanol: nitric acid electrolyte at -55°C and about 20V. Observations were carried out in a Philips EM400 equipped with a "cooling" stage which allowed temperatures of the specimen to vary between -170 and +140°C.

III. Results and Discussion

The results of cyclic heating and cooling the NiTi alloy from 23 to 115°C are presented in Figures 1 through 3. In all cases the heating and cooling rates were rather slow, i.e. 20°C/hr., in order to reduce thermal instabilities in the specimen which would reduce the image quality. The vacuum in the microscope was of a high enough quality that all of the photos in this paper were taken from the same area of the specimen which experienced over 10 hrs. of beam exposure without signs of surface contamination. It was possible to revert the fully martensitic structure at room temperature to the B2 high temperature phase at less than 100°C in all but the thinnest areas of the specimen, apart from a few very stable plates of martensite which resisted transformation (along with the thinnest areas) even at 137°C, the highest temperature obtained. As observed by others, the martensite which formed upong cooling invariably started to grow in the thicker parts of the foil moving towards the thinner areas [4,5].

Figure 1a, taken at 115°C, is a $[111]_{B2}$ zone axis SAD exhibiting the diffuse scattering found by many investigators. Upon slow cooling the first detectable spots at $1/3(110)_{B2}$ occurred at 74°C. These spots appeared to intensify upon cooling but not upon isothermal ageing. This gives credibility to the interpretation that these extra spots are due to a lattice vibration mode as opposed to an ordering phenomena. Figure 1b shows a symmetrical pattern containing the $1/3(110)_{B2}$ reflections at 59°C where the spots have obtained appreciable intensity. Figure 1c shows the onset of the $\frac{1}{2}(110)_{B2}$ reflections that were considered by Purdy et al. [6] as evidence for a premartensitic phase with rhombohedral symmetry. The bright field image of the area used for this diffraction pattern is shown in Figure 2c. This new structure which formed in a burst at 55.5°C can be interpreted as two variants of the monoclinic martensite phase observed by most investigators [7]. It is noted that the $1/3(110)_{B2}$ reflections are still present in the diffraction pattern from the untransformed austenite region in Figure 2c. The area completed transformation at 38.5°C. Figure 1d is a room temperature pattern of the completely transformed area. The $1/3(110)_{B2}$ reflections have completely disappeared whilst the $\frac{1}{2}(110)_{B2}$ reflections have intensified.

Figure 2 is a series of bright field images showing the transformation behavior upon cooling and heating. The stable martensite plate in

the lower right corner of each photo served as a convenient positional datum. Figure 2a is the room temperature martensitic structure. The curved-banded morphology is a result of previous temperature cycling and is not characteristic of the linear primary-quenched structure. The morphology is similar to the wavy martensite observed by Zijlstra et al. [5]. Figure 2b is above A_f and the major contrast is a bend center indicating a $[111]_{B2}$ orientation. Along the bend contours a striation contrast is observable which also has been noted by previous investigators [6,8]. Figure 2c is at M_s and shows the very curved interface generated between the martensite and B2 phases. Figure 2d is the same area at room temperature again. The most salient feature of the micrograph is that the arrangement of plates is not exactly the same as in Figure 2a. Thus the growth of the martensite here is not completely reversible as noted by Zijlstra et al. [5]. Upon slow heating, the austenite was first noted to form at 79°C starting from the upper left corner of Figure 2e. Again the transformation is discontinuous and the martensite does not revert back to austenite along exactly the same path as it initially formed. At high temperature the area always appears as a single austenite grain in the same $[111]_{B2}$ orientation independently of the initial martensite morphology. This observation demonstrates the concept that martensite variants from an austenite grain have only one crystallographic path back to form austenite again. On repeated cycling, all temperatures are completely reproducible for this specimen area.

Figure 3 is a dark field from one of the $\frac{1}{2}(110)_{B2}$ spots showing the fine structure of the martensite. The corresponding diffraction pattern, which is correctly oriented with respect to the image, shows that the boundary planes are perpendicular to the streaks passing through $\{010\}_M$ planes (using the lattice parameters of Hehemann et al. [8]). Figure 3 corresponds closely to the morphology and orientation relations found by Gupta et al. [7] in bulk material heat treated at 200°C before thinning.

IV Summary

This paper is intended as an example of the potential for in situ studies of NiTi using a cooling/heating stage. The major advancement is that with a much cleaner vacuum an area can be studied almost indefinitely eliminating problems with surface contamination that plagued previous investigations [6,9]. The premartensitic phase postulated by Purdy et. al. [6] was not found. The formation of martensite was found not to be ideally reversible, although the final austenite morphology and orientation is always reproduced. Finally, the similarity between striated-curved martensite plates observed by Gupta et al. [7] in bulk material aged at low temperatures and the structures observed by heat treatment of thinned material in the microscope supports the argument that these results are not thinned-foil phenomena, but are representative of bulk behavior Thus further detailed investigation of the transformation by high resolution TEM examination is feasible. It may be of some significance that the cycled morphology and primary-quenched microstructure are so different and this aspect is being studied further.

The help of Raychem Corp. who supplied the alloy, is gratefully acknowledged. Financial support has been provided by the National Science Foundation through the Center for Materials Research, Stanford University.

References

[1] C.M. Jackson, H.J. Wagner and R.J. Wasilewski, 55-Nitinol--The Alloy with a Memory, its Physical Metallurgy, Properties and Applications, NASA Report SP 5110 (1972).

[2] R. Sinclair, J. Physique 38, C7-453 (1977).

[3] G.M. Michal, Proc. 9th International Congress on Electron Microscopy, Vol. 1, p. 610 (1978).

[4] K. Otsuka, T. Sawamura and K. Shimizu, Physica Stat. Sol. 5, 457 (1971).

[5] S.R. Zijlstra, J.B. Beijer and J.A. Klostermann, J. Mat. Sci. 9, 145 (1974).

[6] K. Chandra and G.R. Purdy, J. Appl. Phys. 39, 2176 (1968).

[7] S.P. Gupta and A.A. Johnson, Trans. Jap. Inst. Metals 14, 292 (1973).

[8] G.D. Sandrock, A.J. Perkins and R.F. Hehemann, Met. Trans. 2, 2769 (1971).

[9] J. Perkins, Ph.D. Thesis, Case Western Reserve U. (1969).

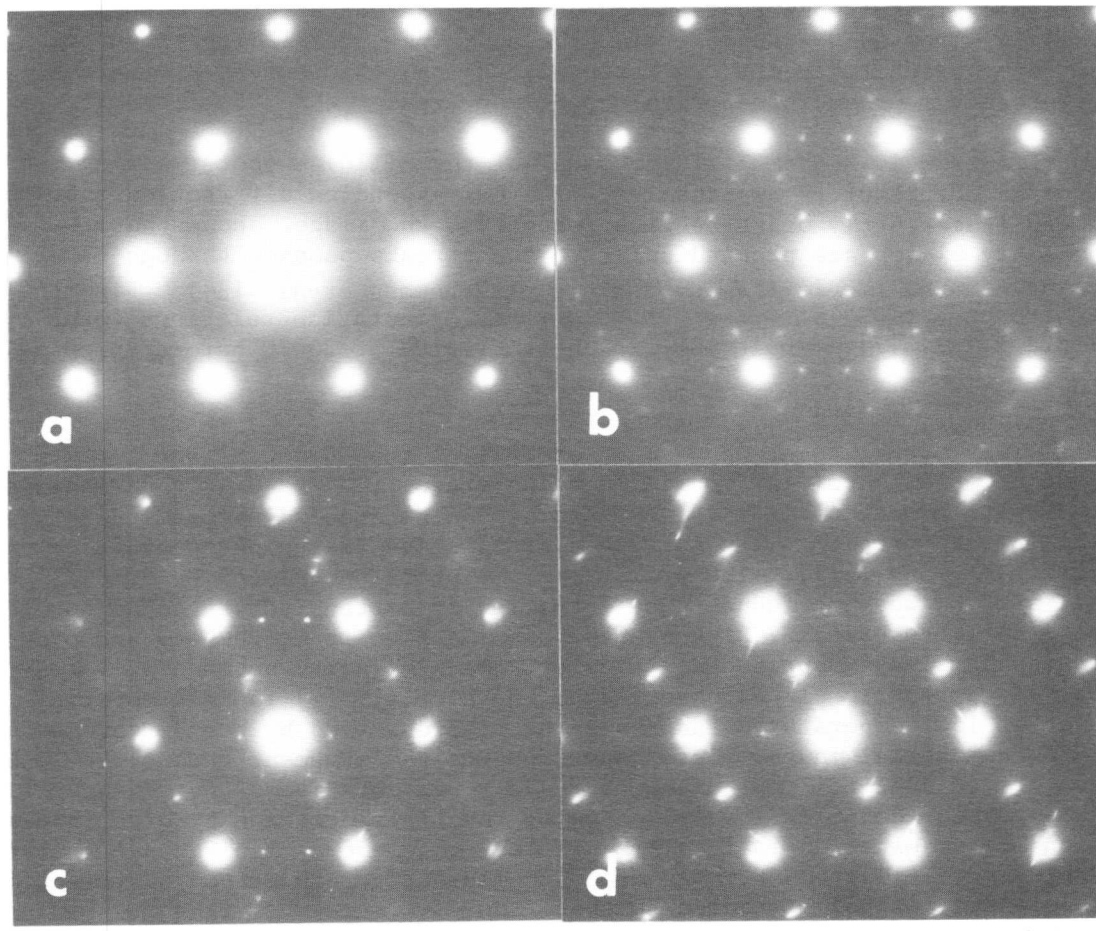

Figure 1 Selected area diffraction patterns from the area depicted in Figure 2 showing the various diffraction effects occurring upon cooling the B2 phase to form martensite: (a) T=115°C; (c) T=M_S=55.5°C (d) T=23°C.

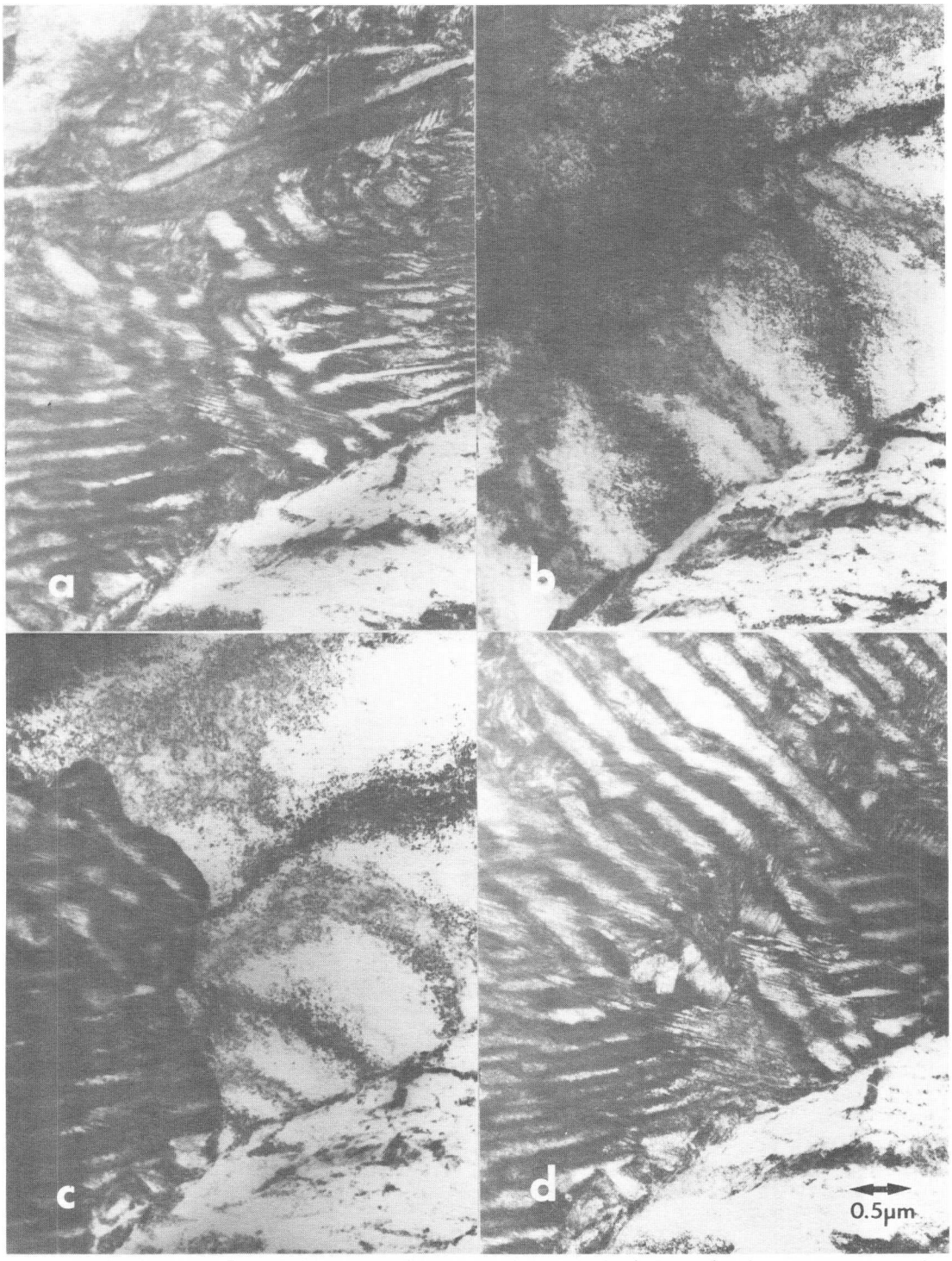

Figure 2 Bright field images showing the morphological changes occurring upon temperature cycling between the B2 phase and the martensite: (a) T= 23°C; (b) T=115°C; (c) T=M_s=55.5°C; (d) T=23°C; (e) T=94°C; (f) T=A_f=99°C.

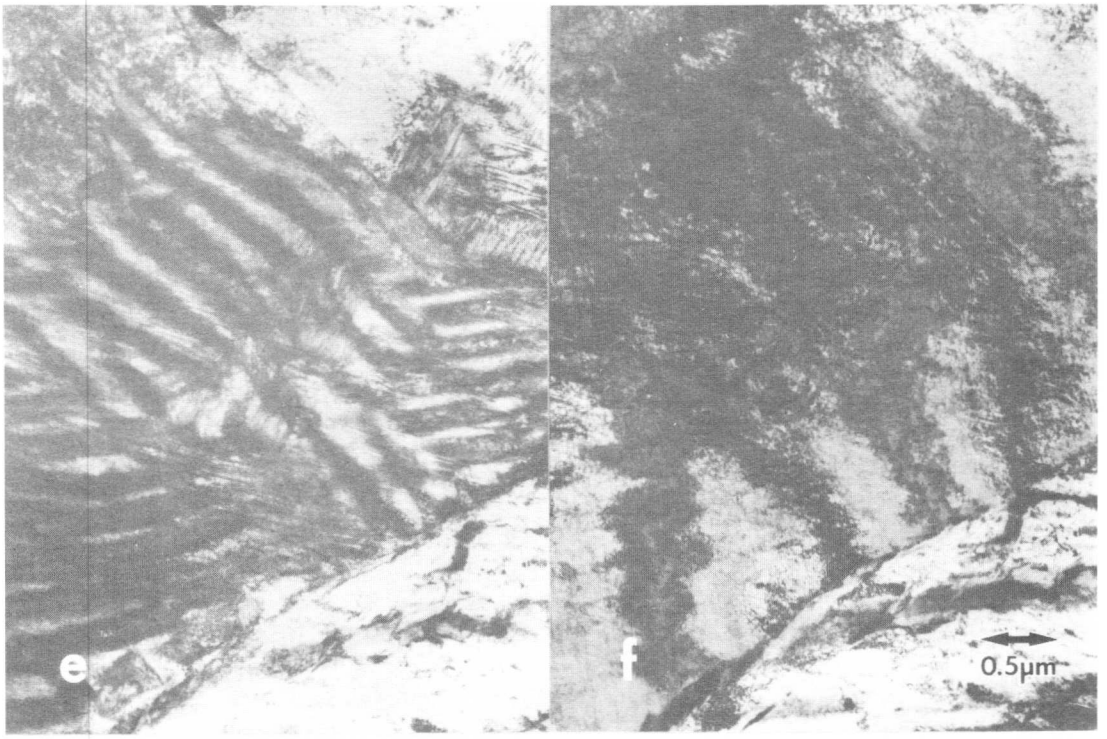

Figure 2 continued.

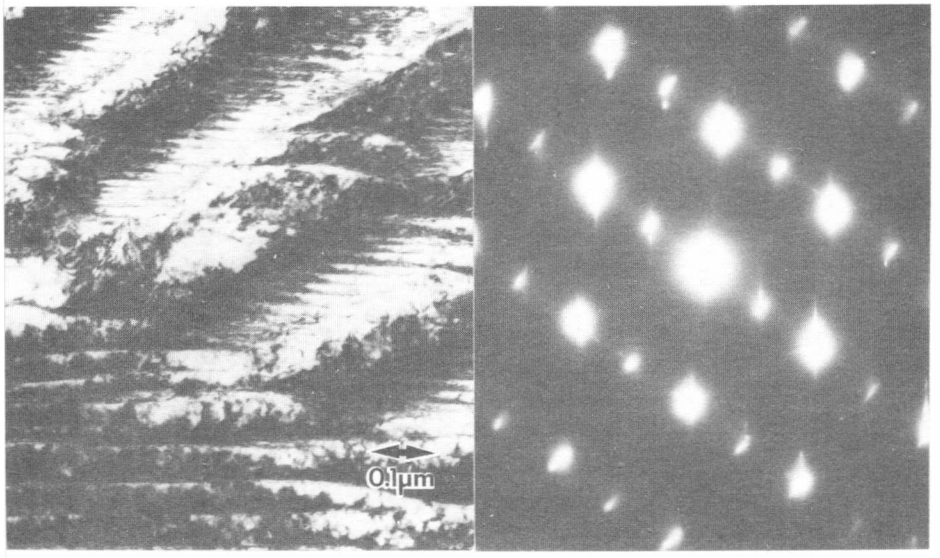

Figure 3 Dark field image of the fine structure of the martensite using a $\frac{1}{2}(110)_{B2}$ $\bar{g}$. The corresponding SAD is correctly oriented with respect to the image and shows that the boundary are perpendicular to streaks through $\bar{g}_{\{010\}M'}$

Lattice Image Study of the Deformation-Induced Transformation from 9R to 3R Martensite

M. Fukamachi and S. Kajiwara

The sequence of structural change in the transformation from the 9R martensite to the 3R martensite are studied by means of lattice image technique using Cu-Zn-Si alloy. The 9R martensite transforms into the 3R martensite in a form of thin plate of twinned structure with an application of slight plastic deformation. With further increment of plastic deformation, the twin plates with favourable orientation grow at the expense of the twin plates with unfavourable orientation, and the simple 3R martensite without twin is formed. The martensitic transformation at the twin-type $(11\bar{4})_{9R}$ grain boundary is also examined. A rotation of grain takes place during the transformation, and the thin plates of the twinned 3R martensite become continuous across the grain boundary. With further increment of plastic deformation, the plates with favourable orientation grow and whole region changes into a single grain of 3R martensite.

I. Introduction

9R martensite transforms into other crystal structures by an application of plastic deformation [1-3]. Extensive studies on this kind of transformation have been carried out on Cu-Al alloys [2-4]. The 9R martensite of the Cu-Al alloy transforms into the fcc, the hcp and the mixture of fcc and hcp structures in accordance with the variation of chemical composition of the alloy. These crystals have the close-packed structures which are expressed by models constructed by stacking the planes of closely-packed hard spheres in respective sequences. In addition to these crystals, the 9R martensite with various amount of stacking faults and several kinds of crystals which are produced by the changes in the stacking sequences of close-packed planes are found in the deformed alloy with the X-ray and the electron diffraction studies.

The 9R martensite transforms into the 3R martensite by introduction of glide on the close-packed planes in a regular manner. It is not clear whether the 9R martensite transforms directly into the 3R martensite or there are some intermediate stages of arrangement of atoms during the transformation. The purpose of this study is to examine the structures of the 9R and the 3R martensites with the electron microscopy and to investigate the sequence of structural change in the 9R to 3R martensitic transformation.

II. Experimental Procedures

The material used for this study is Cu-33.40Zn-1.58Si (at.%) alloy in a form of plate 0.5 mm thick. The 9R martensite was obtained by quenching the alloy from 1153 K. The quenched specimens were plastically deformed in tension to give the 9R to 3R martensitic trans-

National Research Institute for Metals, 2-3-12, Nakameguro, Meguro-ku, Tokyo, Japan 153

formation. Thin foils for the electron microscope observation were prepared by an electropolishing in a solution of phosphoric acid and water. The thin foils were examined in a Hitachi H-500 electron microscope operated at 125 kV fitted with a tilting stage. The diffracted beams of $[1\bar{1}0]_{9R}$ zone, i.e., $(11\bar{1})$, $(11\bar{4})$ and $(11\bar{7})$ spots,were allowed through the objective aperture to form the lattice image with the illumination tilted such that the $(11\bar{4})$ beam was coincided with the optical axis of the microscope.

III. Results

The as-quenched martensite and the deformation-induced martensite have the modified 9R (monoclinic, a = 0.436, b = 0.259, c = 1.881 nm, $\beta = 89°$) and the fct (a = 0.366, c = 0.359 nm) structures. However, the 9R and the fcc structures are good approximation to represent the structures of martensites. In this report, the as-quenched and the deformation-induced martensites are represented simply as the 9R and the 3R martensites, respectively.

(1) 9R to 3R martensitic transformation in the interior of grain

General features of the sequence of structural change in the 9R to 3R martensitic transformation were observed at the low magnification and the results are reproduced in Fig.1. At the extension of two per cent, about eighty per cent of grains transform from the 9R martensite (Fig.1a) to the 3R martensite in a form of thin plate of twinned structure (Fig.1b) and twenty per cent of grains remain as the 9R martensite with many stacking faults. When the plastic deformation increases to the extension of ten per cent, about fifty per cent of grains have the simple 3R martensite without twin (Fig.1c), forty per cent of grains have the twinned structure of 3R martensite and ten per cent of grains are the 9R martensite with many stacking faults.

Results of the observation of the lattice image as well as the selected-area diffraction pattern are summarized in Fig.2. The diffraction spots of $[1\bar{1}0]_{9R}$ zone {or $[10\bar{1}]_{3R}$ zone} and the lattice image are shown at the right side and at the left side of the figure, respectively. Six kinds of grains are found in the specimens. These are denoted by letters a,b,c,d,e and f in the figure. In addition to the 9R martensite of as-quenched specimen (type a) and the 3R martensites with (type e) and without (type f) twin of deformed specimen, there are three kinds of grains (type b,c,d) are found in the deformed specimens, which were classified above as the 9R martensite with many stacking faults. Lattice images with good contrast are obtained in the a-type and the b-type grains. The spacing of lattice fringes is 0.63 nm and is three times as large as the interplanner spacing of the close-packed planes to an accuracy of experiment. The diffraction spot $11\bar{1}$ of as-quenched grain moves to 11 $\overline{1.2}$ in the b-type grain. In the c-type grain of deformed specimen (Fig.2c), the contrast of lattice image becomes poor and the spacing of fringes is 0.72 - 0.76 nm. The diffraction spot $11\bar{1}_{9R}$ in the a-type grain of as-quenched specimen moves to 11 $\overline{1.4}$ and the diffraction spot $11\bar{7}_{9R}$ becomes obscure. The separation between the 11 $\overline{1.4}$ and the $11\bar{4}$ spots agree with the spacing of fringes of lattice image. In the d-type grain which are observed only in the specimen extended to ten per cent, the $11\bar{4}_{9R}$ spot is observed between the $11\bar{3}$ and the $11\bar{6}$ spots of twinned martensite (in the notation of the 9R martensite). The bright fringes observed in

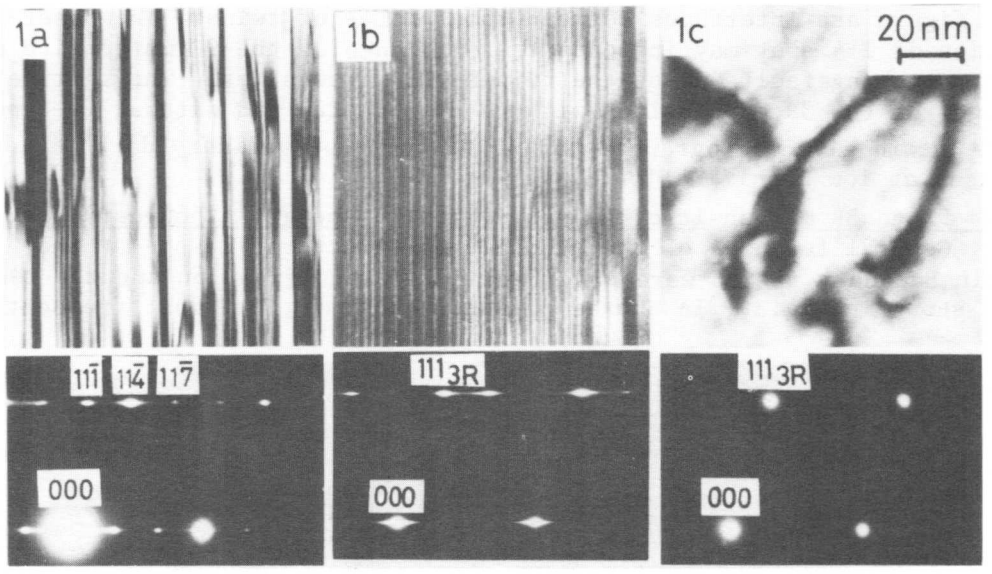

Fig.1 Interference micrographs of Cu-Zn-Si alloy at low magnification taken with the spots of $[1\bar{1}0]_{9R}$ and $[10\bar{1}]_{3R}$ zones for the 9R and the 3R martensites, respectively.

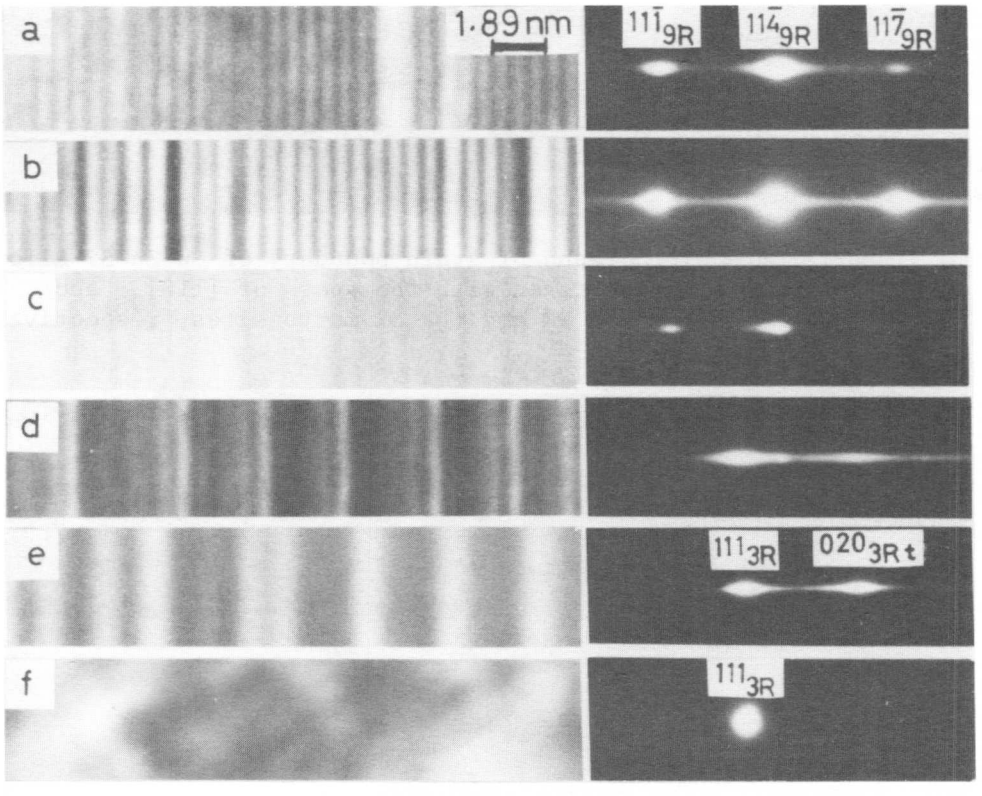

Fig.2 Interference micrographs at high magnification taken with the same spots as Fig.1. The spots of $[1\bar{1}0]_{9R}$ and $[10\bar{1}]_{3R}$ zones are shown.

the figure are interfaces between thin plates of twins. The observation of $11\bar{4}$ spot may indicate the existence of the 9R martensite wit many stacking faults among the twinned 3R martensites. The lattice images of the 3R martensites with (e-type grain) and without (f-type grain) twin give micrographs similar to those of ordinary dark-field images at low magnification.

(2) 9R to 3R martensitic transformation in the grain boundary region

General features of the sequence of structural change at the grain boundary region were observed at low magnification and the result are shown in Fig.3. In the as-quenched specimen, the most frequent

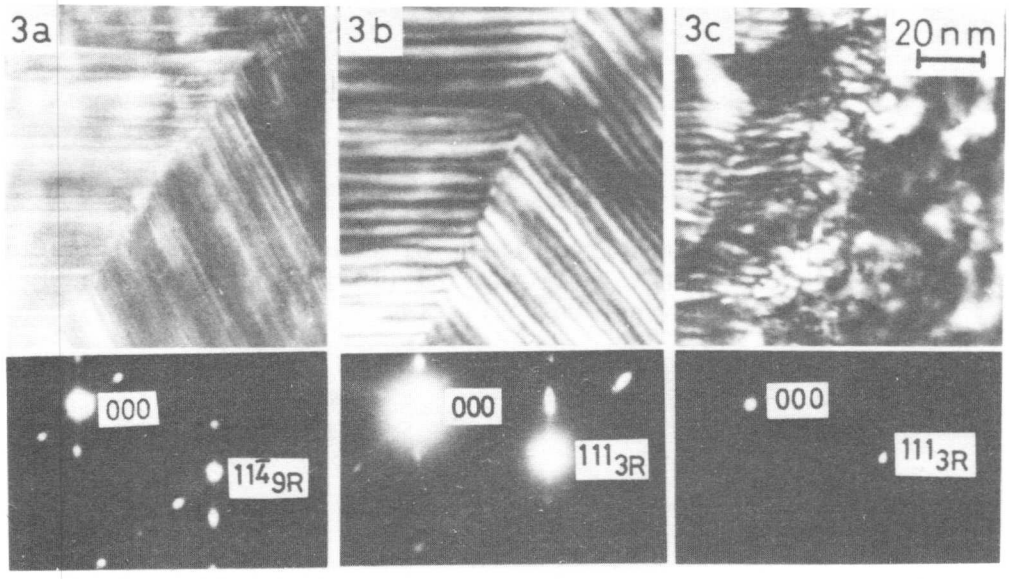

Fig.3 Interference micrographs of grain boundary of Cu-Zn Si alloy at low magnification taken with the spots of $[1\bar{1}0]_{9R}$ and $[10\bar{1}]_{3R}$ zones for the 9R and the 3R martensites, respectively.

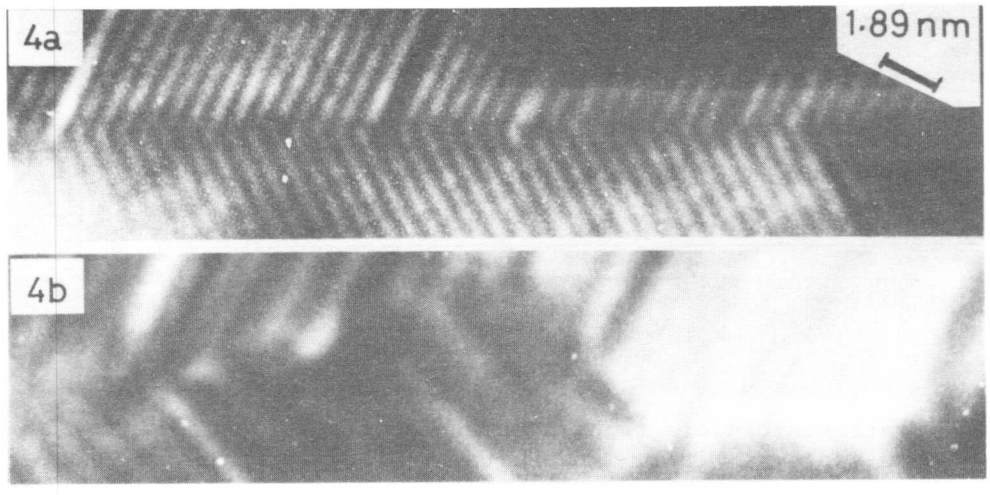

Fig.4 Interference micrographs of grain boundary at high magnification taken with the same spots as Fig.3.

boundary is of the twin type $(11\bar{4})_{9R}$ boundary (Fig.3a). The same martensites with twinned structure formed in the interior of grain are formed at the grain boundary region (Fig.3b) at the extension of two per cent. These thin twin plates are continuous across the grain boundary. When the extension increases further, the twinned structure disappears and the previous existence of grain boundary can be detected by the change in directions of traces of stacking faults (Fig.3c).

Results of lattice image observation at the grain boundary are summarized in Fig.4, (a) being in the as-quenched specimens and (b) in the deformed specimens. With an application of plastic deformation, lattice image becomes obscure as a results of introduction of many stacking faults. The boundary becomes irregular and the difference in directions of lattice image or the traces of stacking faults in the adjacent grains changes from 50° to 70°. The rotation of grain is necessary to make the 3R martensite continuous across the grain boundary, because the angles between the close-packed planes in the $(11\bar{4})_{9R}$ type twins of the 9R martensite and in the 3R martensite are 50° and 70°, respectively. The grains rotate around an axis parallel to the $(11\bar{4})_{9R}$ type twin boundary during the transformation to make the 3R martensite continuous across the boundary and the grain boundary disappears.

IV. Discussion

The 9R martensite and the 3R martensite have the close-packed structures with the stacking sequences ABCBCACAB and ABC, respectively. The transformation from the 9R martensite (Fig.5a) to the 3R martensite (Fig.5 b,c) takes place by giving glides on all of the close-packed planes that are easy to glide. The total amounts of shears necessary for the transformations to the 3R martensites shown in Fig.5b and Fig.5c are -3γ and 6γ, respectively, where γ is the amount of shear strain equal to one glide (a/3) at every nine layers, i.e., 0.074. The 3R martensite shown in Fig.5b and Fig.5c have the twin relation observed in the twinned 3R martensite. The specimens used for this experiment are polycrystals. The amount of plastic deforma-

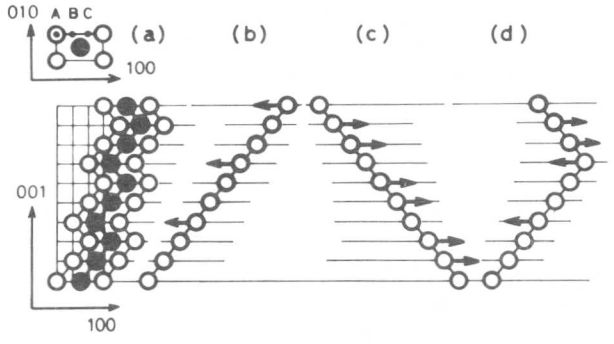

Fig.5 Models for the movements of close-packed planes in the transformation from the 9R(a) to the 3R (b,c,d) martensites.

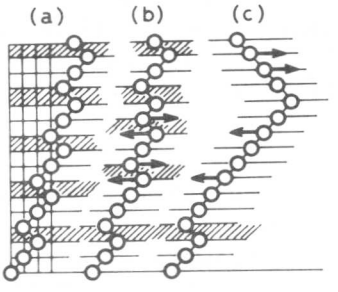

Fig.6 Models for the movements of close-packed planes in the transformation from the 9R martensite (a) to the 9R martensite with many stacking faults (b) and to the 3R martensite with twin (c).

tion varies in individual grains. In order to simplify the discussion the grains with the maximum resolved shear stress is taken to represent the structural change in transformation. Eighty per cent of grains transform from the 9R to the 3R martensites at the extension of two per cent (0.5γ). When the specimen is extended by ten per cent (2.7γ), the twinned structure disappears in fifty per cent of grains. These facts show that the 9R to 3R martensitic transformation takes place with small amount of extension and the further increment of extension is used to change the twinned structure into the simple 3R martensite without twin. The 9R to 3R martensitic transformation can take place with the total amount of shear less than -3γ (or 6γ) by the formation of twinned structure, and the transformation is possible even with the zero net shear as shown in Fig.5b. The twinned martensite changes into a simple 3R martensite such as shown in Fig.5b and Fig.5c by giving the net shears, -3γ and 6γ, respectively. If the orientations of grains are distributed randomly in the specimen, fifty per cent of grains will have the structure of 3R martensite of Fig.5b at the extension of about ten per cent (-2.7γ).

A small number of grains from twenty to ten per cent do not transform into the 3R martensite and remain as the 9R martensite with many stacking faults. In order to investigate if these grains represent the intermediate stages of the transformation, the lattice image of b-type grain which shows clear lattice image is analysed. The results are summarized in Fig.6. The lattice fringes were shifted by one third of the spacing of the lattice fringes at the stacking faults introduced by deformation. This shift of lattice fringes can take place by introducing the glides on the close-packed planes in a manner as shown in Fig. 6b. When the glides take place in such a way as shown in Fig. 6c, the 3R martensite with twinned structure is formed. However, the 9R martensite remains after the introduction of glides, when the glides in both directions occur in the same region as shown in Fig.6b. When polycrystals are deformed, complex plastic deformations take place at the grain boundary to keep the aggregate of grains together. In the grains which do not transform into the 3R martensite, a severe plastic deformation of this kind will be added to the glides necessary for the 9R to 3R martensitic transformation and the 9R martensite with many stacking faults will be produced. In conclusion, most of grains of Cu-Zn-Si alloy transform directly from the 9R martensite to the 3R martensite without passing intermediate stages.

References

[1] I.Isaitshew, E.Kaminsky and G.Kurdjumow: Trans. AIME 128 (1938) 361.

[2] S. Kajiwara: Trans. Japan Inst. Met., 9(1968), Suppl., p.543.

[3] S. Kajiwara: J. Phys. Soc. Japan 23(1967) 656.

[4] S. Kajiwara: J. Phys. Soc. Japan 27(1969) 712.

Crystallography of Stress-induced Transformation in BCC Copper Base Alloys

J. De Vos, L. Delaey, E. Aernoudt and P. Van Houtte

In this paper, a generalized mathematical model is presented for the crystallography of the bcc to 9R martensitic transformation (β to β') observed in copper base alloys. It allows to compute the total deformation gradients for each of the 24 variants. The results of the model were used for the prediction of the martensite plate variant which will be formed in a tensile test for a given orientation of the matrix phase. The maximal pseudoelastic elongations were calculated for two basic assumptions: free deformation and constrained deformation (Taylor model).

Computer Solution of the Phenomenological Theory

The computer model described here is basically the mathematical translation of the phenomenological theory of Wechsler, Lieberman and Read [1]. Analytical approaches were already reported by Saburi et al. [2], by Ledbetter and Wayman [3] and by Schroeder and Wayman [4]. In the present model, which gives the orientation relationships, the habit planes and the transformation strain for all 24 variants, the martensite transformation is split up into the following stages :

1.a. The bcc lattice of the β-phase (a_β) transforms into an fcc lattice. In each bcc-lattice, a face-centered unit cell having the size $a_\beta\sqrt{2}$, $a_\beta\sqrt{2}$, a_β can be found (Fig. 1). The normals on the faces of this unit cell are parallel with the [110], [1$\bar{1}$0] and [001] directions of the bcc lattice, the latter being the Bain axis. A simple axisymmetrical tensile strain of approximately 26 % along the [001] direction transforms this unit cell into a true cubic cell; the lattice parameter is $a = ra_\beta$. No volume change occurs if $r = \sqrt[3]{2}$.

1.b. A small additional axisymmetric strain along the [001] axis is sometimes required. An fct unit cell is then obtained. The lattice parameters are c_1 (along the [001] axis) and a_1 (perpendicular on it). They are fully characterised by the ratio $\psi = c_1/a_1$ and the condition that there is no more volume change: $a_1^2 c_1 = a^3$.

2. The {111} planes of the hypothetical fcc or fct intermediary lattice are close-packed lattice planes. They should become the basal planes of the resulting β' martensite, which has an ABCBCACAB stacking and is therefore called 9R [1]. This stacking order can be obtained by a shear on a hypothetical (1$\bar{1}$1) [$\bar{1}$12] slip system of the fcc (or fct) lattice.

Departement Metaalkunde, Katholieke Universiteit Leuven, Belgium

[1] It is called 18R if the super-lattice structure is accounted for; but this difference is unimportant with regard to the present analysis.

Not all such systems are allowed (Swann and Warlimont [5]). The value of the shear required for this transition can readily be obtained from geometrical considerations (De Vos [6]).

3. An additional shear along the basal slip system of the 9R lattice is still required. There must be an invariant plane of the transformation (habit plane), which is the interface between the non-transformed part of the parent β-lattice and the newly formed martensite. The deformation gradient tensor describing the strain [2] must satisfy the following condition for a habit plane to exist [1,6]:

$$(F^t F - I) = 0 \qquad (1)$$

The additional shear is found by solving (1).

4. The orientation of the habit plane can be found by analyzing F. F usually causes an unwanted rotation of the habit plane. This rotation is counteracted by applying an additional rotation as last stage.

The strains associated with these four stages of the transformation (and with the total strain), can be described analytically using deformation gradient tensors which have been given in detail elsewhere [6,7]. They are functions of the only two unknown parameters left : r and ψ (stage 1). The resulting lattice parameters a", b", c" of the 9R structure (Fig. 2) are functions of r, ψ and a_β. Experimental data concerning a", b" and c" cannot be independent. They must obey to the relationship

$$b"c" = 9a" \sqrt{b"^2 - a"^2} \qquad (2)$$

A deviation of maximal 0.59 % was found while checking experimental data [7].

In several stages of this transformation, different equivalent choices can be made or equivalent solutions are found. All possibilities combined lead to 24 differently oriented martensite variants, all having the same 9R-structure.

Discussion of the Results of the Crystallographic Model

The results of the present model were found to be very insensitive to the values of r and ψ [7]. It can therefore be stated that the results given below are representative for most β Cu-Zn-Al alloys. Figure 3 shows the position of all habit plane normals for a particular case ($r = \sqrt[3]{2}$; i.e. no volume change and $\psi = 0.95$). Figure 4 shows the position of the basal planes for the same case.

The analysis given above takes the volume change due to the martensitic transformation into account. It is characterised by the dilatation $V_r = a"b"c"/9a_\beta^3$ which has typical values ranging from 0.99 to 1

[2] The strain transforms a vector v into a vector v' given by v' = Fv.

for Cu-Zn-Al alloys(the volume change is smaller than 1 %). Kubo and Hirano [8] reported relative errors $\Delta a/a = 0.3$ % for the measured values of the lattice parameters. A statistical analysis of the error on V_r leads to

$$\frac{\Delta V_r}{V_r} = \sqrt{12}.\ \frac{\Delta a}{a} \approx 1\ \% \qquad (3)$$

Hence the volume changes reported above are not significant, i.e., the hypothesis that the volume does not change during the transformation is not in contradiction with the measured lattice parameters. The total strain associated with the transformation simply is a pure shear when this hypothesis is accepted. The habit plane would be the shear plane which contains the shear direction; there would be no dilatation in the direction perpendicular to the shear plane.

Application on Stress-induced Martensite

Assume that a β-crystal of a Cu-Zn-Al alloy is subjected to a tensile test just above M_s. The load will induce a $\beta \rightarrow \beta'$ transformation, causing a pseudoelastic strain, which is reversible on condition that the load is not increased beyond the point where 100 % of the material has transformed into β'. The elongation achieved at that moment will be called "maximal pseudoelastic elongation".

The analytical expressions derived for the strain, associated with the formation of each variant [6, 7, 9] easily allows to predict the variant which will be formed. Assume that a volume fraction df^p of variant p is formed. The transformation strain is a combination of a shear γ_o along the habit plane and a dilatation in the direction perpendicular to it. Assume that the work required for the transformation, per unit transformed volume, is a material constant w (at a given temperature). K_p is the deformation gradient tensor of the strain associated with variant p. It is described in an orthogonal reference system, whose x_3 axis is the tensile axis [3]. Thus the elongation caused by the transformation is equal to $k^p_{33}df^p$. Let σ^{p*} be the macroscopic tensile stress if the variant p would be the first to be formed. The external work must be equal to the work required to form the martensitic variant:

$$\sigma^{p*}k^p_{33}df^p = wdf^p \qquad \text{or} \qquad \sigma^{p*} = w/k^p_{33} \qquad (4)$$

in which w is a constant and k^p_{33} is known for all variants. Hence σ^{p*} can be calculated for all variants. The first to be formed is the variant which requires the smallest tensile stress σ^{p*}. Thus the variant for which k^p_{33} is the largest will be formed. This is nothing else than the criterion formulated eight years ago by Tas et al. [10] : "the variant producing the largest elongation will be formed".

---

[3] Let K^c_p be the deformation gradient with respect to the bcc cube axes. Then $K_p = T^{-1}\ K^c_p\ T$ where the matrix T describes the orientation of the crystal [12].

The transformation strain is a pure shear of magnitude γ_o along the habit plane if the volume change is neglected. Let the angles between the tensile axis and respectively the habit plane normal and the shear direction be α^p and β^p. One could define a Schmid factor $m^p = \cos\alpha^p \cos\beta^p$. It can be demonstrated that $k^p_{33} = \gamma_o m^p$ when there is no volume change. Thus the maximal elongation criterion is equivalent with a maximal Schmid factor criterion, as used by Otsuka et al. [11] , when the volume change is neglected.

k^p_{33} was calculated for all variants and for a number of tensile axis orientations within the fundamental triangle 001-011-111. It appeared that variant no. 3 (Figs. 3 - 4) always gave the maximal elongation ε_o, which is plotted out in fig. 5. These results can be used for any other fundamental triangle as well, because of the cubic symmetry of the β-crystal (Van Houtte and Aernoudt [12]). The variant which is formed in such a triangle can be derived from variant 3 (figs. 3 - 4) by the same symmetry operation which allows to derive the considered triangle from the 001-011-111 triangle. The results of fig. 5 are not essentially different from the results obtained by Otsuka et al. [11] for a Cu-Al-Ni alloy.

The Case of Constrained Deformation

The maximal elongation criterion or the Schmid factor criterion cannot be used for β-polycrystals. Only one variant can be predicted this way in each grain. There is no reason why the corresponding strains should be compatible in adjacent grains. It makes more sense to assume a homogeneous strain field, i.e. impose a prescribed strain upon each grain, instead of a prescribed stress [13]. Such a model has very recently been developed, introducing the $\beta \rightarrow \beta'$ transformation as one of the possible deformation mechanisms considered in the Taylor theory [14]. The details of the analysis will be published in the near future [15]. Fig. 6 gives the results for the maximal pseudoelastic elongation ε_o as a function of the position of the tensile axis with respect to the lattice orientation of a grain of the β-phase. The result is only valid in so far no further transformation or mechanical twinning takes place. The model can be used for any desired strain mode and has already been used for plane strain deformation [16].

References

[1] M.S. Wechsler, D.S. Lieberman and T.A. Read: Trans. AIME, 197 (1953), 1503.
[2] T. Saburi, S. Nenno, S. Kato and K. Takata: J. Less Common Metals, 50 (1976), 223.
[3] H.M. Ledbetter and C.M. Wayman: Mat. Sci. Eng., 7 (1971), 151.
[4] T.A. Schroeder and C.M. Wayman: Acta Met., 25 (1977), 1375.
[5] P.R. Swann and H. Warlimont: Acta Met., 11 (1963), 511.
[6] J. De Vos: Ph.D. Thesis, Departement Metaalkunde, K.U.Leuven, 1978.
[7] J. De Vos, E. Aernoudt and L. Delaey: Z. Metallkde., 69 (1978), 438.
[8] H. Kubo and K. Hirano: Acta Met., 21 (1973), 1669.
[9] J. De Vos, L. Delaey and E. Aernoudt: Z. Metallkde., 69 (1978),511.
[10] H. Tas, L. Delaey and A. Deruyttere: Z. Metallkde., 64 (1973), 855.
[11] K. Otsuka, C.M. Wayman, K. Nakai, H. Sakamoto and K. Shimizu: Acta Met., 24 (1976), 207.
[12] P. Van Houtte and E. Aernoudt: Mat. Sci. Eng., 23 (1976), 11.
[13] U.F. Kocks: Met. Trans., 1 (1970), 1121.
[14] G.I. Taylor: J. Inst. Metals, 62 (1938),307.
[15] P. Van Houtte, J. De Vos, E. Aernoudt and L. Delaey: Proceedings of the 5th International Conference on the Strength of Materials and Alloys, Aachen, 1979.
[16] P. Van Houtte: To be published.

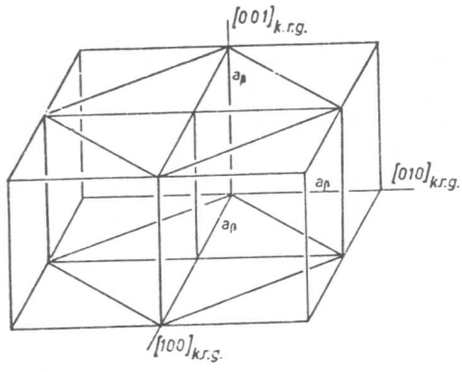

Fig. 1 An fcc unit cell, the faces of which are (001), (110) and (1$\bar{1}$0), can be found in a bcc lattice.

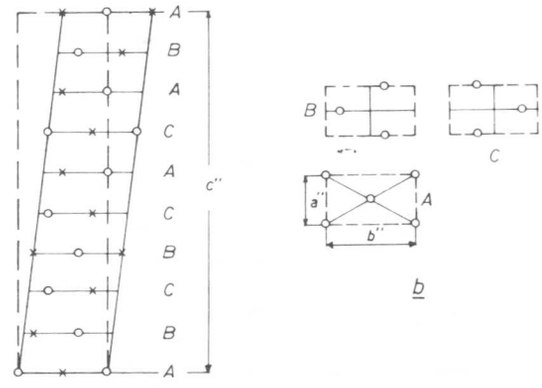

Fig. 2 The unit cell of the 9R martensite.

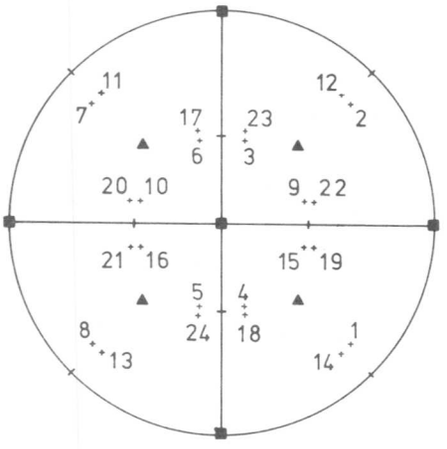

Fig. 3 The position of the habit planes for the 24 variants. r = 1.26 ψ = 0.95

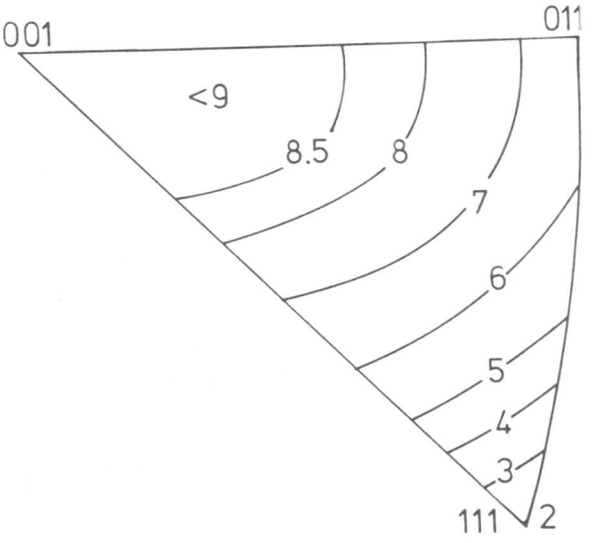

Fig. 5 The maximal pseudoelastic elongation (%) in a a tensile test as a function of the orientation of the tensile axis with respect to the β-crystal. Case of free deformation.

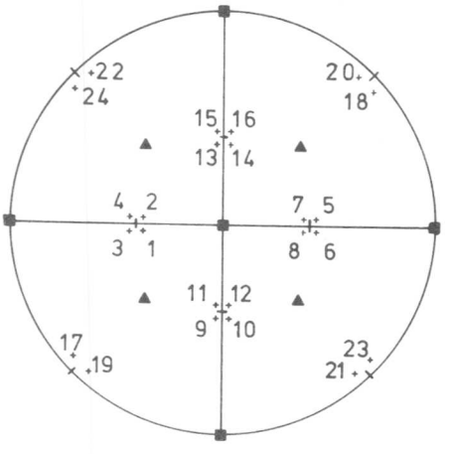

Fig. 4 The position of the basal planes of the 24 variants, same case as fig. 3.

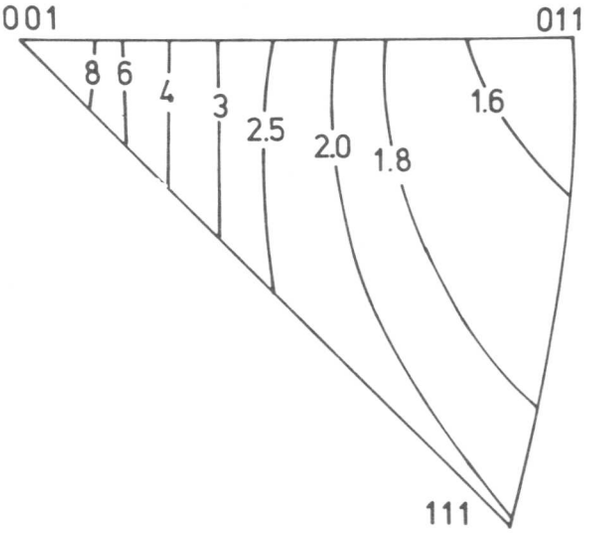

Fig. 6 The maximal pseudoelastic elongation (%) in a tensile test as a function of the orientation of the tensile axis. Case of the constrained deformation (Taylor theory).

A New Stress-Induced Phase Transformation and The Mechanical Properties of Cu+13.4 wT/o Al Alloys

D.Rios-Jara[+], H.Armendariz-Verduzco* and G.Torres-Villaseñor[+*]

The mechanical properties of the Cu+13.4 wT/o Al alloy were studied at room temperature under compression. The alloy quenched to room temperature from 960°C shows an extensive plastic deformation. Optical metallography studies of the structure of the undeformed-specimens shows big grains of gamma-2 phase in a perlitic matrix. After deformation the structure is martensitic with some rosette-type grains. Electron microscopy studies shows that some gamma-2 grains transform under stress to martensite disordered beta. It is known that the gamma-2 phase is stable when it is deformed at high temperature or high hydrostatic pressure, so we propose the existance of a metastable copper rich gamma-2 phase which could transform to beta martensite by a continuous shear of the type a/3 101 , on (330) compact planes of the copper rich gamma-2 phase.

I. Introduction

The mechanical properties of β(Cu-Al) alloys with aluminium content higher than 13 wT/o, have not been studied as much as those with lower aluminium concentration, mainly because the high content of the brittle gamma-2 phase reduces considerably the ductility of these alloys.

In the present study the mechanical properties of the structures formed in the alloys with 13.4 wT/o Al, after intermediate cooling rates (air quench) were investigated. In particular it was found that extensive deformation was achived in the alloy quenched from 900°C→20°C. This extensive deformation was atributed to the transformation of a gamma-2 copper rich phase, obtained by the type of cooling used in this work, to β' disordered martensite.

II. Experimental Procedure

The alloy Cu+13.4 wT/o Al, was prepared by melting in a He atmosphere, in a graphite crucible, 50 grs. charges of the appropiate amounts of electrolitic copper and aluminium analytic quality. The ingot was annealed at 950°C for 24 hours to ensure homogeneity. The resulting material was analyzed for copper by chemical methods. The aluminium content was determined by difference.

+ Centro de Investigación de Materiales, Apartado Postal 70-360, Universidad Nacional Autónoma de México, México 20, D.F., México

* Departamento de Ciencia de Materiales de la E.S.F.yM. del Instituto Politécnico Nacional, Zacatenco, México, D.F., México.

The ingot was divided in three equal parts and reheated to 960°C. One part was air quenched from 960°C, in an effort to develop some Cu-rich or Al-rich structures. A second set of specimens was air quenched from 600°C, in an attempt to develop the martensite plus gamma-2 phase structure and a third one was furnace-cooled in order to obtain stable structures.

For the mechanical testing experiments, compression specimens were cut with a diamond saw in the form of parallelograms (having a base of 3 x 3 mm^2 and 6 mm height), from each of the thermally treated ingots. After sawing, the faces of the specimen were polished, and finally chemical etched with a mixture of 5 gr. of $FeCl_3$, 2ml of HCl in 95 ml of methyl alcohol, in order to observe by means of optical microscopy the microstructure of the specimens before mechanically testing them in an Instron machine at a crosshead speed of 0.01 mm/min. Thin foils suitable for electron microscopy were prepared by conventional electro-thinning methods.

III. Results and Discussion

1. Mechanical Behavior

The mechanical stress-strain behavior in uniaxial compression tests of the alloys Cu+13.4wT/o Al, air quenched from 960, 600°C and slowly cooled, is shown in Figure 1. The specimens which were air quenched from 600°C and slowly cooled show a similar stress-strain curve, with rapid rates of strain hardening and a plastic deformation better than 14% in both cases. The yield stress for the quenched from 600°C material, is around 50 Kg/mm^2 and 70 Kg/mm^2 for the furnace cooled material.

In contrast, the air quenched from 960°C specimens show a quite different mechanical behavior (Figure 1) and microstructure consisting mainly of grains of gamma-2 phase, distributed as dispersed round type and rosette type grains (figure 2-a). From the plastic region of the stress-strain curve, it is observed that the quenched from 960°C material, shows a yield point of around 34 kg/mm^2. After this point, the material deforms with rapid rates of strain hardening, similar to those observed in the quenched from 600°C and furnace cooled material. At around 6% of deformation, it is observed a drastic change in the rate of deformation. The material starts to flow in an easy glide way, and at 20% of deformation, it shows rapid rates of work hardening again. Figure 2-b is an optical photograph, showing the microstructure of the material after deformation to fracture. It is observed that a type of transformation has occurred. The round type grains of gamma-2 have disappeared, and in contrast, we can observe a great number of parallel martensite plates (0.3-0.7 μm long). However, the rosette type grains kept stable up to deformation to fracture of the specimen.

2. Electron Microscopy Observations

Foils for transmission electron microscopy were prepared from the air-quenched from 960°C non-deformed and deformed material. Before deformation they show grains of gamma-2 phase, in a matrix of very fine β' and γ' martensites. The width of the martensite plates varies from 300 to 900 A (Figure 3-a). The diffraction characteristics of the round type and rosette type gamma-2 grains were studied, by electron diffraction techniques and no appreciable differences in the diffraction patterns and

contrast of the images were found between them.

An orientation relationship can be obtained from the composite diffraction pattern in Figure 3-b by assuming that the zones of gamma-2 and martensites producing the observed reflections are parallel and by noting that the planes $(208)_{\beta^1}$ and $(330)_{\gamma_2}$ are parallel. The result is:

$$(208)|010|_{\beta^1}//(330)|\bar{1}11|_{\gamma_2}$$

here, we used the Nishiyama's (1) orthorhombic structure for β^1, since it takes into account the stacking faults in every three (111) plane, of the equivalent cubic F. cell proposed by Swann (2). The (208) planes of the Nishiyama's structure corresponds to (111) planes of the Swann's cubic F. structure, which are the most compact planes of the structure.

The electron transmission microscopy observations from the deformed material, are in agreement with the optical Microscopy observations; the parallel arranged plates observed in Figure 2-b were identified from the diffraction patterns, as highly texturized β' disordered plates, and no gamma-2 round type grains were detected. Figure 4-a shows a typical area of the deformed material and Figure 4-b is the selected area diffraction pattern of the parallel martensite plates; these plates are β' disordered martensites, crossed by thin bands identified as stacking faults.

The fact that deformation of this alloy results into a great reduction in the amount of gamma-2 round type grains and a great increase in size and number of β' martensite plates, lead us to think that the gamma-2 grains transform by plastic deformation into β' martensites. It is known that the gamma-2 phase is stable when it is deformed at high temperature (3) or under high hydrostatic pressure (4) and shows a brittle behavior when deformed under normal conditions, so the observed round type grains with the gamma-2 microstructure are proposed to be some type of retained metastable copper rich gamma-2 phase (γ_2), which could be formed during quenching, at selected sites of the lattice and grows at the expence of the aluminium content of surrounding β phase. The untransformed rosette type grains could be the stable form of the γ_2 phase. This could be the reason why the rosette type grains remains stable until fracture of the sample.

It was not possible however, to distinguish by electron diffraction in the microscope, between a normal gamma-2 phase and a copper-rich gamma-2 phase. Several spot intensity calculation were made, using an H. P. 9830 calculator varing the amount and position of copper and aluminium atoms in the unit cell, with respect to the normal gamma-2 structure. Table I shows a comparation in reflection intensities between the stable gamma-2 phase and the limit case when all the stable vacancy sites of the gamma-2 structure have been filled with copper atoms and the remained atoms reacomodated to result in a structure equivalent to the stacking of 3 x 3 cubic I ordered cells. It is observed from Table I, that the differences in correspondicng reflection intensities can not be distinguishables by conventional electron microscopy techniques.

3. The Transformation $\gamma_2^+ \rightarrow \beta'$

According to the orientation relationships found before, the (330) planes of the γ_2 structure are parallel to the (208) planes of the β' disordered martensite. By analysis of the atom's positions on a computer's reproduction of these planes, Figure 5 it was possible to observe, that the transformation can occur by a continuous shear of the $a/3\cdot|110|$ type, on each (330) compact plane of the copper-rich gamma-2 limit case proposed structure. The calculated interatomic distance in the $|111|_{\gamma_2}$ and $|010|_{\beta'}$ directions differ by 3.27% and 0.92% in the $|11\bar{2}|_{\gamma_2}$ and $|401|_{\beta'}$ directions and the $(330)_{\gamma_2}$ interplanar distance requires a small calculated shrink of 0.97% to attain the $(208)_{\beta'}$ interplanar distance. It is therefore concluded that the β' stress induced martensite is produced by a shear and a small amount of diffusion which do not overflows one interatomic distance.

The easy glide like region observed in the σ-ε curves is associated to the deformation of the β' martensite, microhardness measurements (5) have shown that the β' martensite is 20% softer than the supersaturated γ_2^+ structure and 35% softer than the normal γ_2 structure, so the transformation tends to produce a softer material.

References

(1) Z.Nishiyama and S.Kajiwara; Japanese Journal of Applied Physics 2 (1963), 478.
(2) P.R.Swann and H.Warlimont; Acta Metallurgica 11(1963), 511.
(3) D.J.Mack, A.J.Birkle, and W.L.Krubsack; "Mechanical Properties of Intermetallic Compounds" edited by J.H.Westbrook, John Wiley and Sons Inc., New York, 1960 pag. 320.
(4) G.Torres-Villaseñor, M.Avalos-Borja and S.V.Radcliffe. Metallurgical Transactions. In press.
(5) H.Armendariz-Verduzco and G.Torres-Villaseñor. Proceedings of the "Academia Nacional de Ingeniería". Monterrey, N.L. 1(1976), 441.

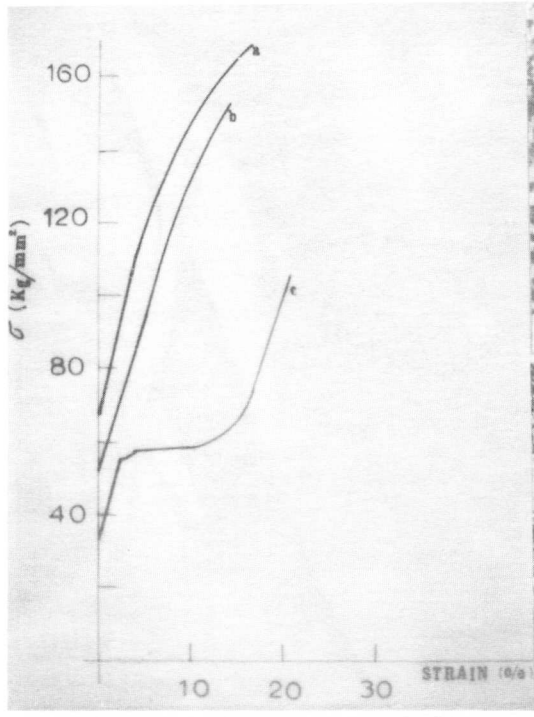

Figura 1 Stress-strain behavior of Cu+13.4wT/o Al. a)Slowly cooled samples. b) Air-cooled specimens from 600°C. c) Air-cooled specimens from 960°C.

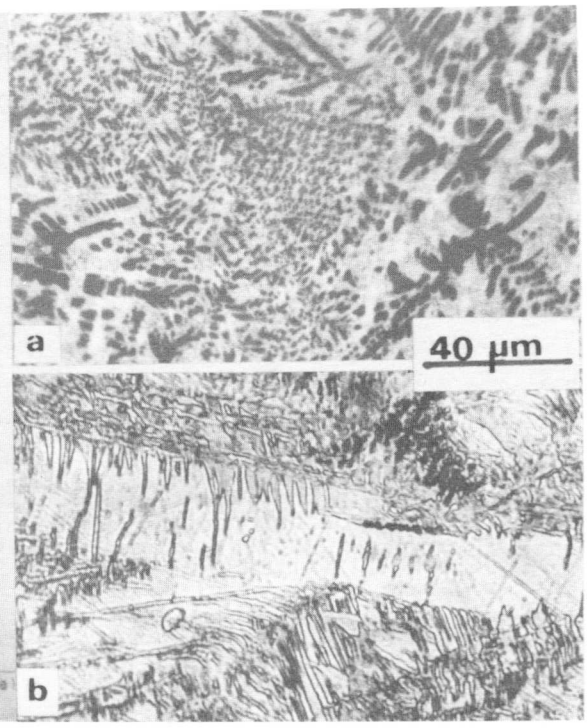

Figure 2 Cu+13.4wT/o Al. a) Quenched from 960°C in air. b) Same specimen after deformation to fracture.

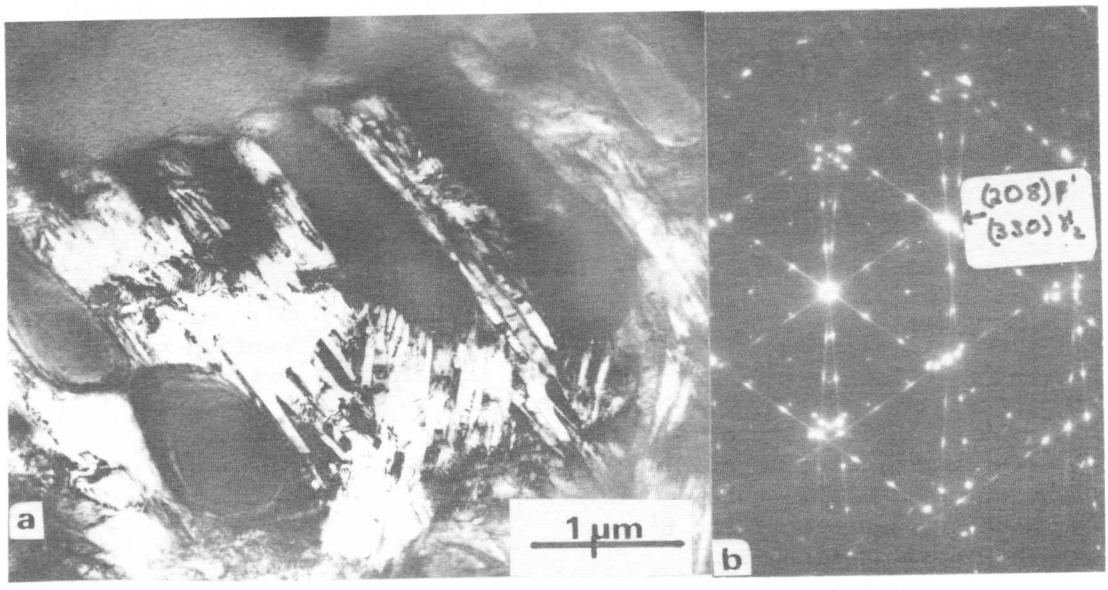

Figure 3 Transmission electron micrographs of Cu+13wT/o Al. a) Before deformation, showing round grains. b) Diffraction pattern of the area shown in (a).

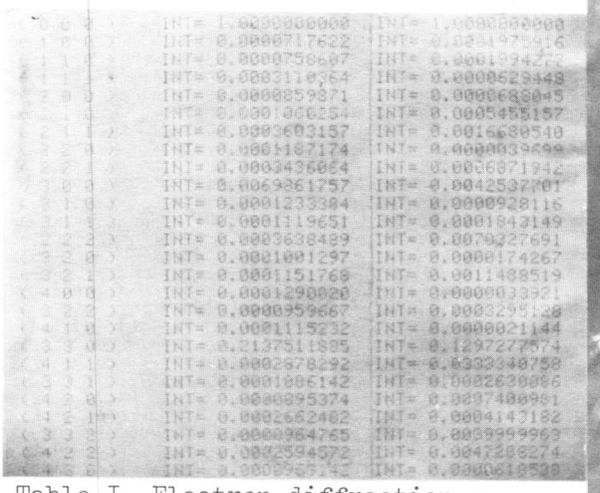

Table I Electron diffraction intensities for a) γ_2^+ b) normal γ_2.

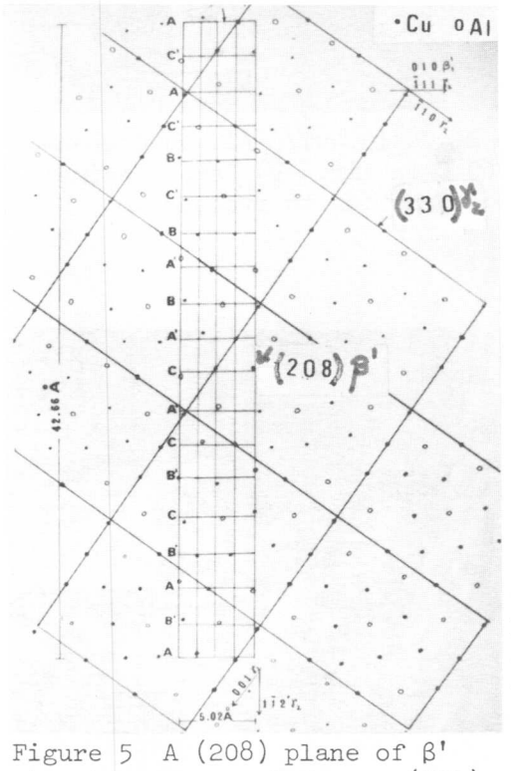

Figure 5 A (208) plane of β' structure, proyected on a (330) plane of gamma-2 structure. The staking sequence of the β' martensite is obtained by a continuous shear of the type $\frac{a}{3}|101|$ of these (330) planes.

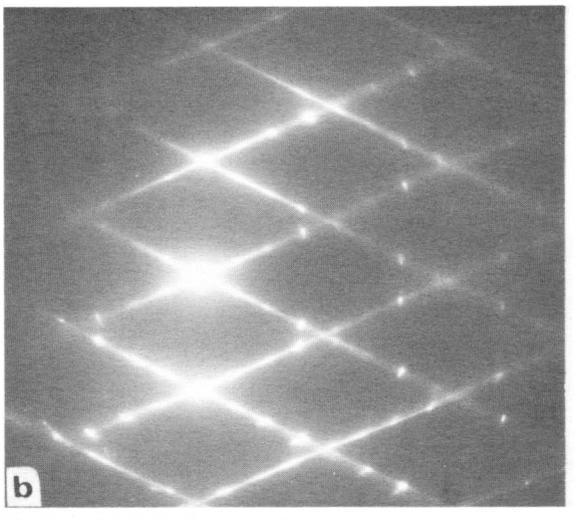

Figure 4 a) Cu+13.4wT/o Al alloy after deformation. b) Diffraction pattern of the β' transformed martensites (010) zone axis.

Morphology and Crystal Structure of Martensite Formed in Quenched Au-47.5 at% Cd

T. Tadaki* and C. M. Wayman*

A Au-47.5 at% Cd alloy was quenched from elevated temperatures to temperatures both above (a) and below (b) the normal M_s temperature corresponding to the formation of γ_2' martensite in slowly cooled specimens. After treatments (a) and (b) specimens were examined by optical microscopy and electron microscopy and diffraction. The major product after treatment (a) is unambiguously shown to be the trigonal ζ_2' martensite typical of alloys containing about 50 at% Cd. Internal defects corresponding to a lattice invariant deformation were not observed in the ζ_2' martensite in the present case, consistent with a previous report of no identifiable substructure in the ζ_2' martensite formed in Au-50 at% Cd. The present ζ_2' martensite was found to be much coarser than that in Au-50 at% Cd, and consequently its morphology could not be clarified. By contrast, treatment (b), on the whole, resulted in the formation of three types of martensite, γ_2', β_2' and ζ_2' which gave rise to highly complicated microstructures. The main products were found to be γ_2' and β_2' with only minor amounts of ζ_2'.

I. Introduction

It is well established that the Au-47.5 at% Cd alloy when slowly cooled from the parent β_2 phase transforms into the γ_2' martensite (modified 2H structure [1]) at about 333K, which will henceforth be considered to be the normal M_s temperature. The formation of γ_2' results in a corresponding decrease ($\sim$ 20%) in electrical resistivity [2]. On the other hand, a Au-50.0 at% Cd alloy when similarly treated transforms to a trigonal ζ_2' martensite at about 306K with a corresponding increase ($\sim$ 20%) in electrical resistivity [3-5]. However, when the Au-47.5 at% Cd alloy is quenched from high temperatures to just above the normal M_s and further slowly cooled, electrical resistivity-temperature relationships very similar to those found for the Au $\sim$ 50% Cd alloy are observed [2]. Because of this similarity, it has been considered that the quenching treatment resulted in the occurrence of the $\beta_2 \rightarrow \zeta_2'$ transformation even in the Au-47.5 at% Cd alloy. However, the kind of martensite produced by quenching has not been clearly established, and morphological aspects of the quenched alloy are not clear. The present study was thus carried out in an attempt to clarify these points.

---

* Department of Metallurgy and Mining Engineering and Materials Research Laboratory, University of Illinois at Urbana-Champaign, Urbana, IL

II. Experimental Procedure

An ingot of nominal composition Au-47.5 at% Cd was prepared by melting Au (99.999%) and Cd (99.999%) at 1173K in an evacuated quartz tube back-filled with argon. The detailed procedure for the preparation of ingots 3 mm in diameter and length ~ 70 mm has been described elsewhere [1]. After homogenizing the ingot at 823K for 3.6×10^5 sec, the difference in weight before melting and after heat treatment was found to be less than 0.05%. Disc-shaped specimens about 0.2 mm thick were cut from the ingot using a slow-speed diamond saw, solution treated at 773K for 3.6×10^3 sec in quartz tubes filled with argon, and given two different quenching treatments: quenching into hot water at 353K, above the normal M_s and quenching into ice water at 273K, below M_s, the former followed by air cooling to room temperature. Upon quenching, the quartz tubes were immediately broken. The specimens treated as above were then electropolished as previously done [1] at about 288K. Some of the specimens used for optical microscopy were occasionally electropolished at about 343K in order to obtain smooth surfaces prior to transformation. Optical microscopy was carried out using polarized light and a thermoelectric stage which allowed cooling to 213K and heating to 398K. The thin foil specimens were examined at 125 KV at room temperature in a Hitachi-H500 electron microscope equipped with a tilt (±60°)-rotation (360°) stage.

III. Results and Discussion

1. Quenching to above the normal M_s

Figure 1(a) is an example of the optical micrographs taken from quenched specimens after light electropolishing at 288K. In spite of the fact that the specimens were carefully examined in polarized light, it proved very difficult to discern microstructures characteristic of martensite formation, as is shown in Fig. 1(a). This result is in marked contrast with that obtained in a specimen slowly cooled from the quenching temperature, an example of which is shown in Fig. 1(b) for comparison. As previously examined in some detail [1], the spear-like morphology in Fig. 1(b) is typical of the 2H-type γ_2' martensite. As a further attempt, a specimen such as that shown in Fig. 1(a) was further cooled to about 213K and examined, but no change was observed. As a yet additional attempt, some such specimens were further electropolished at 343K (likely in the matrix-phase condition) and reexamined at room temperature. Nevertheless, it was still difficult to detect surface relief features characteristic of martensite formation. Then, in order to determine what happened in the quenched specimens, some specimens were electropolished to thin foils and observed in the electron microscope.

Figure 2(a) is a typical example of the electron micrographs obtained from specimens as shown in Fig. 1(a). Figure 2(a) does not show any typical morphologies usually associated with martensite formation

other than some domain-like or mottled structures. However, the corresponding diffraction patterns showed clearly the presence of so-called "one-third" reflections. The diffraction patterns, Fig. 2(b) and (c) show typical examples, which were taken from an almost identical region in Fig. 2(a) by tilting the specimen. These diffraction patterns are very similar to some sections of the reciprocal lattice of the trigonal ζ_2' martensite formed in a Au-50.0 at% Cd alloy [3-5]. As a result of further comparison, all such diffraction patterns were found to be highly consistent with the trigonal structure. The diffraction patterns Fig. 2(b) and (c) are thusly indexed to be the [001] and [$\bar{2}$01] zones, respectively, of the ζ_2' martensite. Consequently, the martensite produced by quenching is concluded to be the ζ_2' martensite, as expected, essentially identical to that found in the Au-50.0 at% Cd alloy. However, the precise determination of the lattice parameters was not attempted and the morphologies remain unclear.

No characteristic planar defects such as internal twins or stacking faults were observed in the ζ_2' martensite produced by quenching. Only domain-like or mottled structures were observed, as shown in Fig. 2(a). This observation is parallel to that made for a Au-50.0 at% Cd ζ_2 martensite [5] where the domain-like contrast was attributed to artifacts formed during electropolishing. It thus appears that the ζ_2' martensite in the present case, as previously found for the ζ_2' martensite in the Au-50.0 at% Cd alloy [5], shows no evidence of a lattice invariant deformation.

While the Au-50.0 at% Cd ζ_2' martensite appears as bands or parallelograms a few μm wide [5], the ζ_2' in the present quenched alloy did not show these features even when observed by electron microscopy. This probably indicates that the martensite is more coarse in the quenched alloy. Further aspects of the morphology of the ζ_2' martensite are obscured by the very small shape strain characteristic of this martensite, and possibly by texturing of the ingot.

The macroscopic aspect of most specimens quenched as above is given by Fig. 1(a), and the product phase consisted of the ζ_2' martensite. However, it should be added that the same quenching treatment also frequently gave rise to highly complex microstructures, which appeared to correspond to the formation of more than one type of martensite. Such a range of results may arise from slight differences in quenching stress and/or chemical composition from specimen to specimen. These complex microstructures, on the whole, were very similar to those obtained by quenching to below the normal M_s, which is described below.

2. Quenching to below the normal M_s

The specimens thus treated exhibited, in general, microstructures which were considered too complex to correspond to a single type of martensite. Figure 3 is an example.

Thin foils were observed by electron microscopy. In some cases banded structures as shown in Fig. 4(a) were observed over wide regions of the foils. The corresponding diffraction patterns revealed that the

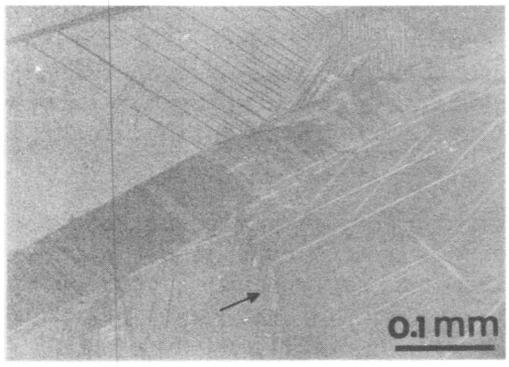

Fig. 3. Example of optical micrographs taken as for Fig. 1 but for specimen quenched to below the normal M_s.

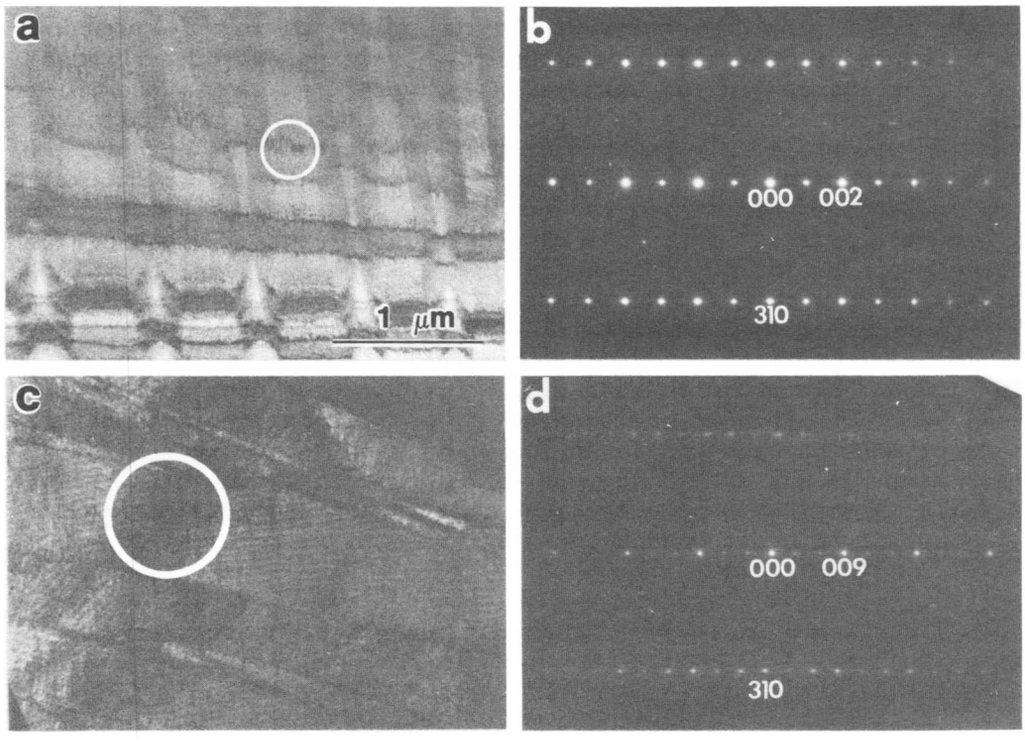

Fig. 4. Electron micrographs (a) and (c) and the respective corresponding diffraction patterns (b) and (d), taken from thin foils of specimens as shown in Fig. 3. (b) and (d) show the [1$\bar{3}$0] zonal patterns of γ_2' martensite with M2H structure and β_2' martensite with M9R structure, respectively.

Relations between Crystal Structures and Electrical Resistivity Changes of Martensites in Au-Cd Alloys

Toshiharu Suzuki, Akira Nagasawa and Norihiko Nakanishi*

The effect of quenching on the structures of martensites in Au-Cd alloys were investigated by electrical resistivity and X-ray diffraction measurements. In the Au-47.5at%Cd alloy, both β_1'(M2H) and β_1''(trigonal) martensites were observed by quenching from 723 K to ice water. Both the martensites transformed to the β_1(CsCl) phase at about 348 K cooperatively with a slight increase in resistivity. On successive cooling, the transformation from the β_1 to both the β_1' and β_1'' martensites occurred at about 313 K with a increase in resistivity. Up to the present, the latter transformation has been recognized as that from the β_1 to the β_1''. During the process of heating and cooling, a wide variation of the resistivity behaviors was observed, but after upon heating to near or above 385 K, only the $\beta_1 \leftrightarrow \beta_1'$ transformation was found; disappearing the $\beta_1 \leftrightarrow \beta_1''$ transformation. In the Au-49.0at%Cd alloy, in which the $\beta_1 \leftrightarrow \beta_1''$ transformation occurs, the transformation temperature was increased by more than 50 K by quenching, which corresponds to the temperature of the disappearing the $\beta_1 \leftrightarrow \beta_1''$ transformation in the quenched Au-47.5at%Cd alloy. These results suggest that the wide variation of the resistivity behaviors appearing by quenching arises from cooperative reactions of the β_1' and β_1'' martensites as well as the effect of lattice defects.

I. Introduction

From results of many investigations of the crystal structures of martensites in Au-Cd alloys have been indicated that two major martensites appear in the range of 47 to 52 at%Cd; as with increasing Cd content, the orthorhombic β_1' which is so-called modified 2H structure[1] and the trigonal β_1'' which contains 18 atoms in a unit cell[2-4] are found to exist as equiribrium phases.

Furthermore, as a result of electrical resistivity measurements[5], it has been shown that the effect of quenching is very striking, especially in a Au-47.5at%Cd alloy. Namely, when quenched from high temperatures to just above the $\beta_1 \rightarrow \beta_1'$ transformation temperature or room temperature, an increase in resistivity occurs through the transformation upon cooling while a usual decrease in resistivity associated with the $\beta_1 \rightarrow \beta_1'$ transformation is observed in slow-cooled condition. It has long been believed that in the case of quenching, the $\beta_1 \leftrightarrow \beta_1''$ transformation occurs instead of the $\beta_1 \leftrightarrow \beta_1'$ transformation, because the similar resistivity increase has been obtained in a Au-49.0at%Cd alloy which typically transforms into the β_1'' martensite. It is, however, still an unclear point whether the increase in resistivity through the transformation in the quenched Au-47.5at%Cd alloy is, in fact, due to the $\beta_1 \rightarrow \beta_1''$ transformation.

Department of Physics, Nara Women's University, Nara, Japan.
*Department of Chemistry, Konan University, Kobe, Japan.

Hence, in this work we make the effect of quenching on the structures of martensites in Au-Cd alloys clear by means of electrical resistivity and X-ray diffraction measurements.

II. Experimental

Two Au-Cd alloys containing 47.5 and 49.0 at%Cd were prepared by melting from preweighted mixtures of 99.999% Au and Cd in a sealed quartz tube filled with argon, shaking vigorously several times in order to ensure homogeneity. The polycrystalline alloys employed to the resistivity measurements were cut into some strips of sheet 0.4 mm thick. The resistivity measurements were carried out by a conventional potentiometric method under an argon atmosphere. X-ray diffraction studies were performed using powder specimens of the Au-47.5 and -49.0 at%Cd alloys and a single crystal of the Au-47.5at%Cd alloy which was examined as a case of the bulk state. At-temperature X-ray diffraction profiles were taken by a high-temperature X-ray goniometer with copper K_α radiation under a vaccum atmosphere. The single crystal was grown by the Bridgman method, and then cut into a rectangular block (5x7x10 mm) to produce a flat surface parallel to the (110) plane. The orientation was determined by the Laue back-reflection technique at about 373 K at which the crystal was in the β_1 phase.

Just before the measurements, all the specimens used throughout this work were annealed at 723 K for 30 min in a glass tube filled with argon and then subsequently quenched into ice water where the glass was immediately broken. All the measurements started from room temperature, and heating and cooling rates were about 2 K/min.

III. Results and Discussion

Fig.1 shows the electrical resistivity curves of the quenched Au-47.5at%Cd alloy. In the initial heating process denoted by (1), a slight increase in resistivity was observed in the temperature range of 332-348 K. After upon heating to 361 K, four thermal cycles were performed successively, varying the maximum heating temperature from 361 K to 388 K as indicated by vertical arrows. As is clearly seen, two distinct resistivity behaviors exist; one is characterized by a resistivity increase, and the other a resistivity decrease through the transformation to the martensites. These characteristics have already been found by Nakanishi and Wayman[5]. From the figure it is apparent that as with increasing the maximum heating temperature, these two characteristics become mixed, and after upon heating above 385 K the resistivity behaviors coincide with those of a slow-cooled case during cooling and heating. Up to the present, as mentioned in the Introduction, it has been considered that hysteresis regions in the curves of (2)-(3) and (4)-(5) are attributed to the $\beta_1 \leftrightarrow \beta_1''$ transformation.

Fig.2 shows partial X-ray diffraction profiles of the quenched single crystal of the Au-47.5at%Cd alloy together with that of the powder specimen. In the measurements observations were restricted to the necessary temperature points, in order to reduce the aging during the measurements, and to approach the same condition as that of resistivity measurements. With the aid of the previous investigations[1-4], all the diffraction lines in the as-quenched state were consistently explained as the mixture

of the β_1' and β_1'' martensites (Fig.2-a). In the case of the single crystal intensities of (111) and (222) of the β_1' martensite seem to be weaker than those of (030) and (060) of the β_1'' martensite, but became stronger by tilting the crystal by 1.0° as shown in Fig.2-a'. This result shows that even if the specimen is quenched, the formation of the β_1' martensite cannot be prevented entirely. After the transformation from both the martensites to the β_1 phase was accomplished upon heating to 376 K (Fig.2-b), the β_1 was found to be stable at least to 327 K upon cooling. On further cooling to room temperature, two martensites β_1' and β_1'' were present again (Fig.2-c). Although any quantitative information for the volume ratio of the β_1' and β_1'' martensites cannot be obtained because of the preferred orientation, it can be seen that after upon heating to 376 K, on successive cooling the $\beta_1 \rightarrow \beta_1''$ transformation is predominant than the $\beta_1 \rightarrow \beta_1'$ transformation compared with the as-quenched state. Further, after reheating to 423 K, cooling resulted in the usual $\beta_1 \rightarrow \beta_1'$ transformation (Fig.2-d). From the comparison with the resistivity curves of Fig.1, it is considered that in the case of quenching, both the β_1' and β_1'' martensites are produced and two transformations $\beta_1 \leftrightarrow \beta_1'$ and $\beta_1 \leftrightarrow \beta_1''$ always occur cooperatively unless, during the process of heating, temperatures become higher than about 385 K. Hence the transformation behaviors associated with the resistivity behaviors are as depicted in Fig.1.

In this work no X-ray analysis was made for the transformation process corresponding to the resistivity curve (6) or (7). Nevertheless, it is natural to consider that in these cases the $\beta_1 \leftrightarrow \beta_1'$ transformation is predominant rather than the $\beta_1 \leftrightarrow \beta_1''$ transformation, because the transformations take place over a broad range of temperatures and the transformation temperature approaches that of the $\beta_1 \leftrightarrow \beta_1'$ transformation.

At the present stage, it becomes very important to study the effect of quenching on the β_1'' martensite. Fig.3 shows the resistivity curves of the quenched Au-49.0at%Cd alloy in which the $\beta_1 \leftrightarrow \beta_1''$ transformation occurs typically. It is clearly seen that the initial transformation temperature is increased by more than 50 K. Wechsler and Read[6] reported that when quenched from 715 K to 313 K, just above M_s, the transformation temperature was decreased by few degrees upon further cooling. This discrepancy probably arises from the difference of the quenching condition; such a increase in transformation temperature in our case is due to the quenching to the martensitic phase.

To check the structural changes through the transformation in the quenched Au-49.0at%Cd alloy, powder X-ray diffraction profiles were obtained. The result is shown partially in Fig.4. Although in the as-quenched state a small amount of the β_1' martensite exists, the $\beta_1 \leftrightarrow \beta_1''$ transformation is found to be essential in this alloy. In the resistivity curves of Fig.3, it should be noted that a temperature at which the initial $\beta_1 \rightarrow \beta_1''$ transformation occurs is about 373 K and very close to that of the disappearing the $\beta_1 \leftrightarrow \beta_1''$ transformation in the quenched Au-47.5at% Cd alloy (~385 K).

These results may lead to some understanding of the complicated resistivity behaviors in the quenched Au-47.5at%Cd alloy; following explanation is possible. By the existence of the β_1' martensite, the $\beta_1 \leftrightarrow \beta_1''$ transformation occurs cooperatively with the $\beta_1 \leftrightarrow \beta_1$ transformation at a temperature below 373 K. But since in essential the β_1'' martensite tends

to exist stably up to or above 373 K by quenching, a very small amount of the β_1'' martensite still remains as a trigger by which the $\beta_1 \leftrightarrow \beta_1''$ transformation is favored, even after the cooperative transformation to the β_1 phase. As a result, during heating and cooling with a temperature range below about 385 K, both the $\beta_1 \leftrightarrow \beta_1'$ and $\beta_1 \leftrightarrow \beta_1''$ transformations are observed.

Finally, it should be noted that it is important to establish the mechanism of the interaction between the β_1' and β_1'' martensites through the transformation, since the results obtained in this work suggest that the wide variation of the resistivity behaviors are associated with the cooperative transformation of the $\beta_1 \leftrightarrow \beta_1'$ and $\beta_1 \leftrightarrow \beta_1''$.

We are grateful to Miss M.Matsunaga and Miss M.Takagi for their collaboration in the experimental work.

References

[1] T.Tadaki, S.Hamada and K.Shimizu: Trans. JIM, 18(1977), 135.
[2] S.Vatanayon and R.F.Hehemann: Shape Memory Effects in Alloys, Ed. by J.Perkins, Plenum Press, (1975), 115.
[3] K.M.Alasafi and K.Schubert: J. Less-Common Metals, 55(1977), 1.
[4] T.Tadaki, Y.Katano and K.Shimizu: Acta Metall., 26(1978), 883.
[5] N.Nakanishi and C.M.Wayman: Trans. JIM, 4(1963), 179.
[6] M.S.Wechsler and T.A.Read: J. Appl. Phys., 27(1956), 194.

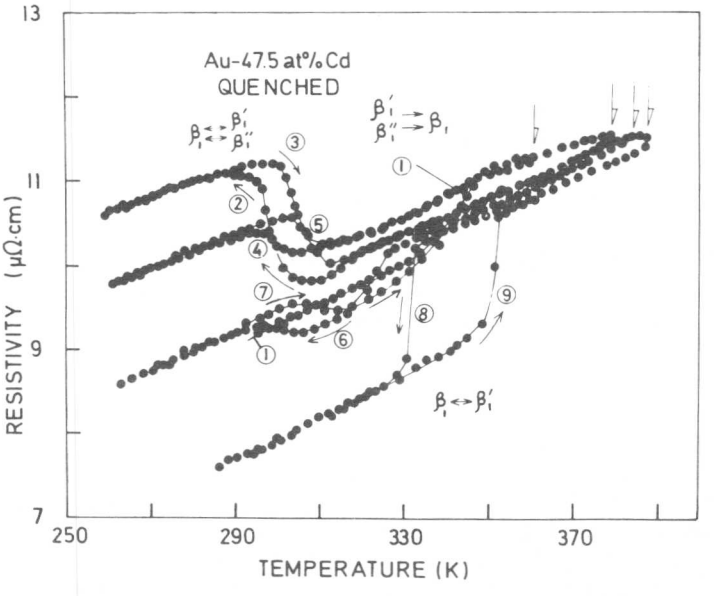

Fig.1: Electrical resistivity vs. temperature curves of the quenched Au-47.5at%Cd alloy, showing the variation due to varying the maximum heating temperature from 361 K to 388 K which are indicated by vertical arrows.

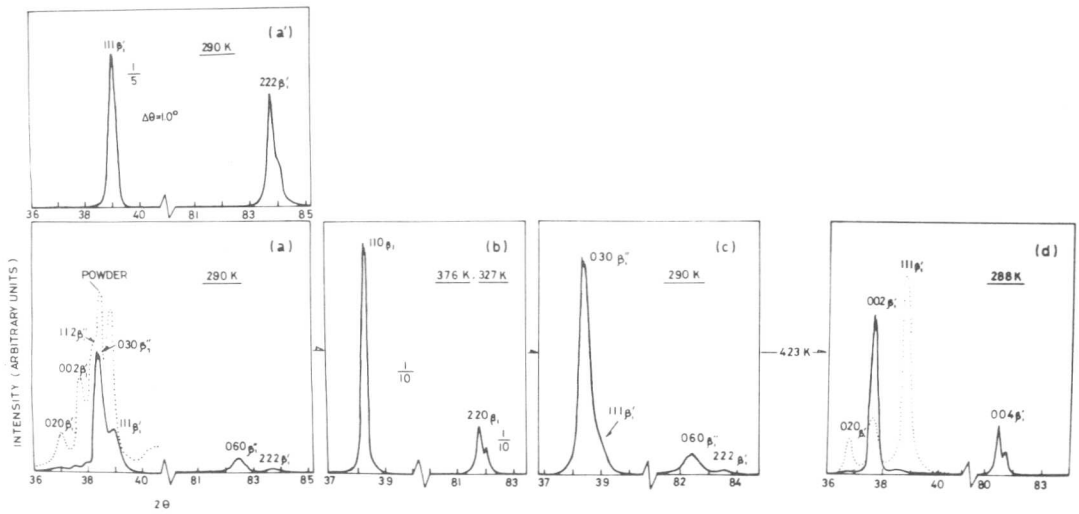

Fig.2: Partial X-ray diffraction profiles of the single crystal of the quenched Au-47.5at%Cd alloy in the vicinity of the $(110)_{\beta_1}$ and $(220)_{\beta_1}$ diffraction angles during heating and cooling. Dotted curves indicate those of the powder specimen in the vicinity of the $(110)_{\beta_1}$ diffraction angle for comparison.

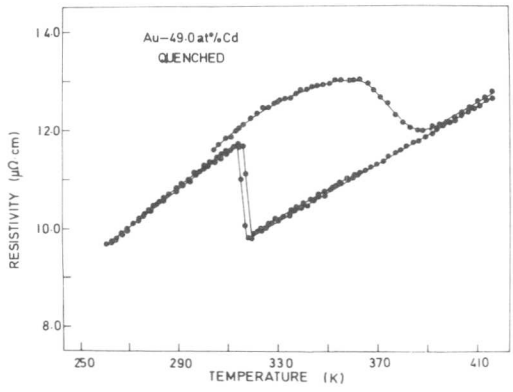

Fig.3: Electrical resistivity vs. temperature curves of the quenched Au-49.0at%Cd alloy.

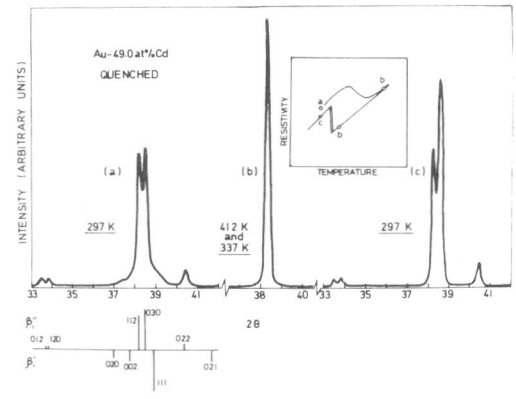

Fig.4: Powder X-ray diffraction profiles of the quenched Au-49.0 at%Cd alloy in the vicinity of the $(110)_{\beta_1}$ diffraction angle during heating and cooling.

The Substitution of Cu for Ni in Martensitic NiTiCu Shape Memory Alloys

K.N. Melton and R.H. Bricknell *

It is shown that up to 35 wt% of Ni in the NiTi alloy can be replaced by Cu whilst retaining a high temperature β phase with the CsCℓ structure which transforms to a martensitic phase showing the shape memory effect. The addition of Cu was found to have little effect on the Ms temperature, in contrast to most ternary martensitic systems. In a combined electron microscopy and X-ray diffraction study it was found that the martensite has a monoclinic structure with similar morphology and lattice parameters to those previously reported for the binary NiTi alloy. Initial substitution of Cu for Ni produced slight changes in the lattice parameters of both the high and low temperature phases, then these remain remarkably constant on further addition of Cu.

I. Introduction

The equiatomic or near equiatomic NiTi alloy is perhaps the best known and best characterised shape memory alloy. A shape memory effect is shown on heating material deformed in the vicinity of Ms such that reversion to the parent austenitic phase occurs, which has the ordered b.c.c. CsCℓ structure [1]. Ms has been reported to be very strongly dependent on the alloy composition, decreasing the Ti content leading to a rapid lowering of Ms [2]. There is only limited information on the influence of ternary additions and in most cases these lead to a decrease in Ms. Currently the main use of alloying elements in NiTi is thus to lower Ms and As where this is required for certain applications, and to improve the strength.
As part of a programme investigating the properties of shape memory alloys we have found that substantial amounts of Ni in NiTi can be replaced by Cu [3-6]. In this paper the effects of such a substitution on Ms and on the structures of the martensite and austenite phases are reported.

II. Experimental

Argon are melted buttons were vacuum induction remelted in a

Brown Boveri Research Center, CH 5405 Baden-Dättwil, Switzerland. * Present address General Electric Research and Development Center, Schenectady NY 12301, USA

graphite crucible to form rods 8 mm diameter. These were canned in stainless steel, hot swaged at 800°C to 5 mm diameter when the canning was removed before final hot swaging to 3 mm diameter. Sample preparation was completed by a 1 h anneal in argon at 950°C and air cooling. Ms temperatures were measured using an A.C. electrical resistivity techniques. For the X-ray diffraction study, discs were machined directly from the as-cast alloys in order to minimise texture effects.

III. Results and Discussion

It was found that alloys which were martensitic at room temperature could be obtained with copper contents of up to 35 wt%, and within this range of copper contents both the one-way and two-way shape memory effects were observed in the rapidly cooled as-cast and wrought conditions. An optical micrograph of a 32 wt% Cu alloy is shown in Fig. 1 and it can be seen that the alloy is martensitic and largely free from precipitates of a second phase. The Ms temperature determined by electrical resistivity is shown in Fig. 2 as a function of copper content for a constant titanium content of 46 wt%. Except for three shallow minima at 2%, 12% and 32% Cu, Ms is seen to remain markedly constant. This is in contrast to the reported effect [7] of replacing Ni by Co, where a strong dependence of Ms on composition was observed. A further observation of the effect of Cu is that the Ms dependence on the Ti content is reduced. This is illustrated in Fig. 3 for an alloy containing 5 wt% Cu. Also shown is the corresponding curve for the binary NiTi alloy prepared from the same starting materials and using the identical processing methods, and it can be seen that Ms decreases less rapidly with decreasing Ti content for the copper containing alloy.

An example of the fine structure of the martensite in a NiTiCu alloy is shown in the transmission electron micrograph of Fig. 4. The appearance of each foil of a given composition varied from region to region, both in the plate sizes observed and in the number and occurence of intersecting variants. These local differences within a foil were as great as those observed between the various compositions studied (up to 29 wt% Cu and including the binary alloy) and it was not possible to distinguish the foils using this criterion. Higher magnification revealed the plates to be internally twinned. The morphology of the martensite in NiTi in thus largely unaffected by the replacement of Ni by Cu.

In-situ heating of the foils in the electron microscope resulted in a burst-like transformation to a distinct high temperature phase whose electron diffraction patterns could be indexed in terms of an ordered b.c.c. CsCl structure with lattice parameters close to 3.0 Å. An example is shown in Fig. 5 for a 22 wt% Cu alloy.

The structural similarity of the high temperature phase was confirmed by X-ray diffractometry on bulk samples at 155°C. The lattice parameters of the austenitic phase, desired from measurements of the {211} diffraction peak, are plotted in Fig. 6 as a function of copper content. It can be seen that there is initially a slight increase in the lattice size on Cu additions but then a remarkably constant value is obtained.

Similar X-ray diffraction traces at room temperature, i.e. in the martensitic phase, were obtained from the copper containing alloys and binary NiTi. Although the relative intensities of the peaks varied, they could be consistently indexed in a similar manner to those of the binary alloy [8] and a similar monoclinic lattice derived. The lattice parameters of the martensites are plotted on Fig. 6 as a function of copper content. The monoclinic angle β was found to be constant at $97 \pm 0{,}1^{o}$, up to 10% Cu and then decreased slightly to $95{,}4^{o} \pm 0{,}1^{o}$ for alloys containing 22 and 29 wt% Cu.

It can be concluded from Fig. 6 that the structure of both austenitic and martensitic phases is very little changed by large copper substitutions. However within this framework it can be seen that the effect of these additions is to initially increase b_0 while decreasing c_0, and then to produce virtually constant lattice parameters, at least up to 22 wt% Cu.

The orthorhombic distortion needed for the step-wise mechanism for the formation of martensite in NiTi, proposed by Hehemann and Sandrock [9], in which an f.c. tetragonal cell derived from four b.c.c. cells is initially distorted to form an orthorhombic lattice and then sheared to the monoclinic martensite, can be derived from the differences in parameters between the f.c.t. and orthorhombic cells. The transformation distortion suffered in the a, b and c directions is thus given by the differences between a_0 and a_β, b_0 and $\sqrt{2}\, a_\beta$ and c_0 and $\sqrt{2}\, a_\beta$ respectively. $\sqrt{2}\, a_\beta$ is also shown in Fig. 6 and it can be seen that the lattice distortion in the a_0 direction remains reasonably constant with Cu additions (at least up to 22 wt% Cu) but that for less orthorhombic distortion is needed in the b_0 and particularly c_0 directions.

Conclusions

1. Copper can be used as a substituent atom for nickel in NiTi shape memory alloys resulting in material whose Ms temperature is less sensitive to composition fluctuations.

2. The high temperature phase remains ordered CsCl

3. All alloys undergo the same transformation as is observed

in binary NiTi alloys to produce a martensite with similar morphology.

4. The structures and lattice parameters of both austenitic and martensitic phases remain remarkably constant as Cu is substituted for Ni.

References

|1| W.J. Buehler, J.V. Gilfrich and R.C. Wiley: I. Appl. Phys. 34 (1963) 1475.
|2| J.E. Hanlon, S.R. Butler and R.I. Wasilewski: Trans. AIME 239 (1967) 1323.
|3| K.N. Melton and O. Mercier: Scripta Met. 12 (1978) 5.
|4| K.N. Melton and O. Mercier: Met. Trans. 9A (1978) 1487.
|5| O. Mercier and K.N. Melton: Met. Trans. in press
|6| R.H. Bricknell, K.N. Melton and O. Mercier: Met. Trans in press
|7| F.E. Wang: Proc. 1st Int. Conf. Fracture, Sendai, Japan 2 (1965) 899.
|8| K. Otsuka, T. Sauramura and K. Shimiza: Phys. Stat. Sol. 5A (1971) 457.
|9| R.F. Hehemann and G.D. Sandrock, Scripta Met. 5 (1971) 801.

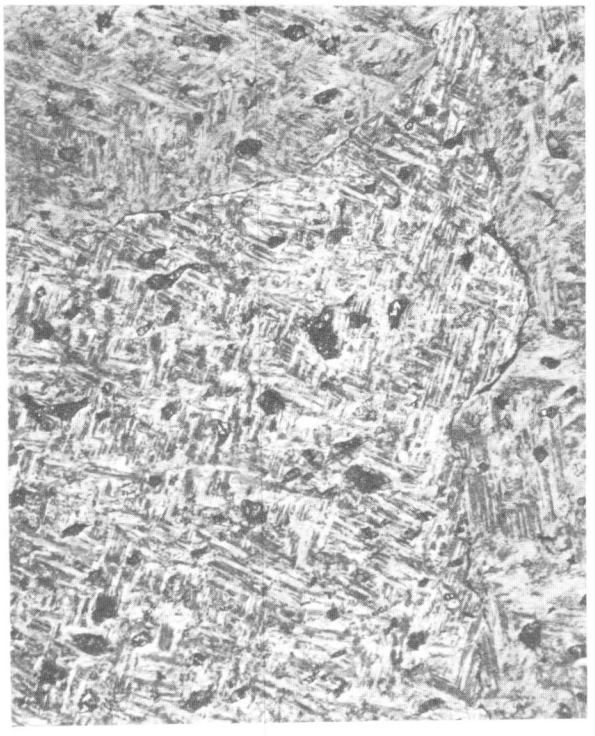

Fig. 1. An optical micrograph (x 200) showing the microstructure of a 46 wt% Ti 22 wt% Ni 32 wt% Cu alloy.

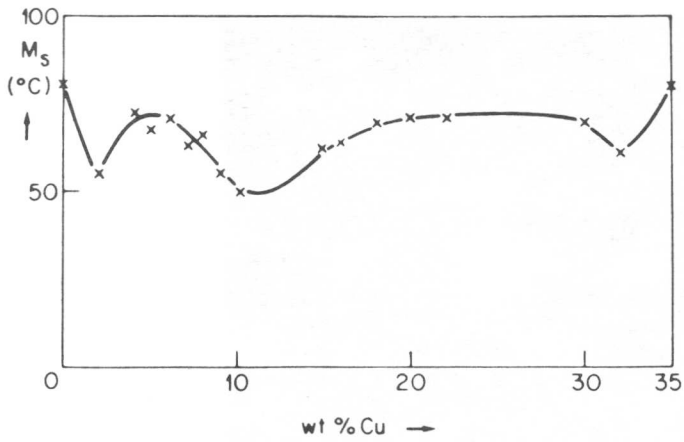

Fig. 2: M_S as a function of copper content for alloys with a constant titanium content of 46 wt%.

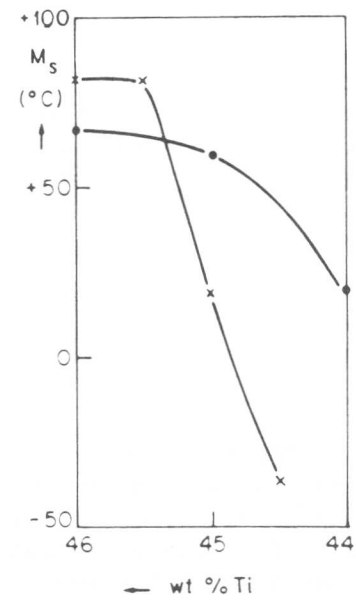

Fig. 3: M_S as a function of titanium content
x binary NiTi
. alloys with a constant Cu content of 5 wtE

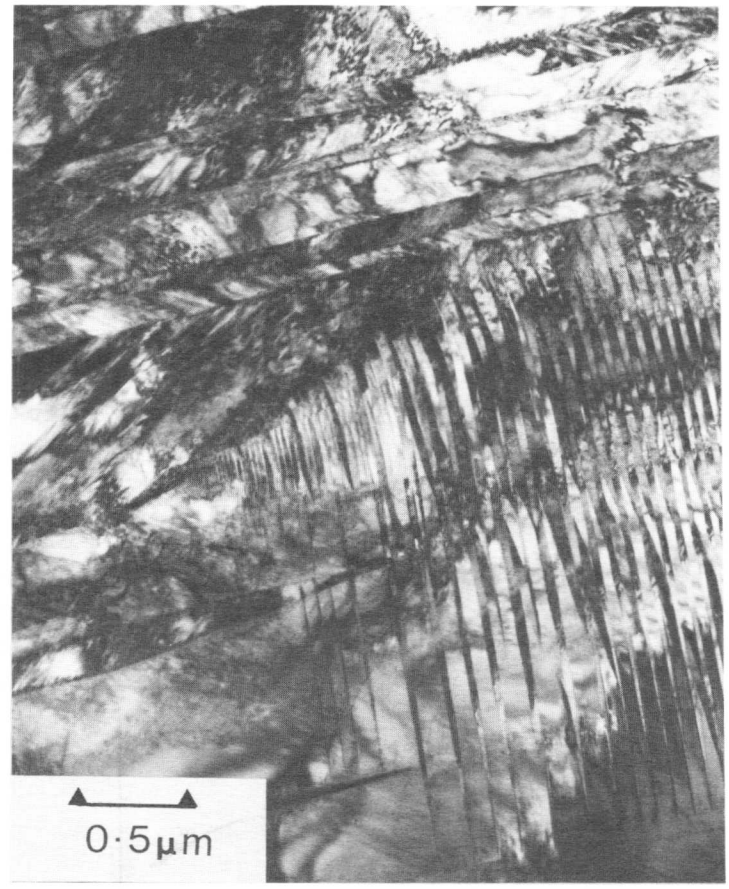

Fig. 4: Transmission electron micrograph of martensite plates in a 7 wt% Cu alloy.

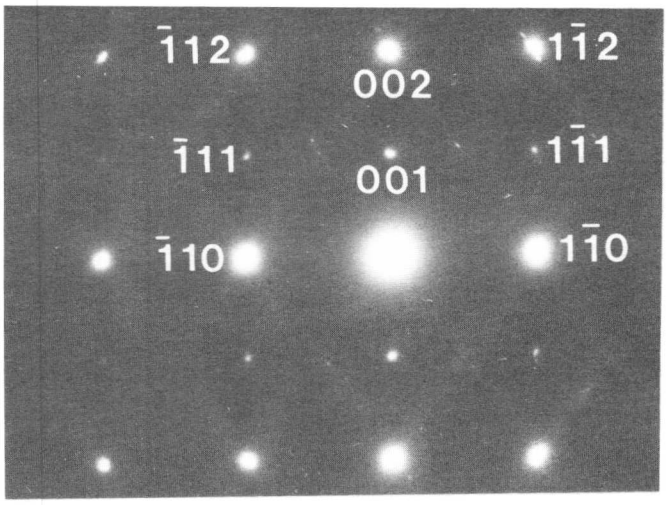

Fig. 5: Electron diffraction pattern from the austenitic phase of the 22 wt% Cu alloy Zone axis in <110> and the 001 ordering spots of the C_5Cl structure are seen.

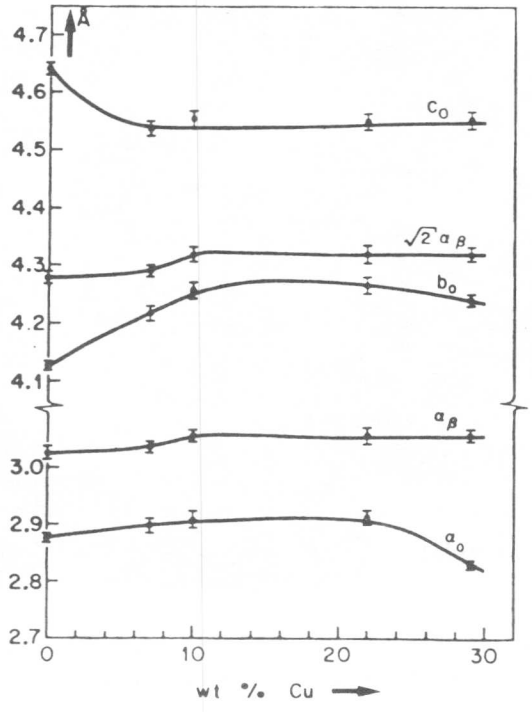

Fig. 6: The room temperature lattice constants of the martensite phase a_o, b_o, C_o plotted as a function of Cu content. Also shown are the lattice constant of the high temperature β phase and of the f.c.t. phase derived from it.

Considerations of Symmetry for the Thermoelastic Martensitic Transformation

Denis Gratias and Richard Portier

The description of the behaviour of a system submitted to a "sollicitation" (for instance the modification of the temperature, the application of an external stress or of a magnetic field...) is usely extremely difficult to formulate. However, this behaviour and the "resulting products of the transformation" satisfy simple symmetry rules which take into account the common symmetry of all the parameters involved : symmetry of the object, of the sollicitation, of the initial conditions. For the study of the martensitic transformation,such a point of view is not frequent (excepted in a paper by J.W. Cahn [1] based on a phenomenological treatment) but, in fact, symmetry considerations are always present. For instance, to say that it exists a single way of return to the parent phase from a martensitic phase when the transformation is crystallography reversible, is also simply described in terms of symmetry.

Preliminary results are presented here, but we must keep in mind that the symmetry rules only consist of necessary conditions (like selection rules in spectroscopy) and that many other factors (thermodynamical...), omitted here, can be preponderant.

I. Principle of superposition of symmetries : Curie's law

The first Curie's law states that when a cause induce some effects, the symmetry elements of the cause exist for the effects. Here the cause represents the interaction between a crystal and a sollicitation (temperature or applied stress). The symmetry of the cause is the common symmetry of these two components (symmetry elements belonging to the intersection group of the space group of the parent crystal $\mathcal{G}_0$ and the invariance group of the sollicitation $\mathcal{G}$ *) so this intersection group $\mathcal{H}_0 = \mathcal{G}_0 \cap \mathcal{G}$, leaving invariant the reaction, is the group of isoprobability of nucleation of the products of the transformation. For a specific nuclei of martensite, defined by a space groupe $\mathcal{G}_I$, every

---

*) If the sollicitation is the temperature, its invariance group is the symmetry group of the sphere : SO_3, if it is an applied stress, its invariance group is the symmetry group of the cylinder along the tensile axis : $\mathcal{D}_{\infty h}$.

C.E.C.M./C.N.R.S. 15, rue Georges Urbain, 94400 Vitry-sur-Seine, France

nuclei deduced from G_I by an operation of $\mathcal{H}_0$ appears with the same probability. There is no special relation between $\mathcal{H}_0$ and G_I but if some operations of symmetry of $\mathcal{H}_0$ also are operations of symmetry of G_I , they will not induce new equivalent nuclei of martensite and they must be omitted. These common operations belong to the group $\mathcal{N}_{0I}$, intersection of $\mathcal{H}_0$ and G_I and the only operations of symmetry which will induce new equivalent nuclei from G_I are the operations of $\mathcal{H}_0$ which do not belong to $\mathcal{N}_{0I}$. So the number of variants of martensite appearing during the transformation is (m_{01}) the index of $\mathcal{H}_0$ on $\mathcal{N}_{0I}$. Moreover, the decomposition of $\mathcal{H}_0$ (supergroup) into cosets of $\mathcal{N}_{0I}$ (subgroup) gives the $m_{01} - 1$ operations of symmetry which related the generated variants of martensite.

Remark 1 : starting from a single crystal of martensite, the inverse transformation can be expressed in the same manner.

Remark 2 : we can only use for the martensitic transformation, the point symmetry group : assuming that a rigorous treatment, using spatial group leads to many difficulties because the metric between the parent and martensitic phases changes. The difference of translations creates some mismatches and we think that the internal defects (twins, faults) of martensites plates, or some interface dislocations can eliminate these mismatches.

Remark 3 : this treatment requires the knowledge of the exact orientation of the respective point groups.

So, a possible scheme for the transformation is :

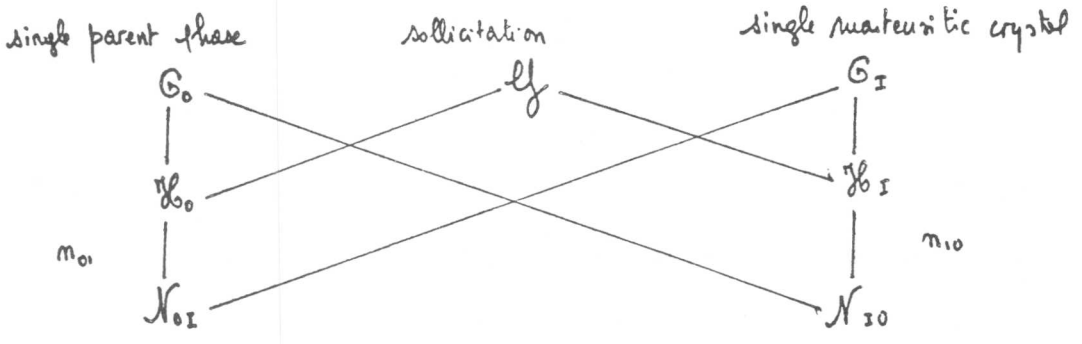

the number of variants of martensite from a single parent phase :

$$m_{01} = i\left(\mathcal{H}_0 / \mathcal{N}_{0I}\right)$$

. number of variants of parent from a single martensitic phase

$$m_{10} = i\left(\mathcal{H}_I / \mathcal{N}_{I0}\right)$$

As an example : NiAl

- Transformation with temperature

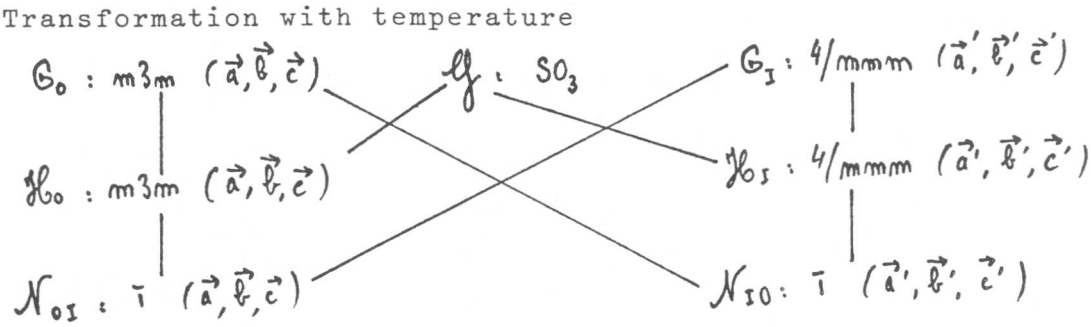

$$n_{01} = i\left(\frac{m3m}{\bar{1}}\right) = \frac{48}{2} = 24$$

$$n_{10} = i\left(\frac{4/mmm}{\bar{1}}\right) = \frac{16}{2} = 8$$

- Transformation under a stress with $[100]_{parent}$ as a tensile axis.

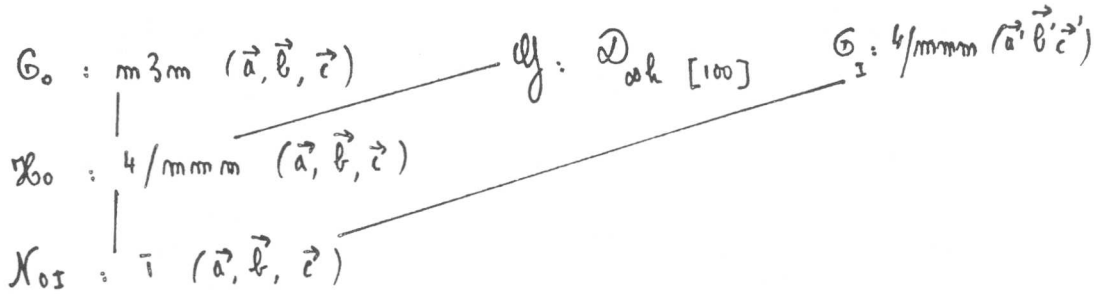

$$n_{01} = i\left(\frac{4/mmm}{\bar{1}}\right) = \frac{16}{2} = 8$$

Remark 4 : for such a treatment we use the crystallographic data of the literature. Obviously, for instance a monoclinic distortion of the martensite will change the group $\mathcal{G}_I$, and hence the number of variants.

Remark 5 : the decomposition of $\mathcal{H}_0$ into cosets of $\mathcal{N}_{0I}$

$$\mathcal{H}_0 = [\,1 + h_1 + \dots + h_{n_{01}-1}\,]\,\mathcal{N}_{0I}$$

gives the operations relating two variants of martensites : for instance $\mathcal{G}_I \xrightarrow{h_1} \mathcal{G}_{II}$; $\mathcal{G}_I = h_1^{-1}\,\mathcal{G}_I\,h_1$

In fact, this relation must be written $h_1 \circ \mathcal{G}_I$, because the

variant I is invariant by its own symmetry operations.

II. Crystallographic reversibility

It means, starting from a single variant of parent phase that m_{0I} variants of martensite will be generated but at the reversion, the same single variant of parent phase will be obtained again. Obviously this appears if $m_{10} = 1$, that means $\mathcal{G}_1$ is a subgroup of $\mathcal{G}_0$. But for NiAl, this is not the case. In fact, for a thermoelastic transformation which presents this character, the transformation appears to be a reversible movement of interfaces. Any product of transformation appearing at the level of an interface between two variants gives rise to an other one with the same probability by an operation of symmetry common to the two variants. If all these operations are also operations of symmetry of the parent phase, no new variant of this parent phase will be generated at the reversion. So the condition for this reversibility (and for thermoelastic behaviour) is that :. between the parent phase and the variant $\mathcal{G}_I$ of martensite $(\mathcal{G}_0 \cap \mathcal{G}) \subset \mathcal{G}_0$ (obvious)
. between two variants of martensite $\mathcal{G}_I$ and $\mathcal{G}_{II}$

(the sign $\subset$ means subgroup). $(\mathcal{G}_I \cap \mathcal{G}_{II}) \subset \mathcal{G}_0$

We can easily see that this is the case for NiAl.

III. Internal defects of the martensitic plates

The latter condition has to be verified for instance between $\mathcal{G}_I$ and $\mathcal{G}'_{II}$, $\mathcal{G}'_{II}$ deduced from $\mathcal{G}_{II}$ by the twin operation. For NiAl, the twin operations correspond to the lost {110} mirrors of the parent phase. In this case they are not able to generate new variants of $\mathcal{G}_0$.

In case of faulted martensite, the local group has to be examined.

IV. Pseudoelasticity

The previous condition obtained for a reaction in temperature is easily extended to a reaction under an applied stress by considering also the symmetry of the stress :

$$(\mathcal{G}_I \cap \mathcal{G}_{II} \cap \mathcal{G}_f) \subset \mathcal{G}_0 .$$

So, a thermoelastic alloy is also pseudoelastic but it seems possible that a non thermoelastic alloy submitted to an applied stress with a specific tensile axis can be pseudoelastic.

V. Shape Memory Effect

It appears that the condition for this effect is a thermoelastic character. This requires the existence of a group for the parent phase which is only possible for an

ordered alloy or a totally disordered alloy (InTl). The case of twins or faults is examined for the crystallographic reversibility.

VI. Some remarks on long period stacking martensites

3R, 2H, 9R... martensites can be considered as different stacking of $[111]_m$ planes. In a simple model, from a B2 parent phase, three $[111]_m$ planes are noticed: A, B, C.

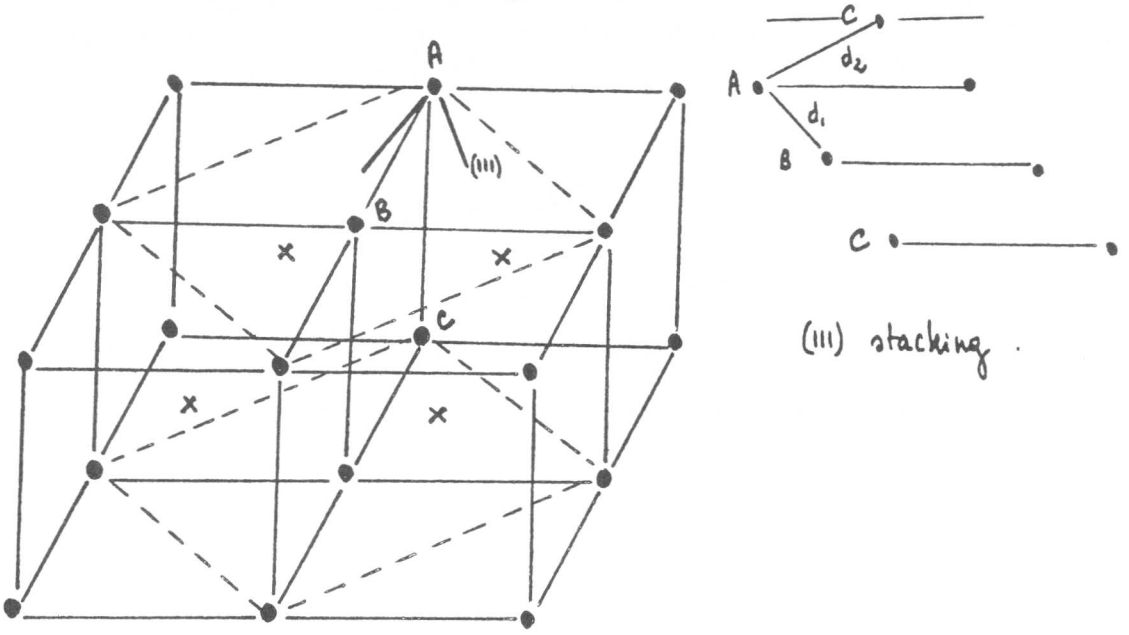

Two distances appear in the stacking :

AB = first neighbour distance (of the same kind of atoms) 1/2 1/2 0 of the "C.F.C." martensite and corresponding to an old 100 B2 distance (forst neighbour)

AC = second neighbour distance (001 of "C.F.C." corresponding to an old 001 - B2 distance (first neighbour).

If during the transformation AB and AC are equal, we have a structure of undiscernibility of first and second neighbour (a similar treatment for the twinning was given by Dubertret and Le Lann [2]). This unstable structure can be relaxed into two possibilities

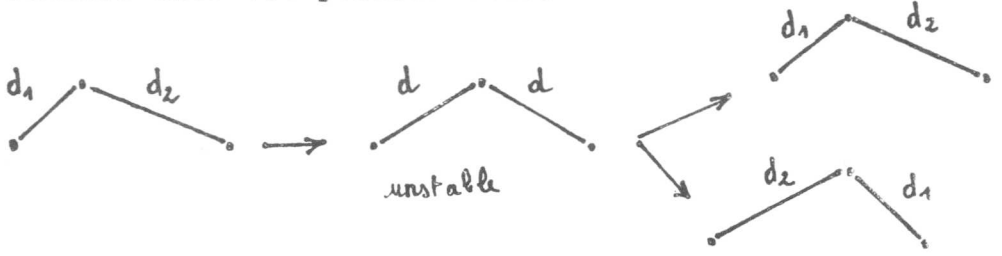

Assuming the fact all these martensites lead to the same non stable structure of indiscernibility, this can be an easy way for their mutual transformations. In the same manner the internal twinning can be presented. Moreover, we can notice that the undiscernible structure of the martensite in the example is similar to the parent phase, so we can imagine that the transformation (martensite → martensite, or twinning) passes through the parent phase which is unstable under the conditions of the transformation. This result has to be compared with the paper of Wasilewski on the mechanical twinning as result of a stress assisted martensitic transformation [3] .

References

1 J.W. CAHN : Acta Met., 25 (1977), 72

2 A. LE LANN and A. DUBERTRET : Phys. Stat. Sol. A, to be published.

3 R.J. WASILEWSKI : Met. Trans., 8 A (1977), 391

Reversibility of $\gamma \rightleftarrows \varepsilon$ Transformation in Fe-18Cr-14Ni Alloy Single Crystals

A. Sato, H. Kasuga and T. Mori

Macroscopic shape change associated with the $\gamma \rightleftarrows \varepsilon$ martensitic transformation under an external stress is examined on Fe-18%Cr-14%Ni alloy single crystals. It is demonstrated that a crystal elongated below Md temperature, 220 K, shows substantial shrinkage by warming-up above 260 K due to the $\varepsilon \rightarrow \gamma$ reverse transformation. Results of the quantitative measurements of the shrinkage are summarized as follows: 1) The largest shrinkage occurs when a crystal was elongated along the [414] direction, introducing a single variant of ε-martensites. 2) Formation of α-martensites impedes the $\varepsilon \rightarrow \gamma$ reverse transformation and suppresses the amount of shrinkage. 3) Application of a tensile stress during the reverse transformation reduces the shrinkage drastically. With increase of a stress above a critical value, a crystal manifests elongation by the reverse transformation. These observations are well described by the motion of particular Shockley partial dislocations under the influence of chemical driving force and the internal and external stresses. Based on these findings, correlation between the martensitic transformation and a shape memory effect is discussed.

I. Introduction

The reversible shape memory (RSM) effect has recently been found in a variety of materials including some iron based alloys [1,2], in which the origin is suggested to come from the reversibility of the shape change due to the $\gamma \rightleftarrows \varepsilon$ martensitic transformation. The current studies of the RSM effect in the iron based alloys have been made on polycrystalline materials and the method of the mechanical test has been limited to a bending. In these studies, however, it is difficult to find an exact correlation between the involved mechanism and the relevant physical properties, which are inherent to the crystal structure.

An external stress required to cause the $\gamma \rightarrow \varepsilon$ transformation has been found to satisfy the Schmidt law for a $\langle 11\bar{2} \rangle \{111\}$ shear [3]. This is because the fcc $\rightarrow$ hcp transformation occurs mainly by operation of a simple shear which is carried by motion of Shockley partial dislocations. Therefore, it is possible to introduce a single variant of ε-martensites by applying an external stress along a proper crystallographic direction. With this in mind, in the present study, an exact measurement of the shape change associated with the $\gamma \rightleftarrows \varepsilon$ transformation will be made under various experimental conditions. The results will then be applied to discuss the mechanism of the RSM effect in the iron based alloys. In the course of the study it will also become apparent that some of the earlier conclusions [4,5] must be examined carefully by taking account of the $\varepsilon \rightarrow \gamma$ reverse transformation.

Department of Materials Science and Engineering, Tokyo Institute of Technology, Ookayama, Meguro, Tokyo 152, Japan.

II. Experimental Procedure

Rectangular flat specimens of 0.5 x 2 x 5 mm were cut from a single crystal of an Fe-18%Cr-14%Ni alloy grown under vacuum by the Bridgeman method. They were annealed in an argon atmosphere at 1273 K for 1 h, quenched into water and electrolytically polished to remove the surface contamination. Specimen orientations are shown in Fig. 1. ε-martensites were introduced by tensile deformation on an Instron type testing machine or by cooling a specimen under a constant load on a creep machine. Measurement of the shape change was made on micro-Vickers markings placed on a flat surface of a specimen by using a precision machinary microscope. During the measurement, a specimen was immersed in an alchohol bath cooled at a desired temperature below 300 K. For the more accurate length change measurement, a creep machine, by which the length change occured under an external stress was measured, was used. the specimens undergone the $\gamma \rightarrow \varepsilon \rightarrow \gamma$ transformation cycle were examined by an interference microscope and subsequently by a 200 KV electron microscope equipped with a 60° tilt and 360° rotation goniometer.

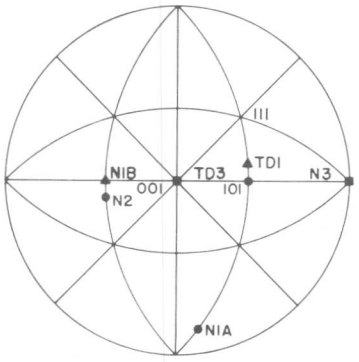

Fig. 1 Stereographic projection of tensile axes (TD) and flat surface normals (N).

III. Experimental Results

Among the specimens with three different tensile axes (cf. Fig.1) the specimen with the [414] tensile axis exhibited largest shrinkage by the warming-up. As it will become apparent shortly, this is attributable to the lowest probability of formation of α-martensites for this orientation compared with others. In this report the results of the [414] specimens with the surface normals N1A (type A) and N1B (type B) will be presented.

A few representative examples of the shape change measurements made on type B crystals are shown in Figs. 2(a) and (b). The deformation temperature corresponds to the left end of each curve in the figure. As shown in (a) the shrinkage is largest for the specimen deformed just below Md(ε) temperature, it is zero for the one deformed above Md(ε), and it is not zero but smaller for the one deformed in the visinity of Md(α) temperature. These observations, together with three micrographs shown in Fig. 3, can be taken as evidence that the shrinkage comes from the $\varepsilon \rightarrow \gamma$ reverse transformation, and that formation of the α-martensites prevents the $\varepsilon \rightarrow \gamma$ reverse transformation. By comparing the 223 K deformation data in the two figures, Figs. 2(a) and (b), it is noted that the elongation along the tensile axis and the shrinkage along the width is complimentary, assuring that the only a single variant of ε-martensites were introduced by the operation of a single shear system, $[121](1\bar{1}1)$. It is also noted that the amount of the recovery strain is

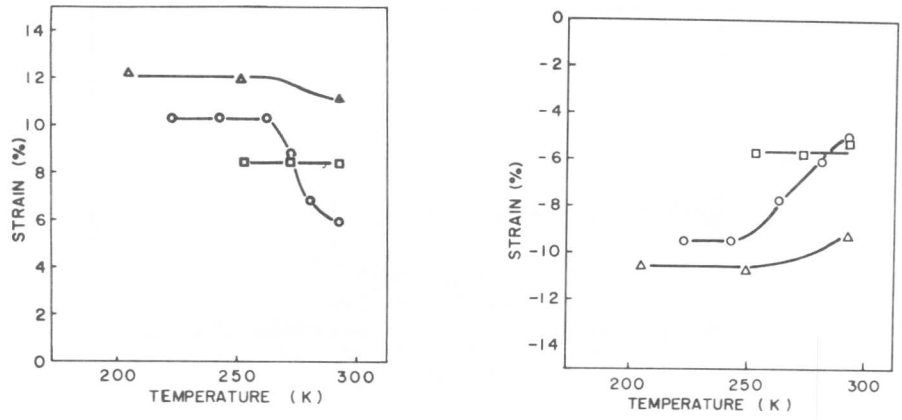

(a) (b)

Fig. 2 Length changes measured along the tensile axis (a), and along the transverse direction (b) on a flat surface.

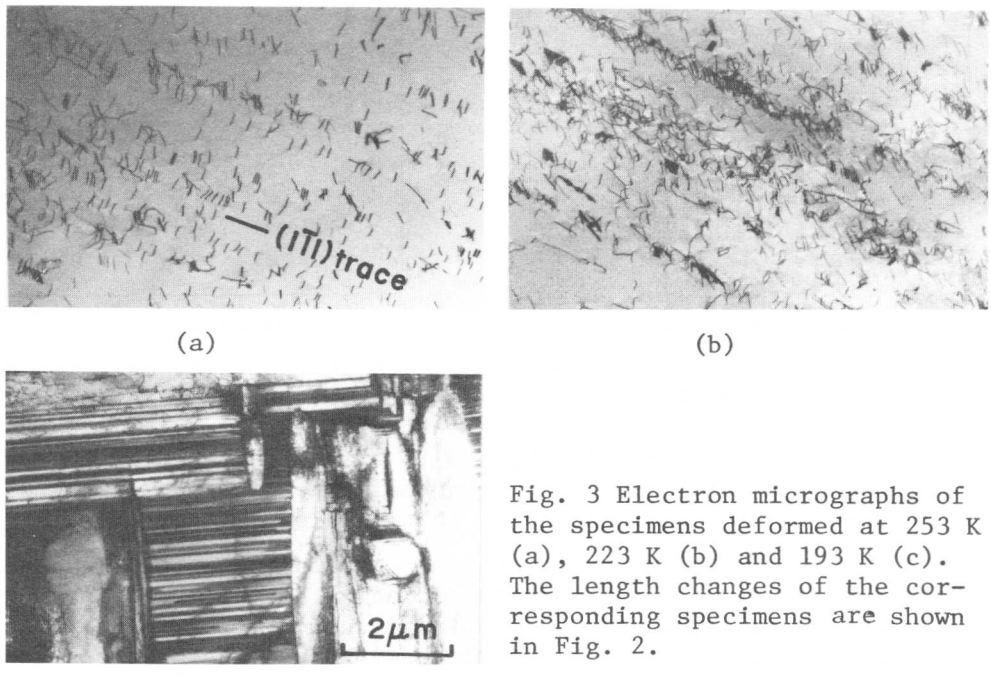

(a) (b)

(c)

Fig. 3 Electron micrographs of the specimens deformed at 253 K (a), 223 K (b) and 193 K (c). The length changes of the corresponding specimens are shown in Fig. 2.

smaller than the initial deformation strain, despite that the reverse transformation was completed in this specimen. This means that the $\varepsilon \rightarrow \gamma$ reverse transformation occurs by the concurrent operation of other shear systems, presumably $[21\bar{1}](1\bar{1}1)$ and $[\bar{1}12](1\bar{1}\bar{1})$, in addition to the $[\bar{1}\bar{2}\bar{1}](\bar{1}11)$ shear system in absence of an external stress.

The length change due to the reverse transformation varied with the amount of a strain given at a low temperature as well as with the variation of an external stress applied during the reverse transformation. Figure 4 shows the shrinkage measured along the tensile axis by a creep machine (filled symbols) and by a precision machinary microscope (open

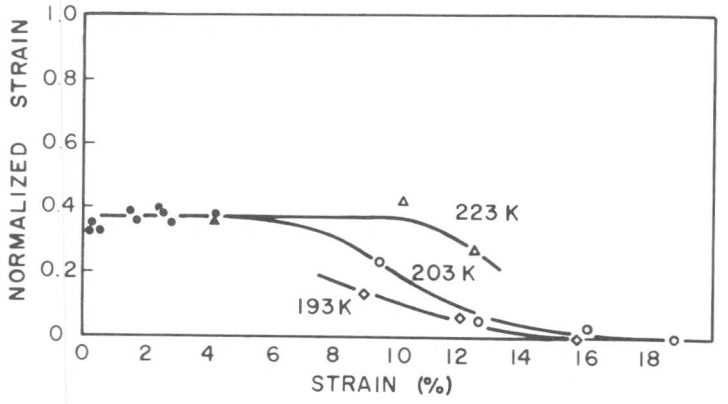

Fig. 4 Shrinkage versus initial elongation. The amount of the shrinkage is normalized with respect to the initial elongation. The deformation temperature is indicated on the corresponding curve.

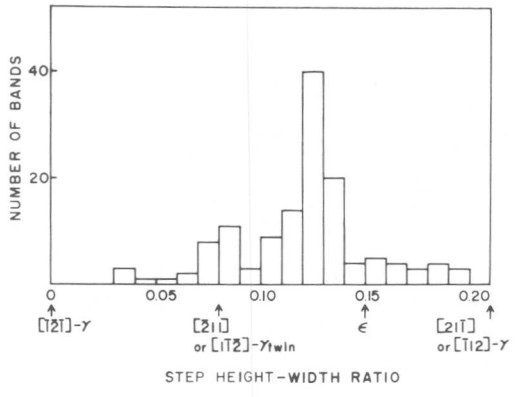

Fig. 5 Distribution of step height-width ratio. The geometrically conceivable ratios of an ε-martensite and a γ-twin are indicated by arrows with the shear directions of the reverse transformation.

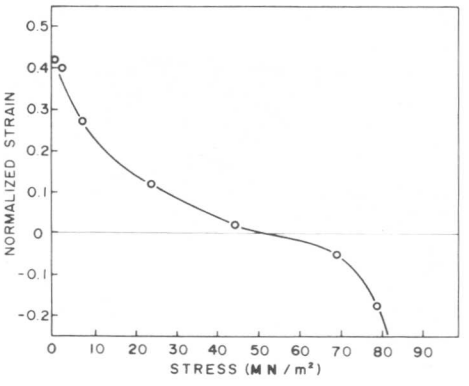

Fig. 6 Influence of an external stress on the shape change due to reverse transformation. The ordinate axis shows the length change normalized with respect to the initial elongation.

symbols), after giving various amount of deformation at the temperature indicated on each curve. An important finding here is that the shrinkage is constant and about 40% of the initial elongation in the small strain region, and it starts to decrease with incsease of the strain and eventually disappears. In order to obtain the further information with regard to the incomplete recovery of the shape change, step height was measured on the flat surface of a type A specimen by an interference microscope. The result is shown by a histogram of a step height-width ratio in Fig. 5. An arrow with a symbol, ε, shows the ratio for an ε-martensite which is supposed to have been formed by the low temperature deformation. The observed ratio distributes in a rather wide range but with its average value somewhat smaller than that for the ε-martensite. This observation is in good accordance with the results of the macroscopic measurements (Fig. 2). As will be discussed later, these results are well explained by a particular situation of the internal stress and

the density of Shockley partial dislocations.

As shown in Fig. 6 the amount of shrinkage decreases rapidly with increase of an external stress applied during the reverse transformation, it becomes zero at 48 MN/m^2, and elongation takes place above it. Since the tensile stress was limited within 80% of the yield stress at room temperature no slip deformation should have occured in the above tests. This is supported by the fact that the temperature, at which the length change became notable and saturated, was same regardless of the magnitude of the stress.

IV. Discussion

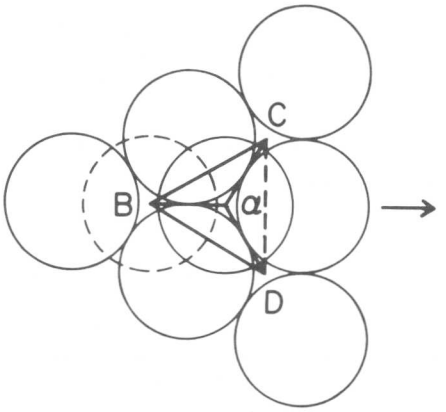

Fig. 7 Illustration of the $(1\bar{1}1)$ plane and the permissible shear directions for the reverse transformation. An arrow indicates the projection of the $[414]$ direction on the $(1\bar{1}1)$ plane.

The 40% recovery of the shape change observed after the $\gamma \rightarrow \varepsilon \rightarrow \gamma$ transformation cycle is a large shape memory effect compared with the earlier works [1,2]. A possible explanation can be given as follows: Figure 7 illustrates the three permissible shear directions, $\alpha B=[\bar{1}\bar{2}1]$, $\alpha C=[\bar{1}12]$ and $\alpha D=[21\bar{1}]$ on a $(1\bar{1}1)$ plane to cause the reverse transformation. BC, CD and DB are the Burgers vector directions of a perfect dislocation. In absence of external and internal stresses the three shear systems, αB, αC and αD, will operate equally provided that the number of the partial dislocations are same. If so, no shape change will result by the reverse transformation. In the actual measurements, however, the specimen showed a large shrinkage. From the electron micrographs shown in Fig. 3(b) and the ones taken with other g vectors, the dislocations introduced by the transformation cycle were found to be almost exclusively the BC and BD types. This means that the number of the αB dislocations should have been equal to the sum of the αC and αD dislocations when they were split on the $(1\bar{1}1)$ plane. If all of the partial dislocations are assumed to move the same distance, the strain produced by the reverse transformation will be 1/4† of that introduced by the $\gamma \rightarrow \varepsilon$ transformation. Thus, the substantial part of the shrinkage can be attrib-

† Suppose that an ε-martensite, introduced by the operation of the $B\alpha$ shear, transforms back to γ by the αB, αC and αD. One half of the reverse transformation occurs by the operation of the αB type shear. Since contribution of the αC and αD shears to the shrinkage is negative and a half of the αB shear in its magnitude as seen in the figure, the resultant shrinkage strain becomes 1/4 of the initial elongation.

uted to the particular situation of the partial dislocation densities. Judging from the sensible stress dependence of the shrinkage shown in Fig. 6, rest of it can be attributed to the influence of an internal stress, possibly developed during the $\gamma \rightarrow \varepsilon$ transformation by the uniaxial deformation.

Although the observed maximum recovery in the shape change was 40%, a complete recovery is yet expected depending on an experimental means. For instance, if it is allowed to extrapolate the result shown in Fig. 6 towards a negative stress, corresponding to compression, a 100% recovery is to be attained at 30 MN/m^2. This expectation implies that the RSM effect may occur by the $\gamma \rightleftarrows \varepsilon$ martensitic transformation when a specimen is situated under an appropriate internal stress. In the present crystal, however, formation of α-martensites will make the situation difficult: As shown in the previous study [6], α-martensites are usually formed as closely spaced and twin related pairs. Therefore, long range internal stress produced by the α-martensites are canceled. Moreover, partial dislocations, which carry the $\gamma \rightleftarrows \varepsilon$ transformation, are likely to be trapped and altered in its character at the ε-α martensite boundary, thus destroying the species required for the shape memory effect to manifest.

Finally, apart from the discussion of the shape memory effect, we would like to mention about the possible influence of the $\varepsilon \rightarrow \gamma$ reverse transformation on some of the earlier works [4,5] based on the present experimental observations. Although micrographs are not shown in this report the structure observed by Dash and Otte, and that by Fujita and Ueda resembled well with those of the partially reverse transformed specimens in the present study. That is, ε-martensites bounded by a twin related pair of α-martensites or by other variant of ε-martensites were left otherwise disappeared by the reverse transformation. It means that a special care must be exercised in order to examine a phenomenon involving the $\gamma \rightarrow \varepsilon$ martensitic transformation for which the Ms-As temperature gap is generally small but influenced by the presence of other imperfections.

REFERENCES

[1] K. Enami, A. Nagasawa and S. Nenno: Scripta Met., 9(1975), 941.
[2] K. Enami, A. Nagasawa and S. Nenno: Proc. 1st Japan Inst. Metals Int. Symp., Kobe, (1976), 239.
[3] A. Sato, Y. Sunaga and T. Mori: Acta Met., 25(1977), 627.
[4] J. Dash and H. M. Otte: Acta Met., 11(1963), 1169.
[5] H. Fujita and S. Ueda: Proc. 1st Japan Inst. Metals Int. Symp., Kobe, (1976), 351.
[6] Y. Higo, F. Lecroisey and T. Mori, Acta Met., 22(1974), 313.

The Decomposition of δ-Ferrite to Austenite by a Martensitic Mechanism in a Duplex Stainless Steel

P D Southwick and R W K Honeycombe

As part of a detailed microstructural investigation of the decomposition of δ-ferrite in an AISI 329-type stainless steel, it was found that on ageing the fully ferritic structure below 600°C, the precipitated austenite was different in morphology and crystallography from that formed at higher temperatures. After very short ageing times (c. 5 secs) very long thin plates of austenite were found (30nm x 5000nm), which exhibited a Nishiyama-Wasserman orientation relationship with the ferrite. The habit plane of the austenite was $\{133\}_\alpha$ and the plates were heavily faulted, with one fault every 1-2nm; STEM microanalysis indicated that the austenite was of the same composition as the matrix. These results suggest that the transformation occurs via a martensitic mechanism. The lattice imaging technique applied to the austenite-ferrite interface indicated that the fault energy may be more important than the usual concept of lattice mismatch, and although the results were not directly interpretable, they showed qualitative agreement with the Olsen-Cohen model for the BCC → FCC transformation.

I. Introduction

In duplex stainless steels, the microstructure consists of austenite and ferrite at most temperatures, including room temperature. By adjustment of the temperature, the stable volume fraction of austenite and ferrite can be changed, and above 1250°C, the alloys become fully ferritic. This single phase microstructure can be retained to room temperature by water quenching, and subsequent ageing in the temperature range 300°C to 1200°C results in the precipitation of austenite (1). In spite of the reverse nature of the transformation, i.e. ferrite transforming to austenite, it has been shown (1,2) that the high temperature (>600°C) precipitation reactions model those which occur in low alloy steels. These stainless steels have been used to gain information on the growth kinetics of the austenite (1,2) and the interface structure between the austenite and the ferrite (1,3). The results agree with those obtained in low alloy steels (4,5,6) and with the theoretical predictions for both growth kinetics and interfacial structure (7). However, the most elusive transformation in low alloy steels is the martensite reaction; the nature of the reaction precludes, in general, the detailed examination of the martensite nuclei or of the interfacial structure. While the phenomenological theories (9,10) have had considerable success in describing the reaction, and predicting the habit planes found, mechanistic nucleation theories (11) have little practical evidence to support them. The most recent theoretical models for martensite nucleation have been provided by Olsen and Cohen (12). The general principles are outlined in their work, and specific

---

Department of Metallurgy and Materials Science, University of Cambridge, Cambridge, UK.

transformations are dealt with; one of which is the BCC → FCC transformation. The precipitation of austenite in the duplex stainless steel in the temperature range 300°C to 600°C appears to form via a martensitic mechanism; the evidence for this conclusion is presented below, and the agreement with the Olsen-Cohen model is pointed out.

II. Experimental Procedure

The steel used in this investigation was of composition Fe-26.5%Cr-4.9%Ni-1.3%Mo-0.03%C; specimens were solution treated at 1300°C for 30 seconds and subsequently water quenched to give a fully ferritic microstructure. Specimens were then aged at temperatures between 300°C and 600°C in a tin bath for times between 5 seconds and 100 hours. Thin foils were prepared, and were examined in a Philips EM400 TEM/STEM with microanalytical facilities, and in a JEOL 120CX for the high resolution microscopy.

III. Results

A typical microstructure of the transformation which occurs above 600°C is shown in Figure 1, which was aged for ½ hour at 700°C. The predominant morphology of the austenite is Widmanstätten sideplates, although this is less marked at higher temperatures. It is shown elsewhere (1,2) that the precipitation in this temperature range produces morphologies which correlate with the Dubé morphological classification (13). The austenite exhibits a Kurdjumov-Sachs orientation relationship with the matrix (14) which is more strictly obeyed as growth proceeds (1,2). The initial growth direction is $\langle 112 \rangle_\alpha$, which leads to a macroscopic habit plane of $\{110\}_\alpha$ in the later stages of growth. Analysis of the growth kinetics has shown that the precipitation of the austenite occurs by a nucleation and growth process which is diffusion controlled (1,2). This is in marked contrast to the morphology shown in Figure 2a, which is formed after 5 seconds at 500°C; the austenite has a plate-like morphology, and is twinned at the centre of the plate. A more general area is shown in Figure 2b, formed after 10 seconds at 400°C; the particle marked A is almost parallel to the 001_α beam direction, and the orientation relationship with the ferrite is shown in Figure 2c, an SADP, which is indexed consistently with the Nishiyama-Wasserman orientation relationship (15); the austenite habit plane was shown to be $\{133\}_\alpha$ by trace analysis. In order to determine the composition of the austenite, the energy dispersive X-ray analysis (EDAX) facility on a Philips EM400 TEM/STEM was used. Full details of this technique are described elsewhere by Thompson (16). The results for both high and low temperature austenite precipitates are shown in Table 1. Within the accuracy of the microanalytical technique, calculated to be $\sim$5% of the value obtained, the analyses for the low temperature austenite and ferrite matrix are identical, whereas the analyses of the high temperature reaction products are clearly different. This implies that the low temperature reaction occurs by a diffusionless process.

Close examination of Figure 2a shows that there are dislocations present in the austenite-ferrite interface, which are giving rise to lobe-contrast in the ferrite, indicating that they are being observed end on. No lobe contrast is observed near the tip of the austenite

plates, but there is strong strain field contrast, implying that no dislocations are present, and that the local mismatch is being accommodated elastically. To investigate this more fully, the lattice imaging technique was used, and Figure 3 shows the tip of an austenite plate formed after 5 seconds at 400°C. The beam direction is near 001_α, and the $111_\gamma/110_\alpha$ planes are imaged; the lattice fringes are continuous across the tip, but gradually rotate up to $\sim 5.6^\circ$ away from the tip, and this relative rotation is maintained at greater distances from the plate tip. The spacings of the fringes are consistent with spacings of the lattice planes, measured to be 1.9776Å for the 110_α planes and 2.0244Å for the 111_γ planes from X-ray powder photographs. The lattice fringes near to the plate tip tend to be curved in both phases, due both to the strain in the two lattices and to local changes in foil orientation, shown by the variation in background intensity. Therefore, no simple direct analysis of the curvatures can be performed.

Lattice fringe terminations can be seen at A in Figure 3 at the austenite-ferrite interface, $\sim$290Å from the plate tip and those near B are apparently of variable sense; these fringe terminations are associated with local irregularities in the otherwise progressive change in orientation of the $\{111\}_\gamma$ planes up to the $\sim 5.6^\circ$ rotation. From Figure 3 it can be seen that there are no other dislocations near the plate tip with the same particular Burgers vector.

In addition to the interfacial dislocation structure, the austenite plates exhibit internal structure. This is closely shown in Figure 4a, where the austenite is inclined to the electron beam. A set of fine lines are observed within the austenite which have a spacing of the order of 20Å. An SADP of this austenite, shown in Figure 4b, shows that there is heavy streaking in a direction normal to the lines; this is consistent with the lines being stacking faults, which are spaced approximately every 10 lattice planes. Figure 5 shows a lattice image of an austenite plane, imaged with an 001_α beam direction, where the lattice fringes now run along the trace of the austenite plate. It can be seen that the relative rotation of the $110_\alpha/111_\gamma$ fringes is much smaller than in Figure 3, where the 110_α fringes are perpendicular to those imaged in Figure 4; the relative rotation is $\sim 2^\circ$. The stacking faults which cross the austenite plate can be clearly seen in this micrograph, and the 111_γ fringes are shifted from side to side as they cross the faults.

IV. Discussion

These results show conclusively that the decomposition of ferrite to austenite in a stainless steel which is normally duplex occurs by two substantially different reaction mechanisms, depending upon the transformation temperature. The high temperature reaction occurs by a diffusional nucleation and growth process, and the low temperature reaction by a diffusionless martensitic transformation. The absence of a composition difference with the matrix, the markedly different morphology, the orientation relationship, irrational habit plane and the internal structure associated with the low temperature produce as compared with the high temperature austenite are similar features to those observed in the martensite and pro-eutectoid ferrite reactions in low alloy steels. This indicates further the comparability between the two types of alloy in

spite of the reactions occurring in reverse crystallographic directions. The martensitic austenite is similar in habit plane and orientation relationship to the thermally activated martensite formed in Ag-Zn (17); the Nishiyama-Wasserman relationship is normally only observed where the reaction mechanism is at least partly shear. However, most of the factors discussed above are phenomological, while evidence for the reaction mechanism must exist on a finer scale. The lattice image shown in Figure 3 shows that the first dislocation exists 290Å from the plate tip. The Olsen-Cohen (12) dislocation model for the transformation shows the second shear of the transformation is $a_{FCC}/18(1\bar{2}1)$ which must be spread by a displacement every 9th plane is displaced in order to prevent rotation of the fault plane. The irregularities arrowed in Figure 3 where the fringes cross the interphase boundary are spaced by 8-10 fringes and may be associated with this spreading. However, since the fringes were taken in the Bragg orientation, rather than the symmetric orientation, and because of local changes in foil orientation, a projected potential image would be necessary to provide conclusive evidence for these shifts.

The lattice image shown in Figure 5 indicates that there is closer parallelism between the 111_γ and 110_α planes which are near to parallel with the trace of the plate than with those near to perpendicular to the trace. Since two sets of 111_γ and 110_α planes cannot be parallel at the same time (18) the orientations observed arise due to a compromise between the possible extreme orientations. This will be the lowest energy situation, and as it is the unfaulted 111_γ planes which show the closer parallelism, i.e. the faulted 111_γ planes are those which cross the plate in Figure 3, this suggests that it is the minimisation of the total fault energy, rather than the mismatch across the interphase interface which is controlling the orientation and morphology. The importance of the fault energy is indicated in the Olsen-Cohen model (12). As with Figure 3, projected potential images are necessary to give more quantitative agreement between the theory and experiment.

The authors wish to thank the Science Research Council, UK, for supporting this work.

References

(1) P D Southwick, PhD Thesis, University of Cambridge, England 1978.
(2) P D Southwick and R W K Honeycombe: In preparation 1979.
(3) P D Southwick, P R Howell and R W K Honeycombe, Phil. Mag. In press 1979.
(4) K R Kinsman, E Eichen and H I Aaronson, Met.Trans. 6 303 (1975).
(5) J R Bradley, J M Rigsbee and H I Aaronson, Met.Trans. 8 323 (1977).
(6) R A Ricks, P R Howell and R W K Honeycombe, Met.Trans. In press (1979).
(7) W Bollman, Phys.Stat.Sol. (a) 21 543 (1974).
(8) J S Bowles and J K Mackenzie, Acta Met. 2, 129,138,224 (1954).
(9) B A Bilby and J W Christian, Inst. of Metals Monograph 18 121 (1956).
(10) J W Christian, 'The Theory of Transformations in Metals & Alloys', Pergamon Press, Oxford 1965.

(11) C L Magee, Phase Transformations, Metals Park, Ohio (1970).
(12) G B Olsen and M Cohen, Met.Trans. 7 1897, 1905, 1915 (1976).
(13) C Dube, H I Aaronson and R F Mehl, Rev.Met. 55 201 (1958).
(14) G V Kurdjumov and G Sachs, Z. Physik 64, 325 (1930).
(15) Z Nishiyama, Sci. Rep. Tohoku Univ. 23, 637 (1934).
(16) M Thompson, Philips EM Bulletin 110 1977/3.
(17) J D Ayers, Acta Met. 22 611 (1974).
(18) M Hall, K R Kinsman and H I Aaronson, Surf. Sci. 31 257 (1972).

Table 1

Heat treatment and microstructure:	Fe wt.%	Ni wt.%	Cr wt.%
δ-Ferrite: 1300°C 30 secs. W.Q.	67.7	5.0	26.0
δ-Ferrite (1300°C 30 secs. W.Q.)	65.4	4.0	28.8
Austenite (1000°C 30 mins. W.Q.)	68.2	7.0	24.1
δ-Ferrite (1300°C 30 secs. W.Q.)	67.6	4.9	25.9
Austenite (500°C 10 secs. W.Q.)	67.6	5.0	26.1

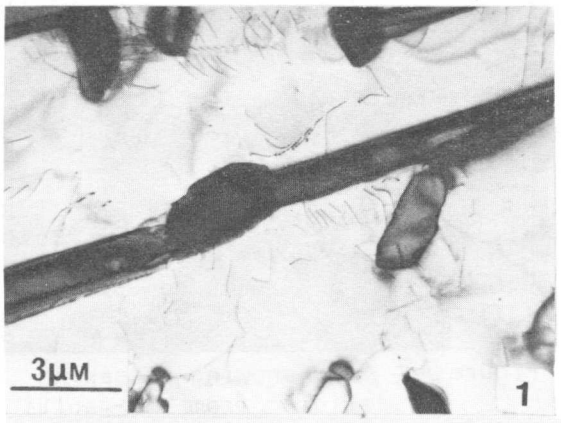

Fig. 1 Widmanstätten γ formed at 700°C

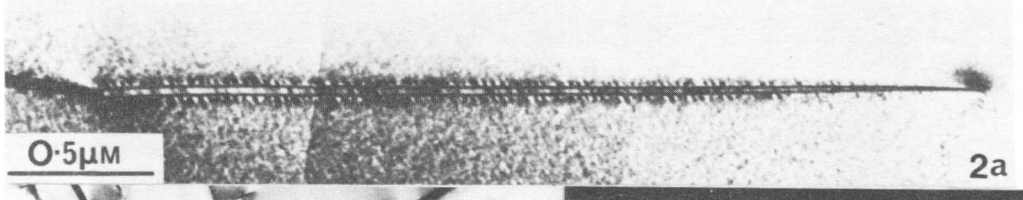

Fig. 2a Martensitic γ formed at 500°C

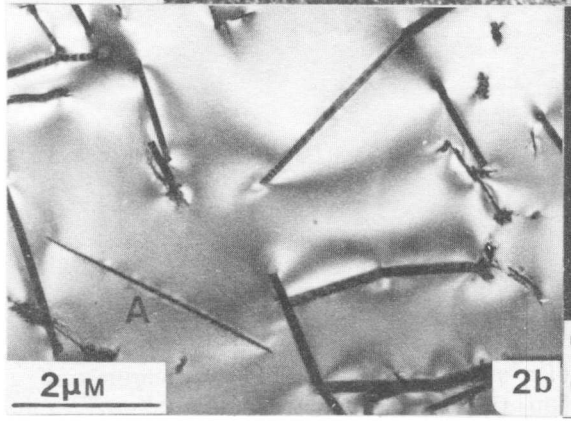

Fig. 2b Martensitic γ formed at 400°C

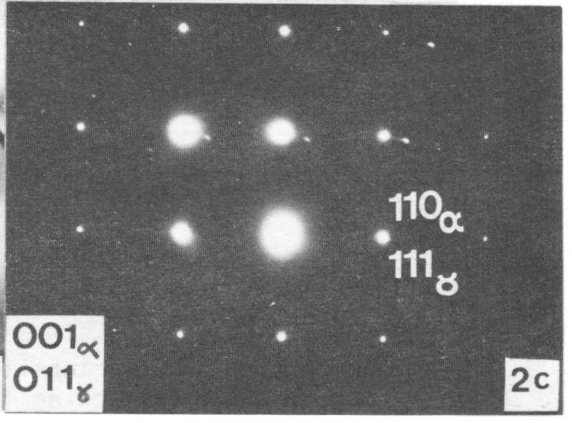

Fig. 2c SADP of Figure 2b

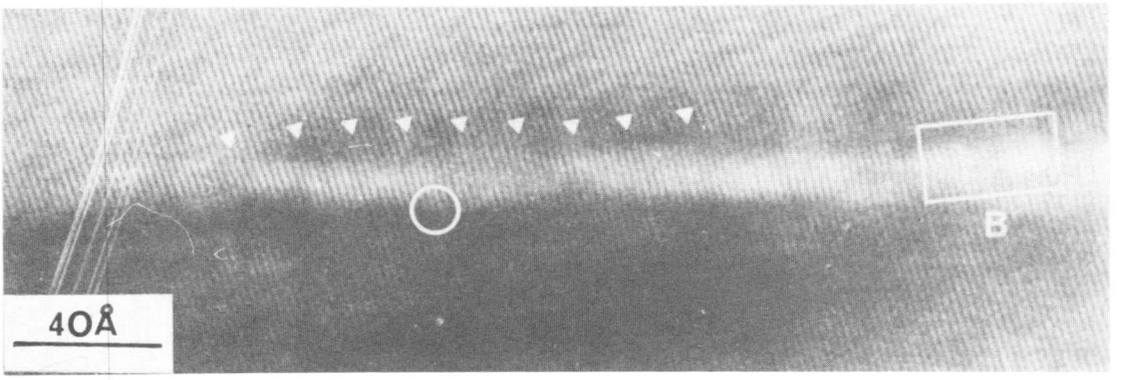

Figure 3 Lattice image of the top of a martensitic γ plate showing $110_\alpha/111_\gamma$ fringes

Figure 4a BF of austenite showing stacking faults

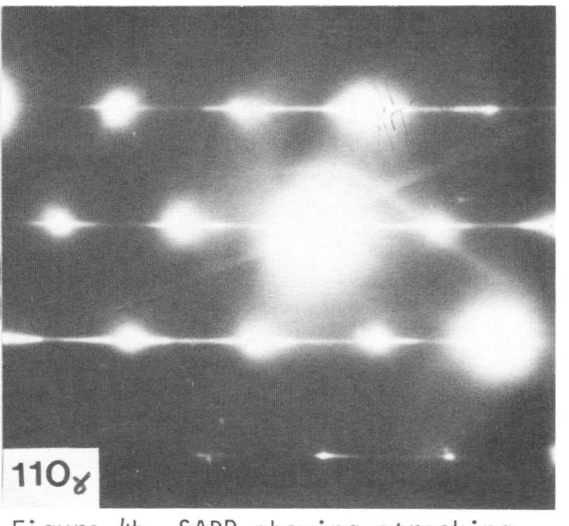

Figure 4b SADP showing streaking arising from the faults

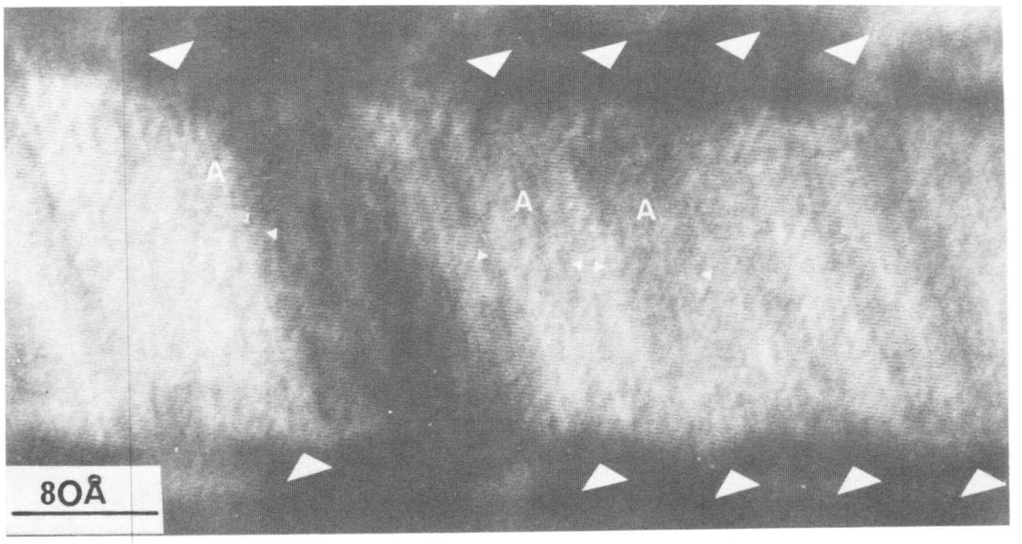

Figure 5 Lattice image of martensitic γ showing $110_\alpha/111_\gamma$ fringes and the presence of stacking faults (arrowed)

Martensitic Transformation in Splat-Quenched Zirconium Alloys

S. Banerjee*+ and B. Cantor+

Microstructures produced in unalloyed zirconium and Zr-Nb alloys by rapid quenching from the liquid state were studied by transmission electron microscopy. The fine cellular structure resulting from segregation of impurities (silicon and oxygen), during the solidification process (Liquid → β) was found to influence the size, the distribution and the substructure of the martensite formed subsequently. While the martensite laths in Zr and Zr-2.5Nb samples were seen to be continuous across the Si rich cell boundary phase the growth of the martensite plates in Zr-5.5Nb was restricted by cell walls. In samples of Zr-5.5Nb free from impurity pick up, it was possible to suppress the β→α martensitic transformation by splat quenching, the β phase alternatively undergoing an athermal β→ω transformation. This preference of the displacive ω-transformation over the martensitic transformation in the splat quenched Zr-5.5Nb alloy has been explained in terms of a higher concentration of vacancies which is known to stabilize the ω-like defects prior to the transformation event.

Experimental

The alloys (Zr-2.5%Nb, Zr-5.5%Nb, Zr-10%Nb and Zr-20%Nb) were prepared by nonconsumable arc melting and they contained about 3000 ppm of interstitials. Splat quenching of these alloys and unalloyed zirconium was carried out in a two piston apparatus described earlier (1). During levitation melting two different techniques were used for holding the specimens. In one set of experiments samples were allowed to rest on a Silica funnel which was used to protect the levitation coil. These samples were levitated but during melting intermittent contact between the Silica funnel and the molten drop could not be avoided. This resulted in oxygen and silicon pick up in these samples (designated as A). In the second set of experiments samples were suspended by Zr-wire (0.5mm dia) inside the levitation coil which was not protected by a Silica funnel. These samples (designated as B), in molten condition, did not come in contact with any 'crucible' material and thus did not pick up impurities during melting.

+ School of Engineering and Applied Sciences, University of Sussex, Brighton, U.K.

* Metallurgy Division, Bhabha Atomic Research Centre, Bombay, India.

Samples A

Samples contaminated with Si and O during melting showed fine scale solidification structures resulting from segregation of these impurities. In a few samples of this set the α phase formed directly from liquid as evidenced from the cellular-α microstructure (Fig 1). No sign of β→α transformation was noticed in these. Detailed description of this structure and the discussion on the direct liquid to α transformation will be published elsewhere. Martensitic transformation occurred in samples of Zr, Zr-2.5Nb and Zr-5.5Nb which solidified into the β phase. Solidification of these alloys containing Si resulted in the formation of fine cellular structure of the β phase which subsequently transformed into martensite. Fig. 2 shows a representative microstructure of lath martensite observed in Zr and Zr-2.5Nb. Martensite laths are seen to be present on a background of cells, a group of which belong to a single β grain. Energy dispersive compositional analysis of the interior and the boundaries of cells revealed that the latter is richer in Si and Nb than the former. SAD patterns taken from the Si rich cell boundary regions could be indexed in terms of an ordered tetragonal structure based on the bcc β-zirconium lattice. Close similarity of this structure with the reported Zr_3Si and Nb_3Si structures (2) suggested that the cell boundary phase is likely to be $(ZrNb)_3Si$. The most important observation was that the martensite laths were often found to be continuous across these cell boundaries. This is illustrated with the bright and dark field pair of micrographs in Fig. 3.

The morphological transition from the lath to the plate type was noticed as Nb content was raised to 5.5%. In contrast with the observed continuity of laths across cell boundaries, the plates were seen to be confined within β cells (Fig. 4). This caused a considerable refinement of the martensite plate size. SAD patterns taken from the interior of cells showed superimposed zones of hcp reciprocal lattice sections which could be indexed in terms of different Burgers variants, arising from a single β crystal (Fig. 5). Dark field images using strong α reflections showed that the same group of martensite variants were present in a group of neighbouring cells (Fig. 6) as they all correspond to a single β orientation. Internal twinning was very rarely encountered in these martensite plates.

Samples B

In samples free from Si and O contamination TEM studies were confined to regions which did not show any solidification structure implying that solidification in these regions was diffusionless. In one or two localized regions, however, relatively coarse cells or dendrites could be seen by optical microscopy. In contrast to the observations made on β-quenched samples (3), splat quenched martensite in Zr-2.5Nb exhibited lath morphology where parallely stacked laths were separated from their neighbours by small angle boundaries (Fig 7). The dislocations constituting such boundaries could be imaged with (0002) refelection suggesting that these dislocations had non basal

Burgers vector and were not the normal slip dislocations. This is expected because the most likely slip shear associated with the lattice invariant deformation in $\beta \rightarrow \alpha$ transformation of Ti (or Zr) is along $\langle 11\bar{2}3 \rangle$ direction (4).

X-ray diffraction indicated that in some of the Zr-5.5Nb samples most of β transformed to α while in others no α was detected. TEM observations on transformed samples showed plate morphology typical of high Nb content (3). As there was no fine scale segregation, the martensite plates were quite large and many of them were internally twinned on $\{10\bar{1}1\}$ planes (Fig. 8). The size of the pre-existing β grains in transfromed samples was estimated to be 10-15μm from the lengths of largest martensite plates. Samples which did not transform to α exhibited a much samller β grain size (1-2μm) characteristic of a higher cooling rate. The equiaxed morphology of β grains (Fig. 9) and the absence of any sign of microsegregation again suggested that solidification of these regions occurred in a diffusionless manner. Presence of the ω phase in the retained β matrix was detected by both x-ray and electron diffraction (Fig. 10). Dark field images taken from ω-reflections clearly showed ω-particles dispersed in the β-matrix (Fig. 11).

As Nb content was progressively increased from 5.5 to 20%, discrete ω-reflections gradually became more and more diffused and Zr-20Nb showed characteristic diffuse intensity lying on $\{111\}$ rel-planes (Fig. 12).

Discussions

In this section attemps have been made to rationalize the following two important observations:

a) propagation of martensite laths across the silicide phase in the cell boundary, and
b) athermal $\beta \rightarrow \omega$ transformation in Zr-5.5Nb suppressing $\beta \rightarrow \alpha$ martensitic transformation.

Propagation of martensite laths through the cell boundary phase suggested that at the instant of martensitic transformation continuity of the lattice was maintained from one cell to its neighbours. As the silicide phase at cell boundaries can be viewed as an ordered structure based on the β-Zr lattice, it is attractive to envisage that immediately before the formation of lath martensite, a β grain consisted of several solute lean cells separated by solute rich boundaries but the average lattice within a grain was continuous. At this stage the long range order necessary to generate the silicide superlattice was perhaps not established. Under such circumstances the transformation shear could propagate across a number of cells belonging to a β-grain. The formation of a continuous layer of silicide crystal along the cell boundary regions appeared to have occurred in a subsequent stage presumably by a diffusional mechanism.

When the martensitic transformation occurred at a lower temperature as in the case of formation of plate martensite in Zr-5.5Nb alloy, the ordering of the cell boundary regions to form the silicide lattice might have occurred prior to the martensitic transformation. As a consequence

β grains were partitioned by the cell walls which prevented the growth of martensites across these boundaries.

β-quenching treatment is known to induce β→α martensitic transformation in Zr-Nb alloys containing less that 7%Nb while higher Nb content alloys undergo a displacive β→ω transformation (5). High speed thermal analysis work by Stewart et al (6) showed that in Zr-5Nb athermal ω-formation can occur after incomplete β→α martensitic transformation when quenching rate exceeds 800°C/sec. According to their results, $M_s(\alpha)$ and $M_s(\omega)$ are depressed by 50°C and 100°C respectively as the cooling rate is increased from 800°C/sec to 5000°C/sec. As faster quenching rate depresses $M_s(\omega)$ more than $M_s(\alpha)$, the observed transformation of β to ω in preference to β to α in splat quenched Zr-5.5Nb alloy does not appear to be a direct consequence of the increased quenching rate. However rapid quenching from the liquid state might be responsible for retention of a higher concentration of excess vacancies or point defect clusters particularly in a sample which is not very fine grained. Diffraction experiments have clearly revealed ω-like structural fluctuations in many ω-forming systems at temperatures much higher than $M_s(\omega)$ and proposed structural model (7) of such ω-embryos (or defects) consist of a vacancy around which rows of atoms are displaced along one <111> direction. It is possible that the excess vacancies present in the splat quenched alloys are stabilizing the ω-embryos which upon cooling through the transition temperature condense to form the ω phase.

Acknowledgements

We would like to thank the Science Research Council and the U S Office of Naval Research for financial support of this research programme and Professor R W Cahn for many helpful discussions.

References

1 R.W. Cahn, K.D. Krishnand, M. Laridjani, M. Greenholz and R. Hill, Mat. Sci. Eng. 23 (1976) 83.
2 F.A. Shunk, Constitution of Binary Alloys, McGraw-Hill, (1969).
3 S. Banerjee and R. Krishnan, Acta Met. 19 (1971) 1317.
4 H.M. Otte, The Science Technology and Application of Titanium, Ed. R.I. Jaffee and N.E. Promisel, Pergammon (1970) 646.
5 S.L. Sass, J. Less Comm. Metals 28, (1972) 157.
6 D. Stewart, B A Hatt and J.A. Roberts, Brit. J. App. Phy. 16 (1965) 1081.
7 T.S. Kuan and S.L. Sass, Acta Met. 24 (1976) 1053.

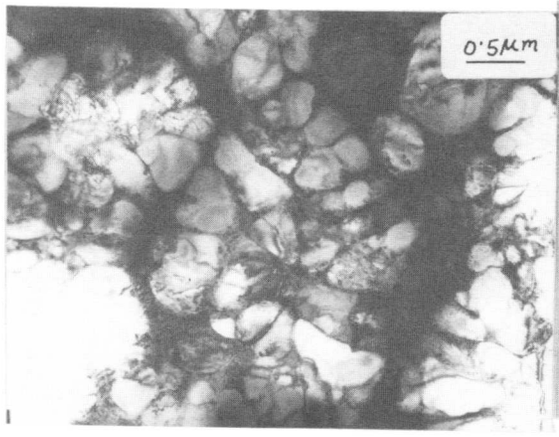

Figure 1: Unalloyed Zr; cellular α microstructure

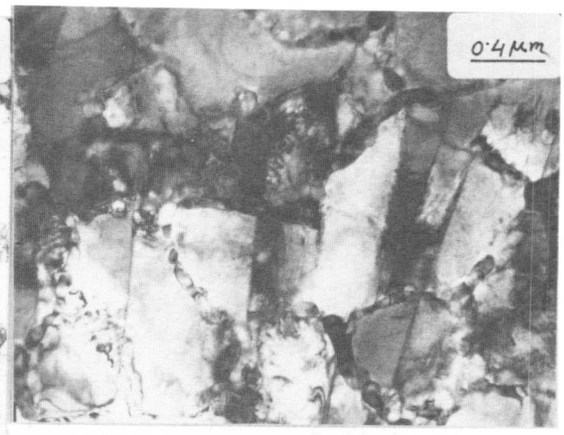

Figure 2: Zr-2.5Nb(A); Lath martensite in the matrix of pre-existing cells

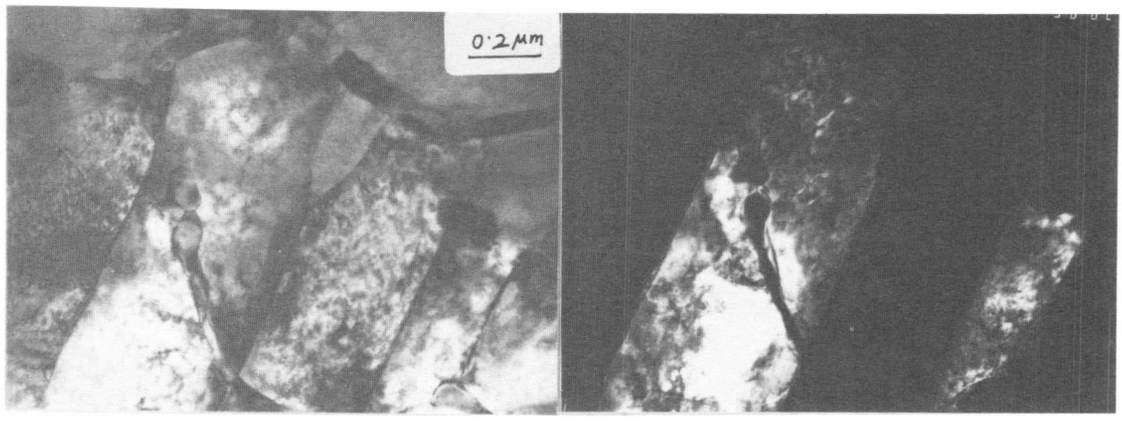

Figure 3: Zr-2.5Nb(A); Bright (a) and dark (b) field micrographs showing continuity of lath through the cell boundary

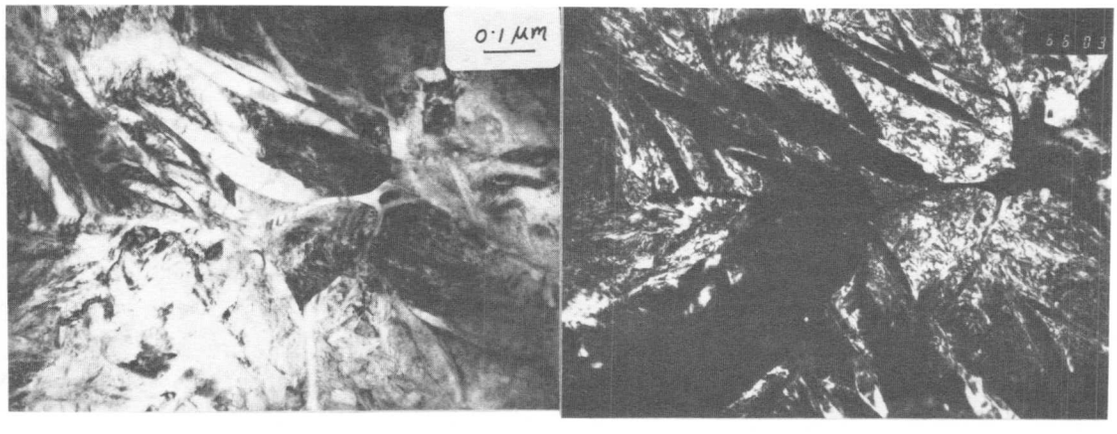

Figure 4: Zr-5.5Nb(A); Martensite plates confined within β cells, (a) bright field and (b) dark field

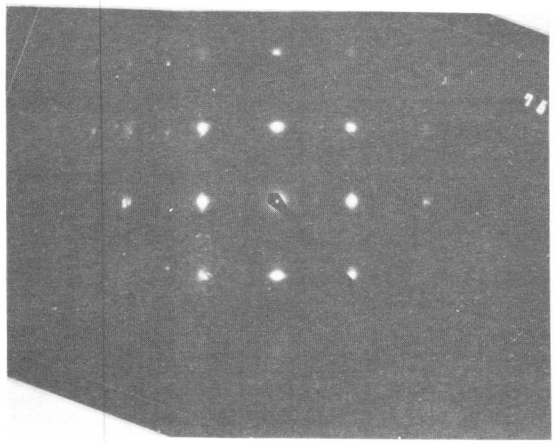

Figure 5: Zr-5.5Nb(A); SAD pattern (a) and key (b) to demonstrate the operation of Burgers orientation relation

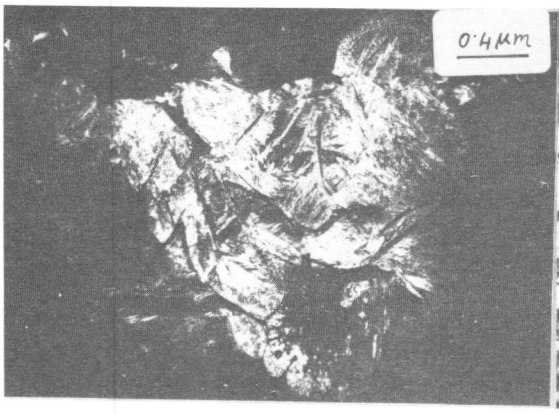

Figure 6: Zr-5.5Nb(A); Martensite plates from a group of cells simultaneously in contrast in the dark field image with $(10\bar{1}1)$ reflection

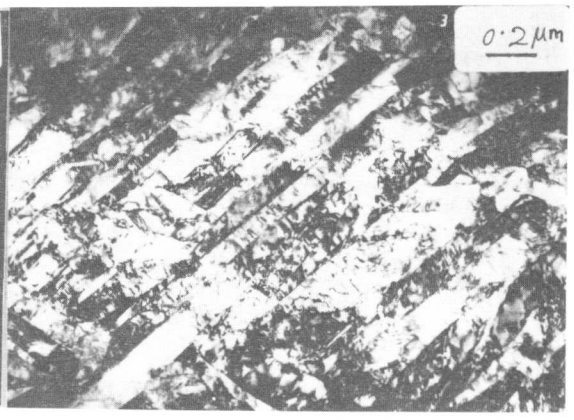

Figure 7(a): Zr-2.5Nb(B); Lath martensite structure

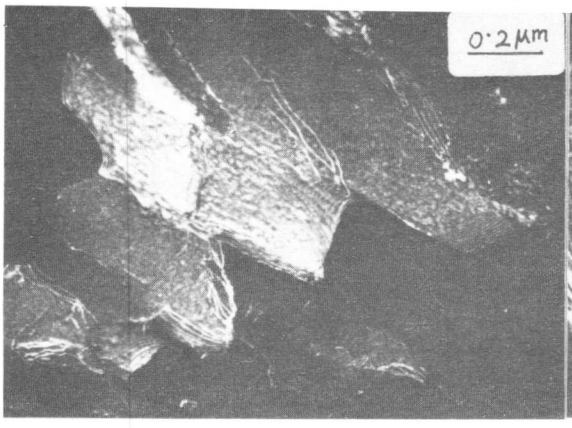

Figure 7(b): Zr-2.5Nb(B); Interlath boundary in dark field (g=0002)

Figure 8(a): Zr-5.5Nb(B); Internally twinned plate martensite

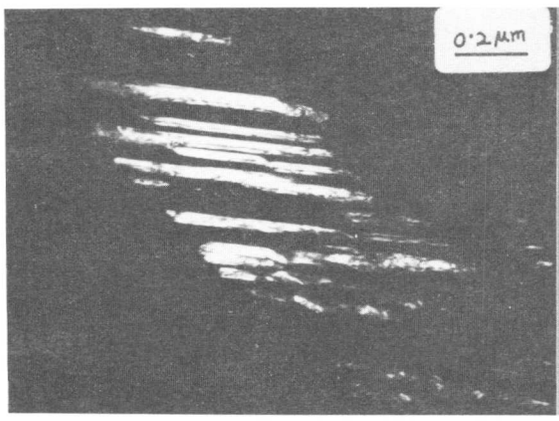

Figure 8(b): Zr-5.5Nb(B); $(10\bar{1}1)$ twins in dark field

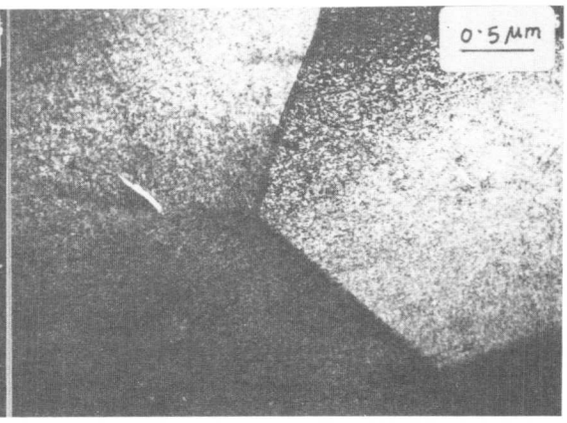

Figure 9: Zr-5.5Nb(B); equiaxed retained β grains with mottling due to ω-formation

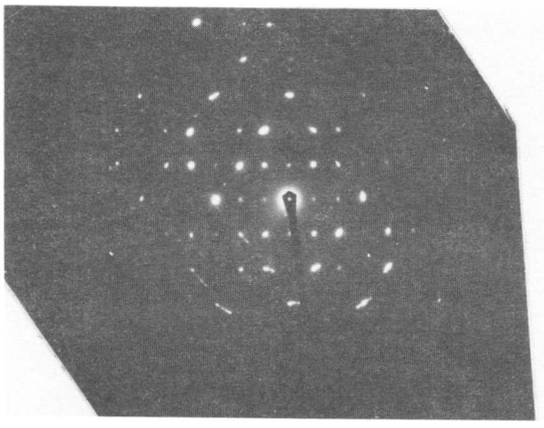

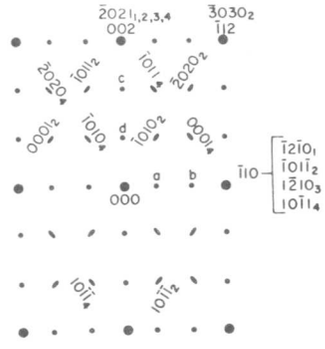

Figure 10: Zr-5.5Nb(B); SAD pattern (a) and key (b) showing four variants of ω in β

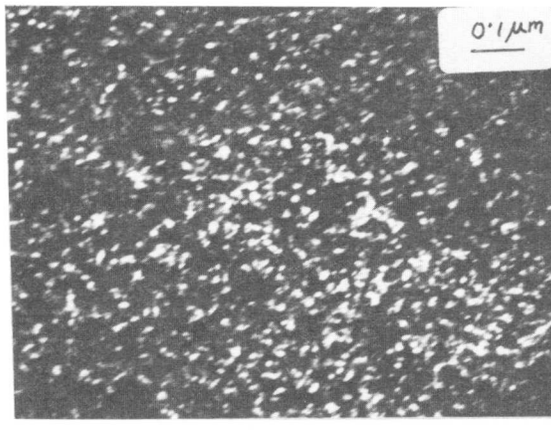

Figure 11: Zr-5.5Nb(B); ω-particles in dark field $g=(10\bar{1}1)\omega$

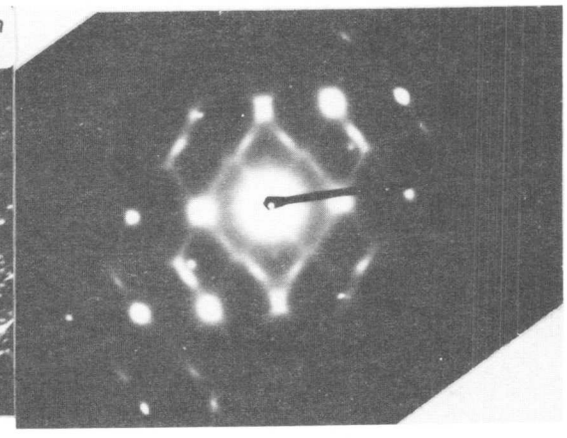

Figure 12: Zr-20Nb(B); Diffuse ω-streaks shown in $(11O)_\beta$ zone

CRYSTALLOGRAPHY OF SHEAR TRANSFORMATIONS IN ZIRCONIUM HYDRIDES

M. P. Cassidy* and C. M. Wayman**

The phenomenological crystallographic theory of martensitic transformations was applied to the transformation from δ to γ and ε zirconium hydrides. The crystallography was determined by transmission electron microscopy and diffraction, interference microscopy and measurement of fiducial scratch displacements.

Good agreement between the predicted and measured crystallography was obtained for the γ formed from δ if hydrogen diffusion was assumed. The predicted and observed lattice invariant shear was twinning on $\{101\}$.

Good agreement between the predicted and measured crystallography for the δ and ε hydride transformation was obtained. For a given plate, the measured habit plane, twin plane, unique Bain contraction axis, and orientation relationship were consistent with the respective predictions for a single variant. The lattice invariant shear was twinning on $\{101\}$, within alternating bands of hydride variants, producing a herringbone morphology.

The interfaces separating the ε hydride bands were found to be of two types, which alternated. This morphology is explained by a mechanism in which each spear nucleates independently as a pair of ε hydride plates with twins which "match-up" across the plane separating the plates, termed a spear interface. When growing spears impinge, the resulting interface, termed an impingement interface, does not "match-up".

I. Introduction

In a recent study [1] the crystallography of the formation of β vanadium hydride has been compared with the predictions [2] of the phenomenological crystallographic theory of martensitic transformations. The success of this phenomenological approach has suggested a mechanism for the transformation from α vanadium to β vanadium hydride, in which the vanadium atoms undergo a martensitic shear while the hydrogen atoms presumably diffuse to their new ordered positions. This mechanism has been likened to the well-known bainite reaction in steels. It has been suggested that hydrides in the Nb-H and Ta-H systems may form in a manner similar to that of vanadium hydride [3].

Several authors [4-8] have suggested similar "bainitic" shear transformations coupled with simultaneous hydrogen diffusion, as well as

---

*Western Electric Engineering Research Center, Princeton, NJ
**Department of Metallurgy and Mining Engineering and Materials Research Laboratory, University of Illinois, Urbana, IL

"classical" diffusionless martensitic transformations between various phases in the Zr-H system. However, the quantitative crystallography of these transformations has not been thoroughly investigated. Only superficial comparisons with the phenomenological theory of martensitic transformations have been made, and the interfaces that form during these transformations have not been studied directly.

To extend the validity of this phenomenological approach, the crystallography and substructure of the transformations which have been hypothesized as involving martensitic shears and which occur between zirconium hydrides were investigated. This paper describes the results of the study of the δ to γ and the δ to ε transformations.

II. Experimental Procedure

The starting material for this work was "Marz" grade zirconium rod, obtained from the Materials Research Corporation. Three different specimen shapes were prepared. All of these specimen geometries were then outgassed following a technique previously demonstrated to produce well annealed specimens with a low interstitial content [9]. Desired hydride compositions were produced by the controlled reaction of the annealed zirconium with a continuous supply of "Ultra Pure Grade" hydrogen gas, following the procedure described by Barraclough and Beevers [10]. The final composition was determined from the weight gain.

Thin foils were produced by a two-stage electropolishing technique. The transmission electron microscopy was performed on a Hitachi H-500 microscope, operated at 125 Kv. All measurements were made directly on glass plates.

III. Results and Discussion

III.1 The $\delta \rightarrow \gamma$ transformation

Figure 1 shows the surface relief produced by a specimen which was polished flat, then hydrided to a composition of 57 at.% hydrogen. The distinctive surface relief produced by an invariant plane strain is clearly revealed. Two surface analyses were utilized to determine the habit plane of the γ hydride in the δ matrix. Three scratches which were easily observed on the negative and which were separated by as much as 14° were selected for the shape strain measurements. The average of the three pairs of scratch measurements for the plate labelled "A" in Figure 1 gave a magnitude of the shape strain, m_1, of 0.0415. The crystallographic results are plotted in Figure 2.

In all γ plates observed (Figure 3 shows a typical electron micrograph) twins were present. Trace analysis was consistent with the twin plane being of the (101) type. Measurements of six twin pairs from

Figure 3 resulted in an average width for "Twin 1" of 582 Å, while for "Twin 2" the average width is 437 Å. Therefore, the lattice invariant shear magnitude, m_2, is 0.031. The average for all specimens measured is 0.051, while the maximum value for any plate is 0.114.

The crystallography predicted by the phenomenological theory of martensitic transformations was investigated by utilizing a computer program [11] based on the Bowles and Mackenzie formulation of the phenomenlogical theory [12]. The observed twin plane and direction, the observed identify correspondence, a dilatation parameter of 1.000, and the Bain strain determined from the lattice parameters were input to the computer program. The use of reported values of the room temperature lattice parameters for the δ and γ hydrides failed to produce any solutions to the geometric equations which establish the habit plane even when the possibility of large experimental errors were considered. Allowance for the mechanism proposed by Rashid and Scott [3], in which the hydrogen atoms diffuse prior to the shear transformation to produce localized regions of composition at or near the product phase composition, or the mathematically equivalent mechanism in which hydrogen atoms are expelled from the γ hydride ahead of the advancing interface, was made by extrapolating the variation of the δ hydride lattice parameter with hydrogen content to lower hydrogen contents. The resulting predictions for the plate in Figure 1 are plotted in Figure 2. All of the measurements were in good agreement with the predicted values. The predicted value of 0.073595 for m_2 is within the range of measurements obtained. The large error was due to the very few twin pairs which could be measured. More importantly, though, all measurements for each γ plate were internally consistent with the predictions for a single variant. Thus, excluding the uncertainty in the lattice parameters, it appears that the transformation from the δ hydride to the γ hydride in zirconium behaves according to the martensite crystallography theory with the transformation occurring in an interface region depleted in hydrogen.

III.2 The $\delta \rightarrow \varepsilon$ transformation

Under polarized light, the ε hydride showed a "black-white" contrast in long straight bands. Some faint contrast from subbands within each main band could be seen, producing a herringbone pattern. This "black-white" contrast has been termed the spear morphology in martensites. The surface relief observed was that of one main band tilted up, the adjacent main band tilted down. Each type of tilt can be related on a one-to-one basis to the bands in the "black-white" contrast. This indicates that in addition to being formed with different twin systens, adjacent bands have roughly opposing shape strain directions. This opposition results in a net reduction in the shape strain produced by a pair of bands in that the two variants are self-accommodating.

In Figure 4, the dislocation density is seen to be quite low. This was typical of the specimens which were completely ε, but not of those containing isolated plates of ε. The difference in dislocation density is apparently due to the effectiveness of the self-accommodation of the shape strain in adjacent main bands.

Specimens containing both δ and ε hydrides were used for habit plane measurements. All results obtained from the single pole loci technique were consistent with habit plane normals within 6° of $\{011\}_\delta$ type planes. Stereographic analysis of a typical result is shown in Figure 5.

In all ε hydride plates observed, the internal inhomogeneity was twinning. Trace analysis was consistent with the twin plane being of the $\{011\}_\varepsilon$ type. With the twin plane parallel to the electron beam, the magnitude of the lattice invariant shear, m_2, was determined by measuring more than 50 twin pairs. The measured m_2 is 0.055 while the predicted value for 63.8 at.% hydrogen is 0.056.

The observed surface relief, corresponds to that produced by an invariant plane strain, and the observation of twins demonstrates the existence of an inhomogeneous shear; thus the transformation appears to be geometrically martensitic. All measurements performed were consistent with the predictions of the theory, but more importantly, all measurements for each ε plate were consistent with the predictions for a single variant.

The contrast observed at ε-ε interfaces is complex. The predictions of the crystallographic theory provide a model of the interface, however, which is of considerable help in understanding the interface structure and the contrast it produces. Two different interface structures, which alternate, were observed in many specimens and can be understood by turning to the phenomenological theory where the twin thickness ratio enters into the fundamental equation. The actual thickness of the twins does not appear in the equations, but is variable, depending on a balancing of the energy of the twin boundaries versus the energy of the microscopic interface. Thus it would be expected that plates which nucleate separately would not have precisely identical twin thicknesses and that on impingement these twins would not exactly "match-up". It is therefore evident that the two main bands which are separated by the interface labelled "A-B" in Figure 4, and have twins that "match-up", grew together as a spear. The other main band, separated by the interface labelled "C-D" has twins which do not "match-up" and therefore nucleated separately. This mechanism is illustrated schematically in Figure 6.

The question of the motion of the hydrogen atoms during the formation of the ε hydride has been addressed in part, by previous authors [6], but still cannot be completely answered. The finding [13] that at room temperature, the δ hydride is disordered, while the ε hydride is ordered would suggest that there is motion of the hydrogen atoms during the transformation. Thus the ε hydride resembles bainite in ferrous alloys. At room temperature, however, the δ and ε hydrides have different compositions, and the hydrogen ordering, or lack of ordering, could be due to this composition difference. Hydrogen ordering reflections were clearly present in the completely ε specimens. In the specimens containing both δ and ε, ordered spots were occasionally observed, but were weak in intensity. Due to the near identity orientation relationship between the δ and ε hydrides, it was impossible to

to determine whether the ordered spots originated from one or both of the hydrides.

In summary, each of the hydride transformations for which the detailed crystallography and substructure has been analyzed and has been shown to behave according to the phenomenological crystallographic theory of martensitic transformations. This research was supported by the National Science Foundation, Grant GH-76-01058 and the Energy Research and Development Administration under Contract (11-1)-1198 through the Materials Research Laboratory at the University of Illinois.

References

[1] M. P. Cassidy, B. C. Muddle, T. C. Scott, C. M. Wayman, and J. S. Bowles: Acta Met., 25 (1977) 829.

[2] J. S. Bowles, B. C. Muddle, and C. M. Wayman: Acta Met., 25 (1977) 513.

[3] M. S. Rashid and T. E. Scott: J. Less Common Metals, 31 (1973) 377.

[4] R. Chang: J. Nucl. Mat., 2 (1960) 335.

[5] R. L. Beck: Trans. ASM, 55 (1962) 542.

[6] K. G. Barraclough and C. J. Beevers: J. Nucl. Mat., 34 (1970) 125.

[7] J. S. Bradbrook, G. W. Lorimer, and N. Ridley: J. Nucl. Mat., 42 (1972) 142.

[8] G. C. Carpenter, J. F. Watters, and R. W. Gilbert: J. Nucl. Mat., 48 (1973) 267.

[9] C. R. Cupp and P. Flubacher: J. Nucl. Mat., 6 (1962) 213.

[10] K. G. Barraclough and C. J. Beevers: J. Nucl. Mat., 33 (1969) 296.

[11] H. M. Ledbetter and C. M. Wayman: Mat. Sci. & Eng., 7 (1971) 151.

[12] J. S. Bowles and J. K. Mackenzie: Acta Met., 2 (1954) 129.

[13] G. G. Libowitz: J. Nucl. Mat., 5 (1962) 228.

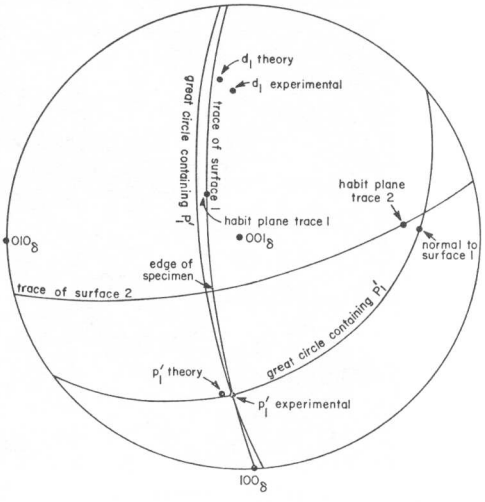

Fig. 2. Stereographic projection showing crystallographic data obtained for plate "A" in Fig. 1

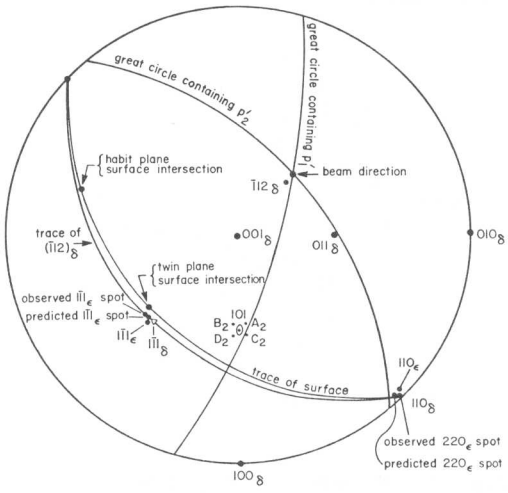

Fig. 5. Stereographic projection showing typical trace analysis and orientation relationship results for $\delta \rightarrow \varepsilon$ transformation

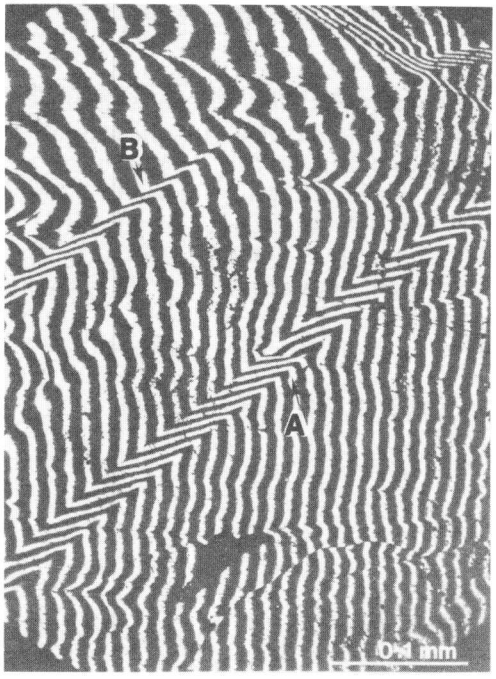

Fig. 1. Interference micrograph of γ hydride plates

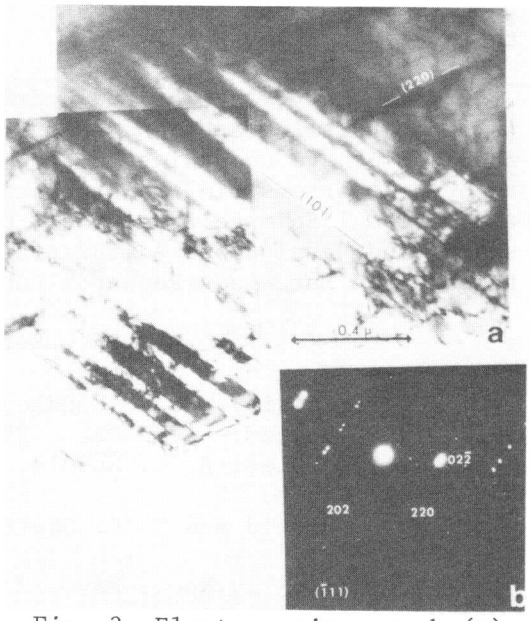

Fig. 3. Electron micrograph (a) and selected area diffraction pattern (b) obtained with the electron beam parallel to the twin plane of the γ hydride

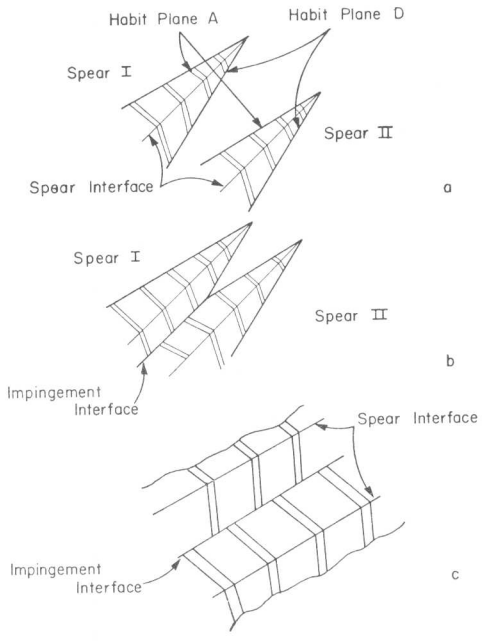

Fig. 6. Schematic representation of the separate nucleation (a) and impingement (b) of two martensite spears. Complete transformation is shown in (c)

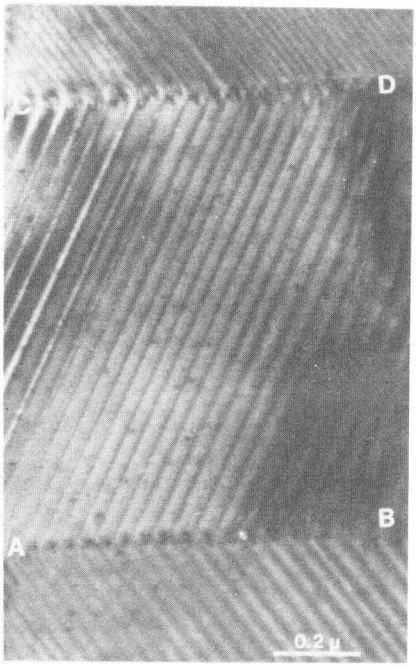

Fig. 4. High magnification TEM of two ε-ε hydride interfaces. "A-B" is a spear interface, while "C-D" is an impingement plane

Structural Transformations in KNO_3, $RbNO_3$ and NH_4Br

S. W. Kennedy, W. M. Kriven* and W. L. Fraser†

Evidence based on x-ray diffraction, some electron diffraction, and light microscopy is presented for martensitic transformation mechanisms in rubidium nitrate (NaCl - cubic → rhombohedral → cubic) and ammonium bromide (NaCl cubic → CsCl cubic), and for cooperative mechanisms in potassium nitrate (aragonite → calcite). In NH_4Br there is a coordination change of 6 to 8 and the lattice deformation is large. The same lattice correspondence applies to $RbNO_3$ and the two are compared. It is concluded that whilst the lattice invariant shear in NH_4Br is (100)[011] (referred to the parent NaCl phase), in $RbNO_3$ I → II it is (110)[001]. $RbNO_3$ shows twinned main bands. Subsequent to the transformation several processes of detwinning, besides recrystallization, remove this texture. KNO_3 shows shape changes, tilted bands in several orientations, very fine twinning, and several orientation relations, for which lattice deformations can be proposed. The mechanism does not correspond to hcp → ccp, and it appears that in this more complex structure several mechanisms operate.

Introduction

Crystallographic studies have been made of several structural transformations in inorganic crystals in which there is a change of first coordination and the lattice deformations are large. These transformations include the NaCl - CsCl type in ammonium bromide NH_4Br at 137°C (change of coordination 6→8), cubic NaCl-related (phase I) $\xrightarrow{284°C}$ rhombohedral calcite-type (II) $\xrightarrow{219°C}$ cubic CsCl-related (III) in rubidium nitrate $RbNO_3$ (m.p.310°C), and the aragonite to calcite type in potassium nitrate KNO_3 at 128°C.

Studies of $RbNO_3$ and NH_4Br are complementary since the same lattice correspondence applies (with different strains), but twin-related displacements are not visible as twins in the cubic product of NH_4Br whilst in rhombohedral $RbNO_3$ twins are distinguishable, as are plane-normals and directions having the same index. Ions in $RbNO_3$ I have large amplitudes of thermal vibration which might be expected to facilitate a non-martensitic mechanism. The present work shows how the $RbNO_3$ I → II transformation conforms to martensite theory, and for comparison also presents further observations to support the previously reported [1] martensitic mechanism in supercooled NH_4Br. A further interesting result was that in $RbNO_3$ II the martensitic texture was not stable, but relaxed by several mechanisms including twin thickening and recrystallization. Though it is not further discussed here it is noteworthy that a second mechanism was found in $RbNO_3$ giving a different orientation relation (B)

Department of Physical and Inorganic Chemistry, University of Adelaide, S.A. 500, Australia. *Present address: Department of Materials Science and Mineral Engineering, University of California, Berkeley, CA 94720, USA. †Present address: Kodak Research Laboratories, Coburg, Victoria, Australia.

apparently due to a non-martensitic mechanism, and this confirms our limited data on a similar secondary mechanism in NH_4Br. The mechanism can be attributed to a new correspondence which converts {111} (Z=4) into {100} (NaCl).

In the conventional lattice correspondence for NH_4Br and $RbNO_3$ the NaCl cube is converted to a rhombohedron, Z = 4, ($RbNO_3$ II) by relative contraction along a common [111] direction: further contraction converts the primitive rhombohedron of the fcc lattice to the primitive cube of the CsCl structure ($RbNO_3$ III, NH_4Br II). A (110) plane of the primitive cell is a {100} plane of the 4-unit cell, and $\{11\bar{1}\}$ of this become {100} of the primitive cell. The values of the principal distortions are: for $RbNO_3$ I → II, $\eta_1 = \eta_2 = 1.065$, $\eta_3 = 0.850$ ($\|$[111]), $\Delta V < 1\%$; (see [2] for further refs.); for NH_4Br I → II, $\eta_1 = \eta_2 = 1.192$, $\eta_3 = 0.596$ $\Delta V = -16\%$. In a structure change NaCl → CsCl-type, the original 90°cell angle becomes 109°46´. KNO_3 has a pseudo-hexagonal orthorhombic cell (II), Z = 4, below 128°C, and above 128°C the rhombohedral calcite-like cell (I), Z = 4, similar to $RbNO_3$ II. The room temperature aragonite-type pseudohexagonal cell is related to inverse NiAs. As form I is NaCl-related as described above, and NiAs is related to NaCl as hcp to ccp, it has been anticipated that the transformation aragonite - calcite could be similar to hcp → ccp, the "close packed" basal planes and rows in them remaining parallel in the two phases with martensitic accommodation of minor changes in dimensions [3]. This was not found in the present work nor in previous orientation determinations [4,5] but surface effects suggesting other displacements have now been observed.

Experimental

Most orientation relations were measured by X-ray diffraction Laue, oscillation, and precession photography, with use of Polaroid film for $RbNO_3$, but some in KNO_3 were also measured by electron diffraction. Shape changes, habit planes and twinning were examined by transmitted and incident light microscopy including dark field, Nomarski interference contrast and interferometry. The microscope was fitted with a transparent heating stage allowing magnifications up to 600. A smaller microscope was attached temporarily to the X-ray precession camera, the goniometer head of which carried a small heater. Batches of individual crystals of NH_4Br I, 30 to 150 μm wide, were grown on glass coverslips from ethylene glycol solutions at 150 - 200°C. They were of cubic morphology, with good {001} faces. As they did not adhere firmly to the glass they were effectively free from constraints. Cooled specimens, some untransformed, were lightly gold-coated. Rhombohedra of $RbNO_3$ II were similarly grown from polyethylene glycol solutions above 230°C. Single-crystal sheets of $RbNO_3$ were grown from the melt under the microscope. Needles of KNO_3 were grown on the coverslips from aqueous solution at room temperature and dried. Crystals were not disturbed and therefore not stressed. Calculations were made by the Bowles-Mackenzie and Weschsler-Lieberman-Read methods, by programs MARTENS [1] and MRTNST [4], and those on NH_4Br were published [1].

For NH_4Br results are summarized here for rapid supercooling.

Each single crystal of form I produced several orientations of II, for each of which the orientation relation was irrational but close to $\langle 001\rangle_I \parallel \langle 1\bar{1}1\rangle_{II}$, $\{100\}_I \parallel \{10\bar{1}\}_{II}$, implying that within the precision, a face and contained cell edge of the original cube remained unrotated. Most crystals of NH_4Br supercooled to 22°C and persisted for periods from minutes to 50 hours. Each ultimately transformed suddenly and completely. The click-like nature of the transformation was emphasized as it caused some crystals to jump out of the field of view. The shape change (Photo.1) was measurable in smaller crystals as inter-edge angles, though in others it was complicated by the number of variants present, but was visible as surface tilts. The tilted surfaces remained flat, implying homogeneous deformation within the resolution; and they intersected the remainder of the surface in a straight boundary without detectable distortion, suggesting no macroscopic misfit in the boundary, or interface. However conflicting shape change from independent variants caused fracture in some crystals. In other crystals the product II was in the form of plates or laths of volume $< 10\ \mu m^3$. The direction of the trace of these was measured and provisionally taken to indicate habit planes (Photo.2). The martensite analysis produced three types of solution, predicting different shape changes, and habit planes respectively near {310}, 10° from $\{1\bar{1}1\}$ and 5° from $\{210\}_I$. The shape changes and the directions of the traces of the laths agree only with the last, based on LIS $\{110\}\langle 001\rangle_{II} = \{100\}\langle 011\rangle_I$, which could be due to transformation twinning displacements. It is concluded that near room temperature the mechanism is martensitic based on this lattice invariant shear.

$RbNO_3$ I → II. In most melt-grown sheets the orientation relation was the same as in NH_4Br: $(011)_{II} \parallel (010)_I$, $[1\bar{1}1]_{II} \parallel [100]_I$, (primitive cell of II), or $(0\bar{1}0)_{II} \parallel (010)_I$, $[001]_{II} \parallel [001]_I$ ($Z = 4$ for II), both ± 4°. Crystals cycled II → I → II within 10 min of first transformation regained their former orientation in II, but the texture described below was only regained identically if the cycle was reversed within 15 sec.

The rhombohedra transformed by a single interface parallel to an edge and underwent a regular shape change, the morphology becoming orthogonal in phase I. On cooling from I, alternating shape changes produced zig-zag blocks or laths or II. The melt grown crystals when transformed more quickly to II showed a pattern of internally twinned main bands, 0.4 to 2 μm wide (Photo.3). Their surfaces were tilted, each pair forming a ridge. The front propagated in jumps by sudden formation of another band. Often when the tips of bands were in the transformation front no twins were resolvable near the tip, but only several μm back from it. This could be interpreted as due to twin thickening behind the front. By measurements of the traces on {100} and {111} surfaces ($Z=4$) the habit plane of the bands was indexed as close to {100}. The directions of the twin traces within the bands then corresponded to $\{110\}_{II}$ and not $\{100\}_{II}$ twinning. Different groups of bands were at 90° on a {100} face, confirming that they originated from different mutually perpendicular {100} planes.

Martensite calculations were made with (011)[100] and (100)[011] twinning as the LIS. The orientation relation agreed with experiment. With the former LIS the habit plane was 6° from {001}, with the latter 5.5° from {102}. The magnitude of the shape change was 0.163. Thus the observed twinning leads to almost the observed habit plane. This agreement confirms that simple martensite theory describes the transformation rather well. The 6° discrepancy is however somewhat outside the experimental error of this work. Whilst errors in the lattice parameters at the required temperature could vary the H.P. orientation by about 2°, there remains the possibility that some additional mode of accommodation contributes slightly to the LIS.

The twinned lamellar texture was not stable. Within 15 seconds after transformation fine-scale detwinning began and progressed in two ways. First, adjacent twins amalgamated suddenly. This process was spasmodic. Sometimes parts of adjacent main bands themselves combined suddenly, eliminating the ridge. More commonly a random interface moved along the length of the band removing the twinning. Adjacent untwinned bands then joined (Photo.4,5). These relaxed bands did not further alter. After 15 min. in other areas twins and bands gradually lost their sharp outline and merged into a uniform orientation. Alternatively macroscopic recrystallization occured, an advancing random boundary engulfing the bands and leaving a uniform orientation.

$RbNO_3$ I → II → III. Rhombohedra of II also transformed to cubic III with a shape change producing orthogonal morphology, by advance of a single interface several degrees from $\{110\}_{II}$ (Z=4). Thus each transformation with different principal strains has a different interface. In crystals quickly cooled I → II → III the orientation relation was the same as in NH_4Br. However whilst in annealed sheets of II, phase III originated as fine platelets with this interface near {110}, in slow propagation they grew randomly, producing a lace-like appearance in polarized light. Thus here propagation need not be shear-like, and possibly interaction of stress fields from many platelets caused breakdown of the regular propagation seen in the rhombohedra.

Discussion of NH_4Br and $RbNO_3$

According to these results large changes of structure can nevertheless proceed essentially martensitically. It appears that different choices of alternative LIS were favoured in NH_4Br and $RbNO_3$ respectively. The instability of the martensitic texture seen in $RbNO_3$ can be attributed to twin boundary and dislocation energy, the influence of which becomes evident in these relatively low-melting substances in which there is considerable thermal atomic vibration. The fact that a martensitic rather than a "diffusive" mechanism nevertheless operates especially in $RbNO_3$ shows the strong tendency for cooperative minimal displacements in transformations. The early onset of relaxation suggests that at least in these types of material, any stationary martensitic interface would rapidly lose its glissile structure.

Potassium Nitrate

Form II is pseudo hexagonal, (net angle 61.14), symmetry Pmcn. Orthorhombic [001] corresponds to pseudo hexagonal c axis and [100] to a

axis. In one mechanism of transformation II → I the interface was within 3° of the basal $(001)_{II}$ and advanced by discrete jumps producing bands having surface tilts of 14° (Photo.6). An alternative interface was between $\{1k2\}_{II}$ and $\{2k3\}_{II}$. Thin rectangular platelets also nucleated parallel to this. The orientation relation (OR.1) was $[111]_I \parallel [001]_{II}$, $(01\bar{1})_I \parallel (010)_{II}$. This differs by 30° around $[001]_{II}$ from the orientation for hcp → ccp in say Co or ZnS. In other crystals distinct surface steps had traces corresponding to $\{\bar{1}k4\}_{II}$ and near $\{3k2\}_{II}$ (Photo.7). These were accompanied by very fine traces near $\{3k2\}_{II}$ and $\{2k3\}_{II}$. Faint fine traces near {3k2}, {3kl} and $\{\bar{1}k3\}$ also occurred without the large steps: in all these product crystals the extinction was undulose indicating fine twinning. For this type of mechanism twins or laths appeared in the growth front (Photo.8). In some lattice orientations the fine striations were consistent with shear on $\{11\bar{1}\}_{II}$, $\{110\}_I$ or $\{100\}_I$. Other lattice orientations were $(110)_I \parallel (001)_{II}$, $[10\bar{1}]_I \parallel [0\bar{1}0]_{II}$ (OR2); $(111)_I \parallel (1\bar{1}0)_{II} \parallel [1\bar{1}0]_I \parallel [100]_{II}$ (OR3) in which the new 'basal' plane is parallel to a pseudo hexagonal prism plane; and $(11\bar{1})_I \parallel (110)_{II}$, $[1\bar{1}0] \parallel [114]_{II}$ (OR4). OR2 was reported by earlier workers [7]. In the present work the hexagonal pseudo symmetry options of all these also occurred, showing that the deviation from hexagonal symmetry did not affect the mechanism or that pseudo hexagonal twinning of II [4] was incorporated.

In the structure of II the NO_3^- ions are almost in simple hexagonal stacking. Relation (1) could be derived from deformation of the basal $(001)_{II}$ nets and a shear of them along b_{II}. It correlates with the fact that the orientation of the NO_3^- triangles relative to the K atoms in I and II differ by 30°. The deformation allows all ions to move into their new positions without atom rows riding over one another and therefore amounts to a rather complex lattice correspondence. Orientations (2) and (3), though different could be attributed to a correspondence in which a primitive prism of the nitrate ion stacking deforms to become the primitive rhombohedron of phase I, the K atoms falling into position by non-diffusive shuffles, with different tilts of the planes of the nitrate ions for different orientations. A further feasible correspondence requires a deformation of the four-molecule orthorhombic cell to produce the four molecule rhombohedron, with feasible displacements (shuffles) of the second set of ions, but no direct evidence has been found for this. The results so far suggest that where symmetry relations and deformations are complex, more than one mechanism and lattice correspondence may operate

This work was supported by the Australian Research Grants Committee.

References

[1] W. L. Fraser and S. W. Kennedy: Acta Cryst., A30(1974), 13.
[2] S. W. Kennedy and W. M. Kriven: J. Mater. Sci., 11(1976), 1767.
[3] S. Swaminathan and S. Srinivasan: Acta Cryst., A30(1975), 628.
[4] S. W. Kennedy and W. M. Kriven: J. Mater. Sci., 7(1972), 1092.
[5] S. W. Kennedy and M. Odlyha: Acta Cryst., A33(1977), 168.
[6] H. M. Ledbetter and C. M. Wayman, Mater. Sci. Eng., 7(1971), 151.
[7] B. L. Davis and E. H. Oshier, Amer. Mineral. 52(1967), 957.

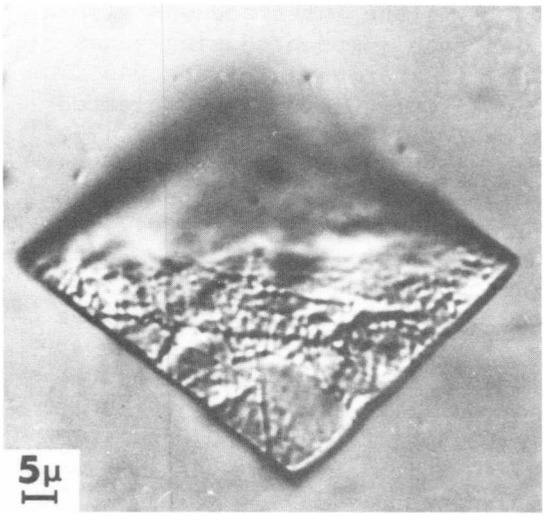

Photo 1. NH_4Br shape change. One variant has lifted from the stage and out of focus.

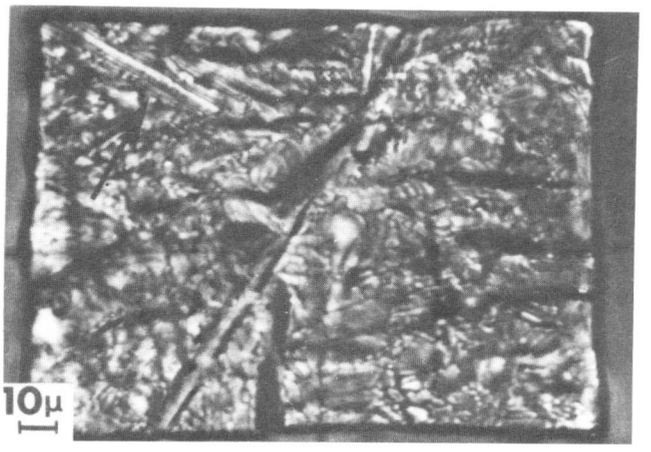

Photo 2. NH_4Br laths and fracture.

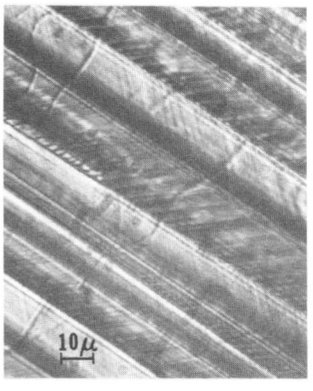

Photo 3. $RbNO_3$ twinned bands.

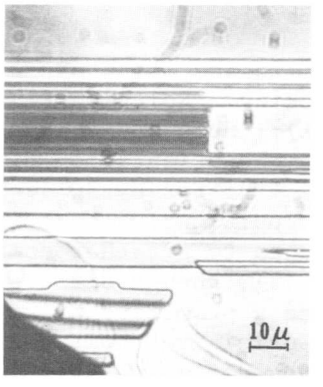

Photos 4 and 5. Movement of detwinning along bands in $RbNO_3$. Recrystallization also appearing.

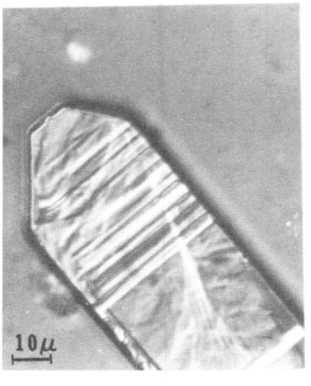

Photo 6. KNO_3 tilted bands on (010) face.

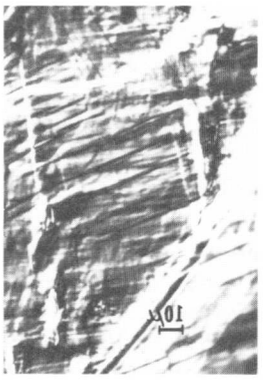

Photo 7. Steps on KNO_3 (010).

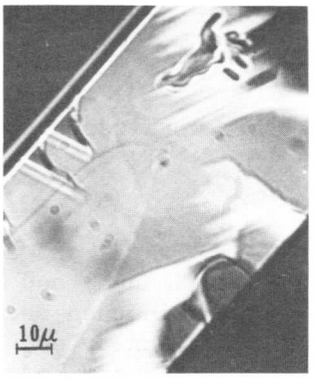

Photo 8. KNO_3 growth front showing laths or twins. Transmitted polarized light.

Diffusionless Phase Transformations in Al_4Ca and Al_3Mg_2

P. Schwellinger*, J. Timm*, H. Warlimont** and H. Zogg***

The phases Al_4Ca and Al_3Mg_2 transform martensitically. This was found by microscopic examination and by measurements of the electrical resistivity and specific heat. By x-ray and electron diffraction it was determined that the tetragonal structure of Al_4Ca transforms to monoclinic symmetry by a shear of 1.1° in the {110} planes of the $D1_3$ structure. The crystallography of the transformation of Al_3Mg_2 could not be clarified in detail. Evidence of small displacements of the atomic positions was found indicating that the transformation is from f.c.c. to lower symmetry.

Introduction

During an investigation of the temperature dependence of some physical properties of the intermetallic phases Al_4Ca and Al_3Mg_2 anomalies were found which lead to the detection of two hitherto unknown diffusionless transformations. Alloys prepared from Al of 99.99%, Mg of 99.95% and Ca of 99.5% purity were used. The procedures of alloy preparation and the measurements of physical and mechanical properties are given elsewhere [1-3]. The present work is mainly based on light and electron microscopy and electron and x-ray diffraction.

Results

Al_4Ca

An alloy containing 14 wt.% Ca was studied. After slow solidification it contained primary Al_4Ca platelets surrounded by the Al-Al_4Ca eutectic in accordance with the phase diagram [4]. Polarized light revealed a heavily twinned structure within the Al_4Ca phase. This structure disappeared upon heating to T ≈ 200°C and reappeared upon cooling, usually with a different twin arrangement. Measurements of the electrical resistivity of Young's modulus and of the specific heat have indicated that the temperature of transformation is T ≈ 130°C [2]. Specimens annealed for 1 d at 160 and 90°C, respectively, and quenched in water of 0°C revealed that the transformation cannot be suppressed. Some single phase Al_4Ca powder was separated from a sample lowered through a temperature gradient and analysed in a precision x-ray diffractometer. The diagram, Fig. 2, taken at room temperature shows that

* Swiss Aluminium Ltd., 8212 Neuhausen, Switzerland
**now: Vacuumschmelze GmbH, 6450 Hanau, Germany
***now: Eidgen. Techn. Hochschule, 8093 Zürich, Switzerland

most of the lines associated with the tetragonal unit cell (marked t) according to Nowotny et al. [5] are split. The splitting can be accounted for by a monoclinic unit cell with a = 0.6158 nm, b = 0.6175 nm, c = 1.118 nm, $\beta = 88.9^{\circ}$ (marked m). This unit cell is related to the unit cell of the tetragonal structure by a shear of 1.1° in $\{110\}_t$ planes with a and b pointing in $[110]_t$ and $[1\bar{1}0]_t$ directions, respectively. At 170°C no corresponding splitting of the lines was observed. An analysis of the lattice correspondence leads to a total of 4 orientation variants of the monoclinic structure that may be derived from the tetragonal structure. Since the microstructure of the main Al_4Ca crystallite in Fig. 1 shows sets of twin lamellae in at least 4 different directions more than one kind of twinning system must be operative. By combining electron microscopy and electron diffraction 4 twinning systems with $\{001\}_m$ and $\{100\}_m$ as twinning planes could be identified. Specimens which had been annealed for 1 d at 160°C and 90°C, respectively, and quenched showed the same microstructure as Fig. 1. However, in these specimens the effects of the electron beam on the foil lead to rearrangements of the boundaries and to the growth and disappearance of lamellae or faults. Figs. 3a and b show such microstructural changes in a time interval of ca. 60 s. The rearrangements were confined to regions near the edge of the foil; they were not observed in slowly cooled specimens.

Al_3Mg_2

According to the Al-Mg phase diagram [4] the Al_3Mg_2 (β) phase extends from ≃ 35.1 to ≃ 37.5 wt.% Mg at room temperature. But the electrical resistivity and the specific heat exhibit anomalies at ≃ 240°C for 35.8 wt.% Mg and at ≃ -20°C for 37.2 wt.% Mg. Thus, the temperature of the transformation to be described is strongly concentration dependent. The transformation cannot be suppressed by water quenching.

A precision x-ray diffractogram of a 37.2 wt.% Mg alloy at room temperature agreed with the f.c.c. structure obtained by Samson [6]. In a transformed 35.8 wt.% Mg specimen a slight distortion of the f.c.c. structure was found. However, the splitting of the lines could not be resolved. Thus, a detailed analysis of the crystal structure and of the crystallography of the transformation could not be carried out. Thin foils of a 35.8 wt.% Mg alloy showed transformed regions with internal lamellae or faults (Fig. 4a). The corresponding diffraction pattern (Fig. 4b) contains streaks in the [111] direction, perpendicular to the defects. Upon heating within the microscope, the faults and streaks disappeared. On subsequent cooling tongue shaped regions of the new phase were formed at the edge of the foil and grew into the interior. Fig. 5a shows an advancing growth front at T ≃ 220°C. In this case a splitting of the diffraction spots was observed (Fig. 5b).

At 37.2 wt.% Mg transformed regions with internal lamellae were found near the edge of the foil (Fig. 6). Since the transformation temperature of bulk material at this composition is below room temperature,

the product has probably been nucleated due to stress relaxation as is well known, e.g. for Fe-Ni alloys. Due to the small difference between the parent and the product structure the nature of the internal lamellae could not yet be resolved.

Discussion

The results show that both Al_4Ca and Al_3Mg_2 undergo diffusionless shear transformations. In Al_3Mg_2 the coexistence of the parent and the product phase could be observed indicating that the characteristics of martensitic transformations occur. In Al_4Ca the light micrograph (Fig. 1) shows a rather domain-like array of twinned regions. Since the transformation could not be observed directly in a two-phase stage its nature could not be determined unambiguously. Two alternatives are likely: a martensitic transformation with a weakly developed plate shape of the product or a gradual shear transformation of the entire volume followed by stress relaxation twinning similar to, e.g., the structural changes associated with antiferromagnetic transitions [7].

References

[1] J. Timm: Die physikalischen Eigenschaften der intermetallischen Phase Al_3Mg_2, Diplomarbeit Universität Konstanz 1978.
[2] H. Zogg, P. Schwellinger: J. Mat. Science, in press
[3] H. Zogg, J. Timm, H. Warlimont: Aluminium, in press
[4] M. Hansen, K. Anderko: Constitution of Binary Alloys Mc Graw-Hill, New York, Toronto, London 1958
[5] H. Nowotny, E. Wormes, A. Mohrnheim: Z. Metallkde, 32(1940), 39.
[6] S. Samson: Acta Cryst. 19(1965),401.
[7] U. Hocke, H. Warlimont: J. Phys. F: Metal Phys. 7(1977), 1145.

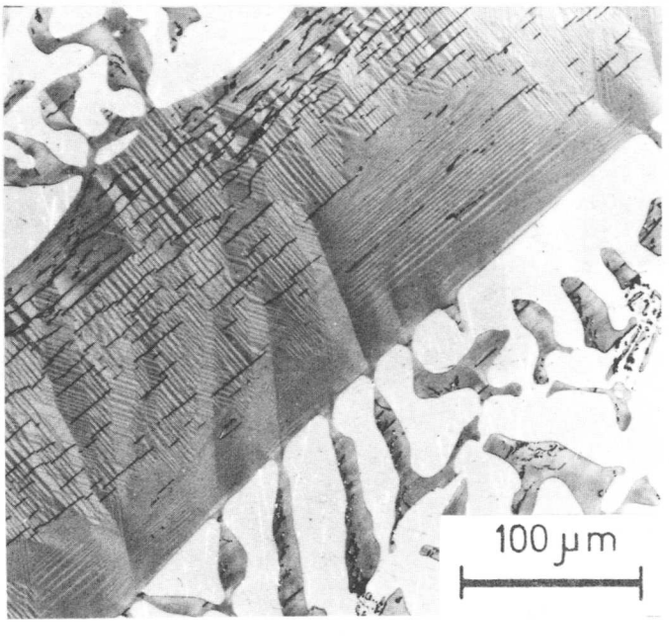

Fig. 1 Internal structure of Al14wt.%Ca showing twin lamellae (polarized light)

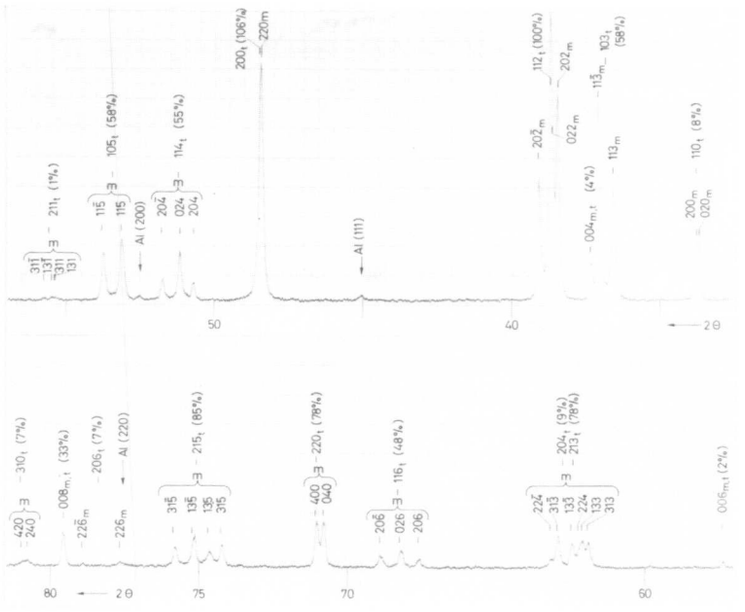

Fig. 2 Room temperature x-ray spectra of Al_4Ca obtained with $CoK_{\alpha 1}$-radiation

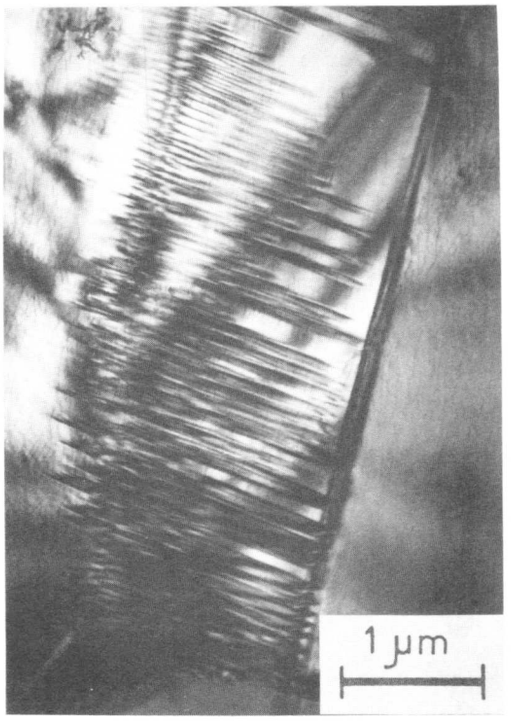

Fig. 3a Electron micrograph of quenched Al_4Ca exposed to the electron beam for the first time. Growing front of faults.

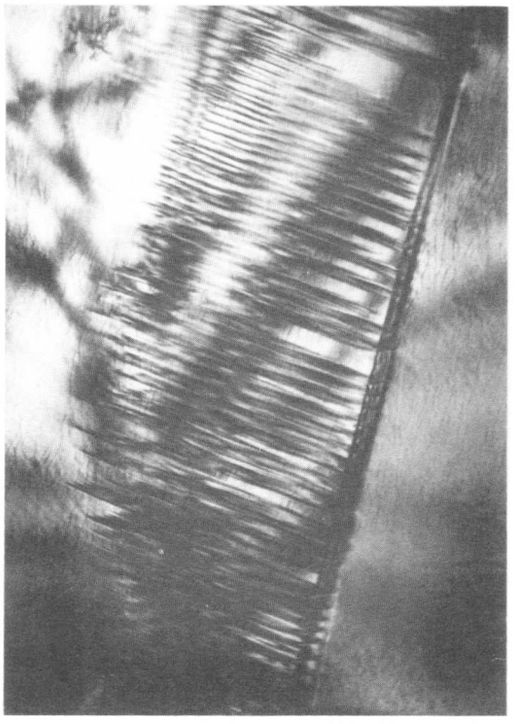

Fig. 3b is taken from the same area ca. 60 s later

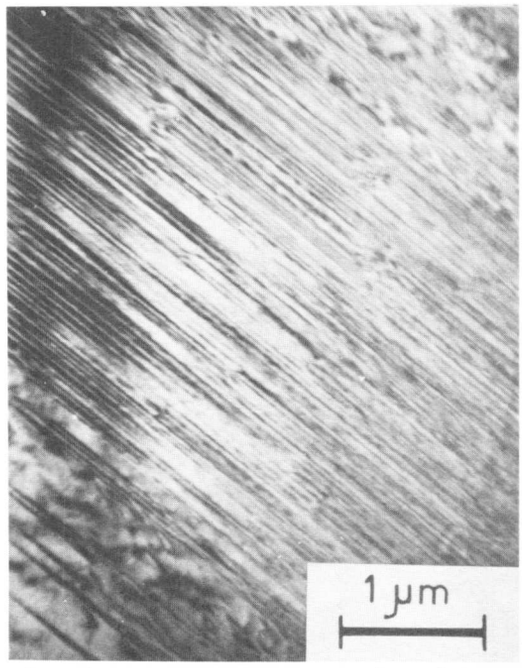

Fig. 4a Transformed region in Al_3Mg_2 (35.8 wt.% Mg)

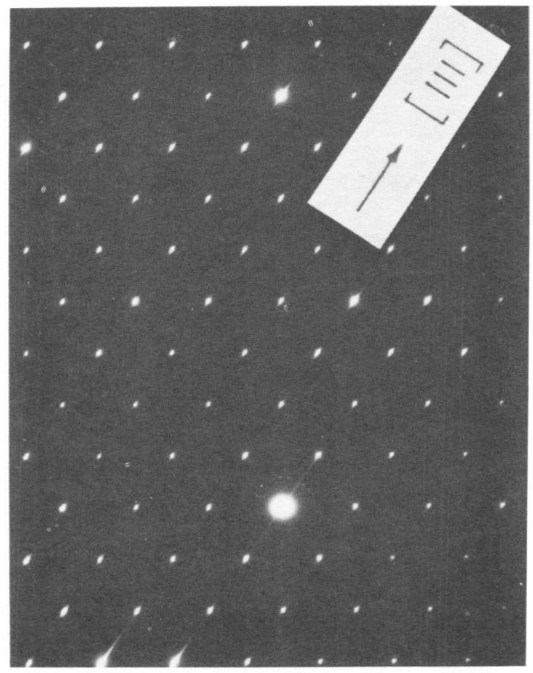

Fig. 4b Corresponding diffraction pattern. Streaking in III direction

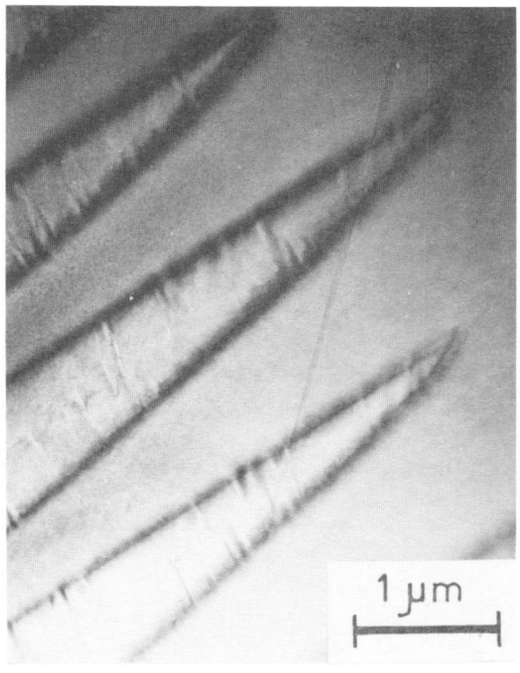

Fig. 5a Advancing growth front in Al_3Mg_2 ($T \approx 220^{\circ}C$, 35.8 wt.% Mg)

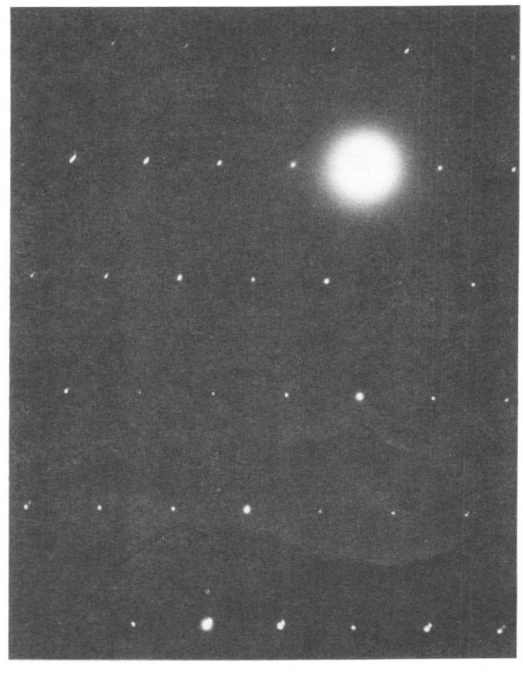

Fig. 5b Corresponding diffraction pattern. Splitting of spots.

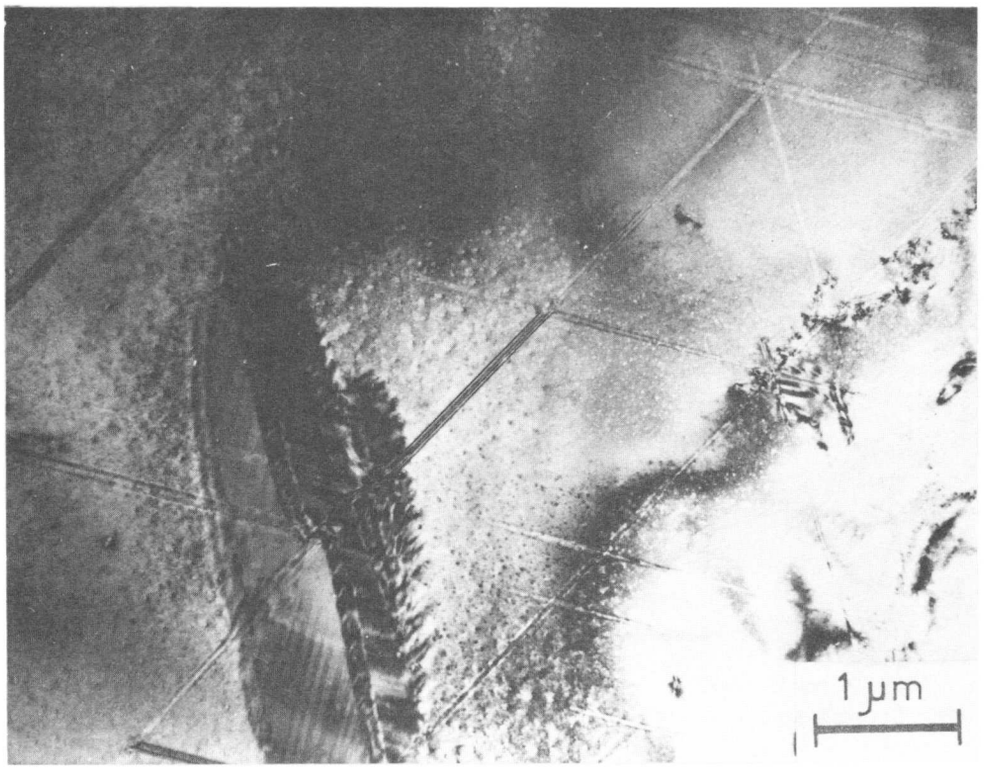

Fig. 6 Transformed region in Al_3Mg_2 (37.2 wt.% Mg).
Internal lamellae. Stacking faults in the parent phase.

Acknowledgement - The technical help of Mr. Koutny and Mr. Scalco is greatly acknowledged.

Thermodynamics and Kinetics of Martensite

J. W. Christian*

I. Introduction

Troiano and Greninger [1] and Kurdjumov [2] considered kinetics to be as important as crystallography in defining the characteristics of martensitic reactions. In supporting this view, I shall ignore the exigencies of the time-table and look backwards to nucleation as well as forwards to today's papers. I take as my starting point the excellent survey of kinetics and nucleation theory in ferrous martensite presented by Magee [3]. He distinguished two kinds of kinetic behaviour, "dynamically stabilized" and "isothermal", and further sub-divided the latter into cases where martensite forms predominantly in bursts during cooling and those in which most of the transformation is isothermal. To these categories, we must add thermoelastic martensite which occurs in many non-ferrous systems.

Magee concluded, in contrast to earlier theories, that the average volume of a martensite plate is independent of the volume fraction of martensite and that nucleation sites which are autocatalytically activated by previously formed plates are overwhelmingly more important than randomly-distributed pre-existing sites. He suggested that the rate-limiting step may be the propagation of the interface.

II. Thermodynamics

Although some displacive phase transitions may be thermodynamically second or higher order, the transformations which the metallurgist recognizes as martensitic involve large distortions of the unit cell and changes in symmetry and are all first order. It is then possible to define an equilibrium T_o temperature by the intersection of two independent free energy curves, and to define a driving force as the difference between these curves (see Fig. 1). The free energy as a continuous function of configuration along some path from A to B in Fig. 1 may, more controversially, be given by a Landau expansion [4]

$$\Delta G = P\eta^2 + Q\eta^3 + R\eta^4 + \ldots \qquad (1)$$

where η is an appropriate order parameter which in the case of martensite represents a finite homogeneous deformation. Fig. 2 shows the relation between ΔG and η at different temperatures; the perfect parent phase becomes mechanically unstable at T_u when the minimum at $\eta = 0$ changes

*National Bureau of Standards, Washington, DC; on leave from Dept. of Metallurgy and Science of Materials, Oxford University

into a maximum and the free energy decreases continuously from $\eta = 0$ to $\eta = \eta_\alpha$. At T_u, $P = 0$, and writing $P = \alpha(T-T_u)$ and neglecting higher terms in (1) $T_o - T_u = Q^2/4\alpha R$. If the parent lattice remains mechanically stable at M_s, $T_u < M_s < T_o$; it is an open question whether even, in principle, T_u exists for most transformations.

Figs. 1 and 2 show the free energies of homogeneous, stress-free volumes of the parent, product and intermediate structures. When a martensite region forms within a constraining matrix, additional energy arises from the non-uniformity of the structure and may be approximately divided into coherency strain energy, surface energy and defect energies. In evaluating experimental thermodynamic data, it is important to take account of this additional stored energy.

2.1. Enthalpies and Free Energies in Ferrous Alloys

According to early calculations [5], the difference ΔG_c in chemical free energies of austenite and martensite is $\sim$1200 J mol^{-1} at the M_s of all binary Fe-C alloys. Later work [6-7] has shown, however, that for both Fe-C and Fe-N alloys, ΔG_c at M_s increases strongly from $\lesssim$ 1100 J mol^{-1} in pure iron (see below) to $\sim$2400 J mol^{-1} at 10 at % solute. Early estimates for substitutional alloys gave too large a variation of ΔG_c with composition; it now appears that ΔG_c increases slightly with solute content and reaches $\sim$1450 J mol^{-1} at Fe-10 at % Cr. Ternary solutes in Fe-Ni may either raise or lower ΔG_c [8].

There is still uncertainty about the value of M_s and hence ΔG_c for pure iron. The limiting arrest temperature of $\sim$820K found in very fast cooling curves [9-15] represents a reasonable extrapolation of the Fe-N data [6], but if M_s varies rapidly with interstitial content at low levels, the experimental values may be lowered by residual interstitials [1]. An alternative is $M_s \simeq$970-1000K which is consistent with extrapolation of dilute substitutional alloy data; much depends on whether the arrest temperatures observed in these alloys represent bainitic or martensitic reactions [16-18]. In recent work, four different arrest plateaux are reported by Wilson [13,19] and three by Morozov et al [14-15] who used high purity zone refined iron. Both groups obtained metallographic evidence that the transformation at 820K produces lath martensite, and in a rapidly cooled Fe-0.01% C alloy Morozov et al also found an arrest at 690K which is attributed to lenticular martensite. The value of 820K for M_s appears more probable and hence $\Delta G_c \simeq$1100 J mol^{-1} [20]. If M_s is 970K, ΔG_c is $\sim$400 J mol^{-1} and calorimetric data on alloys indicate that this is inadequate to produce heavily dislocated lath martensite.

Recent calorimetric measurements [21] indicate that the stored energy of ferrous martensite varies with the morphology and substructure. The heat evolved when lath martensite is formed in Fe-29 wt% Ni at 266-133K corresponds to an enthalpy of transformation (evaluated at 570K) of $\sim$1600 J mol^{-1} independent of transformation temperature and volume fraction. The enthalpy change is similar for Fe-30.3 wt% Ni transformed at 243-198K, but at lower temperatures, where plate